Practical estimates of rock mass strength

E. Hoek and E.T. Brown

Published in the *International Journal of Rock Mechanics and Mining Sciences*, Vol 34, No 8, 1997, pages 1165-1186

Practical estimates of rock mass strength

E. HOEK[⌖]
E.T. BROWN[⌖⌖]

The Hoek-Brown failure criterion was originally developed for estimating the strengths of hard rock masses. Because of the lack of suitable alternatives, the criterion has been applied to a variety of rock masses including very poor quality rocks, which could almost be classed as engineering soils. These applications have necessitated changes to the original criterion. One of the principal problems has been the determination of equivalent cohesive strengths and friction angles to meet the demands of software written in terms of the Mohr-Coulomb failure criterion. This paper summarises the interpretation of the Hoek-Brown failure criterion which has been found to work best in dealing with practical engineering problems.

INTRODUCTION

Since its introduction in 1980 [1], the Hoek-Brown failure criterion has evolved to meet the needs of users who have applied it to conditions which were not visualised when it was originally developed. In particular, the increasing number of applications to very poor quality rock masses has necessitated some significant changes. The key equations involved in each of the successive changes are summarised in Appendix A.

The criterion is purely empirical and hence there are no 'correct' ways to interpret the various relationships which can be derived. Under the circumstances, it is not surprising that there have been a few less than useful mutations and that some users have been confused by the alternative interpretations which have been published.

This paper is an attempt to set the record straight and to present an interpretation of the criterion which covers the complete range of rock mass types and which has been found to work well in practice.

GENERALISED HOEK-BROWN CRITERION

The Generalised Hoek-Brown failure criterion for jointed rock masses is defined by:

$$\sigma'_1 = \sigma'_3 + \sigma_{ci}\left(m_b \frac{\sigma'_3}{\sigma_{ci}} + s\right)^a \tag{1}$$

where σ'_1 and σ'_3 are the maximum and minimum effective stresses at failure respectively,

m_b is the value of the Hoek-Brown constant m for the rock mass,

s and a are constants which depend upon the characteristics of the rock mass, and

σ_{ci} is the uniaxial compressive strength of the intact rock pieces.

It is possible to derive some exact mathematical relationships between the Hoek-Brown criterion, expressed in terms of the major and minor principal stresses, and the Mohr envelope, relating normal and shear stresses. However, these relationships are cumbersome and the original approach used by Hoek and Brown [1] is more practical. In this approach, equation (1) is used to generate a series of triaxial test values, simulating full scale field tests, and a statistical curve fitting process is used to derive an equivalent Mohr envelope defined by the equation:

$$\tau = A\sigma_{ci}\left(\frac{\sigma'_n - \sigma_{tm}}{\sigma_{ci}}\right)^B \tag{2}$$

where A and B are material constants

σ'_n is the normal effective stress, and

σ_{tm} is the 'tensile' strength of the rock mass.

This 'tensile' strength, which reflects the interlocking of the rock particles when they are not free to dilate, is given by:

$$\sigma_{tm} = \frac{\sigma_{ci}}{2}\left(m_b - \sqrt{m_b^2 + 4s}\right) \tag{3}$$

In order to use the Hoek-Brown criterion for estimating the strength and deformability of jointed rock masses, three 'properties' of the rock mass have to be estimated. These are

⌖ Evert Hoek Consulting Engineer Inc.
P.O. Box 75516, North Vancouver
British Columbia, Canada, V7R 4X1
⌖⌖ Senior Deputy Vice Chancellor
The University of Queensland
Brisbane, Queensland 4072, Australia

1. the uniaxial compressive strength σ_{ci} of the intact rock pieces in the rock mass,
2. the value of the Hoek-Brown constant m_i for these intact rock pieces, and
3. the value of the Geological Strength Index GSI for the rock mass.

THE EFFECT OF WATER

Many rocks show a significant strength decrease with increasing moisture content. In some cases, such as montmorillonitic clay shales, saturation destroys the specimens completely. More typically, strength losses of 30 to100 % occur in many rocks as a result of chemical deterioration of the cement or clay binder (Broch [2]). Samples which have been left to dry in a core shed for several months, can give a misleading impression of the rock strength. Laboratory tests should be carried out at moisture contents which are as close as possible to those which occur in the field.

A more important effect is the strength reduction which occurs as a result of water pressures in the pore spaces in the rock. Terzaghi [3] formulated the concept of effective stress for porous media such as soils. The effective stress 'law', as it is frequently called, can be expressed as $\sigma' = \sigma - u$ where σ' is the effective or intergranular stress which controls the strength and the deformation of the material, σ is the total stress applied to the specimen and u is the pore water pressure. In a comprehensive review of the applicability of the effective stress concept to soil, concrete and rock, Lade and de Boer [4] conclude that the relationship proposed by Terzaghi works well for stress magnitudes encountered in most geotechnical applications, but that significant deviations can occur at very high stress levels.

The effective stress principle has been used throughout this paper for both intact rock and jointed rock masses. For intact rocks, with very low porosity, it has been assumed that stress changes are slow enough for the pore pressures in the rock specimens to reach steady state conditions (Brace and Martin [5]). In jointed rock masses, it may be expected that the water pressures in the discontinuities will build up and dissipate more rapidly than those in the pores of the intact rock blocks, especially in low porosity and permeability rocks. For this reason, a distinction is sometimes made between joint and pore water pressures in jointed rock masses. When applying the Hoek - Brown criterion to heavily jointed rock masses, isotropic behaviour involving failure on the discontinuities is assumed. In these cases, the water or 'pore' pressures governing the effective stresses will be those generated in the interconnected discontinuities defining the particles in an equivalent isotropic medium.

In applying the failure criterion, expressed in effective stress terms, to practical design problems it is necessary to determine the pore pressure distribution in the rock mass being analysed. This can be done by direct measurement, using piezometers, or estimated from manually constructed or numerically generated flow nets. In the case of slopes, dam foundations and tunnels subjected to fluctuating internal water pressure, the magnitude of the pore pressures can be of the same order as the induced rock stresses and hence it is very important to deal with the analysis in terms of effective stresses. In other cases, particularly when designing under-ground excavations, it can be assumed that the rock mass surrounding these excavations will be fully drained and hence the pore pressures are set to zero.

INTACT ROCK PROPERTIES

For the intact rock pieces that make up the rock mass equation (1) simplifies to:

$$\sigma'_1 = \sigma'_3 + \sigma_{ci}\left(m_i \frac{\sigma'_3}{\sigma_{ci}} + 1\right)^{0.5} \tag{4}$$

The relationship between the effective principal stresses at failure for a given rock is defined by two constants, the uniaxial compressive strength σ_{ci} and a constant m_i. Wherever possible the values of these constants should be determined by statistical analysis of the results of a set of triaxial tests on carefully prepared core samples, as described in Appendix B.

Note that the range of minor principal stress (σ'_3) values over which these tests are carried out is critical in determining reliable values for the two constants. In deriving the original values of σ_{ci} and m_i, Hoek and Brown [1] used a range of $0 < \sigma'_3 < 0.5\sigma_{ci}$ and, in order to be consistent, it is essential that the same range be used in any laboratory triaxial tests on intact rock specimens.

When laboratory tests are not possible, Tables 1 and 2 can be used to obtain estimates of σ_{ci} and m_i. These estimates can be used for preliminary design purposes but, for detailed design studies, laboratory tests should be carried out to obtain values that are more reliable.

When testing very hard brittle rocks it may be worth considering the fact that short-term laboratory tests tend to overestimate the in-situ rock mass strength. Extensive laboratory tests and field studies on excellent quality Lac du Bonnet granite, reported by Martin and Chandler [7], suggest that the in-situ strength of this rock is only about 70% of that measured in the laboratory. This appears to be due to the fact that damage resulting from micro-cracking of the rock initiates and develops critical intensities at lower stress levels in the field than in laboratory tests carried out at higher loading rates on smaller specimens.

Anisotropic and foliated rocks such as slates, schists and phyllites, whose behaviour is dominated by closely spaced planes of weakness, cleavage or schistosity, present particular difficulties in the determination of the uniaxial compressive strengths.

Salcedo [8] has reported the results of a set of directional uniaxial compressive tests on a graphitic phyllite from Venezuela. These results are summarised in Fig. 1. It will be noted that the uniaxial compressive strength of this material varies by a factor of about 5, depending upon the direction of loading. Evidence of the behaviour of this graphitic phyllite in the field suggests that the rock mass properties are dependent upon the strength parallel to schistosity rather than that normal to it.

In deciding upon the value of σ_{ci} for foliated rocks, a decision has to be made on whether to use the highest or the lowest uniaxial compressive strength obtained from results such as those given in Fig. 1. Mineral composition, grain size, grade of metamorphism and tectonic history all play a role in determining the characteristics of the rock mass.

The authors cannot offer any precise guidance on the choice of σ_{ci} but suggest that the maximum value should be used for hard, well interlocked rock masses such as good quality slates. The lowest uniaxial compressive strength should be used for tectonically disturbed, poor quality rock masses such as the graphitic phyllite tested by Salcedo [8].

Table 1. Field estimates of uniaxial compressive strength.

Grade*	Term	Uniaxial Comp. Strength (MPa)	Point Load Index (MPa)	Field estimate of strength	Examples
R6	Extremely Strong	> 250	>10	Specimen can only be chipped with a geological hammer	Fresh basalt, chert, diabase, gneiss, granite, quartzite
R5	Very strong	100 - 250	4 - 10	Specimen requires many blows of a geological hammer to fracture it	Amphibolite, sandstone, basalt, gabbro, gneiss, granodiorite, limestone, marble, rhyolite, tuff
R4	Strong	50 - 100	2 - 4	Specimen requires more than one blow of a geological hammer to fracture it	Limestone, marble, phyllite, sandstone, schist, shale
R3	Medium strong	25 - 50	1 - 2	Cannot be scraped or peeled with a pocket knife, specimen can be fractured with a single blow from a geological hammer	Claystone, coal, concrete, schist, shale, siltstone
R2	Weak	5 - 25	**	Can be peeled with a pocket knife with difficulty, shallow indentation made by firm blow with point of a geological hammer	Chalk, rocksalt, potash
R1	Very weak	1 - 5	**	Crumbles under firm blows with point of a geological hammer, can be peeled by a pocket knife	Highly weathered or altered rock
R0	Extremely weak	0.25 - 1	**	Indented by thumbnail	Stiff fault gouge

* Grade according to Brown [2]
** Point load tests on rocks with a uniaxial compressive strength below 25 MPa are likely to yield ambiguous results.

Table 2. Values of the constant m_i for intact rock, by rock group. Note that values in parenthesis are estimates.

Rock type	Class	Group	Texture: Coarse	Texture: Medium	Texture: Fine	Texture: Very fine
SEDIMENTARY	Clastic		Conglomerate (22)	Sandstone 19	Siltstone 9	Claystone 4
				— Greywacke (18) —		
	Non-Clastic	Organic		— Chalk 7 —		
				— Coal (8-21) —		
		Carbonate	Breccia (20)	Sparitic Limestone (10)	Micritic Limestone 8	
		Chemical		Gypstone 16	Anhydrite 13	
METAMORPHIC	Non Foliated		Marble 9	Hornfels (19)	Quartzite 24	
	Slightly foliated		Migmatite (30)	Amphibolite 25 - 31	Mylonites (6)	
	Foliated*		Gneiss 33	Schists 4 - 8	Phyllites (10)	Slate 9
IGNEOUS	Light		Granite 33		Rhyolite (16)	Obsidian (19)
			Granodiorite (30)		Dacite (17)	
	Dark		Diorite (28)		Andesite 19	
			Gabbro 27	Dolerite (19)	Basalt (17)	
			Norite 22			
	Extrusive pyroclastic type		Agglomerate (20)	Breccia (18)	Tuff (15)	

* These values are for intact rock specimens tested normal to bedding or foliation. The value of m_i will be significantly different if failure occurs along a weakness plane.

Unlike other rocks, coal is organic in origin and therefore has unique constituents and properties. Unless these properties are recognised and allowed for in characterising the coal, the results of any tests will exhibit a large amount of scatter. Medhurst, Brown and Trueman [9] have shown that, by taking into account the ‘brightness’ which reflects the composition and the cleating of the coal, it is possible to differentiate between the mechanical characteristics of different coals.

INFLUENCE OF SAMPLE SIZE

The influence of sample size upon rock strength has been widely discussed in geotechnical literature and it is generally assumed that there is a significant reduction in strength with increasing sample size. Based upon an analysis of published data, Hoek and Brown [1] have suggested that the uniaxial compressive strength σ_{cd} of a rock specimen with a diameter of d mm is related to the uniaxial compressive strength σ_{c50} of a 50 mm diameter sample by equation (5).

$$\sigma_{cd} = \sigma_{c50}\left(\frac{50}{d}\right)^{0.18} \quad (5)$$

This relationship, together with the data upon which it was based, is illustrated in Fig. 2.

The authors suggest that the reduction in strength is due to the greater opportunity for failure through and around grains, the 'building blocks' of the intact rock, as more and more of these grains are included in the test sample. Eventually, when a sufficiently large number of grains are included in the sample, the strength reaches a constant value.

Medhurst and Brown [10] have reported the results of laboratory triaxial tests on samples of 61, 101, 146 and 300 mm diameter samples of a highly cleated mid-brightness coal from the Moura mine in Australia. The results of these tests are summarised in Table 3 and Fig. 3.

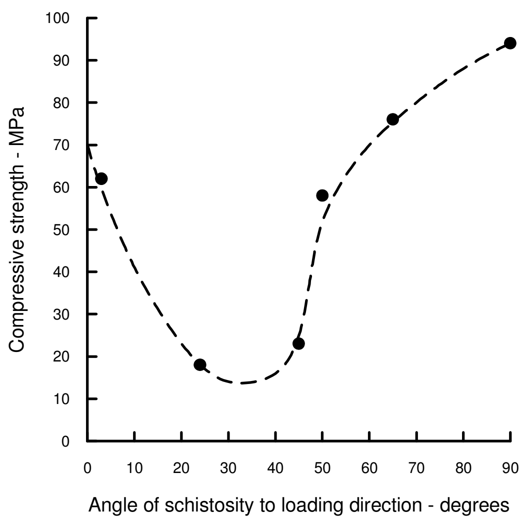

Fig. 1. Influence of loading direction on strength of graphitic phyllite tested by Salcedo [8].

The results obtained by Medhurst and Brown show a significant decrease in strength with increasing sample size. This is attributed to the effects of cleat spacing. For this coal, the persistent cleats are spaced at 0.3 to 1.0 m while non-persistent cleats within vitrain bands and individual lithotypes define blocks of 1 cm or less. This cleating results in a 'critical' sample size of about 1 m above which the strength remains constant.

It is reasonable to extend this argument further and to suggest that, when dealing with large scale rock masses, the strength will reach a constant value when the size of individual rock pieces is sufficiently small in relation to the overall size of the structure being considered. This suggestion is embodied in Fig. 4 which shows the transition from an isotropic intact rock specimen, through a highly anisotropic rock mass in which failure is controlled by one or two discontinuities, to an isotropic heavily jointed rock mass.

The Hoek-Brown failure criterion, which assumes isotropic rock and rock mass behaviour, should only be applied to those rock masses in which there are a sufficient number of closely spaced discontinuities that isotropic behaviour involving failure on discontinuities can be assumed. Where the block size is of the same order as that of the structure being analysed, the Hoek-Brown criterion should not be used. The stability of the structure should be analysed by considering the behaviour of blocks and wedges defined by intersecting structural features. When the slope or underground excavation is large and the block size small in comparison, the rock mass can be treated as a Hoek-Brown material.

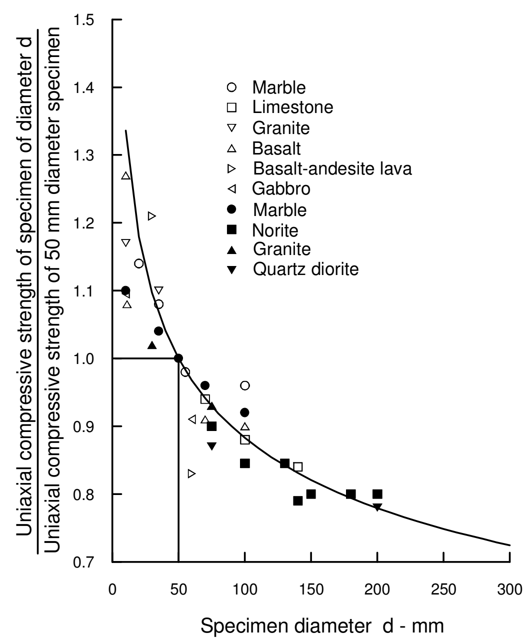

Fig. 2. Influence of specimen size on the strength of intact rock. After Hoek and Brown [1].

Table 3. Peak strength of Moura DU coal in terms of the parameters contained in equation (1), based upon a value of σ_{ci} = 32.7 MPa.

Dia.(mm)	m_b	s	a
61	19.4	1.0	0.5
101	13.3	0.555	0.5
146	10.0	0.236	0.5
300	5.7	0.184	0.6
mass	2.6	0.052	0.65

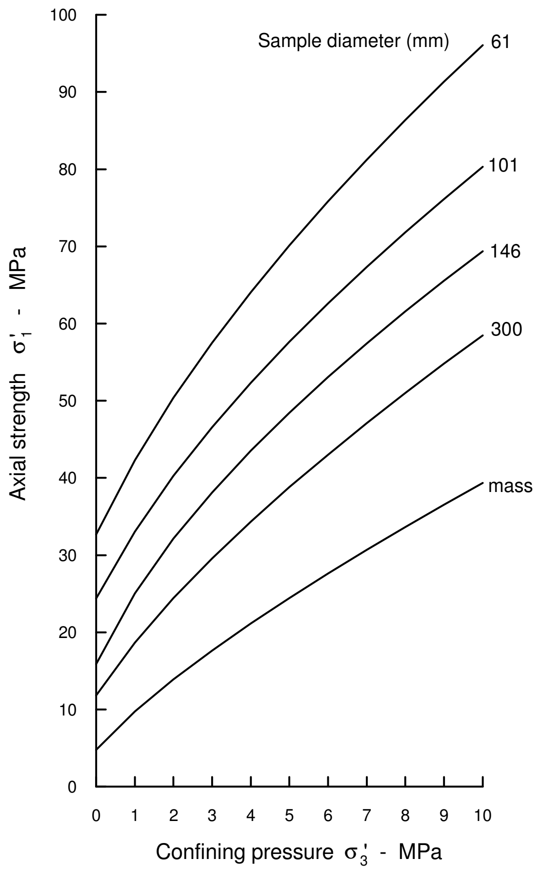

Fig. 3. Peak strength for Australian Moura coal. After Medhurst and Brown [6].

GEOLOGICAL STRENGTH INDEX

The strength of a jointed rock mass depends on the properties of the intact rock pieces and also upon the freedom of these pieces to slide and rotate under different stress conditions. This freedom is controlled by the geometrical shape of the intact rock pieces as well as the condition of the surfaces separating the pieces. Angular rock pieces with clean, rough discontinuity surfaces will result in a much stronger rock mass than one which contains rounded particles surrounded by weathered and altered material.

The Geological Strength Index (GSI), introduced by Hoek [11] and Hoek, Kaiser and Bawden [12] provides a system for estimating the reduction in rock mass strength for different geological conditions. This system is presented in Tables 4 and 5. Experience has shown that Table 4 is sufficient for field observations since it is only necessary to note the letter code which identifies each rock mass category. These codes can then be used to estimate the GSI value from Table 5.

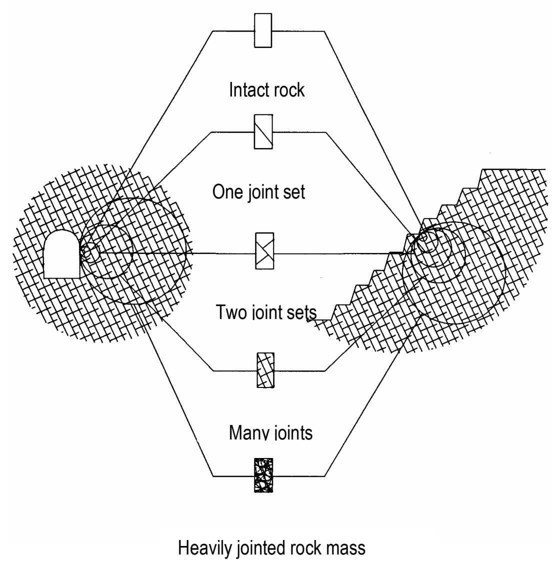

Fig. 4. Idealised diagram showing the transition from intact to a heavily jointed rock mass with increasing sample size.

Once the Geological Strength Index has been estimated, the parameters which describe the rock mass strength characteristics, are calculated as follows:

$$m_b = m_i \exp\left(\frac{GSI - 100}{28}\right) \tag{6}$$

For GSI > 25, i.e. rock masses of good to reasonable quality, the original Hoek-Brown criterion is applicable with

$$s = \exp\left(\frac{GSI - 100}{9}\right) \tag{7}$$

and

$$a = 0.5 \tag{8}$$

For GSI < 25, i.e. rock masses of very poor quality, the modified Hoek-Brown criterion [14] applies with

$$s = 0 \tag{9}$$

and

$$a = 0.65 - \frac{GSI}{200} \tag{10}$$

The choice of GSI = 25 for the switch between the original and modified criteria is purely arbitrary. It could be argued that a switch at GSI = 30 would not introduce a discontinuity in the value of a, but extensive trials have shown that the exact location of this switch has negligible practical significance.

For better quality rock masses (GSI > 25), the value of GSI can be estimated directly from the 1976 version of Bieniawski's Rock Mass Rating, with the Groundwater rating set to 10 (dry) and the Adjustment for Joint Orientation set to 0 (very favourable) [15]. For very poor quality rock masses the value of RMR is very difficult to estimate and the balance between the ratings no longer gives a reliable basis for estimating rock mass strength. Consequently, Bieniawski's RMR classification should not be used for estimating the GSI values for poor quality rock masses.

If the 1989 version of Bieniawski's RMR classification [16] is used, then GSI = RMR_{89}' - 5 where RMR_{89}' has the Groundwater rating set to 15 and the Adjustment for Joint Orientation set to zero.

One of the practical problems which arises when assessing the value of GSI in the field is related to blast damage. As illustrated in Fig. 5, there is a considerable difference in the appearance of a rock face which has been excavated by controlled blasting and a face which has been damaged by bulk blasting. Wherever possible, the undamaged face should be used to estimate the value of GSI since the overall aim is to determine the properties of the undisturbed rock mass. Where all the visible faces have been damaged by blasting, some attempt should be made to compensate for the lower values of GSI obtained from such faces. In recently blasted faces, new discontinuity surfaces will have been created by the blast and these will give a GSI value which may be as much as 10 points lower than that for the undisturbed rock mass. In other words, severe blast damage can be allowed for by moving up one row in Tables 4 and 5. Where blast damaged faces have been exposed for a number of years, it may also be necessary to step as much as one column to the left in order to allow for surface weathering which will have occurred during this exposure. Hence, for example, a badly blast damaged weathered rock surface which has the appearance of a BLOCKY/DISTURBED and FAIR (BD/F in Table 4) rock mass may actually be VERY BLOCKY and GOOD (VB/G) in its unweathered and undisturbed in-situ state.

An additional practical question is whether borehole cores can be used to estimate the GSI value behind the visible faces? For reasonable quality rock masses (GSI > 25) the best approach is to evaluate the core in terms of Bieniawski's RMR classification and then, as described above, to estimate the GSI value from RMR. For poor quality rock masses (GSI < 25), relatively few intact core pieces longer than 100 mm are recovered and it becomes difficult to determine a reliable value for RMR. In these circumstances, the physical appearance of the material recovered in the core should be used as a basis for estimating GSI.

MOHR-COULOMB PARAMETERS

Most geotechnical software is written in terms of the Mohr-Coulomb failure criterion in which the rock mass strength is defined by the cohesive strength c' and the angle of friction ϕ'. The linear relationship between the major and minor principal stresses, σ'_1 and σ'_3, for the Mohr-Coulomb criterion is

$$\sigma'_1 = \sigma_{cm} + k\sigma'_3 \tag{11}$$

where σ_{cm} is the uniaxial compressive strength of the rock mass and k is the slope of the line relating σ'_1 and σ'_3. The values of ϕ' and c' can be calculated from

$$\sin\phi' = \frac{k-1}{k+1} \tag{12}$$

$$c' = \frac{\sigma_{cm}}{2\sqrt{k}} \tag{13}$$

There is no direct correlation between equation (11) and the non-linear Hoek-Brown criterion defined by equation (1). Consequently, determination of the values of c' and ϕ' for a rock mass that has been evaluated as a Hoek-Brown material is a difficult problem.

The authors believe that the most rigorous approach available, for the original Hoek-Brown criterion, is that developed by Dr J.W. Bray and reported by Hoek [17]. For any point on a surface of concern in an analysis such as a slope stability calculation, the effective normal stress is calculated using an appropriate stress analysis technique. The shear strength developed at that value of effective normal stress is then calculated from the equations given in Appendix A. The difficulty in applying this approach in practice is that most of the geotechnical software currently available provides for constant rather than effective normal stress dependent values of c' and ϕ'.

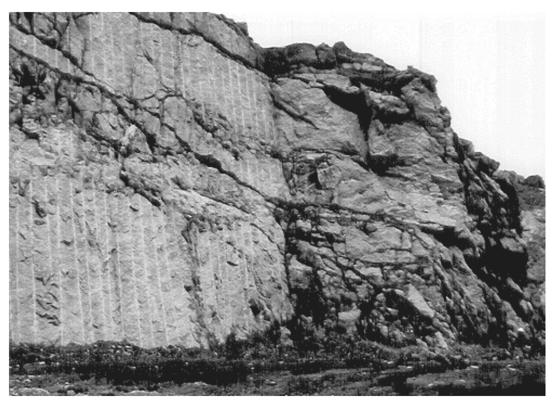

Fig. 5: Comparison between the results achieved by controlled blasting (on the left) and normal bulk blasting for a surface excavation in gneiss.

Table 4. Characterisation of rock masses on the basis of interlocking and joint alteration[1].

ROCK MASS CHARACTERISTICS FOR STRENGTH ESTIMATES

Based upon the appearance of the rock, choose the category that you think gives the best description of the 'average' undisturbed in situ conditions. Note that exposed rock faces that have been created by blasting may give a misleading impression of the quality of the underlying rock. Some adjustment for blast damage may be necessary and examination of diamond drill core or of faces created by pre-split or smooth blasting may be helpful in making these adjustments. It is also important to recognize that the Hoek-Brown criterion should only be applied to rock masses where the size of individual blocks is small compared with the size of the excavation under consideration.

STRUCTURE (DECREASING INTERLOCKING OF ROCK PIECES ↓) / SURFACE CONDITIONS (DECREASING SURFACE QUALITY →)		VERY GOOD Very rough, fresh unweathered surfaces	GOOD Rough, slightly weathered, iron stained surfaces	FAIR Smooth, moderately weathered or altered surfaces	POOR Slickensided, highly weathered surfaces with compact coatings or fillings of angular fragments	VERY POOR Slickensided, highly weathered surfaces with soft clay coatings or fillings
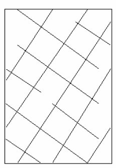	BLOCKY - very well interlocked undisturbed rock mass consisting of cubical blocks formed by three orthogonal discontinuity sets	B/VG	B/G	B/F	B/P	B/VP
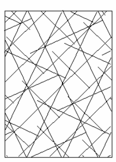	VERY BLOCKY - interlocked, partially disturbed rock mass with multifaceted angular blocks formed by four or more discontinuity sets	VB/VG	VB/G	VB/F	VB/P	VB/VP
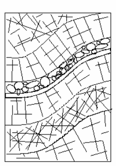	BLOCKY/DISTURBED- folded and/or faulted with angular blocks formed by many intersecting discontinuity sets	BD/VG	BD/G	BD/F	BD/P	BD/VP
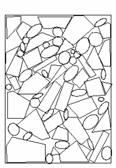	DISINTEGRATED - poorly inter-locked, heavily broken rock mass with a mixture or angular and rounded rock pieces	D/VG	D/G	D/F	D/P	D/VP

[1] In earlier versions of this table the terms BLOCKY/SEAMY and CRUSHED were used, following the terminology used by Terzaghi [9]. However, these terms proved to be misleading and they have been replaced, in this table by BLOCKY/DISTURBED, which more accurately reflects the increased mobility of a rock mass which has undergone some folding and/or faulting, and DISINTEGRATED which encompasses a wider range of particle shapes.

Table 5. Estimate of Geological Strength Index GSI based on geological descriptions.

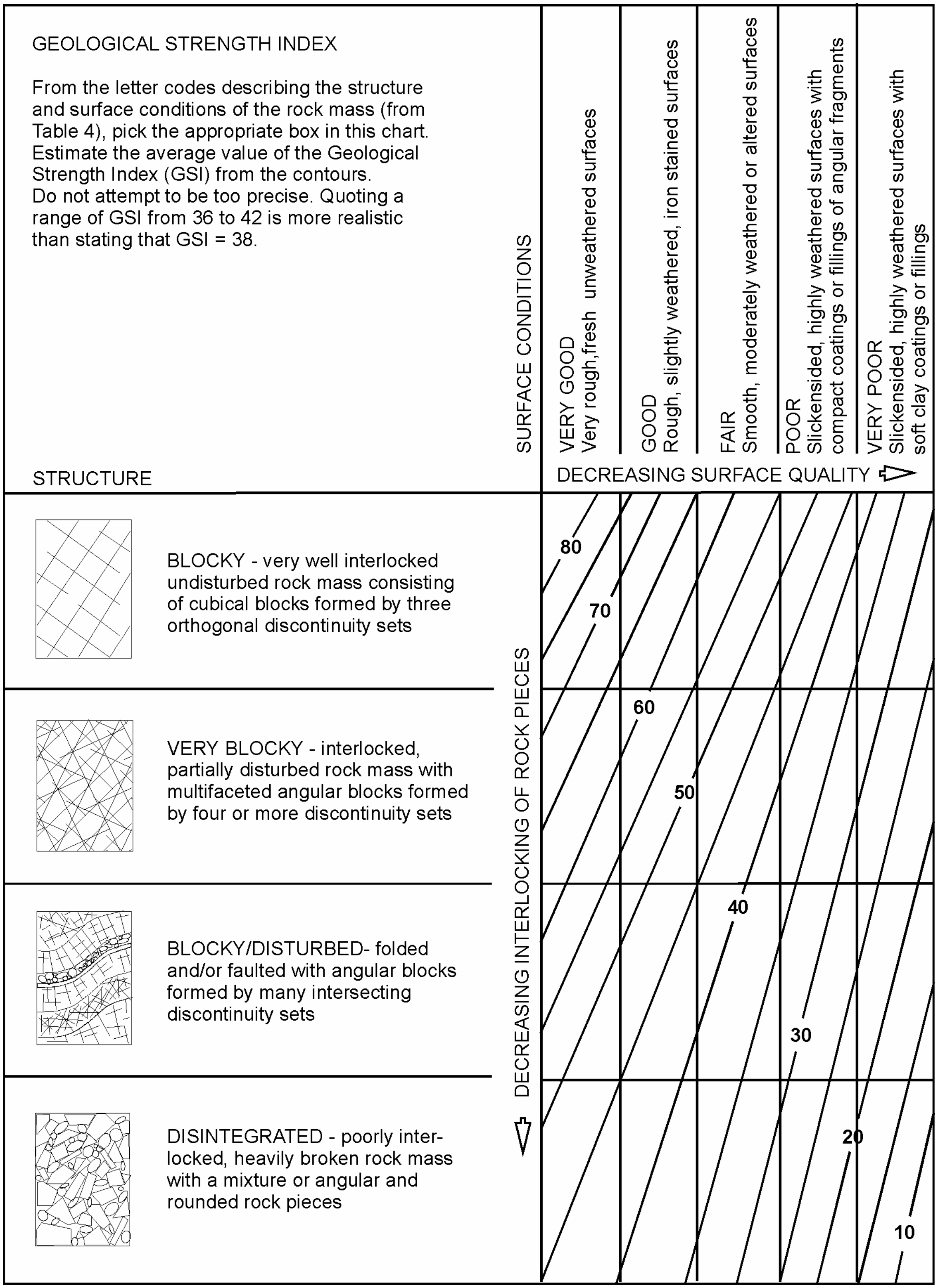

Having evaluated a large number of possible approaches to this problem, it has been concluded that the most practical solution is to treat the problem as an analysis of a set of full-scale triaxial strength tests. The results of such tests are simulated by using the Hoek-Brown equation (1) to generate a series of triaxial test values. Equation (11) is then fitted to these test results by linear regression analysis and the values of c' and ϕ' are determined from equations (12) and (13).

A discussion of all the steps required to determine the parameters A and B (equation (2)) and c' and ϕ' is given in Appendix C. A spreadsheet for carrying out this analysis, with a listing of all the cell formulae, is also given in this appendix.

The values of c' and ϕ' obtained from this analysis are very sensitive to the range of values of the minor principal stress σ'_3 used to generate the simulated full-scale triaxial test results. On the basis of trial and error, it has been found that the most consistent results are obtained when 8 equally spaced values of σ'_3 are used in the range $0 < \sigma'_3 < 0.25\sigma_{ci}$.

An example of the results, which are obtained from this analysis, is given in Fig. 6. Plots of the values of the ratio c'/σ_{ci} and the friction angle ϕ', for different combinations of GSI and m_i are given in Fig. 7 and Fig. 8.

Appendix C includes a calculation for a tangent to the Mohr envelope defined by equation (2). A normal stress has to be specified in order to calculate this tangent and, in Fig. 6, this stress has been chosen so that the friction angle ϕ' is the same for both the tangent and the line defined by c' = 3.3 MPa and ϕ' = 30.1°, determined by the linear regression analysis described earlier. The cohesion intercept for the tangent is c' = 4.1 MPa which is approximately 25% higher than that obtained by linear regression analysis of the simulated triaxial test data.

Fitting a tangent to the curved Mohr envelope gives an upper bound value for the cohesive intercept c'. It is recommended that this value be reduced by about 25% in order to avoid over-estimation of the rock mass strength.

There is a particular class of problem for which extreme caution should be exercised when applying the approach outlined above. In some rock slope stability problems, the effective normal stress on some parts of the failure surface can be quite low, certainly less than 1 MPa. It will be noted that in the example given in Fig. 6, for values of σ'_n of less than about 5 MPa, the straight line, constant c' and ϕ' method overestimates the available shear strength of the rock mass by increasingly significant amounts as σ'_n approaches zero. Under such circumstances, it would be prudent to use values of c' and ϕ' based on a tangent to the shear strength curve in the range of σ'_n values applying in practice.

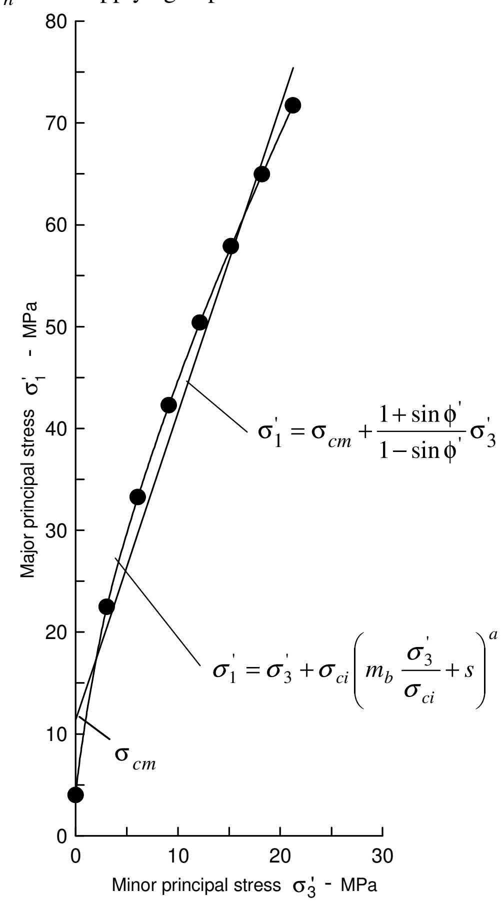

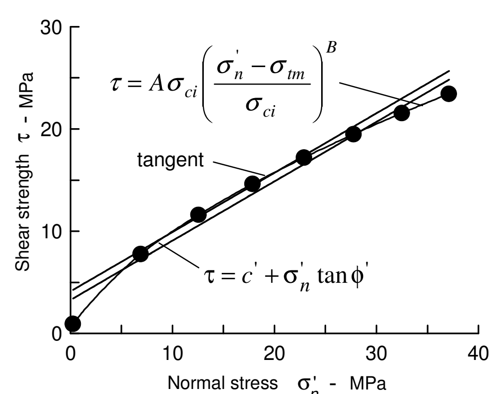

Fig. 6. Plot of results from simulated full scale triaxial tests on a rock mass defined by a uniaxial compressive strength σ_{ci} = 85 MPa, a Hoek-Brown constant m_i = 10 and Geological Strength Index GSI = 45. Detailed calculations are given in Appendix C.

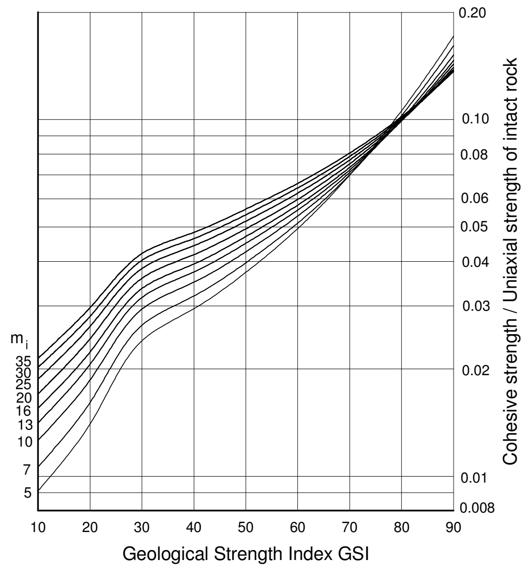

Fig. 7. Relationship between ratio of cohesive strength to uniaxial compressive strength of intact rock c'/σ_{ci} and GSI for different m_i values.

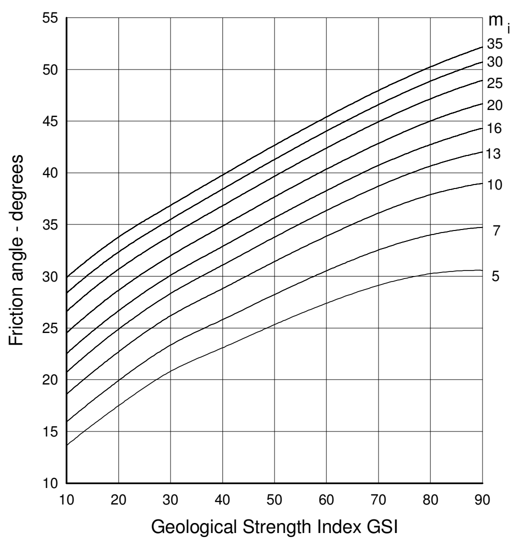

Fig. 8. Friction angle ϕ' for different GSI and m_i values.

DEFORMATION MODULUS

Serafim and Pereira [18] proposed a relationship between the in-situ modulus of deformation and Bieniawski's RMR classification. This relationship is based upon back analysis of dam foundation deformations and it has been found to work well for better quality rocks. However, for many of the poor quality rocks it appears to predict deformation modulus values which are too high.

Based upon practical observations and back analysis of excavation behaviour in poor quality rock masses, the following modification to Serafim and Pereira's equation is proposed for $\sigma_{ci} < 100$:

$$E_m(\text{GPa}) = \sqrt{\frac{\sigma_{ci}}{100}}\,10^{\left(\frac{GSI-10}{40}\right)} \qquad (14)$$

Note that GSI has been substituted for RMR in this equation and that the modulus E_m is reduced progressively as the value of σ_{ci} falls below 100. This reduction is based upon the reasoning that the deformation of better quality rock masses is controlled by the discontinuities while, for poorer quality rock masses, the deformation of the intact rock pieces contributes to the overall deformation process.

Based upon measured deformations, equation (14) appears to work reasonably well in those cases where it has been applied. However, as more field evidence is gathered it may be necessary to modify this relationship.

POST-FAILURE BEHAVIOUR

When using numerical models to study the progressive failure of rock masses, estimates of the post-peak or post-failure characteristics of the rock mass are required. In some of these models, the Hoek-Brown failure criterion is treated as a yield criterion and the analysis is carried out using plasticity theory [e.g. 19]. No definite rules for dealing with this problem can be given but, based upon experience in numerical analysis of a variety of practical problems, the post-failure characteristics illustrated in Fig. 9 are suggested as a starting point.

Very good quality hard rock masses

For very good quality hard rock masses, such as massive granites or quartzites, the analysis of spalling around highly stressed openings [12] suggests that the rock mass behaves in an elastic brittle manner as shown in Fig. 9(a). When the strength of the rock mass is exceeded, a sudden strength drop occurs. This is associated with significant dilation of the broken rock pieces. If this broken rock is confined, for example by rock support, then it can be assumed to behave as a rock fill with a friction angle of approximately $\phi' = 38°$ and zero cohesive strength.

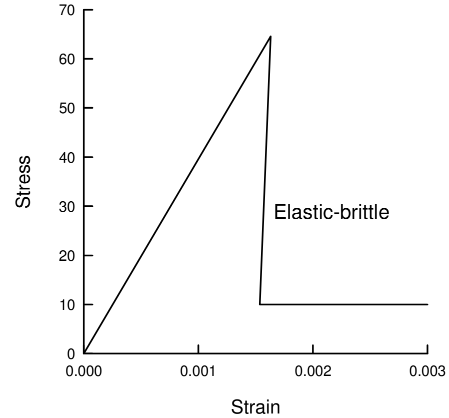

(a) Very good quality hard rock mass

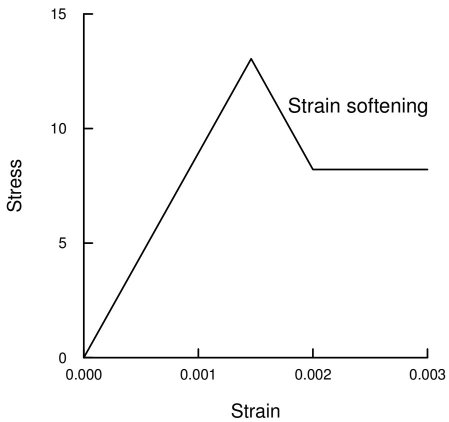

(b) Average quality rock mass

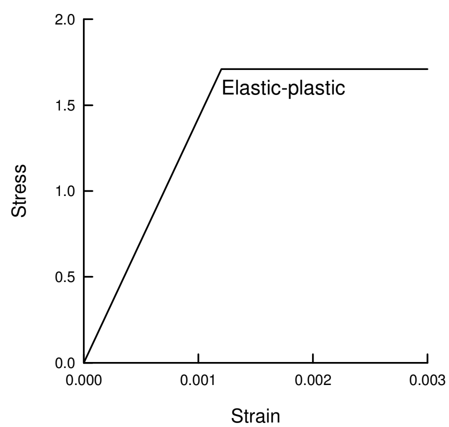

(c) Very poor quality soft rock mass

Fig. 9. Suggested post-failure characteristics for different quality rock masses. Note that the stress scales are different.

Typical properties for this very good quality hard rock mass may be as follows:

Intact rock strength	σ_{ci}	150 MPa
Hoek-Brown constant	m_i	25
Geological Strength Index	GSI	75
Friction angle	ϕ'	46°
Cohesive strength	c'	13 MPa
Rock mass compressive strength	σ_{cm}	64.8 MPa
Rock mass tensile strength	σ_{tm}	-0.9 MPa
Deformation modulus	E_m	42000 MPa
Poisson's ratio	ν	0.2
Dilation angle	α	$\phi'/4 = 11.5°$
Post-peak characteristics		
Friction angle	ϕ_f'	38°
Cohesive strength	c_f'	0
Deformation modulus	E_{fm}	10000 MPa

Average quality rock mass

In the case of an average quality rock mass it is reasonable to assume that the post-failure characteristics can be estimated by reducing the GSI value from the in-situ value to a lower value which characterises the broken rock mass.

The reduction of the rock mass strength from the in-situ to the broken state corresponds to the strain softening behaviour illustrated in Fig. 9(b). In this figure it has been assumed that post failure deformation occurs at a constant stress level, defined by the compressive strength of the broken rock mass. The validity of this assumption is unknown.

Typical properties for this average quality rock mass may be as follows:

Intact rock strength	σ_{ci}	80 MPa
Hoek-Brown constant	m_i	12
Geological Strength Index	GSI	50
Friction angle	ϕ'	33°
Cohesive strength	c'	3.5 MPa
Rock mass compressive strength	σ_{cm}	13 MPa
Rock mass tensile strength	σ_{tm}	-0.15
Deformation modulus	E_m	9000 MPa
Poisson's ratio	ν	0.25
Dilation angle	α	$\phi'/8 = 4°$
Post-peak characteristics		
Broken rock mass strength	σ_{fcm}	8 MPa
Deformation modulus	E_{fm}	5000 MPa

Very poor quality rock mass

Analysis of the progressive failure of very poor quality rock masses surrounding tunnels suggests that the post-failure characteristics of the rock are adequately represented by assuming that it behaves perfectly plastically. This means that it continues to deform at a constant stress level and that no volume change is associated with this ongoing failure. This type of behaviour is illustrated in Fig. 9(c).

Typical properties for this very poor quality rock mass may be as follows:

Intact rock strength	σ_{ci}	20 MPa
Hoek-Brown constant	m_i	8
Geological Strength Index	GSI	30
Friction angle	ϕ'	24°
Cohesive strength	c'	0.55 MPa
Rock mass compressive strength	σ_{cm}	1.7 MPa
Rock mass tensile strength	σ_{tm}	-0.01 MPa
Deformation modulus	E_m	1400 MPa
Poisson's ratio	ν	0.3
Dilation angle	α	zero
Post-peak characteristics		
Broken rock mass strength	σ_{fcm}	1.7 MPa
Deformation modulus	E_{fm}	1400 MPa

PRACTICAL EXAMPLES

Massive weak rock masses

Karzulovic and Diaz [20] have described the results of a program of triaxial tests on a cemented breccia known as Braden Breccia from the El Teniente mine in Chile. In order to design underground openings in this rock, attempts were made to classify the rock mass in accordance with Bieniawski's RMR system. However, as illustrated in Fig. 10, this rock mass has very few discontinuities and so assigning realistic numbers to terms depending upon joint spacing and condition proved to be very difficult. Finally, it was decided to treat the rock mass as a weak but homogeneous 'almost intact' rock and to determine its properties by means of triaxial tests on large diameter specimens.

A series of triaxial tests was carried out on 100 mm diameter core samples, illustrated in Fig. 11. The results of these tests were analysed by means of the regression analysis presented in Appendix A. Back analysis of the behaviour of underground openings in this rock indicate that the in-situ GSI value is approximately 75. From the spreadsheet presented in Appendix C the following parameters were obtained:

Intact rock strength	σ_{ci}	51 MPa
Hoek-Brown constant	m_i	16.3
Geological Strength Index	GSI	75
Hoek-Brown constant	s	0.062
Friction angle	ϕ'	42°
Cohesive strength	c'	4.32 MPa
Deformation modulus	E_m	30000 MPa

Fig. 10. Braden Breccia at El Teniente Mine in Chile. This rock is a cemented breccia with practically no joints. It was dealt with in a manner similar to weak concrete and tests were carried out on 100 mm diameter specimens illustrated in Fig. 11.

Fig. 11. 100 mm diameter by 200 mm long specimens of Braden Breccia from the El Teniente mine in Chile.

A similar approach has been used for dealing with rock masses with very sparse jointing. In one case, 50 mm diameter core specimens of a massive siltstone were successfully prepared and tested in a laboratory very close to the site in order to minimise the effects of very rapid deterioration when this material was subjected to changing moisture content conditions.

Massive strong rock masses

The Rio Grande Pumped Storage Project in Argentina includes a large underground powerhouse and surge control complex and a 6 km long tailrace tunnel. The rock mass surrounding these excavations is a massive gneiss with very few joints. A typical core from this rock mass is illustrated in Fig. 12. The appearance of the rock at the surface is illustrated in Fig. 5, which shows a cutting for the dam spillway.

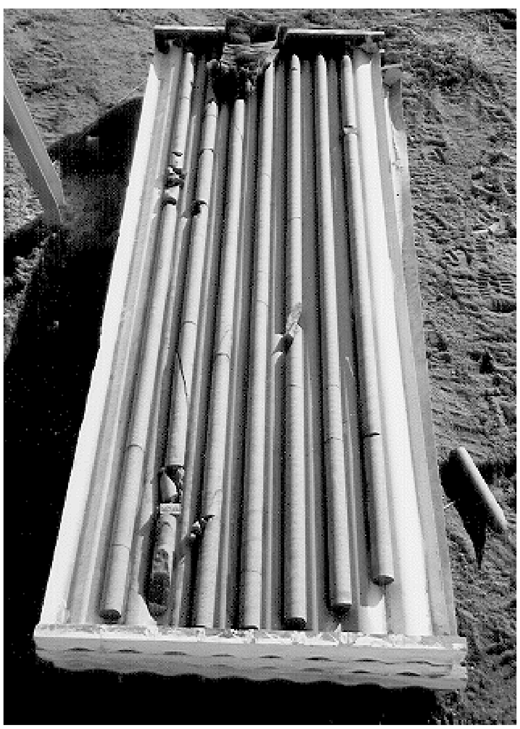

Fig. 12. Excellent quality core from a hard strong rock mass with very few discontinuities.

The rock mass can be described as BLOCKY/VERY GOOD and the GSI value, from Table 5, is 75. Typical characteristics for the rock mass are as follows:

Intact rock strength	σ_{ci}	110 MPa
Hoek-Brown constant	m_i	17.7
Geological Strength Index	GSI	75 (assumed)
Hoek-Brown constant	m_b	7.25
Hoek-Brown constant	s	0.062
Constant	a	0.5
Friction angle	ϕ'	43°
Cohesive strength	c'	9.4 MPa
Rock mass compressive strength	σ_{cm}	43 MPa
Rock mass tensile strength	σ_{tm}	-0.94 MPa
Deformation modulus	E_m	42000 MPa

Fig. 13 illustrates the 8 m high 12 m span top heading for the tailrace tunnel. The final tunnel height of 18 m was achieved by blasting two 5 m benches. The top heading was excavated by full-face drill and blast and, because of the excellent quality of the rock mass and the tight control on blasting quality, most of the top heading did not require any support.

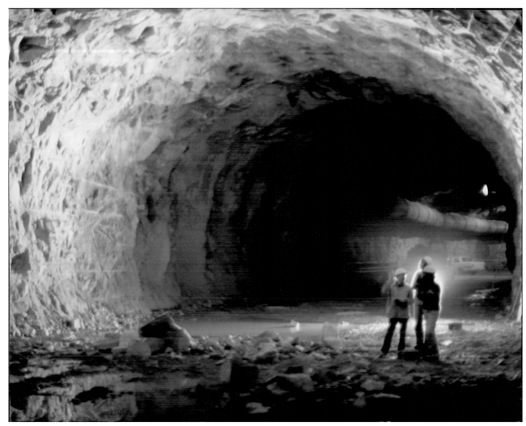

Fig. 13. Top heading for the 12 m span, 18 m high tailrace tunnel for the Rio Grande Pumped Storage Project.

Details of this project are to be found in Moretto et al [21]. Hammett and Hoek [22] have described the design of the support system for the 25 m span underground powerhouse in which a few structurally controlled wedges were identified and stabilised during excavation.

Average quality rock mass

The partially excavated powerhouse cavern in the Nathpa Jhakri Hydroelectric project in Himachel Pradesh, India is illustrated in Fig. 14. The rock is a jointed quartz mica schist, which has been extensively evaluated by the Geological Survey of India as described by Jalote et al [23]. An average GSI value of 65 was chosen to estimate the rock mass properties which were used for the cavern support design. Additional support, installed on the instructions of the Engineers, was placed in weaker rock zones.

Fig. 14. Partially completed 20 m span, 42.5 m high underground powerhouse cavern of the Nathpa Jhakri Hydroelectric project in Himachel Pradesh in India. The cavern is approximately 300 m below the surface.

The assumed rock mass properties are as follows:

Intact rock strength	σ_{ci}	30 MPa
Hoek-Brown constant	m_i	15.6
Geological Strength Index	GSI	65 (average)
Hoek-Brown constant	m_b	4.5
Hoek-Brown constant	s	0.02
Constant	a	0.5
Friction angle	ϕ'	40°
Cohesive strength	c'	2.0 MPa
Rock mass compressive strength	σ_{cm}	8.2 MPa
Rock mass tensile strength	σ_{tm}	-0.14 MPa
Deformation modulus	E_m	13000 MPa

Two and three dimensional stress analyses of the nine stages used to excavate the cavern were carried out to determine the extent of potential rock mass failure and to provide guidance in the design of the support system. An isometric view of one of the three dimensional models is given in Figure 15.

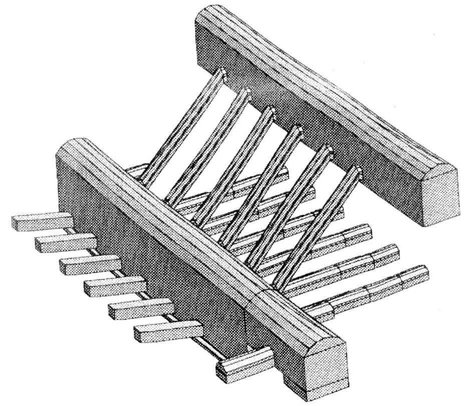

Fig. 15. Isometric view of a 3DEC[2] model of the Underground powerhouse cavern and the transformer gallery of the Nathpa Jhakri Hydroelectric project, analysed by Dr B. Dasgupta[3] .

The support for the powerhouse cavern consists of rockbolts and mesh reinforced shotcrete. Alternating 6 and 8 m long 32 mm diameter bolts on 1 x 1 m and 1.5 x 1.5 m centres are used in the arch. Alternating 9 and 7.5 m long 32 mm diameter bolts are used in the upper and lower sidewalls with alternating 9 and 11 m long 32 mm rockbolts in the centre of the sidewalls, all at a grid spacing of 1.5 m. Shotcrete consists of two 50 mm thick layers of plain shotcrete with an interbedded layer of weldmesh. The support provided by the shotcrete was not included in the support design analysis, which relies upon the rockbolts to provide all the support required.

In the headrace tunnel, some zones of sheared quartz mica schist have been encountered and these have resulted in large displacements as illustrated in Fig. 16. This is a common problem in hard rock tunnelling where the excavation sequence and support system have been designed for 'average' rock mass conditions. Unless very rapid changes in the length of blast rounds and the installed support are made when an abrupt change to poor rock conditions occurs, for example when a fault is encountered, problems with controlling tunnel deformation can arise.

---

[2] Available from ITASCA Consulting Group Inc., Thresher Square East, 708 South Third Street, Suite 310, Minneapolis, Minnesota 55415, USA. Fax 1 612 371 4717

[3] Formerly at the Institute of Rock Mechanics (Kolar), Kolar Gold Fields, Karnataka, now with of Advanced Technology and Engineering Services, Delhi. India.

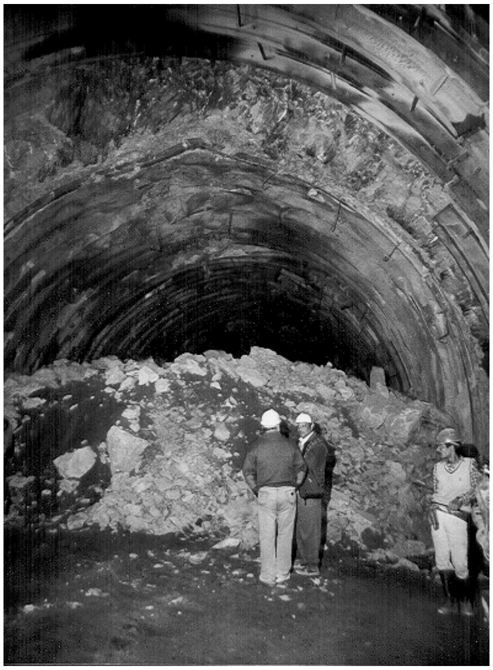

Fig. 16. Large displacements in the top heading of the headrace tunnel of the Nathpa Jhakri hydroelectric project in India.

The only effective way known to the authors for anticipating this type of problem is to keep a probe hole ahead of the advancing face at all times. Typically, a long probe hole is percussion drilled during a maintenance shift and the penetration rate, return water flow and chippings are constantly monitored during drilling. Where significant problems are indicated by this percussion drilling, one or two diamond-drilled holes may be required to investigate these problems in more detail. In some special cases, the use of a pilot tunnel may be more effective in that it permits the ground properties to be defined more accurately than is possible with probe hole drilling. In addition, pilot tunnels allow pre-drainage and pre-reinforcement of the rock ahead of the development of the full excavation profile.

Poor quality rock mass at shallow depth

Kavvadas et al [24] have described some of the geotechnical issues associated with the construction of 18 km of tunnels and the 21 underground stations of the Athens Metro. These excavations are all shallow with typical depths to tunnel crown of between 15 and 20 m. The principal problem is one of surface subsidence rather than failure of the rock mass surrounding the openings.

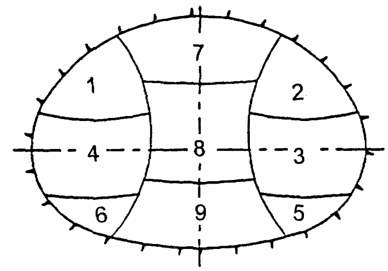

Fig. 17. Twin side drift and central pillar excavation method. Temporary support consists of double wire mesh reinforced 250 - 300 mm thick shotcrete shells with embedded lattice girders or HEB 160 steel sets at 0.75 - 1 m spacing.

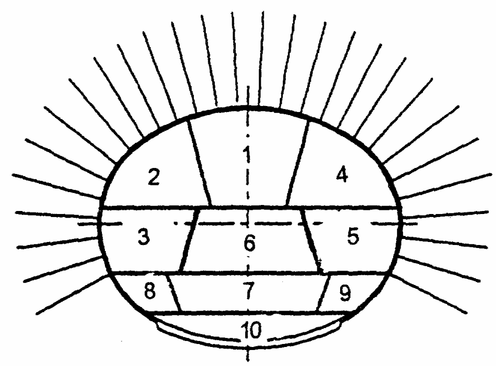

Fig. 18. Top heading and bench method of excavation. Temporary support consists of a 200 mm thick shotcrete shell with 4 and 6 m long untensioned grouted rockbolts at 1.0 - 1.5 m spacing.

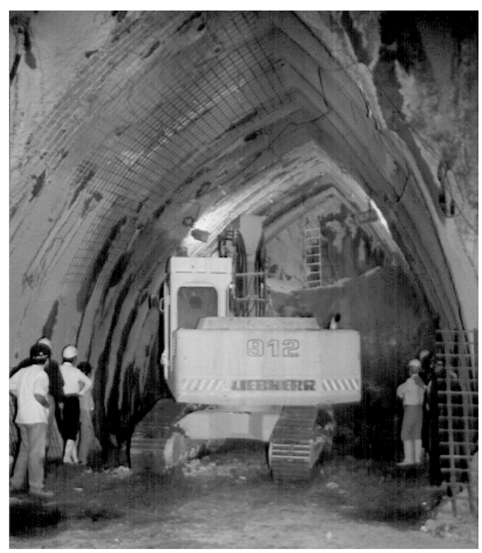

Fig. 19. Side drift in the Athens Metro Olympion station excavation, which was excavated by the method illustrated in Fig. 17. The station has cover depth of approximately 10 m over the crown.

The rock mass is locally known as Athenian schist which is a term erroneously used to describe a sequence of Upper Cretaceous flysch-type sediments including thinly bedded clayey and calcareous sandstones, siltstones (greywackes), slates, shales and limestones. During the Eocene, the Athenian schist formations were subjected to intense folding and thrusting. Later extensive faulting caused extensional fracturing and widespread weathering and alteration of the deposits.

The GSI values, estimated from Bieniawski's 1976 RMR classification, modified as recommended by Hoek, Kaiser and Bawden [12], ranges from about 15 to about 45. The higher values correspond to the intercalated layers of sandstones and limestones, which can be described as BLOCKY/DISTURBED and POOR (Table 5). The completely decomposed schist can be described as DISINTEGRATED and VERY POOR and has GSI values ranging from 15 to 20. Rock mass properties for the completely decomposed schist, using a GSI value of 20, are as follows:

Intact rock strength	σ_{ci}	5-10 MPa
Hoek-Brown constant	m_i	9.6
Geological Strength Index	GSI	20
Hoek-Brown constant	m_b	0.55
Hoek-Brown constant	s	0
Constant	a	0.55
Friction angle	ϕ'	22.4°
Cohesive strength	c'	0.09-0.18 MPa
Rock mass strength	σ_{cm}	0.27-0.53 MPa
Deformation modulus	E_m	398-562 MPa

The Academia, Syntagma, Omonia and Olympion stations were constructed using the New Austrian Tunnelling Method twin side drift and central pillar method as illustrated in Fig. 17. The more conventional top heading and bench method, illustrated in Fig. 18, was used for the excavation of the Ambelokipi station. These stations are all 16.5 m wide and 12.7 m high. The appearance of the rock mass in one of the Olympion station side drift excavations is illustrated in Fig. 19 and Fig. 20.

Numerical analyses of the two excavation methods illustrated in Fig. 17 and Fig. 18 showed that the twin side drift method resulted in slightly less rock mass failure in the crown of the excavation. However, the final surface displacements induced by the two excavation methods were practically identical.

Maximum vertical displacements of the surface above the centre-line of the Omonia station amounted to 51 mm. Of this, 28 mm occurred during the excavation of the side drifts, 14 mm during the removal of the central pillar and a further 9 mm occurred as a time dependent settlement after completion of the excavation. According to Kavvadas et al [24], this time dependent settlement is due to the dissipation of excess pore water pressures which were built up during excavation. In the case of the Omonia station, the excavation of recesses towards the eastern end of the station, after completion of the station excavation, added a further 10 to 12 mm of vertical surface displacement at this end of the station.

Fig.20. Appearance of the very poor quality Athenian schist at the face of the side heading illustrated in Fig. 19.

Poor quality rock mass under high stress

The Yacambú Quibor tunnel in Venezuela is considered to be one of the most difficult tunnels in the world. This 26 km long water supply tunnel through the Andes is being excavated in sandstones and phyllites at depths of up to 1200 m below surface. The graphitic phyllite is a very poor quality rock and gives rise to serious squeezing problems which, without adequate support, result in complete closure of the tunnel. A full-face tunnel-boring machine was completely destroyed in 1979 when trapped by squeezing ground conditions.

At its worst, the graphitic phyllite has an unconfined compressive strength of about 15 MPa (see Fig. 1), and the estimated GSI value is about 24. Typical rock mass properties are as follows:

Intact rock strength	σ_{ci}	15 MPa
Hoek-Brown constant	m_i	10
Geological Strength Index	GSI	24
Hoek-Brown constant	m_b	0.66
Hoek-Brown constant	s	0
Constant	a	0.53
Friction angle	ϕ'	24°
Cohesive strength	c'	0.34 MPa
Rock mass strength	σ_{cm}	1 MPa
Deformation modulus	E_m	870 MPa

Various support methods have been used on this tunnel and only one will be considered here. This was a trial section of tunnel, at a depth of about 600 m, constructed in 1989. The support of the 5.5 m span tunnel was by means of a complete ring of 5 m long, 32 mm diameter untensioned grouted dowels with a

200 mm thick shell of reinforced shotcrete. This support system proved to be very effective but was later abandoned in favour of yielding steel sets (steel sets with sliding joints) because of construction schedule considerations.

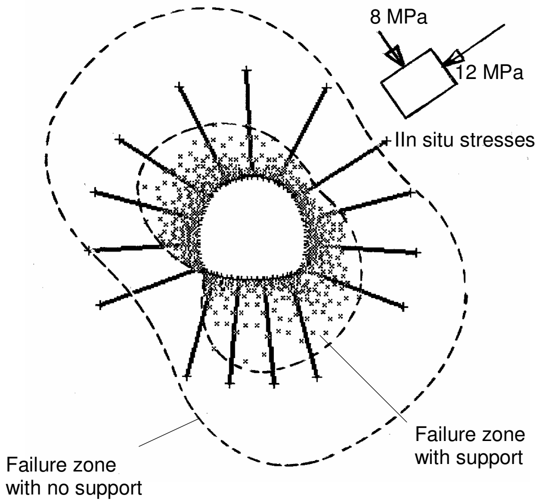

Fig. 21. Results of a numerical analysis of the failure of the rock mass surrounding the Yacambu-Quibor tunnel when excavated in graphitic phyllite at a depth of about 600 m below surface.

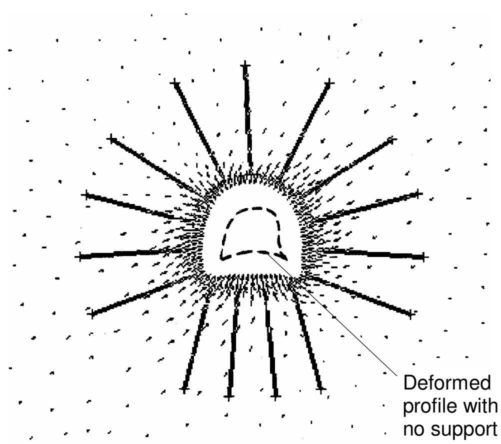

Fig. 22. Displacements in the rock mass surrounding the Yacambu-Quibor tunnel. The maximum calculated displacement is 258 mm with no support and 106 mm with support.

Examples of the results of a typical numerical stress analysis of this trial section, carried out using the program PHASE2[4], are given in Fig. 21 and Fig. 22. Fig. 21 shows the extent of failure, with and without support, while Fig. 22 shows the displacements in the rock mass surrounding the tunnel. Note that the criteria used to judge the effectiveness of the support design are that the zone of failure surrounding the tunnel should lie within the envelope of the rockbolt support, the rockbolts should not be stressed to failure and the displacements should be of reasonable magnitude and should be uniformly distributed around the tunnel. All of these objectives were achieved by the support system described earlier.

Slope stability considerations

When dealing with slope stability problems in rock masses, great care has to be taken in attempting to apply the Hoek-Brown failure criterion, particularly for small steep slopes. As illustrated in Fig. 23, even rock masses which appear to be good candidates for the application of the criterion can suffer shallow structurally controlled failures under the very low stress conditions which exist in such slopes.

As a general rule, when designing slopes in rock, the initial approach should always be to search for potential failures controlled by adverse structural conditions. These may take the form of planar failures on outward dipping features, wedge failures on intersecting features, toppling failures on inward dipping failures or complex failure modes involving all of these processes. Only when the potential for structurally controlled failures has been eliminated should consideration be given to treating the rock mass as an isotropic material as required by the Hoek-Brown failure criterion (see Fig. 4).

Fig. 24 illustrates a case in which the base of a slope failure is defined by an outward dipping fault which does not daylight at the toe of the slope. Circular failure through the poor quality rock mass overlying the fault allows failure of the toe of the slope. Analysis of this problem was carried out by assigning the rock mass at the toe properties which had been determined by application of the Hoek-Brown criterion. A search for the critical failure surface was carried out utilising the program XSTABL[5] which allows complex failure surfaces to be analysed and which includes facilities for the input of non-linear failure characteristics as defined by equation 2.

[4] Available from the Rock Engineering Group, University of Toronto, 31 Balsam Avenue, Toronto, Ontario, Canada M4E 3B5, Fax + 1 416 698 0908, email rockeng@civ. utoronto.ca, Internet www.rockeng.utoronto.ca.

[5] Available from Interactive Software Designs, Inc., 953 N. Cleveland Street, Moscow, Idaho, USA 83843, Fax + 1 208 885 6608

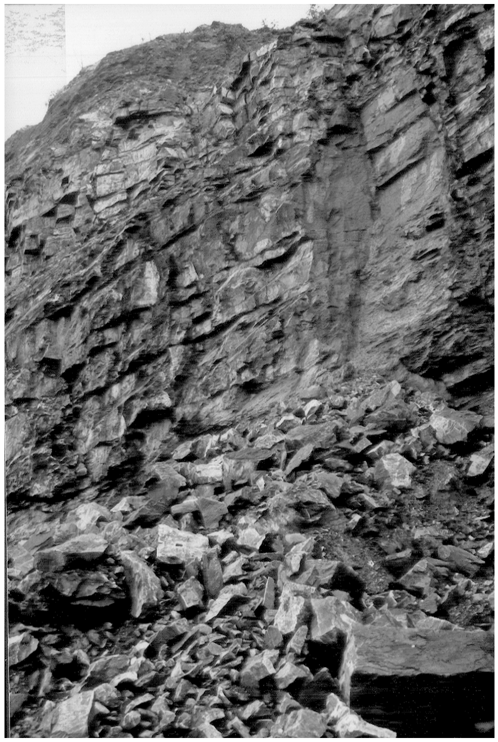

Fig. 23. Structurally controlled failure in the face of a steep bench in a heavily jointed rock mass.

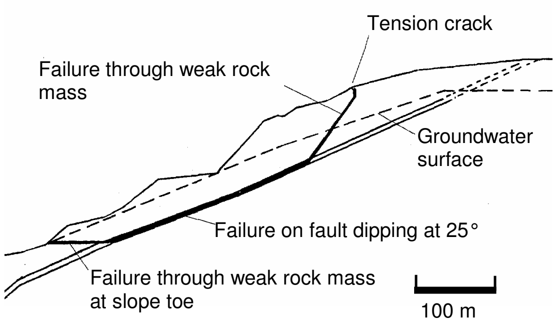

Fig 24. Complex slope failure controlled by an outward dipping basal fault and circular failure through the poor quality rock mass overlying the toe of the slope.

Sancio [25] and Sönmez et al [26] have presented interesting discussions on methods of back analysis of slope failures involving jointed rock masses, the properties of which can be described in terms of the Hoek-Brown failure criterion. Numerical analysis of complex failure processes in very large-scale open pit mine slopes have been described by Board et al [27].

ACKNOWLEDGEMENTS

Many individuals have been involved in the development of the ideas presented in this paper and it is impossible to list them all individually. However, the contributions of the following persons stand out and the authors expresses their sincere gratitude for their assistance and encouragement over the past twenty years: Dr John Bray, a former colleague at Imperial College in London, Mr David Wood, Mr Peter Stacey, Mr Graham Rawlings and Dr Trevor Carter in Canada, Dr John Read and Dr Terry Medhurst in Australia, Professor Z.T. Bieniawski in the USA, Dr Antonio Karzulovic in Chile, Professor Paul Marinos and Dr Michael Kavvadas in Greece, Dr Walter Steiner in Switzerland, Professors Rudolpho Sancio and Daniel Salcedo in Venezuela, Mr. P.M. Jalote, Mr Vinai Kumar and Dr. B. Dasgupta in India.

The authors also acknowledge permission to publish details of current projects by the following organisations: The Nathpa Jhakri Power Corporation Limited, India, Attiko Metro, Greece and Sistema Hidraulico Yacambú Quibor C.A., Venezuela.

REFERENCES

1. Hoek E. and Brown E.T. Underground excavations in rock, p. 527. London, Instn Min. Metall. (1980).
2. Broch E. The influence of water on some rock properties. Proc. 3rd Congress, ISRM, Denver. 74(2), Part A, 33-38 (1974).
3. Terzaghi K. Die Berechnung der Durchlassigkeitsziffer des Tones aus dem Verlauf der hydrodynamischen Spannungserscheinungen. Sber. Akad. Wiss. Wien. 132(105), 125-138 (1923).
4. Lade P.V. and de Boer R. The concept of effective stress for soil, concrete and rock. Géotechnique 47(1), 61-78 (1997).
5. Brace W.F. and Martin R.J. A test of the law of effective stress for crystalline rocks of low porosity. Int. J. Rock Mech. Min. Sci.. 5(5), 415-426 (1968).
6. Brown E.T. (Ed). Rock characterization, testing and monitoring - ISRM suggested methods, 171-183. Oxford, Pergamon (1981).
7. Martin C.D. and Chandler N.A. The progressive failure of Lac du Bonnet granite. Int. J. Rock Mech. Min. Sci. & Geomech. Abstr. 30(7), 643-659 (1994).
8. Salcedo D.A. Macizos Rocosos: Caracterización, Resistencia al Corte y Mecanismos de Rotura. Proc. 25 Aniversario Conferencia Soc. Venezolana de Mecánica del Suelo e Ingeniería de Fundaciones, Caracas. 143-172 (1983).
9. Medhurst T.P., Brown E.T. and Trueman R. Experimental studies of the effects of scale on the strength of coal. In Proc. 8th Int. Congr. Rock Mech, 1, 347-351. Rotterdam, Balkema (1995).

10. Medhurst T.P. and Brown E.T. Large scale laboratory testing of coal. In Proc. 7th ANZ Conf. Geomech., (Edited by Jaksa M.B., Kaggwa W.S. and Cameron D.A.), 203-208, Canberra, IE Australia (1996).
11. Hoek E. Strength of rock and rock masses, ISRM News Journal, 2(2), 4-16 (1994).
12. Hoek E., Kaiser P.K. and Bawden W.F. Support of underground excavations in hard rock. p. 215. Rotterdam, Balkema. (1995).
13. Terzaghi K. Rock defects and loads on tunnel supports. In Rock tunneling with steel supports, (Edited by Proctor R. V. and White T. L.) 1, 17-99. Youngstown, Ohio, Commercial Shearing and Stamping Company (1946).
14. Hoek E., Wood D. and Shah S. A modified Hoek-Brown criterion for jointed rock masses. Proc. Rock Characterization, Symp. Int. Soc. Rock Mech.: Eurock '92, (Edited by Hudson J.A.), 209-214. London, Brit. Geotech. Soc. (1992).
15. Bieniawski Z.T. Rock mass classification in rock engineering. In Exploration for Rock Engineering, Proc. of the Symp., (Edited by Bieniawski Z.T.) 1, 97-106. Cape Town, Balkema (1976).
16. Bieniawski Z.T. Engineering Rock Mass Classifications. p. 251. New York, Wiley (1989).
17. Hoek E. Strength of jointed rock masses, 1983 Rankine Lecture. Géotechnique 33(3), 187-223. (1983).
18. Serafim J.L. and Pereira J.P. Consideration of the geomechanical classification of Bieniawski. Proc. Int. Symp. on Engineering Geology and Underground Construction, Lisbon 1(II), 33-44. (1983).
19. Pan X.D. and Hudson J.A. A simplified three dimensional Hoek-Brown yield criterion. In Rock Mechanics and Power Plants, Proc. ISRM Symp. (Edited by Romana M.), 95-103. Rotterdam, Balkema (1988).
20. Karzulovic A. and Díaz, A. Evaluación de las Propiedades Geomacánicas de la Brecha Braden en Mina El Teniente. Proc. IV Congreso Sudamericano de Mecanica de Rocas, Santiago 1, 39-47. (1994).
21. Moretto O., Sarra Pistone R.E. and Del Rio J.C. A case history in Argentina - Rock Mechanics for underground works in the Pumping Storage Development of Rio Grande No 1. In Comprehensive Rock Engineering. (Edited by Hudson. J.A.) 5, 159-192. Oxford, Pergamon (1993).
22. Hammett R.D. and Hoek E. Design of large underground caverns for hydroelectric projects with particular reference to structurally controlled failure mechanisms. In Recent Developments in Geotechnical Engineering for Hydro Projects. (Edited by Kulhawy F.H.), 192-206. New York, ASCE (1981).
23. Jalote P.M., Kumar A. and Kumar V. Geotechniques applied in the design of the machine hall cavern, Nathpa Jhakri Hydel Project, N.W. Himalaya, India. J. Engng Geol. (India) XXV(1-4), 181-192. (1996).
24. Kavvadas M., Hewison L.R., Lastaratos P.G., Seferoglou C. and Michalis I. Experience in the construction of the Athens Metro. Proc. Int. Symp. Geotechical Aspects of Underground Construction in Soft Ground. (Edited by Mair R.J. and Taylor R.N.), 277-282. London, City University. (1996).
25. Sancio R.T. The use of back-calculations to obtain shear and tensile strength of weathered rock. Proc. Int. Symp. Weak Rock, Tokyo 2, 647-652. (1981).
26. Sönmez H., Ulusay R. and Gökçeoglu, C. Practical procedure for the back analysis of slope failures in closely jointed rock masses. Submitted to Int. J. Rock Mech. Min. Sci. (1997).
27. Board M., Chacon E., Verona P. and Lorig L. Comparative analysis of toppling behaviour at Chuquicamata open pit mine, Chile. Trans. Instn Min. Metall.. 105, A11-21. (1996).
28. Balmer G. A general analytical solution for Mohr's envelope. Am. Soc. Test. Mat. 52, 1260-1271. (1952).
29. Hoek E. and Brown E.T. The Hoek-Brown failure criterion - a 1988 update. In Rock Engineering for Underground Excavations, Proc. 15th Canadian Rock Mech. Symp. (Edited by Curran J.C.), 31-38. Toronto, Dept. Civil Engineering, University of Toronto. (1988).
30. Hoek E. and Franklin J.A. A simple triaxial cell for field and laboratory testing of rock. Trans. Instn Min. Metall. 77, A22-26.

APPENDIX A - HISTORICAL DEVELOPMENT OF THE HOEK-BROWN CRITERION

Publication	*Coverage*	*Equations*
Hoek & Brown [1]	Original criterion for heavily jointed rock masses with no fines. Mohr envelope was obtained by statistical curve fitting to a number of (σ_n', τ) pairs calculated by the method published by Balmer [28]. σ_1', σ_3' are major and minor effective principal stresses at failure, respectively σ_t is the tensile strength of the rock mass *m* and *s* are material constants σ_n', τ are effective normal and shear stresses, respectively.	$\sigma_1' = \sigma_3' + \sigma_{ci}\sqrt{m\sigma_3'/\sigma_{ci} + s}$ $\sigma_t = \frac{\sigma_{ci}}{2}\left(m - \sqrt{m^2 + 4s}\right)$ $\tau = A\sigma_{ci}\left((\sigma_n' - \sigma_t)/\sigma_{ci}\right)^B$ $\sigma_n' = \sigma_3' + \left((\sigma_1' - \sigma_3')/(1 + \partial\sigma_1'/\partial\sigma_3')\right)$ $\tau = (\sigma_n' - \sigma_3')\sqrt{\partial\sigma_1'/\partial\sigma_3'}$ $\partial\sigma_1'/\partial\sigma_3' = m\sigma_{ci}/2(\sigma_1' - \sigma_3')$
Hoek [17]	Original criterion for heavily jointed rock masses with no fines with a discussion on anisotropic failure and an exact solution for the Mohr envelope by Dr J.W. Bray.	$\sigma_1' = \sigma_3' + \sigma_{ci}\sqrt{m\sigma_3'/\sigma_{ci} + s}$ $\tau = \left(Cot\phi_i' - Cos\phi_i'\right)m\sigma_{ci}/8$ $\phi_i' = \arctan\left(1/\sqrt{4h\cos^2\theta - 1}\right)$ $\theta = \left(90 + \arctan(1/\sqrt{h^3 - 1})\right)/3$ $h = 1 + \left(16(m\sigma_n' + s\sigma_{ci})/(3m^2\sigma_{ci})\right)$
Hoek & Brown [29]	As for Hoek [17] but with the addition of relationships between constants *m* and *s* and a modified form of *RMR* (Bieniawski [15]) in which the Groundwater rating was assigned a fixed value of 10 and the Adjustment for Joint Orientation was set at 0. Also a distinction between *disturbed* and *undisturbed* rock masses was introduced together with means of estimating deformation modulus *E* (after Serafim and Pereira [18]).	*Disturbed rock masses:* $m_b/m_i = \exp\left((RMR - 100)/14\right)$ $s = \exp\left((RMR - 100)/6\right)$ *Undisturbed or interlocking rock masses* $m_b/m_i = \exp\left((RMR - 100)/28\right)$ $s = \exp\left((RMR - 100)/9\right)$ $E = 10^{((RMR-10)/40)}$ m_b, m_i are for broken and intact rock, respectively.
Hoek, Wood & Shah [14]	Modified criterion to account for the fact the heavily jointed rock masses have zero tensile strength. Balmer's technique for calculating shear and normal stress pairs was utilised	$\sigma_1' = \sigma_3' + \sigma_{ci}\left(m_b\sigma_3'/\sigma_{ci}\right)^\alpha$ $\sigma_n' = \sigma_3' + \left((\sigma_1' - \sigma_3')/(1 + \partial\sigma_1'/\partial\sigma_3')\right)$ $\tau = (\sigma_n' - \sigma_3')\sqrt{\partial\sigma_1'/\partial\sigma_3'}$ $\partial\sigma_1'/\partial\sigma_3' = 1 + \alpha m_b^\alpha\left(\sigma_3'/\sigma_{ci}\right)^{(\alpha-1)}$
Hoek [11] Hoek, Kaiser & Bawden [12]	Introduction of the Generalised Hoek-Brown criterion, incorporating both the original criterion for fair to very poor quality rock masses and the modified criterion for very poor quality rock masses with increasing fines content. The Geological Strength Index *GSI* was introduced to overcome the deficiencies in Bieniawski's *RMR* for very poor quality rock masses. The distinction between disturbed and undisturbed rock masses was dropped on the basis that disturbance is generally induced by engineering activities and should be allowed for by downgrading the value of *GSI*.	$\sigma_1' = \sigma_3' + \sigma_c\left(m\sigma_3'/\sigma_{ci} + s\right)^a$ for $GSI > 25$ $m_b/m_i = \exp\left((GSI - 100)/28\right)$ $s = \exp\left((GSI - 100)/9\right)$ $a = 0.5$ for $GSI < 25$ $s = 0$ $a = 0.65 - GSI/200$

APPENDIX B - TRIAXIAL TESTS TO DETERMINE σ_{ci} AND m_i

Determination of the intact rock uniaxial compressive strength σ_{ci} and the Hoek-Brown constant m_i should be carried out by triaxial testing wherever possible. The tests should be carried out over a confining stress range from zero to one half of the uniaxial compressive strength. At lease five data points should be included in the analysis.

One type of triaxial cell which can be used for these tests is illustrated in Fig. B1. This cell, described by Hoek and Franklin [26], does not require draining between tests and is convenient for the rapid testing or a large number of specimens. More sophisticated cells are available for research purposes but the results obtained from the cell illustrated in Fig. B1 are adequate for the rock strength estimates described in this paper. This cell has the additional advantage that it can be used in the field when testing materials such as coals, shales and phyllites which are extremely difficult to preserve during transportation and normal specimen preparation for laboratory testing.

Once the five or more triaxial test results have been obtained, they can be analysed to determine the uniaxial compressive strength σ_{ci} and the Hoek-Brown constant m_i as described by Hoek and Brown [1]. In this analysis, equation (4) is re-written in the form:

$$y = m\sigma_{ci}x + s\sigma_{ci} \tag{B1}$$

where $x = \sigma_3'$ and $y = (\sigma_1' - \sigma_3')^2$

The uniaxial compressive strength σ_{ci} and the constant m_i are calculated from:

$$\sigma_{ci}^2 = \frac{\sum y}{n} - \left[\frac{\sum xy - \left(\sum x \sum y/n\right)}{\sum x^2 - \left(\left(\sum x\right)^2/n\right)}\right]\frac{\sum x}{n} \tag{B2}$$

$$m_i = \frac{1}{\sigma_{ci}}\left[\frac{\sum xy - \left(\sum x \sum y/n\right)}{\sum x^2 - \left(\left(\sum x\right)^2/n\right)}\right] \tag{B3}$$

The coefficient of determination r^2 is given by:

$$r^2 = \frac{\left[\sum xy - \left(\sum x \sum y/n\right)\right]^2}{\left[\sum x^2 - \left(\sum x\right)^2/n\right]\left[\sum y^2 - \left(\sum y\right)^2/n\right]} \tag{B4}$$

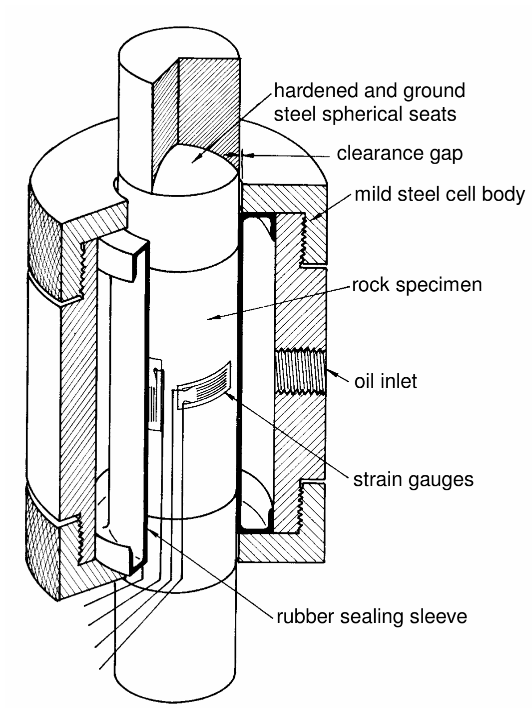

Fig. B1. Cut-away view of the triaxial cell designed by Hoek and Franklin [26].

Fig. B2. Spreadsheet for calculation of σ_{ci} and m_i from triaxial test data

Triaxial test data

x		y	xy	xsq	ysq
sig3	sig1				
0	38.3	1466.89	0.0	0.0	2151766
5	72.4	4542.76	22713.8	25.0	20636668
7.5	80.5	5329.00	39967.5	56.3	28398241
15	115.6	10120.36	151805.4	225.0	102421687
20	134.3	13064.49	261289.8	400.0	170680899
47.5	441.1	34523.50	475776.5	706.3	324289261
sumx		sumy	sumxy	sumxsq	sumysq

Calculation

Number of tests	n =	5
Uniaxial strength	sigci =	37.4
Hoek-Brown constant	mi =	15.50
Hoek-Brown constant	s =	1.00
Coefficient of determination	r2 =	0.997

Cell formulae

y = (sig1-sig3)^2
sigci = SQRT(sumy/n - (sumxy-sumx*sumy/n)/(sumxsq-(sumx^2)/n)*sumx/n)
mi = (1/sigci)*((sumxy-sumx*sumy/n)/(sumxsq-(sumx^2)/n))
r2 = ((sumxy-(sumx*sumy/n))^2)/((sumxsq-(sumx^2)/n)*(sumysq-(sumy^2)/n))

APPENDIX C - CALCULATION OF MOHR-COULOMB PARAMETERS

The relationship between the normal and shear stresses can be expressed in terms of the corresponding principal effective stresses as suggested by Balmer [24]:

$$\sigma'_n = \sigma'_3 + \frac{\sigma'_1 - \sigma'_3}{\partial\sigma'_1 / \partial\sigma'_3 + 1} \qquad \text{(C1)}$$

$$\tau = (\sigma'_1 - \sigma'_3)\sqrt{\partial\sigma'_1 / \partial\sigma'_3} \qquad \text{(C2)}$$

For the *GSI* > 25, when $a = 0.5$:

$$\frac{\partial\sigma'_1}{\partial\sigma'_3} = 1 + \frac{m_b \sigma_{ci}}{2(\sigma'_1 - \sigma'_3)} \qquad \text{(C3)}$$

For *GSI* < 25, when $s = 0$:

$$\frac{\partial\sigma'_1}{\partial\sigma'_3} = 1 + a m_b^a \left(\frac{\sigma'_3}{\sigma_{ci}}\right)^{a-1} \qquad \text{(C4)}$$

The tensile strength of the rock mass is calculated from:

$$\sigma_{tm} = \frac{\sigma_{ci}}{2}\left(m_b - \sqrt{m_b^2 + 4s}\right) \qquad \text{(C5)}$$

The equivalent Mohr envelope, defined by equation (4), may be written in the form:

$$Y = \log A + BX \qquad \text{(C6)}$$

where

$$Y = \log\frac{\tau}{\sigma_{ci}}, \quad X = \log\left(\frac{\sigma'_n - \sigma_{tm}}{\sigma_{ci}}\right) \qquad \text{(C7)}$$

Using the value of σ_{tm} calculated from equation (C5) and a range of values of τ and σ'_n calculated from equations (C1) and (C2), the values of A and B are determined by linear regression where :

$$B = \frac{\sum XY - \left(\sum X \sum Y\right)/T}{\sum X^2 - \left(\sum X\right)^2 / T} \qquad \text{(C8)}$$

$$A = 10\text{^}\left(\sum Y/T - B\left(\sum X/T\right)\right) \qquad \text{(C9)}$$

and T is the total number of data pairs included in the regression analysis.

The most critical step in this process is the selection of the range of σ'_3 values. As far as the authors are aware, there are no theoretically correct methods for choosing this range and a trial and error method, based upon practical compromise, has been used for selecting the range included in the spreadsheet presented in Fig. C1.

For a Mohr envelope defined by equation (4), the friction angle ϕ'_i for a specified normal stress σ'_{ni} is given by:

$$\phi'_i = \arctan\left(AB\left(\frac{\sigma'_{ni} - \sigma_{tm}}{\sigma_{ci}}\right)^{B-1}\right) \qquad \text{(C10)}$$

The corresponding cohesive strength c'_i is given by:

$$c'_i = \tau - \sigma'_{ni} \tan\phi'_i \qquad \text{(C11)}$$

and the corresponding uniaxial compressive strength of the rock mass is :

$$\sigma_{cmi} = \frac{2c'_i \cos\phi'_i}{1 - \sin\phi'_i} \qquad \text{(C12)}$$

Note that the cohesive strength c'_i given by equation (C11) is an upper bound value and that it is prudent to reduce this to about 75% of the calculated value for practical applications.

Fig. C1. Spreadsheet for calculation of Hoek-Brown and equivalent Mohr-Coulomb parameters

Hoek-Brown and equivalent Mohr Coulomb failure criteria

Input:	sigci =	85	MPa	mi =	10		GSI =	45			
Output:	mb =	1.40		s =	0.0022		a =	0.5			
	sigtm =	-0.13	MPa	A =	0.50		B =	0.70			
	k =	3.01		phi =	30.12	degrees	coh =	3.27	MPa		
	sigcm =	11.36	MPa	E =	6913.7	MPa					
Tangent:	signt =	15.97	MPa	phit=	30.12	degrees	coht =	4.12	MPa		

Calculation:

									Sums
sig3	1E-10	3.04	6.07	9.1	12.14	15.18	18.21	21.25	85.00
sig1	4.00	22.48	33.27	42.30	50.40	57.91	64.98	71.74	347.08
ds1ds3	15.89	4.07	3.19	2.80	2.56	2.40	2.27	2.18	35.35
sign	0.24	6.87	12.56	17.85	22.90	27.76	32.50	37.13	157.80
tau	0.94	7.74	11.59	14.62	17.20	19.48	21.54	23.44	116.55
x	-2.36	-1.08	-0.83	-0.67	-0.57	-0.48	-0.42	-0.36	-6.77
y	-1.95	-1.04	-0.87	-0.76	-0.69	-0.64	-0.60	-0.56	-7.11
xy	4.61	1.13	0.71	0.52	0.39	0.31	0.25	0.20	8.12
xsq	5.57	1.17	0.68	0.45	0.32	0.23	0.17	0.13	8.74
sig3sig1	0.00	68.23	202.01	385.23	612.01	878.92	1183.65	1524.51	4855
sig3sq	0.00	9.22	36.86	82.94	147.45	230.39	331.76	451.56	1290
taucalc	0.96	7.48	11.33	14.45	17.18	19.64	21.91	24.04	
sig1sig3fit	11.36	20.51	29.66	38.81	47.96	57.11	66.26	75.42	
signtaufit	3.41	7.26	10.56	13.63	16.55	19.38	22.12	24.81	
tangent	4.253087	8.103211	11.40318	14.47286	17.3991	20.2235	22.97025	25.65501	

Cell formulae:

```
      mb = mi*EXP((GSI-100)/28)
       s = IF(GSI>25,EXP((GSI-100)/9),0)
       a = IF(GSI>25,0.5,0.65-GSI/200)
   sigtm = 0.5*sigci*(mb-SQRT(mb^2+4*s))
       A =  acalc =  10^(sumy/8 - bcalc*sumx/8)
       B =  bcalc =  (sumxy - (sumx*sumy)/8)/(sumxsq - (sumx^2)/8)
       k = (sumsig3sig1 - (sumsig3*sumsig1)/8)/(sumsig3sq-(sumsig3^2)/8)
     phi = ASIN((k-1)/(k+1))*180/PI()
     coh = sigcm/(2*SQRT(k))
   sigcm = sumsig1/8 - k*sumsig3/8
       E = IF(sigci>100,1000*10^((GSI-10)/40),SQRT(sigci/100)*1000*10^((GSI-10)/40))
    phit = (ATAN(acalc*bcalc*((signt-sigtm)/sigci)^(bcalc-1)))*180/PI()
    coht = acalc*sigci*((signt-sigtm)/sigci)^bcalc-signt*TAN(phit*PI()/180)
    sig3 = Start at 1E-10 (to avoid zero errors) and increment in 7 steps of  sigci/28 to 0.25*sigci
    sig1 = sig3+sigci*(((mb*sig3)/sigci)+s)^a
  ds1ds3 = IF(GSI>25,(1+(mb*sigci)/(2*(sig1-sig3))),1+(a*mb^a)*(sig3/sigci)^(a-1))
    sign = sig3+(sig1-sig3)/(1+ds1ds3)
     tau = (sign-sig3)*SQRT(ds1ds3)
       x = LOG((sign-sigtm)/sigci)
       y = LOG(tau/sigci)
      xy = x*y          x sq = x^2          sig3sig1= sig3*sig1          sig3sq = sig3^2
 taucalc = acalc*sigci*((sign-sigtm)/sigci)^bcalc
  s3sifit = sigcm+k*sig3
sntaufit =  coh+sign*TAN(phi*PI()/180)
 tangent = coht+sign*TAN(phit*PI()/180)
```

Putting numbers to geology – an engineer's viewpoint

Evert Hoek

The Second Glossop Lecture – presented to the Geological Society, London.

Published in the *Quarterly Journal of Engineering Geology,*
Vol. 32, No. 1, 1999, pages 1 – 19.

The Second Glossop Lecture

Putting Numbers to Geology – an Engineer's Viewpoint

Evert Hoek
3034 Edgemont Boulevard, North Vancouver, British Columbia, Canada V7R 4X1

Abstract

Assigning numbers to geology requires a delicate balance between the commonly held opinion that geology cannot be quantified and the over-optimistic view that every physical quantity can be described in precise mathematical terms. In reality, many geological characteristics cannot be quantified precisely and intelligent guesses based upon experience and logical arguments are the best that can be hoped for.

This paper explores the processes used to make some of these guesses and describes how the results are then applied to engineering design. It is shown that, with care, rational engineering decisions can be made in spite of the limitations of the input data. In recent years the development of computer hardware and software has made it much easier to investigate the influence of ranges of values for each of the input parameters. However, care has to be taken that the design is driven by sound geological reasoning and rigorous engineering logic rather than by the very attractive images that appear on the computer screen.

Introduction

Professor Peter Fookes, in the First Glossop lecture (Fookes 1997), gave an excellent description of the numerous steps required in the development of a Geological Model. This model, whether conceptual, hand-drawn or in the form of a computer generated three-dimensional solid model, is the basic building block upon which the design of any major construction project must be based. A good geological model will enable the geologists and engineers involved in the project to understand the interactions of the many components that make up the earth's crust and to make rational engineering decisions based on this understanding. On projects where an adequate geological model does not exist, decisions can only be made on an ad hoc basis and the risks of construction problems due to unforeseen geological conditions are very high.

In this, the Second Glossop lecture, I would like to take the process of design to the next step. I will attempt to describe how an engineer puts numbers to the largely qualitative model described by Fookes. Many geologists are uncomfortable with this requirement to assign numbers to geology and many will contend that geological materials, not being man-made like steel or concrete, cannot be quantified. While I have some sympathy with these views, I have to face the reality that engineering design requires numbers in the form of in situ stress, pore water pressure, rock mass strength and deformation modulus. These numbers are required for the calculation of the stability of slopes, the bearing capacity of foundations, the support capacity for underground excavations and the movement of groundwater contaminants. Without these numbers the process of engineering design is not possible.

Of course rock and soil are not man-made and their properties can vary greatly over short distances. The interactions of different components in a rock mass can be very complex and these interactions are difficult to quantify. These variations must be recognised and incorporated into the numbers themselves and the use to which the numbers are put in the engineering design process. Quoting a rock mass classification value to three decimal places betrays a complete lack of understanding of the process of quantifying rock mass properties. On the other hand, assigning excessively large ranges to each parameter can result in equally meaningless results.

A good engineering geologist and a good geotechnical engineer, working as a team, can usually make realistic educated guesses for each of the parameters required for a particular engineering analysis. It is the selection of reasonable values for the parameters and the choice of appropriate engineering design methods that I wish to explore in this paper.

Help for artistically challenged geologists

The three-dimensional block drawings and sections included in the written version of the first Glossop Lecture, prepared by or with the assistance of Mr G. Pettifer, are miniature masterpieces of geological art. If only such drawings were available on all construction sites.

Unfortunately, I have to say that in my thirty-five odd years of consulting around the world I have seldom come across geological drawings that come close to the these in terms of clarity of presentation and transmission of useful engineering geology information. The converse is generally the case and I have spent many uncomfortable hours attempting to decipher geological plans and sections of less than adequate quality. Of course, it is not the artistic ability of the geologist that determines that accuracy of the geological interpretations being presented but it certainly helps when the drawings are well executed, clearly captioned and approximately to scale.

Help for artistically challenged geologists is on the way in the form of computer generated three-dimensional solid models. Such models are now relatively common in mechanical and structural engineering and even in the medical field. The models of greatest interest to geologists were developed to meet the needs of the mineral exploration geologists in their efforts to define the three dimensional shapes and ore grade distribution of sub-surface mineral deposits. For many years these geologists have used sophisticated statistical techniques and trend surface analysis to interpolate and extrapolate between borehole intersections. The evolution into three-dimensional computer modelling was a natural step.

The mining industry has embraced these computer modelling techniques and such models can now be found in mine planning and geotechnical departments as well as in the offices of the exploration and mining geologists.

One of the most spectacular examples of such a model has been constructed by the Geotechnical Group of the Chuquicamata open pit copper mine in northern Chile, illustrated in Figure 1. An example of a typical three-dimensional block model is illustrated in Figure 2. The 1998 shell of the Chuquicamata mine, showing the geological units exposed in the walls, is illustrated in Figure 3. In this case the computer operators are the geologists themselves and it is not unusual to see a geologist come in from the field and sit down immediately to enter the latest data into the model. This ensures that the model reflects the understanding and interpretation of the geologists and that it is not simply an illustration prepared by a computer technician who may not understand the on-going thinking that goes into building the geological model.

The advantages of these three-dimensional computer generated models are enormous. The model can be rotated and viewed from any direction, enlarged, sectioned and components can be removed or added at will. Trend surfaces representing interpolations or extrapolations between boreholes can be adjusted to fit the geologist's understanding of the tectonic processes involved in the formation of the rock mass. Work is now going on to take data from one of these models and to feed it directly into limit equilibrium slope stability analyses or numerical analyses of the stress and failure conditions around underground excavations.

The current cost of the hardware and software required for the generation of these three-dimensional models is approximately £50,000. This places it outside the range of all but the very largest civil engineering projects. However, with dramatic advances in computer software and the ever decreasing cost of computer hardware, it is conceivable that installations costing one tenth of the current system costs will be available within a few years. This would put these systems within reach of most agencies or consulting organisations with the need to interpret and present engineering geology data. I look forward with eager anticipation to the day when I see one of these models being used on a civil engineering project.

The geotechnical engineering design process

The end product of the work carried out by a geotechnical engineer is generally the complete design of a slope, a foundation or an underground excavation. An example of a typical flow path for a geotechnical engineering design, adapted from Hoek and Brown (1980), is illustrated in Figure 4. In this case, the design is for an underground excavation but a similar diagram can be constructed for any other structure for which the geotechnical engineer is responsible

From this figure it will be obvious that the design process progresses from a largely qualitative preliminary assessment of potential problems to a highly quantitative analysis of support capacity and excavation performance for the situations that require such an analysis.

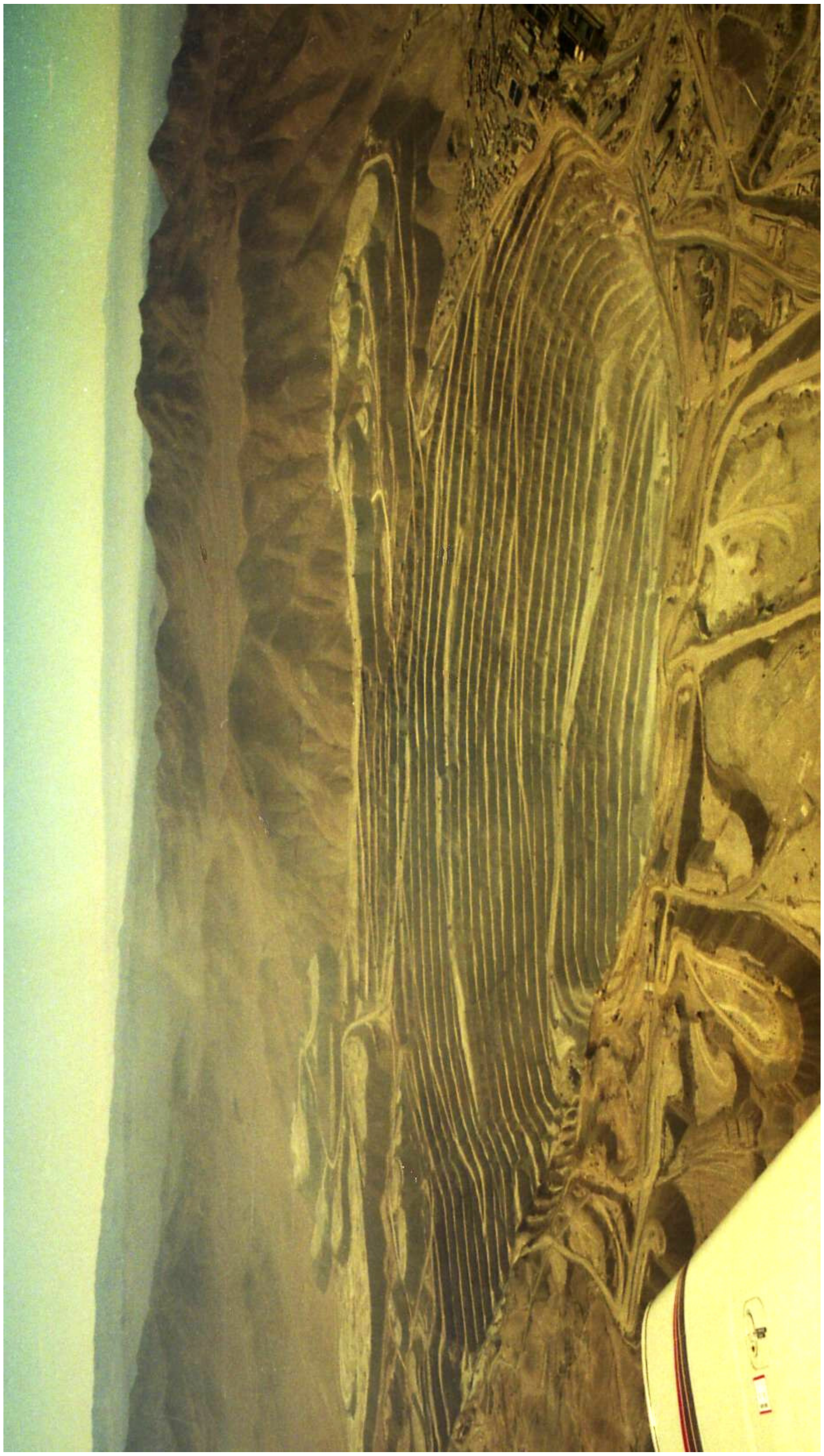

Fig **1**: Arial view of the Chuquicamata open pit copper mine in northern Chile.

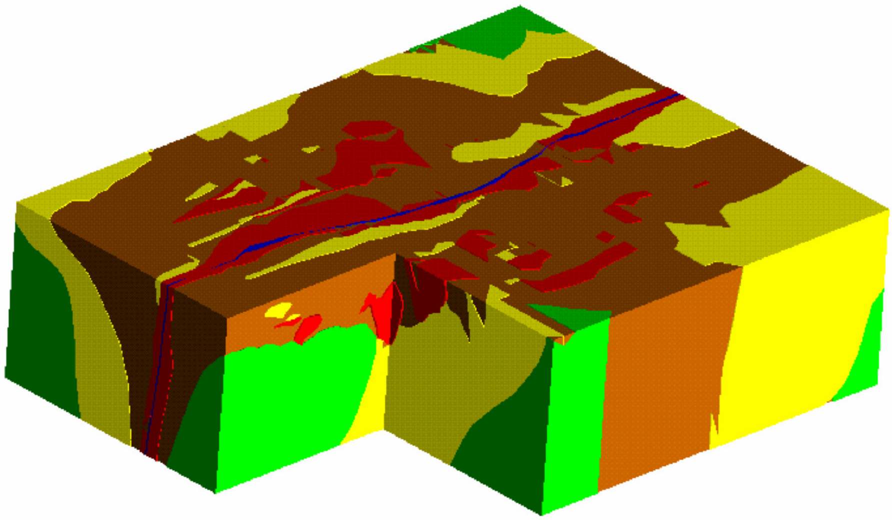

Fig. **2**: Example of a computer generated three-dimensional solid model of the rock mass in which the Chuquicamata open pit copper mine in northern Chile is being mined.

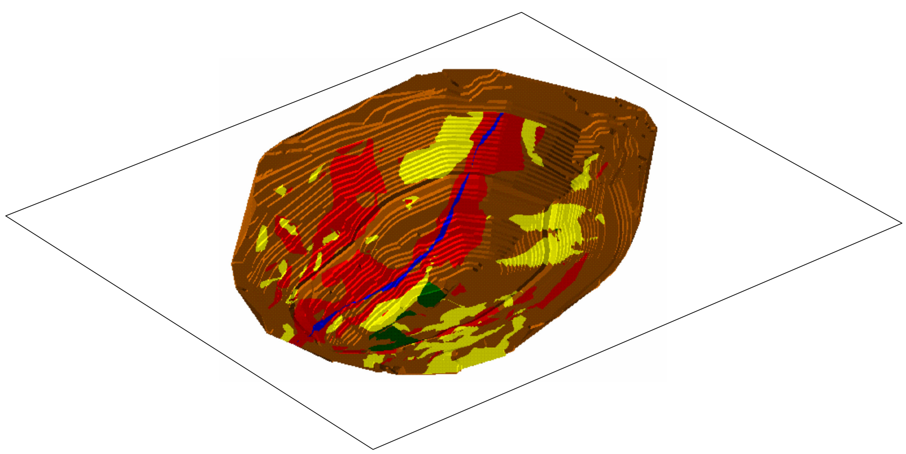

Fig. **3**: Chuquicamata open pit mine in 1998 showing the geological units exposed in the walls of the 750 m deep pit. Figures 2 and 3 were prepared by Mr Ricardo Torres of the Chuquicamata Geotechnical Group using the program Vulcan[1].

[1] Available from Maptek Perth, 92 Roe Street, Northbridge, Western Australia 6003, Phone: + 61 8 9328 4111, Fax: + 61 8 9328 4422, email: info@perth.maptek.com.au

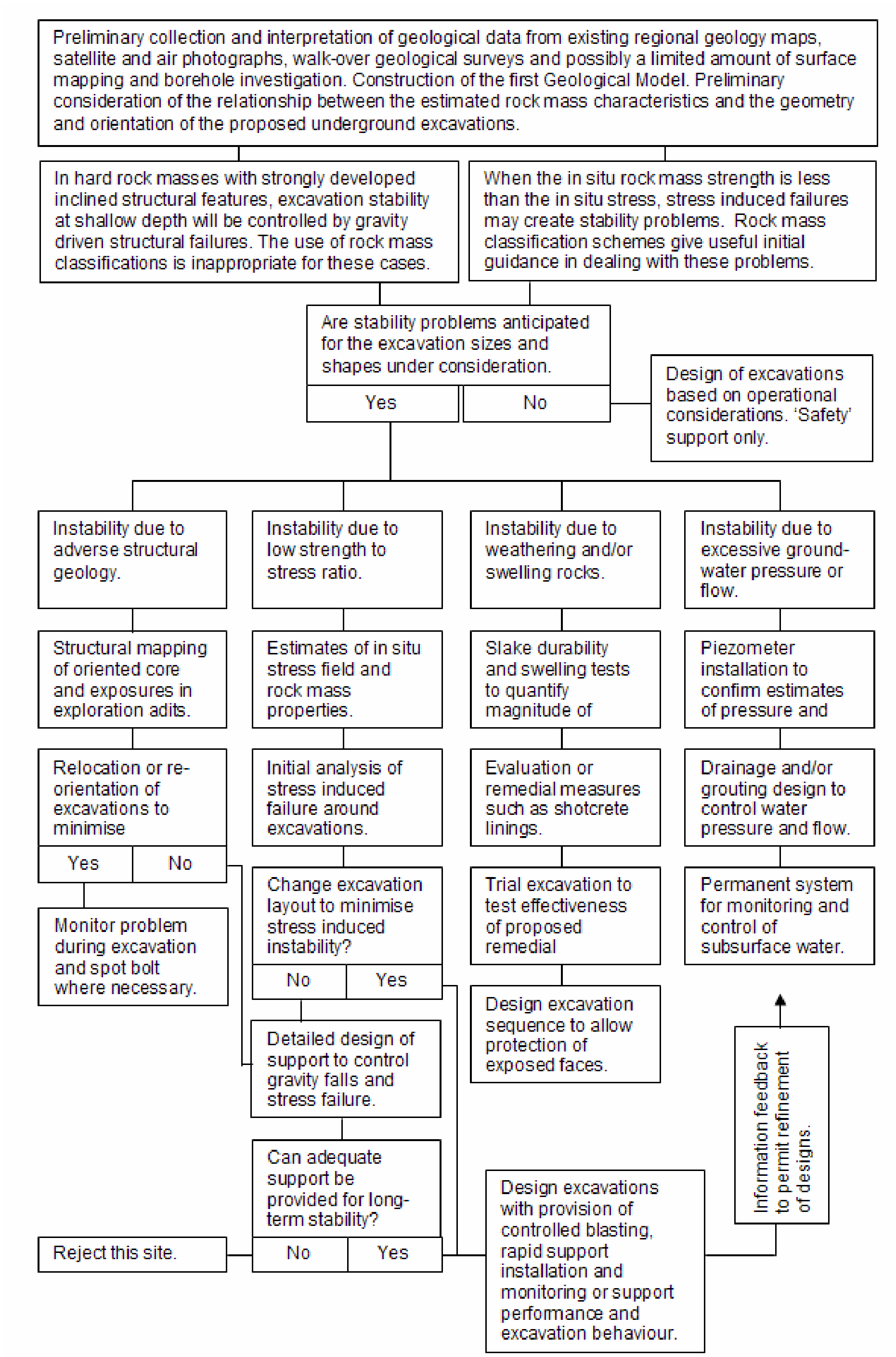

Fig. **4**: Flow path for the geotechnical design of underground excavations in rock. (Hoek and Brown 1980).

Note that the engineering design process need only be taken as far as necessary to satisfy the designer that the requirements of safety and stability have been met. It may be possible, on the basis of a very simple semi-quantitative analysis, to conclude that there are no conditions likely to lead to instability and to terminate the design at this point. On the other hand, in cases where the structural conditions are very unfavourable or where the rock mass strength is very low compared to the in situ stresses, a very detailed numerical analysis may be required.

In complex cases it may be necessary to run the numerical analysis concurrently with construction and adjust the excavation sequence and support systems to satisfy the design requirements established by back-analysis of the observed excavation behaviour.

Note that the geological model is a dynamic tool that changes as more information is exposed during the excavation process. It is only for very simple geological environments that the geological model can be established early in the site investigation and design process and left unaltered for the remainder of the project. The more usual condition is that the model is continually refined as the project progresses through the various stages of design and construction.

Preliminary project feasibility assessment

During the very early stages of project evaluation and design, when practically no quantitative information is available and when the geological model is fairly crude, the design process relies heavily on precedent experience and very general rules of thumb. For example, in evaluating three alternative highway routes through mountainous terrain, the engineering geologist or geotechnical engineer would look for routes with the minimum number of unstable landforms, ancient landslides, difficult river crossings and the minimum number of tunnels. Simple common sense says that all of these factors represent problems and the potential for increased cost.

This may sound a trivial example but it is amazing how often a highway will be laid out by transportation engineers with more concern for lines of sight and radii of curves than for the geological conditions which happen to occur along the route. It is then up to the engineering geologists and geotechnical engineers to sort out the problems and, where necessary, to propose an alignment that is more appropriate for the geological conditions.

Precedent experience is also an important consideration at this stage of the design process. When evaluating the potential problems along a proposed tunnel route it is very useful to visit and to talk to engineers and contractors who have worked on tunnels in similar geological conditions within a few tens of kilometres of the site, if such tunnels exist.

Care has to be exercised in how this precedent experience is interpreted and applied. I remember visiting an open pit mine in the United Kingdom many years ago and asking why the slopes had been designed at the unusual angle of 53 degrees. The answer I received was that the company's mines in the United States seemed to operate successfully at this angle – hardly an appropriate extrapolation by any stretch of the imagination.

During the preliminary design stage, the engineer is probably less important than the geologist. The engineer is there to convey the general requirements and constraints of the project and it is up to the geologist, based on the geological model, to provide the qualitative assessment of whether these conditions can easily be met or whether it would be better to look for another site.

Preliminary engineering evaluation

Once the qualitative process described above has been exhausted and the options have been narrowed down to one or two, it may become necessary to move into a more quantitative process in which the engineer starts to assume the leading role in the design process. It is at this stage in the design process (and, in my opinion, only at this stage) that classification schemes play an important role.

These classifications, based upon experience and the back analysis of a large number of case histories, attempt to quantify the general rock mass conditions in terms of relatively simple numerical ratings. The final 'score' is then used to provide guidance on tunnel support, slope stability, the problems of excavating rock masses or the ease with which a rock mass will cave in a block caving mining operation. The rock mass classification systems commonly used in the English language world have been summarised by Bieniawski (1989) and it is not my intention to discuss these classifications further here. Incidentally, there are at least seven different rock mass classification systems in use in Japan and probably similar numbers in other non-English speaking countries.

Table 1: Rockfall Hazard Rating System. After Pierson and van Vickle (1993).

CATEGORY	RATING CRITERIA AND SCORE			
	POINTS 3	POINTS 9	POINTS 27	POINTS 81
SLOPE HEIGHT	25 FT	50 FT	75 FT	100 FT
DITCH EFFECTIVENESS	Good catchment	Moderate catchment	Limited catchment	No catchment
AVERAGE VEHICLE RISK	25% of the time	50% of the time	75% of the time	100% of the time
PERCENT OF DECISION SIGHT DISTANCE	Adequate site distance, 100% of low design value	Moderate sight distance, 80% of low design value	Limited site distance, 60% of low design value	Very limited sight distance, 40% of low design value
ROADWAY WIDTH INCLUDING PAVED SHOULDERS	44 feet	36 feet	28 feet	20 feet
GEOLOGIC CHARACTER — CASE 1 — STRUCTURAL CONDITION	Discontinuous joints, favorable orientation	Discontinuous joints, random orientation	Discontinuous joints, adverse orientation	Continuous joints, adverse orientation
GEOLOGIC CHARACTER — CASE 1 — ROCK FRICTION	Rough, irregular	Undulating	Planar	Clay infilling or slickensided
GEOLOGIC CHARACTER — CASE 2 — STRUCTURAL CONDITION	Few differential erosion features	Occasional erosion features	Many erosion features	Major erosion features
GEOLOGIC CHARACTER — CASE 2 — DIFFERENCE IN EROSION RATES	Small difference	Moderate difference	Large difference	Extreme difference
BLOCK SIZE / QUANTITY OF ROCKFALL/EVENT	1 FT / 3 cubic yards	2 FT / 6 cubic yards	3 FT / 9 cubic yards	4 FT / 12 cubic yards
CLIMATE AND PRESENCE OF WATER ON SLOPE	Low to moderate precipitation; no freezing periods, no water on slope	Moderate precipitation or short freezing periods or intermittent water on slope	High precipitation or long freezing periods or continual water on slope	High precipitation and long freezing periods or continual water on slope and long freezing periods
ROCKFALL HISTORY	Few falls	Occasional falls	Many falls	Constant falls

Table 2: Example of the application of the Rockfall Hazard Rating System

Category	*Description*	*Points*
Slope height	30 m	81
Ditch effectiveness	Limited catchment	27
Average vehicle risk	50% of the time	9
Percentage of decision sight distance	Very limited sight distance, 40% of low design value	81
Roadway width, including paved shoulders	28 feet / 8.5 m	27
Geologic character – Case 1	Discontinuous joints, adverse orientation, Planar	27
Block size / quantity of rockfall	3 ft (1.3 m) / 12 cu. yards or cu. metres	81
Climate and presence of water on slope	Moderate precipitation or short freezing periods or intermittent water on slope	9
Rockfall history	Many falls	27
	Total score	369

A classification system that is probably almost completely unknown in the United Kingdom but which, for me, embodies the essential elements of a good classification system for preliminary engineering design is the 'Rockfall Hazard Rating System'. This system was developed by the Federal Highway Administration in the United States for the preliminary evaluation of rockfall hazards and the allocation of priorities for remedial work (Pierson and van Vickle 1993). The key elements of this rating system are contained in the table reproduced as Table 1. Detailed instructions and examples on the evaluation of each of the nine components of the system are given in the FHWA manual.

I like this classification because it is based on a set of simple visual observations, most of which can be carried out from a slow moving vehicle as would be required for the preliminary evaluation of miles of mountain highway. The system also contains all the components required for a complete engineering evaluation of the risks to the public. These include highway design factors as well as geometrical and geotechnical factors, all presented in clear and unambiguous terms.

An example of a typical rockfall hazard evaluation, based on this system, is given in Table 2. The authors of the FHWA manual give no direct instructions on how the total score obtained from this rating system should be used. It is intended for use as a tool to assist management in the allocation of resources and these decisions will vary from state to state. From personal discussions with one of the authors I learned that, in the State of Oregon, slopes with a rating of less than 300 are assigned a very low priority while slopes with a rating of more than 500 are identified for urgent remedial action.

Returning to the question of the preliminary evaluation of a construction project, the aim should be to divide the problems into a series of approximate categories, depending upon the severity of each problem. Whatever numerical process is used, these categories should be treated as approximate guidelines rather than absolute design values. The whole purpose of the preliminary evaluation is to decide which components justify additional site investigations and analysis. The detailed design follows later.

Detailed engineering design

Having identified those components of a construction project that require detailed analysis, the next step is to select the appropriate method of analysis and the input data required for this analysis. There are too many geotechnical problems and methods of analysis for me to cover in this paper so I will deal with only one - the design of underground excavations in weak rocks.

In the context of this discussion I will define rock as weak when the in situ uniaxial compressive strength is less than the in situ stress level. Hence, a jointed rock mass with a uniaxial compressive strength of 3 MPa will behave as a weak rock at depths of more than about 120 m. Under these conditions a tunnel would begin to show the first signs of stress induced failure.

In order to carry out a meaningful analysis of the stresses induced by the excavation of a tunnel or cavern it is necessary to estimate the in situ stresses in the rock mass and also the properties of the rock mass.

Estimates of in situ stress

Of all of the quantities that the geotechnical engineer is required to estimate or to measure, the in situ stress field in a rock mass is one of the most difficult. The vertical stress can be approximated, to an acceptable level of accuracy, by the product of the depth below surface and the unit weight of the rock mass. On the other hand, the horizontal stresses of interest to civil engineers are influenced by global factors such as plate tectonics and also by local topographic features.

Zoback (199) described the World Stress Map project that was designed to create a global database of contemporary tectonic stress data. The data included in this map were derived mainly from geological observations on earthquake focal mechanisms, volcanic alignments and fault slip interpretations.

The results included in this map are very interesting to geologists but are of limited value to engineers concerned with the upper few hundred metres of the earth's crust. The local variations in the in situ stress field are simply too small to show up on the global scale.

A more useful basis for estimating horizontal in situ stresses was proposed by Sheorey (1994). He developed an elasto-static thermal stress model of the earth. This model considers curvature of the crust and variations of elastic constants, density and thermal expansion coefficients through the crust and mantle. A plot of the ratio of horizontal to vertical stress predicted by Sheorey's analysis, for a range of horizontal rock mass deformation moduli, is given in Figure 5. This plot is very similar in appearance to that derived by Hoek and Brown (1980) on the basis of measured in situ stresses around the world. While this similarity does not constitute a proof of the correctness of Sheorey's solution, it is at least comforting to find this correlation between theory and observations.

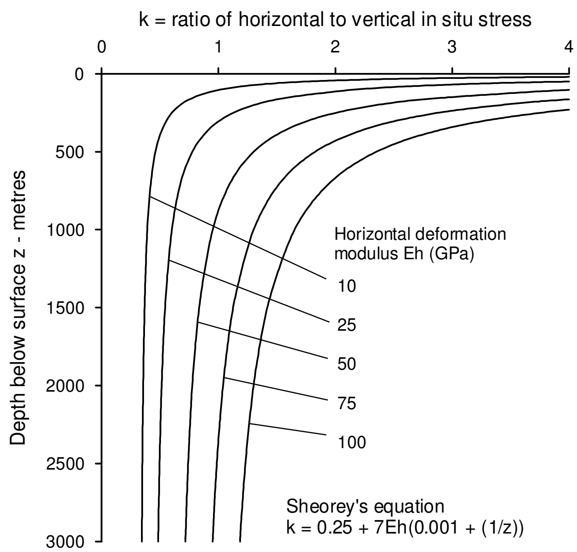

Fig. **5**. Ratio of horizontal to vertical in situ stress versus depth below surface. (Sheorey 1994)

Note that neither Sheorey's equation nor the trends established by Hoek and Brown account for local topographic influences on the in situ stress field. Hence, when making estimates of the in situ stress field in a mountainous area, adjustments must be made to account for these topographic factors. For example, the general relationships discussed above may indicate a horizontal stress of approximately twice the vertical stress for the rock mass at a depth of 300 m. In deciding upon the in situ stresses to be applied to the analysis of an underground powerhouse to be located at this depth in the side of a steep valley, the horizontal stress at right angles to the valley axis could be reduced to a value equal to the vertical stress. This would account for the stress relief due to the down-cutting of the valley. No such stress relief would occur parallel to the valley axis and so the horizontal stress in this direction would be kept at twice the vertical stress.

In carrying out an analysis of the stresses induced by the creation of an underground excavation, it is prudent to consider a range of possible in situ stresses. In the example discussed above, the horizontal stress at right angles to the valley axis could be varied from one half the vertical stress to twice the vertical stress. The stress parallel to the valley could be varied from a minimum value equal to the vertical stress to a maximum value of three times the vertical stress. An exploration of the effects of all possible combinations of these stress values would give a good indication of whether or not these in situ stresses would be critical to the design of the underground excavations. In cases where a preliminary analysis indicates that the design is very sensitive to the in situ stresses, measurement of the in situ stresses has to be considered a priority in the ongoing site investigation and design process.

Estimates of rock mass properties

Hoek and Brown (1980) proposed a methodology for estimating the strength of jointed rock masses. This technique has been refined and expanded over the years and the latest version is described in a recent paper and technical note. (Hoek and Brown 1997, Hoek 1998).

The basic input consists of estimates or measurements of the uniaxial compressive strength (σ_{ci}) and a material constant (m_i) that is related to the frictional properties of the rock. Ideally, these basic properties should be determined by laboratory testing as described by Hoek and Brown (1997) but, in may cases, the information is required before laboratory tests have been completed. To meet this need, tables that can be used to estimate values for these parameters are reproduced in Tables 3 and 4.

Table 3: Field estimates of uniaxial compressive strength.

Grade*	Term	Uniaxial Comp. Strength (MPa)	Point Load Index (MPa)	Field estimate of strength	Examples
R6	Extremely Strong	> 250	>10	Specimen can only be chipped with a geological hammer	Fresh basalt, chert, diabase, gneiss, granite, quartzite
R5	Very strong	100 - 250	4 - 10	Specimen requires many blows of a geological hammer to fracture it	Amphibolite, sandstone, basalt, gabbro, gneiss, granodiorite, limestone, marble, rhyolite, tuff
R4	Strong	50 - 100	2 - 4	Specimen requires more than one blow of a geological hammer to fracture it	Limestone, marble, phyllite, sandstone, schist, shale
R3	Medium strong	25 - 50	1 - 2	Cannot be scraped or peeled with a pocket knife, specimen can be fractured with a single blow from a geological hammer	Claystone, coal, concrete, schist, shale, siltstone
R2	Weak	5 - 25	**	Can be peeled with a pocket knife with difficulty, shallow indentation made by firm blow with point of a geological hammer	Chalk, rocksalt, potash
R1	Very weak	1 - 5	**	Crumbles under firm blows with point of a geological hammer, can be peeled by a pocket knife	Highly weathered or altered rock
R0	Extremely Weak	0.25 - 1	**	Indented by thumbnail	Stiff fault gouge

*Grade according to Brown (1981).
**Point load tests will give highly ambiguous results on rocks with a uniaxial compressive strength of less than 25 MPa.

Table 4: Values for the constant m_i for intact rock,. Note that the values in parenthesis are estimates.

Rock type	Class	Group	Texture			
			Coarse	Medium	Fine	Very fine
SEDIMENTARY	Clastic		Conglomerate (22)	Sandstone 19	Siltstone 9	Claystone 4
				Greywacke (18)		
	Non-Clastic	Organic		Chalk 7		
				Coal (8-21)		
		Carbonate	Breccia (20)	Sparitic Limestone (10)	Micritic Limestone 8	
		Chemical		Gypstone 16	Anhydrite 13	
METAMORPHIC	Non Foliated		Marble 9	Hornfels (19)	Quartzite 24	
	Slightly foliated		Migmatite (30)	Amphibolite 25 - 31	Mylonites (6)	
	Foliated*		Gneiss 33	Schists 4 - 8	Phyllites (10)	Slate 9
IGNEOUS	Light		Granite 33		Rhyolite (16)	Obsidian (19)
			Granodiorite (30)		Dacite (17)	
			Diorite (28)		Andesite 19	
	Dark		Gabbro 27	Dolerite (19)	Basalt (17)	
			Norite 22			
	Extrusive pyroclastic type		Agglomerate (20)	Breccia (18)	Tuff (15)	

* These values are for intact rock specimens tested normal to bedding or foliation. The value of m_i will be significantly different if failure occurs along a weakness plane.

The most important component of the Hoek-Brown system is the process of reducing the material constants σ_{ci} and m_i from their 'laboratory' values to appropriate in situ values. This is accomplished through the Geological Strength Index GSI that is defined in Figure 6.

In the context of this paper, the GSI is a real case of putting numbers to geology. It has been developed over many years of discussions with engineering geologists with whom I have worked around the world. Careful consideration has been given to the precise wording in each box and to the relative weights assigned to each combination of structural and surface conditions.

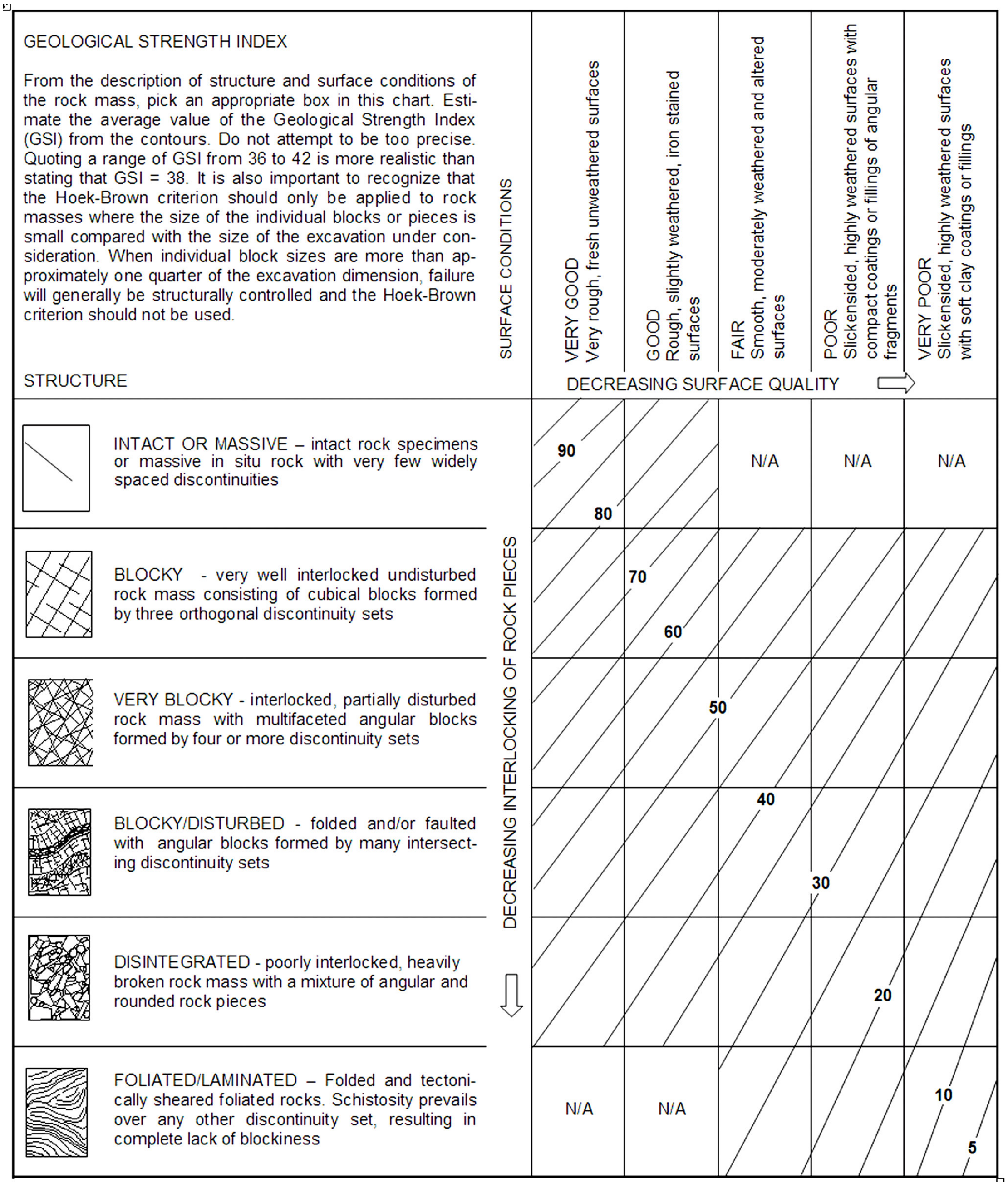

Fig. **6**: Geological Strength Index GSI on the basis of geological observations.

The version of the GSI chart presented in Figure 6 contains two new rows that have not yet been published elsewhere. The top row on 'intact or massive' rock is the result of work in Chile on cemented breccias that behave very much like weak concrete (personal communication from Dr Antonio Karzulovic). The bottom row on 'foliated/laminated/sheared' rock has been inserted to deal with very poor quality phyllites encountered in Venezuela (personal communications from Professors Rudolpho Sancio and Daniel Salcedo) and the weak schists being tunnelled through for the Athens Metro (Hoek, Marinos and Benissi 1998). It is probable that this figure will continue to evolve as experience is gained in the use of GSI for estimating rock mass properties in the wide range of geological environments to which it is being applied.

Based on intuition, experience and the back analysis of a number of case histories, relationships have been developed between GSI, σ_{ci} and m_i and the various rock mass properties required for engineering analyses,. These relationships, described in detail by Hoek and Brown (1997), have been used to generate the charts for cohesion, friction angle and modulus of deformation given in Figures 7, 8 and 9.

These charts can be used to obtain approximate values for in situ properties. It is an absolute requirement that the engineer making these estimates should check their appropriateness by back analysis of the measured or observed excavation behaviour, once construction commences.

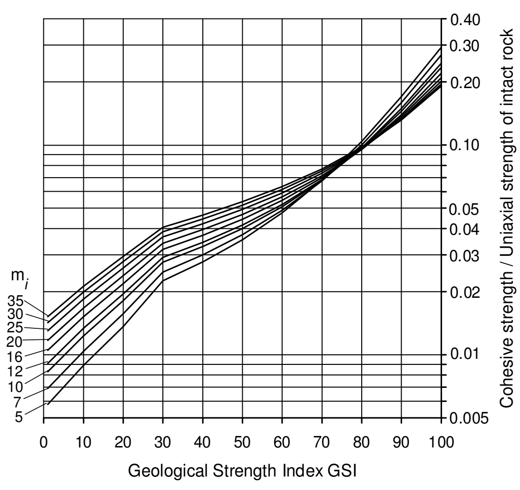

Fig. **7**: Cohesive strength versus GSI.

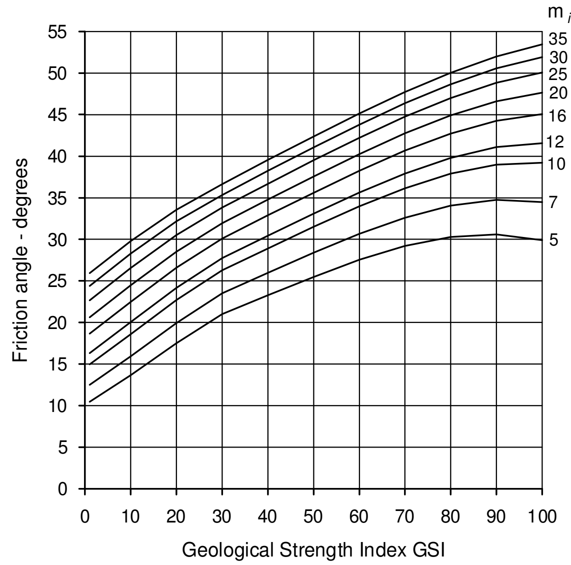

Fig. **8**: Friction angle versus GSI.

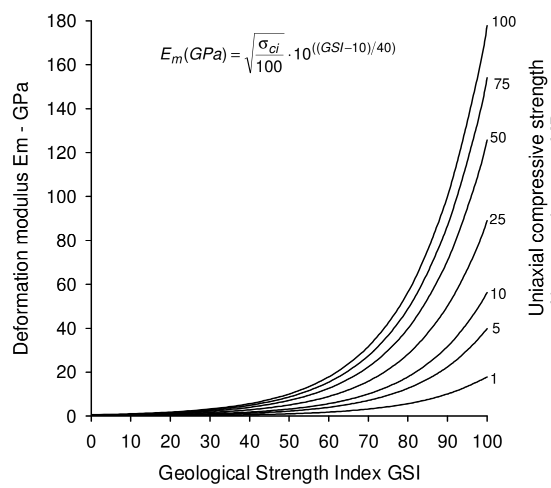

Fig **9**: Deformation modulus versus GSI.

Practical example

A 27 km long, 10 m internal diameter concrete-lined headrace tunnel is currently under construction as part of the 1500 MW Nathpa Jhakri hydroelectric project on the Satluj river in Himachel Pradesh, India. The rock masses through which the tunnel passes are either metamorphic, consisting of gneisses, schists, quartzites and amphibolites or igneous consisting of granites and pegmatites. The engineering geological conditions associated with the project have been evaluated by the Geological Survey of India (Geological Survey of India 1988, Jalote *et al* 1996) on the basis of surface mapping, exploration boreholes and a few exploration adits. Excellent maps and sections were available before the commencement of underground excavation. In addition to conventional descriptive and structural maps, the rock mass has been classified in terms of Bieniawski's RMR system (Bieniawski 1989), Barton, Lien and Lunde's Q system (Barton *et al* 1974) and the GSI system described above.

At the time of writing (May 1998), the bulk of the tunnel excavation has been completed and the prediction of tunnelling conditions provided by the Geological Survey of India has proved to be accurate and a useful guide to the steps to be taken in excavation and support. One of the sections still to be completed is a 360 m long stretch through the Daj Khad shear zone. It is this part of the tunnel that I wish to discuss. The dramatic impact of the Daj Khad shear zone on the stability of the tunnel top heading is illustrated in Figure 10. This shows a closure in excess of one metre due to the heavy loads being imposed on the support system.

The rock mass in the vicinity of the Daj Khad shear zone is predominantly quartz mica schist with some serecite schist and a few gneiss bands and one amphibolite zone. The shear zone itself comprises a number of steeply dipping seams of fractured blocky rock with kaolinised and sericitised material. The uniaxial compressive strength of the schist that makes up the bulk of the rock mass is approximately 10 MPa under the saturated conditions that occur at the tunnel depth of between 200 and 300 m through this zone. The value of the rock mass constant m_i has been assumed equal to 10 for the entire zone (see Table 4). The variation of the Geological Strength Index GSI through the rock mass associated with the Daj Khad can be represented by a truncated normal distribution defined by a mean value of 27, a standard deviation of 7, a minimum value of 6 and a maximum value of 45. This distribution is based on studies carried out by Geodata S.p.A. of Turin, consultants to the Nathpa Jhakri Joint Venture, the contractors on this stretch of headrace tunnel. The methodology employed by Geodata in arriving at this distribution has been described in a recent paper by Russo *et al* (1998).

Fig. **10**: Large convergence in the Nathpa Jhakri headrace tunnel top heading due to the influence of the Daj Khad shear zone.

Based upon this GSI distribution and assuming that the vertical in situ stress is uniformly distributed with a minimum of 5.4 MPa and a maximum of 8.1 MPa, corresponding to depths below surface of 200 and 300 m, a Monte Carlo simulation has been carried out to determine the extent of the plastic zone and the convergence of the rock mass surrounding the 10 m diameter tunnel. This calculation is too detailed for inclusion in this publication but the equations used to set up the spreadsheet for the simulation are described in Hoek and Brown (1997) and Hoek (1998). The results of the simulation are plotted, in dimensionless form, in Figures 11 and 12. Note that these plots are for an unsupported tunnel.

It is evident, from the plots given in these figures, that the size of the plastic zone and the convergence of the tunnel both show dramatic increases when the uniaxial compressive strength of the rock mass falls below about one tenth of the in situ stress. Unless adequate support is provided, the tunnel will almost certainly collapse for the lowest quality rock conditions under the highest in situ stresses. These findings are consistent with the results of as yet unpublished research on tunnelling in weak rocks. I have found that the very unstable conditions develop in unsupported tunnels of almost any shape for rock mass strengths less than 0.1 to 0.2 of the maximum in situ stress.

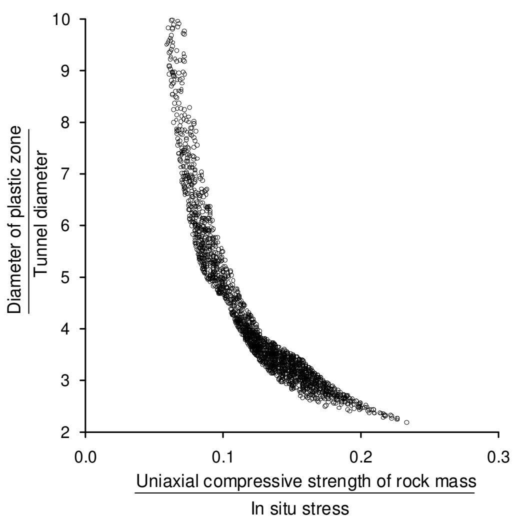

Fig. **11**: Size of plastic zone versus ratio of uniaxial compressive strength of rock mass to in situ stress.

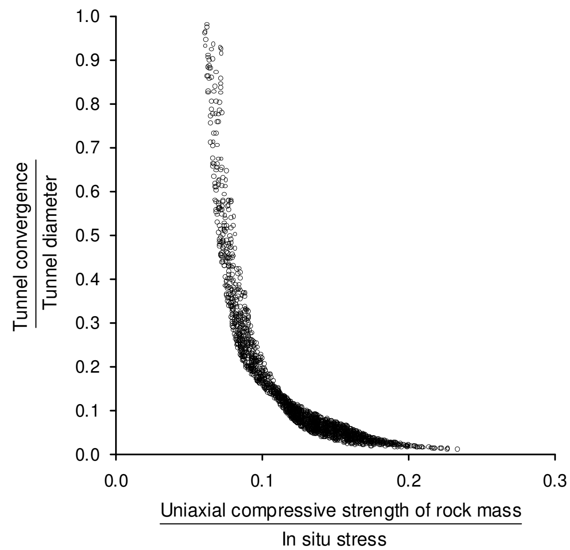

Fig. **12**: Tunnel convergence versus ratio of uniaxial compressive strength of the rock mass to in situ stress.

In passing, it is worth mentioning that trends such as this are of great value to geotechnical engineers. If a trend is found to be consistent over a wide range of conditions, this usually indicates that some basic law is at work and, if this law can be isolated, it may be possible to describe it in mathematical terms. This is an important part of the process of putting numbers to geology.

Taking the study of the Natha Jhakri tunnel to the next stage involves a more refined numerical analysis and, in order to demonstrate this process, I have used the finite element program PHASE2 developed at the University of Toronto. This software is one of a family of user-friendly but powerful programs developed with financial assistance from the Canadian mining industry. Development and distribution of these programs has now been taken over by a spin-off company called Rocscience Inc.[2].

I have considered two cases, one defined by a GSI of 45, representing the better rock mass conditions in this zone, and the other defined by a GSI of 20 that is typical of the shear zone. As discussed earlier, the uniaxial compressive strength of the intact schist is taken as $\sigma_{ci} = 10$ MPa and the value of the material constant m_i

[2] Details available from Rocscience Inc., 31 Balsam Avenue, Toronto, Ontario, Canada M4E 3B5, Fax 1 416 698 0908, Email: software@rocscience.com, Internet: http://www.rocscience.com.

is 10. The corresponding values of cohesion, angle of friction and deformation modulus, estimated from Figures 7, 8 and 9, are given in Table 5. The uniaxial compressive strength (UCS) of the rock mass is calculated from the equation $UCS = 2c\cos\phi/(1-\sin\phi)$ and the values for the two cases are included in this table.

Table 5: Rock mass properties for two examples analysed.

Property	Case 1	Case 2
Intact rock strength σ_{ci} MPa	10	10
Material constant m_i	10	10
Geological Strength Index	45	20
Cohesive strength c MPa	0.4	0.2
Friction angle ϕ degrees	30	23
Deformation modulus MPa	2500	550
Rock mass UCS, MPa	1.4	0.6
In situ stress MPa	6.75	6.75
UCS/in situ stress	0.21	0.09

In situ stresses along the tunnel route have been measured by hydraulic fracturing and by overcoring techniques (Bhasin *et al* 1996). The following values were found for the principal stresses:

σ_1 = 7.1 MPa, approximately parallel to valley,
σ_2 = 5.9 MPa, vertical stress,
σ_3 = 3.9 MPa, approximately normal to valley.

However, because of the general weakness of the rock mass in the region of the Daj Khad shear zone, it has been assumed that the rock mass cannot tolerate significant stress differences and that all three principal in situ stresses are equal. An average tunnel depth of 250 m has been used to derive the in situ stress value of 6.75 MPa used in these analyses.

As shown in Table 5, the ratio of the uniaxial compressive strength of the rock mass to the in situ stress is 0.21 for Case 1 and 0.09 for Case 2. These values fall on either side of the critical ratio of about 0.1 shown in Figures 11 and 12.

The zone of failure for Case 1 is illustrated in Figure 13. The PHASE2 model simulates progressive failure as the tunnel is excavated. The process used to achieve this simulation involves transferring loads that cannot be carried by failed elements onto adjacent elements. A check is then performed to determine whether the loads imposed on these adjacent elements causes them to fail. The process is continued until no more elements are loaded to failure.

For Case 1, as shown in Figure 13, the failure zone extends about 3 m into the rock mass surrounding the 10 m span top heading. The convergence of the roof and haunches is approximately 40 mm and, in this example, the floor heave is also approximately 40 mm. In many cases of weak rock tunnelling, floor heave is significantly larger than roof and wall convergence. This leads to the need for reinforcement of the floor, by rockbolting or by the placement of a concrete invert, in order to stabilise the tunnel.

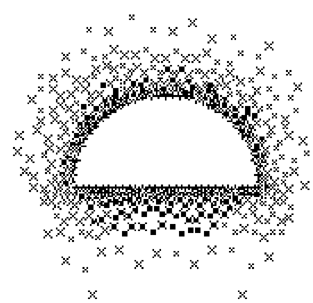

Fig. **13**: Extent of failure zone surrounding the tunnel top heading in a rock mass defined by GSI = 45. Shear failure is represented by the × symbol while tensile failure is denoted by the • symbol.

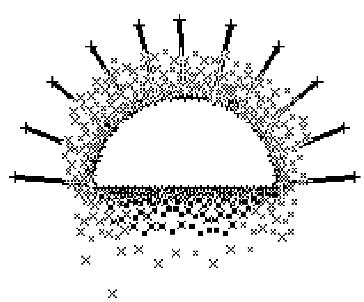

Fig. **14**: Reduced failure zone in the top heading roof due to the installation of untensioned fully-grouted rockbolts and steel fibre reinforced shotcrete.

Figure 14 shows that the top heading in the better quality rock mass (GSI = 45) can be stabilised by a combination of untensioned fully-grouted rockbolts and steel-fibre reinforced shotcrete. The rockbolts are 4 m long, 25 mm diameter and are installed on a grid pattern of 1.5 m x 1.5 m. The shotcrete layer is 100 mm thick. Typically a 25 mm thick layer of shotcrete is placed immediately after the excavation of a tunnel length of two to three metres. This is followed by the installation of the grouted rockbolts to within about 1 m of the face. A second layer of shotcrete is then applied to bring the total thickness up to 100 mm. In this case, no support of the floor is required since this is relatively stable and it will be excavated during the subsequent benching operation.

In deciding upon the adequacy of the support system, the extent of the failure zone in the reinforced rock mass is checked. Rockbolts passing through this failure zone will generally suffer yield of the grout/steel interface. This is not a problem provided that an unyielded anchor length of 1 to 2 m remains outside the zone of failed rock, as shown in Figure 14. The deformations in the rock mass must also be checked to determine whether there are any sections of the excavation perimeter that require additional support.

Note that other support systems, such as steel sets or lattice girders embedded in shotcrete, could also be used to stabilise this particular tunnel. The final choice of the support system depends upon overall cost and scheduling considerations.

The Daj Khad shear zone itself is characterised by a Geological Strength Index of approximately 20. Mining through this poor quality rock mass results in a failure zone that extends about 15 m into the roof and floor, as illustrated in Figure 15. The size of this zone, together with the presence of kaolin, means that rockbolt support will not be effective in this case. Steel set support is also difficult to design because of the large span of the top heading and the heavy squeezing pressures.

The support system chosen for mining through this difficult stretch of tunnel is similar to that used by Geodata on a number of previous projects (Carrieri *et al* 1991, Grasso *et al* 1993). This consists of a series of sub-horizontal holes, up to 24 m long, for geological exploration as well as predrainage and grouting of the rock mass ahead of the tunnel.. These are followed by a 12 m long umbrella of grouted pipe forepoles, forming a protective umbrella under which the tunnel can be excavated. Cemented fibreglass bars are used to stabilise the face and steel sets, radial rockbolts and a shotcrete or concrete invert are also used if required.

Figure 16 shows the equipment used to drill the sub-horizontal holes and to install the forepoles in the Daj Khad stretch of the Nathpa Jhakri headrace tunnel.

The three-dimensional geometry of the tunnel heading and protective umbrella makes it very difficult to analyse this support system. Two-dimensional analyses, such as those described above, are not adequate. Grasso *et al* (1993) used an axisymmetric two-dimensional model to study the support provided by the forepole umbrella. However, I feel that a full three-dimensional analysis of this support system would be justified. Three-dimensional models capable of a full progressive failure analysis for this type of support system are becoming available but are not for the numerically timid. This type of analysis is best left to the numerical model specialist at this stage but they should be available as general design tool within a few years.

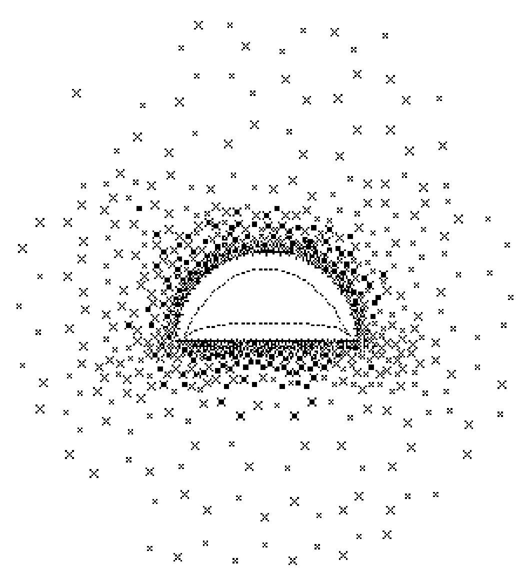

Fig. **15**: Failure zone surrounding the tunnel top heading in the Daj Khad shear zone, defined by a Geological Strength Index of 20. The tunnel convergence, shown by the deformed excavation boundary, is approximately 400 mm.

Fig. **16**: Installation of 12 m long grouted pipe forepoles to form a protective reinforced rock umbrella under which excavation of the top heading can proceed.

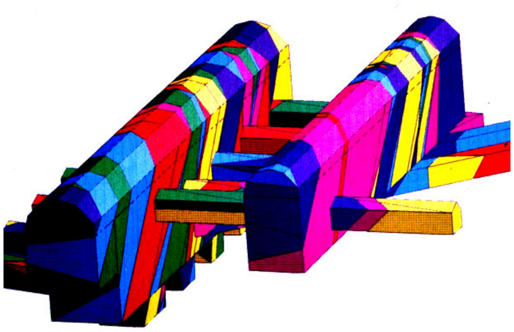

Fig. **17**: Isometric view of the three-dimensional numerical model of the underground powerhouse cavern and transformer gallery of the Nathpa Jhakri Hydroelectric Project.

One example of the type of three-dimensional model that can be used for these studies is illustrated in Figure 17. This 3DEC[3] model has been used in studies of the Nathpa Jhakri underground powerhouse complex, carried out by Dr B. Dasgupta of Advanced Technology and Engineering Services, Delhi. India.

Engineering risk assessment

The inherent variability of geological materials means that each material property should be defined by a range of values rather than by a single number. Hence, the end product of any analysis based on these numbers has to be assessed in terms of probability of occurrence or of engineering risk.

A detailed discussion on techniques for engineering risk assessment is beyond the scope of this paper and the reader is referred to the excellent book by Harr (1987) on this subject. However, the general concepts of this

[3] Available from ITASCA Consulting Group Inc., Thresher Square East, 708 South Third Street, Suite 310, Minneapolis, Minnesota 55415, USA. Fax 1 612 371 4717

form of analysis are illustrated in the following simple example.

The problem is to determine the risk of failure of a slope excavated in a heavily jointed rock mass. The shear strength properties of this rock mass are defined by the normal distributions of cohesion and angle of friction given in Figure 18. These distributions were calculated by means of a Monte Carlo simulation, using assumed normal distributions defined by the following values (Hoek 1998):

Parameter	Mean	Standard deviation
UCS of intact rock, MPa	10	2.5
Intact rock constant m_i	8	1
Geological Strength Index	25	2.5

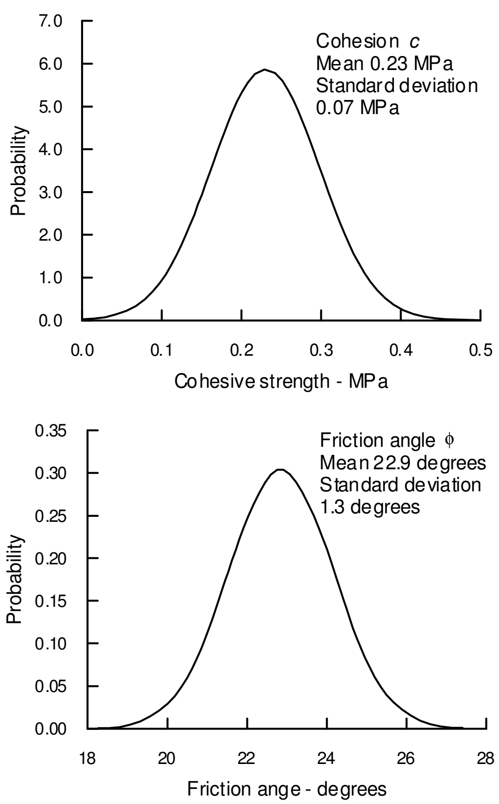

Fig. **18**: Normal distributions of cohesive strength and angle of friction for a heavily jointed rock mass.

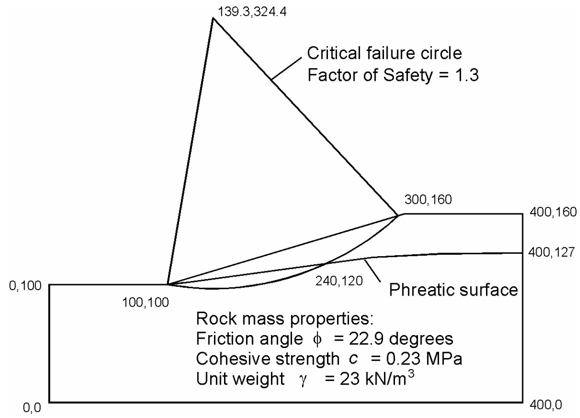

Fig. **19**: Slope and phreatic surface geometry, rock mass properties and critical failure surface for a homogeneous slope.

The geometry of the slope, with a height of 60 m and a slope face angle of 16.7 degrees, is defined in Figure 19. The program SLIDE[4] was used to carry out a critical failure surface search, using Bishop's circular failure analysis. Rosenbleuth's point estimate method (Hoek 1998, Harr 1987) was used to determine the mean and standard deviation of the normal distribution for the factor of the slope. This distribution is plotted in Figure 20.

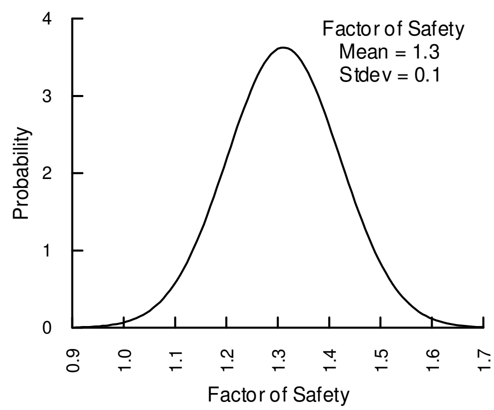

Fig. **20**: Normal distribution of the factor of safety of the slope defined in Figure 19.

[4] Available from Rocscience Inc., 31 Balsam Avenue, Toronto, Ontario, Canada M4E 3B5, Fax 1 416 698 0908, Email: software@rocscience.com, Internet: http://www.rocscience.com.

This plot shows that, for a mean factor of safety of 1.3 with a standard deviation of 0.1, the normal distribution curve extends from 0.9 to 1.7. This range is determined by the high quality of the input data. It was assumed that the uniaxial compressive strength of the intact rock as well as the material constant m_i were determined by laboratory testing and that the Geological Strength Index has been obtained by careful field observations by an experienced engineering geologist. Where poor quality input data is used for such an analysis, the mean value may be the same but the standard deviation and the range of factors of safety contained in the distribution curve will be much higher.

The probability of failure is defined by the ratio of the area under the curve for factors of safety of less than 1.0 divided by the total area under the normal distribution curve. As can be seen from Figure 20, this ratio is very small for the case considered. This suggests that, for this particular slope and for the quality of the input data used, a factor of safety of 1.3 will ensure that the risk of slope failure is negligible.

Finite failure risks are acceptable provided that they are considered in terms of the cost and consequences of failure. For example, a probability of failure of 10% may be acceptable in the case of an open pit bench or a logging road where traffic is restricted to trained personnel and where equipment is available to clear up the failure. On the other hand, this level of risk would be completely unacceptable for the abutment of a dam or the foundation of a high rise building.

Current technology for calculating the probability of failure, as described above, can only be used for relatively simple problems for which a deterministic solution can be obtained. As computer processing speeds increase, the application of these methods to more complex problems, such as the stability of underground excavations, will become feasible.

Note that other techniques are available for making an engineering risk assessment. These include the use of fault and decision tree analysis and some of these techniques are being applied to subjects such as the assessment of dam safety (Nielsen *et al* 1994). The huge societal and economic consequences of dam failures have attracted the attention of researchers in this field for many years and we can expect to see significant advances in risk analysis in the years to come (Anon. 1998).

Conclusion

Engineering design requires numbers. This is true whether the design utilises man-made materials such as steel or concrete or naturally occurring rocks and soils. One of the principal characteristics of natural materials is their variability and this makes it extremely difficult to assign reliable values to the properties required by engineering designers.

This paper has explored some of the methods that can be used by engineering geologists and geotechnical engineers to assess the geological factors that have an impact on engineering design. These start from the very crude estimates that are made during the early stages of a project on the basis of walk-over surveys and studies of available regional geology maps. At the other end of the spectrum are the input requirements of the very sophisticated numerical analyses used to assess the stability and support requirements for complex three-dimensional excavations in rock.

It is easy to conclude that there is never enough information and that, what there is, is unreliable because of the uncertainty associated with the methods of assigning numbers to geology. While these conclusions may be true they are not helpful to the design engineers who have to produce safe and economical designs, whether or not the information is adequate.

I have tried to demonstrate that it is possible to arrive at useable estimates of the properties required for an engineering design. This requires close co-operation between engineering geologists and geotechnical engineers and a good measure of common sense and practical judgement.

I would like to conclude with a statement contained in a general report presented almost 25 years ago: 'The responsibility of the design engineer is not to compute accurately but to judge soundly' (Hoek and Londe 1974). I consider that this statement is still true today.

Acknowledgements

The permission granted by the Chuquicamata Divion of Codelco, Chile, to publish the information contained in Figures 1, 2 and 3 is gratefully acknowledged. Similarly, permission from the Nathpa Jhakri Power Corporation, the Naptha Jhakri Joint Venture and Geodata S.p.A. to include details of tunnelling through the Daj

Khad stretch of the Nathpa Jhakri headrace tunnel is acknowledged.

I would also like to thank my wife Theo for her support and her help in proof-reading the manuscript of this paper.

References

Anon. 1998. Risk-based dam safety evaluations. Workshop report. *Intnl. J. Hydropower and Dams.* **5**(1), 89-97, **5**(2), .

Barton, N.R., Lien, R. and Lunde, J. 1974. Engineering classification of rock masses for the design of tunnel support. *Rock Mech.* **6**(4), 189-239.

Bhasin, R., Barton, N., Grimstad, E. and Chryssanthakis. P. 1996. Engineering geological characterisation of low strength anisotropic rocks in the Himalayan region for assessment of tunnel support. *Proc. Conf. Recent Advances in Tunnelling Technology.* New Delhi. 157-181.

Bieniawshi, Z.T. 1989. *Engineering Rock Mass Classification*. Wiley, New York.

Carrieri, G., Grasso, P., Mahtab, A. and Pelizza, S. 1991. Ten years of experience in the use of umbrella arch for tunnelling. *Proc. Societa Italiana Gallerie Conf. On Soil and Rock Improvement, Milan.* March 1991, Vol. 1, 99-111.

Fookes, P.G. 1997. Geology for Engineers: the Geological Model, Prediction and Performance. *Quarterly Journal of Engineering Geology,* **30**, 293-424.

Geological Survey of India. 1988. *A comprehensive geotechnical report of the studies carried out for Nathpa Jhakri Hydel Project, Shimla and Kinnaur Districts, Himachel Pradesh: Part I of II and II of II.* Compiled by Ashraf, Z. and Chowdhart, A.K., New Delhi.

Grasso, P., Mahtab, M.A., Rabajoli, G. and Pelizza, S. 1993. Consideration for design of shallow tunnels. *Proc. Infrastructures souterraines de transport, Toulon.* October 1993, 19-28.

Harr, M.E. 1987. *Reliability-based design in civil engineering*. New York: McGraw-Hill.

Hoek, E. 1998. Reliability of Hoek-Brown estimates of rock mass properties and their impact on design. *Int. J. Rock Mech. Min. Sci.* **35**(1), 63-68.

Hoek, E. and Brown, E.T. 1980. *Underground Excavations in Rock.* Institution of Mining and Metallurgy, London.

Hoek, E. and Brown, E.T. 1997. Practical estimates of rock mass strength. *Int. J. Rock Mech. Min. Sci.* **34**(8), 1165-1186.

Hoek, E. and Londe, P. 1974. The design of rock slopes and foundations. General Report on Theme III. *Proc. Third Congress Intnl. Soc. Rock Mech., Denver.* **1**(A), 613-752.

Hoek, E., Marinos, P. and Benessi, M. 1998. Applicability of the Geological Strength Index (GSI) classification for very weak and sheared rock masses. The case of the 'Athens Schist' system of formations. *Paper in preparation.*

Jalote, P.M., Kumar, A. and Kumar, V. 1996. Geotechniques applied in the design of the machine hall cavern, Nathpa Jhakri Hydel Project, N.W. Himalaya, India. *J. Engng. Geol. (India)* **XXV**(1-4), 181-192.

Nielsen, N.M., Hartford, D.N.D. and MacDonald. 1994. Selection of tolerable risk criteria for dam safety decision making. *Proc. 1994 Canadian Dam Safety Conference, Winnipeg, Manitoba.* Vancouver: BiTech Publishers, pp 355-369.

Pierson, L.A. and van Vickle, R. 1993. *Rockfall Hazard Rating System – Participants' Manual*. Federal Highway Administration Publication No. FHWA SA-93-057, Washington.

Russo, G., Kalamaras, G.S. and Grasso. P. 1998. A discussion on the concepts of : Geomechanical Classes, Behaviour Categories, and Technical Classes for an Underground Project. *Gallerie e Grandi Opre Sotterranee.* March 1998, No. 54, 41-51.

Sheorey, P.R. 1994. A theory for in situ stresses in isotropic and transversely isotropic rock. *Int. J. Rock Mech. Min. Sci. & Geomech. Abstr.* **31**(1), 23-34.

Zoback, M.L. 1992. First- and second-order patterns of stress in the lithosphere: the World Stress Map Project. *Journal of Geophysical Research.* **97**(B8), 11761-11782.

Estimating the geotechnical properties of heterogeneous rock masses such as Flysch

Paul Marinos and Evert Hoek

Paper published in *Bull. Engg. Geol. Env.* **60**, 85-92, 2001

Paper published in Bull. Engg. Geol. Env. 60, 85-92, 2001

Estimating the geotechnical properties of heterogeneous rock masses such as Flysch

Estimation des propriétés géotechniques des masses rocheuses hétérogènes, comme le flysch

Paul Marinos[1] and Evert Hoek[2]

Abstract

The design of tunnels and slopes in heterogeneous rock masses such as Flysch presents a major challenge to geologists and engineers. The complex structure of these materials, resulting from their depositional and tectonic history, means that they cannot easily be classified in terms of widely used rock mass classification systems. A methodology for estimating the Geological Strength Index and the rock mass properties for these geological formations is presented in this paper.

Résumé

L' étude des tunnels et des talus dans des masses rocheuses hétérogènes, comme le flysch représente un défi majeur pour les géologues et les ingénieurs. La complexité de ces formations, résultat de leur histoire de sédimentation et de leur mise en place tectonique, pose des problémes à leur classification par les systèmes reconnus des classifications géotechniques. Dans ce travail une méthodologie pour l' estimation du GSI et l' évaluation des propriétés des masses rocheuses de flysch, est présentée.

[1] Civil Engineering Department, National Technical University of Athens, Athens, Greece
[2] Consulting Engineer, Vancouver, Canada

Introduction

Many large civil engineering projects are currently under construction in countries where Flysch is a very common geological formation. The design of surface and underground excavations in these materials requires knowledge of the mechanical properties of the rock masses in which these excavations are carried out. The following paper presents a methodology for estimating these properties.

Estimation of rock mass properties

One of the most widely used criteria for estimating rock mass properties is that proposed by Hoek and Brown (1997) and this criterion, with specific adaptations to heterogeneous rock masses such as flysch, is briefly summarised in the following text.

This failure criteria should not be used when the rock mass consists of a strong blocky rock such as sandstone, separated by clay coated and slickensided bedding surfaces. The behaviour of such rock masses will be strongly anisotropic and will be controlled by the fact that the bedding planes are an order of magnitude weaker than any other features. In such rock masses the predominant failure mode will be gravitational falls of wedges or blocks of rock defined by the intersection of the weak bedding planes with other features which act as release surfaces. However, if the rock mass is heavily fractured, the continuity of the bedding surfaces will have been disrupted and the rock may behave as an isotropic mass.

In applying the Hoek and Brown criterion to "isotropic" rock masses, three parameters are required for estimating the strength and deformation properties. These are:

- the uniaxial compressive strength σ_{ci} of the "intact" rock elements that make up the rock mass (as described below, this value may not be the same of the obtained from a laboratory uniaxial compressive strength or UCS test),
- a constant m_i that defined the frictional characteristics of the component minerals in these rock elements, and
- the Geological Strength Index (GSI) that relates the properties of the intact rock elements to those of the overall rock mass.

These parameters are dealt with in the following sub-sections.

Uniaxial compressive strength σ_{ci} of intact rock

In dealing with heterogeneous rock masses such as flysch, it is extremely difficult to obtain a sample of "intact' core for uniaxial compressive testing in the laboratory. The typical appearance of such material in an outcrop, is illustrated in Figure 1.

Practically every sample obtained from rock masses such as that illustrated in Figure 1 will contain discontinuities in the form of bedding and schistosity planes or joints. Consequently, any laboratory tests carried out on core samples will result in a strength value that is lower than the uniaxial compressive strength σ_{ci} required for input into the Hoek-Brown criterion. Using the results of such tests in the will impose a double penalty on the strength (in addition to that imposed by GSI) and will give unrealistically low values for the rock mass strength.

Figure 1: Appearance of sheared siltstone flysch in an outcrop

In some special cases, where the rock mass is very closely jointed and where it has been possible to obtain undisturbed core samples, uniaxial compressive strength tests have been carried out directly on the "rock mass" (Jaeger, 1971). These tests require an extremely high level of skill on the part of the driller and the laboratory technician. The large-scale triaxial test facilities required for such testing are only available in a few laboratories in the world and it is generally not economical or practical considering such tests for routine engineering projects.

One of the few courses of action that can be taken to resolve this dilemma is to use the Point Load Test on samples in which the load can be applied normal to bedding or schistosity block samples. The specimens used for such testing can be either irregular pieces or pieces broken from the core as illustrated in Figure 2. The direction of loading should be as perpendicular to any weakness planes as possible and the fracture created by the test should not show any signs of having followed an existing discontinuity. It is strongly recommended that photographs of the specimens, both before and after testing, should accompany the laboratory report since these enable the user to judge the validity of the test results. The uniaxial compressive strength of the intact rock samples can be estimated, with a reasonable level of accuracy, by multiplying the point load index I_s by 24, where $I_s = P/D^2$. P is the load on the points and D is the distance between the points (Brown, 1981).

In the case of very weak and/or fissile rocks such as clayey shales or sheared siltstones, the indentation of the loading points may cause plastic deformation rather than fracture of the specimen. In such cases the Point Load Test does not give reliable results.

Where it is not possible to obtain samples for Point Load Testing, the only remaining alternative is to turn to a qualitative description of the rock material in order to estimate the uniaxial compressive strength of the intact rock. A table listing such a qualitative description is given in Table 1, based on Hoek and Brown (1997).

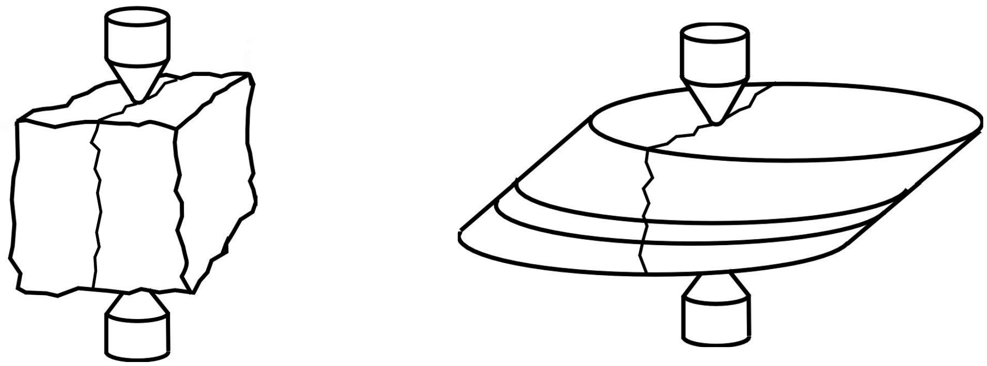

a. Test on sample chosen from surface exposure.

b. Test on sample broken from diamond drill core.

Figure 2: Point Load test options for intact rock samples from heterogeneous rock masses.

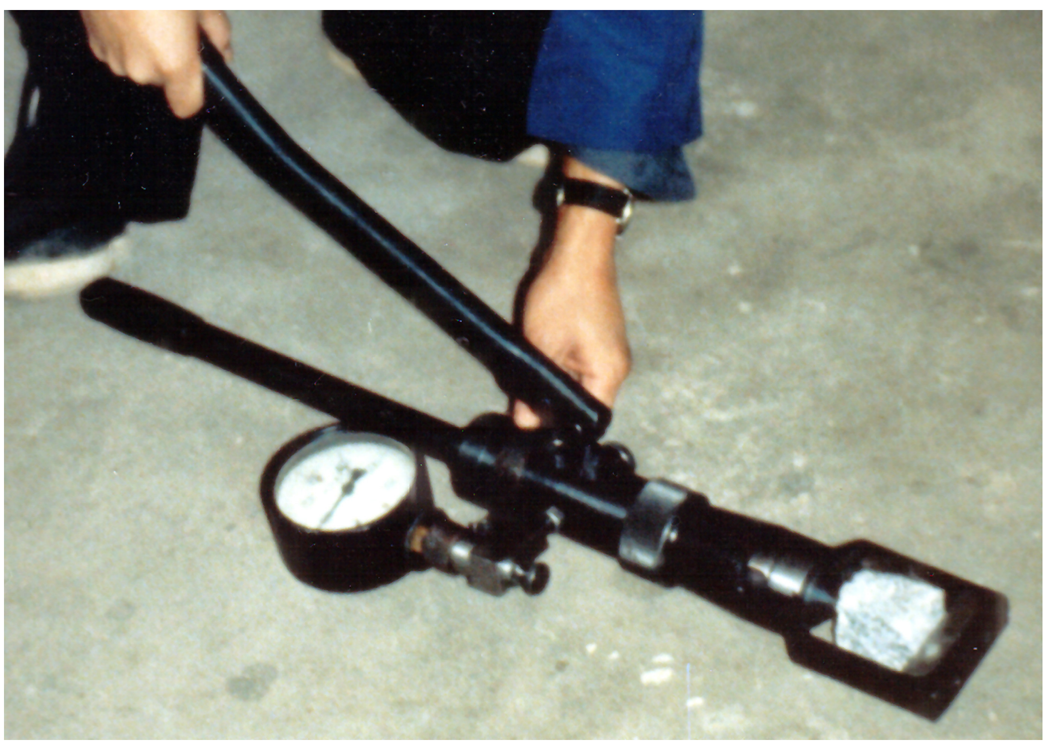

Figure 3: “Portable” point load test device for use in the field.

Table 1: Field estimates of uniaxial compressive strength of intact rock.

Grade*	Term	Uniaxial Comp. Strength (MPa)	Point Load Index (MPa)	Field estimate of strength	Examples
R6	Extremely Strong	> 250	>10	Specimen can only be chipped with a geological hammer	Fresh basalt, chert, diabase, gneiss, granite, quartzite
R5	Very strong	100 - 250	4 - 10	Specimen requires many blows of a geological hammer to fracture it	Amphibolite, sandstone, basalt, gabbro, gneiss, granodiorite, peridotite , rhyolite, tuff
R4	Strong	50 - 100	2 - 4	Specimen requires more than one blow of a geological hammer to fracture it	Limestone, marble, sandstone, schist
R3	Medium strong	25 - 50	1 - 2	Cannot be scraped or peeled with a pocket knife, specimen can be fractured with a single blow from a geological hammer	Concete, phyllite, schist, siltstone
R2	Weak	5 - 25	**	Can be peeled with a pocket knife with difficulty, shallow indentation made by firm blow with point of a geological hammer	Chalk, claystone, potash, marl, siltstone, shale, rocksalt,
R1	Very weak	1 - 5	**	Crumbles under firm blows with point of a geological hammer, can be peeled by a pocket knife	Highly weathered or altered rock, shale
R0	Extremely weak	0.25 - 1	**	Indented by thumbnail	Stiff fault gouge

* Grade according to Brown (1981).
** Point load tests on rocks with a uniaxial compressive strength below 25 MPa are likely to yield highly ambiguous results.

Constant m_i

The Hoek-Brown constant m_i can only be determined by triaxial testing on core samples or estimated from a qualitative description of the rock material as described by Hoek and Brown (1997). This parameter depends upon the frictional characteristics of the component minerals in the intact rock sample and it has a significant influence on the strength characteristics of rock.

When it is not possible to carry out triaxial tests, for the reasons discussed in the previous section, an estimate of m_i can be obtained from Table 2. Most of the values quoted have been derived from triaxial tests on intact core samples and the range of values shown is dependent upon the accuracy of the geological description of each rock type. For example, the term "granite" described a clearly defined rock type and all granites exhibit very similar mechanical characteristics. Hence the value of m_i is defined as 32 ± 3. On the other hand, the term "volcanic breccia" is not very precise in terms of mineral composition and hence the value of m_i is shown as 19 ± 5, denoting a higher level of uncertainty.

Fortunately, in terms of the estimation of rock mass strength, the value of the constant m_i is the least sensitive of the three parameters required. Consequently, the average values given in Table 2 are sufficiently accurate for most practical applications.

Geological Strength Index GSI

The Geological Strength Index (GSI) was introduced by Hoek, Kaiser and Bawden (1995), Hoek and Brown (1997) and extended by Hoek, Marinos and Benissi (1998). A chart for estimating the GSI for Flysch is presented in Table 3.

Mechanical properties of flysch

The term flysch is attributed to the geologist B. Studer and it comes from the German word "fliessen" meaning flow, probably denoting the frequent landslides in areas consisting of these formations.

Flysch consists of varying alternations of clastic sediments that are associated with orogenesis. It closes the cycle of sedimentation of a basin before the "arrival" of the poroxysme folding process. The clastic material derived from erosion of the previously formed neighbouring mountain ridge.

Flysch is characterised by rhythmic alternations of sandstone and fine grained (pelitic) layers. The sandstone may also include conglomerate beds. The fine grained layers contain siltstones, silty shales and clayey shales. Rarely and close to its margins, limestone beds or ophiolitic masses may be found. The thickness of the sandstone beds range from centimetres to metres. The siltstones and schists form layers of the same order but bedding discontinuities may be more frequent, depending upon the fissility of the sediments.

The overall thickness of the flysch is often very large (hundreds to a few thousand metres) albeit it may have been reduced considerably by erosion or by thrusting. The formation may contain different types of alterations and is often affected by reverse faults and thrusts. This, together with consequent normal faulting, results in a degradation of the geotechnical quality of the flysch rock mass. Thus, sheared or even chaotic rock masses can be found at the scale of a typical engineering design.

Table 2: Values of the constant m_i for intact rock, by rock group[3]. Note that values in parenthesis are estimates. The range of values quoted for each material depends upon the granularity and interlocking of the crystal structure – the higher values being associated with tightly interlocked and more frictional characteristics.

Rock type	Class	Group	Texture			
			Coarse	Medium	Fine	Very fine
SEDIMENTARY	Clastic		Conglomerates (21 ± 3) Breccias (19 ± 5)	Sandstones 17 ± 4	Siltstones 7 ± 2 Greywackes (18 ± 3)	Claystones 4 ± 2 Shales (6 ± 2) Marls (7 ± 2)
SEDIMENTARY	Non-Clastic	Carbonates	Crystalline Limestone (12 ± 3)	Sparitic Limestones (10 ± 2)	Micritic Limestones (9 ± 2)	Dolomites (9 ± 3)
SEDIMENTARY	Non-Clastic	Evaporites		Gypsum 8 ± 2	Anhydrite 12 ± 2	
SEDIMENTARY	Non-Clastic	Organic				Chalk 7 ± 2
METAMORPHIC	Non Foliated		Marble 9 ± 3	Hornfels (19 ± 4) Metasandstone (19 ± 3)	Quartzites 20 ± 3	
METAMORPHIC	Slightly foliated		Migmatite (29 ± 3)	Amphibolites 26 ± 6	Gneiss 28 ± 5	
METAMORPHIC	Foliated*			Schists 12 ± 3	Phyllites (7 ± 3)	Slates 7 ± 4
IGNEOUS	Plutonic	Light	Granite 32 ± 3 Granodiorite (29 ± 3)	Diorite 25 ± 5		
IGNEOUS	Plutonic	Dark	Gabbro 27 ± 3 Norite 20 ± 5	Dolerite (16 ± 5)		
IGNEOUS	Hypabyssal		Porphyries (20 ± 5)		Diabase (15 ± 5)	Peridotite (25 ± 5)
IGNEOUS	Volcanic	Lava		Rhyolite (25 ± 5) Andesite 25 ± 5	Dacite (25 ± 3) Basalt (25 ± 5)	
IGNEOUS	Volcanic	Pyroclastic	Agglomerate (19 ± 3)	Volcanic breccia (19 ± 5)	Tuff (13 ± 5)	

* These values are for intact rock specimens tested normal to bedding or foliation. The value of m_i will be significantly different if failure occurs along a weakness plane.

[3] Note that this table contains several changes from previously published versions, These changes have been made to reflect data that has been accumulated from laboratory tests and the experience gained from discussions with geologists and engineering geologists.

Table 3. GSI estimates for heterogeneous rock masses such as Flysch.

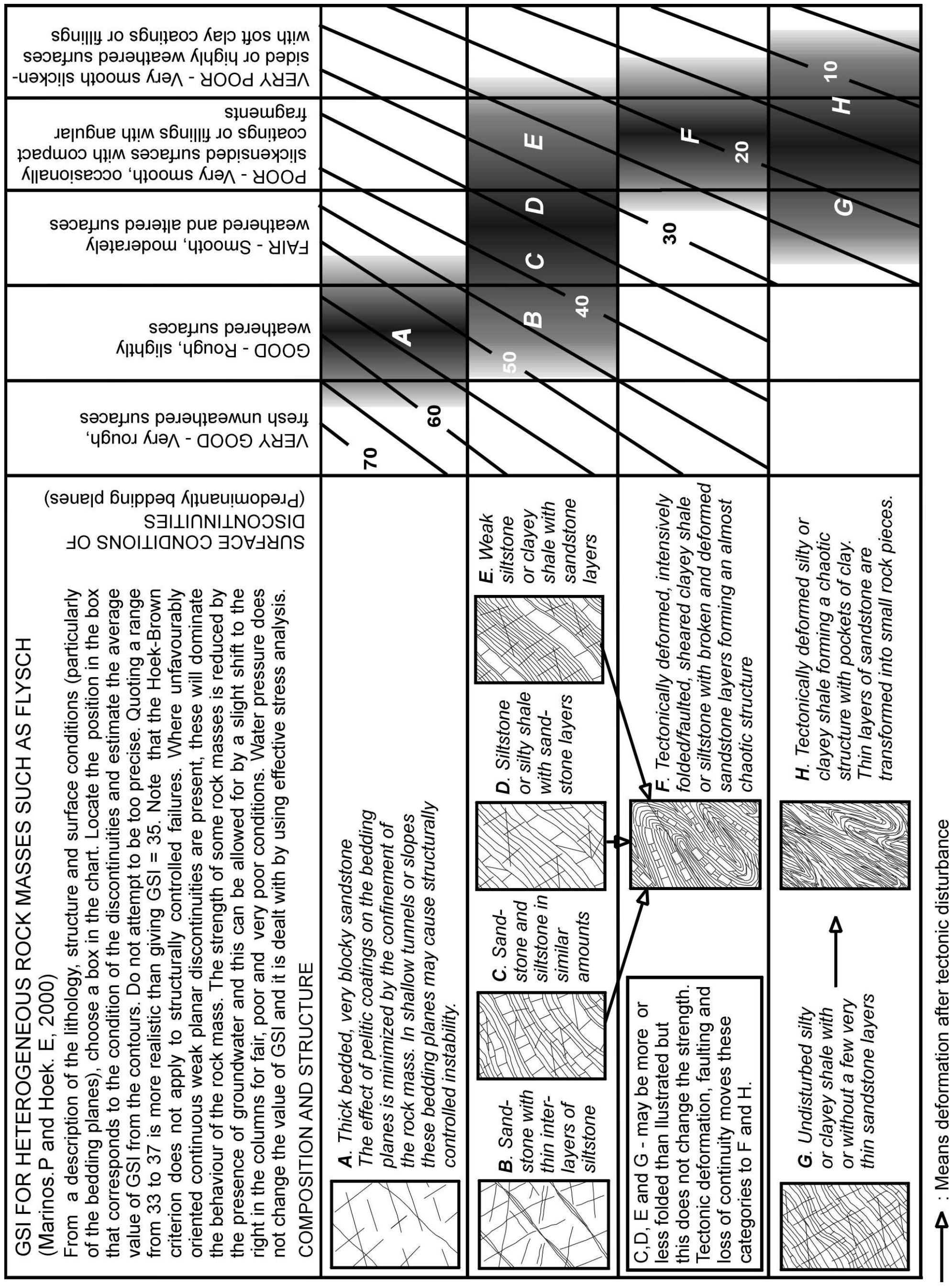

Geotechincally, a flysch rock mass has the following characteristics:

- Heterogeneity: alterations of competent and incompetent members,
- Presence of clay minerals,
- Tectonic fatigue and sheared discontinuities, often resulting in a soil-like material,
- Permeability of flysch rock masses is generally low and, because of the presence of clay minerals, the rock mass may be weakened to a significant degree where free drainage is not present.

Molasse is a term that is used to define a rock mass of similar composition but of post-orogenic origin associated with newly formed mountain ridges. It has the same alternations of strong (sandstones and conglomerates) and weak (marls, siltstones and claystones) but there is no compressional disturbance.

Determination of the Geological Strength Index for these rock masses, composed of frequently tectonically disturbed alternations of strong and weak rocks, presents some special challenges. However, because of the large number of engineering projects under construction in these rock masses, some attempt has to be made to provide better engineering geology tools than those currently available. Hence, in order to accommodate this group of materials in the GSI system, a chart for estimating this parameter has been developed and is presented in Table 3.

Influence of groundwater

The most basic impact of groundwater is upon the mechanical properties of the intact rock components of the rock mass. This is particularly important when dealing with shales, siltstones and similar rocks that are susceptible to changes in moisture content. Many of these materials will disintegrate very quickly if they are allowed to dry out after removal from the core barrel. For this reason testing of the “intact” rock to determine the uniaxial compressive strength σ_{ci} (see above) and the constant m_i must be carried out under conditions that are as close to the in situ moisture conditions as possible. Ideally, a field laboratory should be set up very close to the drill rig and the core prepared and tested immediately after recovery.

In one example in which a siltstone was being investigated for the construction of a power tunnel for a hydroelectric project, cores were carefully sealed in aluminium foil and wax and then transported to a laboratory in which very high quality testing could be carried out. In spite of these precautions, the deterioration of the specimens was such that the test results were meaningless. Consequently, a second investigation program was carried out in which the specimens were transported to a small laboratory about 5 kilometres from the exploration site and the samples were tested within an hour of having been removed from the core barrel. The results of this second series of tests gave very consistent results and values of uniaxial compressive strength σ_{ci} and constant m_i that were considered reliable.

When laboratory testing is not possible, point load tests, using equipment similar to that illustrated in Figure 3, should be carried out as soon after core recovery as possible in order to ensure that the moisture content of the sample is close to the in situ conditions.

Examples of typical Flysch.

In order to assist the reader in using Table 3, examples of typical Flysch outcrops are given in the photographs reproduced in Figure 4.

Figure 4 A. Thick bedded blocky sandstone. Note that structural failure can occur when dip of bedding planes is unfavourable.

Figure 4 B. Sandstone with thin siltstone layers. Small scale structural failures can occur when bedding dip is unfavourable.

Figure 4 C. Sandstone and siltstone in equal proportions

Figure 4 D. Siltstone or silty shale with sandstone

Figure 4 E. Weak siltstone or clayey shale with sandstone layers

Figure F. Tectonically deformed clayey shale or siltstone with broken sandstone

Figure 4 G. Undisturbed silty or clayey shale with a few thin sandstone layers

Figure 4 H. Tectonically deformed clayey shale

Figure 4: Examples of Flysch corresponding to descriptions in Table 3.

Selection of σ_{ci} and m_i for Flysch

In addition to the GSI values presented in Table 3, it is necessary to consider the selection of the other "intact" rock properties σ_{ci} and m_i for heterogeneous rock masses such as Flysch. Because the sandstone layers or usually separated from each other by weaker layers of siltstone or shales, rock-to-rock contact between blocks of sandstone may be limited. Consequently, it is not appropriate to use the properties of the sandstone to determine the overall strength of the rock mass. On the other hand, using the "intact" properties of the siltstone or shale only is too conservative since the sandstone skeleton certainly contributes to the rock mass strength. Therefore, it is proposed that a 'weighted average' of the intact strength properties of the strong and weak layers should be used. Suggested values for the components of this weighted average are given in Table 4.

Table 4: Suggested proportions of parameters σ_{ci} and m_i for estimating rock mass properties for Flysch.

Flysch type see Table 4.	Proportions of values for each rock type to be included in rock mass property determination
A and B	Use values for sandstone beds
C	Reduce sandstone values by 20% and use full values for siltstone
D	Reduce sandstone values by 40% and use full values for siltstone
E	Reduce sandstone values by 40% and use full values for siltstone
F	Reduce sandstone values by 60% and use full values for siltstone
G	Use values for siltstone or shale
H	Use values for siltstone or shale

Estimating rock mass properties

Having defined the parameters σ_{ci}, m_i and GSI as described above, the next step is to estimate the mechanical properties of the rock mass. The procedure making these estimates has been described in detail by Hoek and Brown (1997) it will not be repeated here. A spreadsheet for carrying out these calculations is given in Table 5.

Deep tunnels

For tunnels at depths of greater than 30 m, the rock mass surrounding the tunnel is confined and its properties are calculated on the basis of a minor principal stress or confining pressure σ_3 up to 0.25 σ_{ci}, in accordance with the procedure defined by Hoek and Brown (1997).

For the case of "deep" tunnels, equivalent Mohr Coulomb cohesive strengths and friction angles together with the uniaxial compressive strength σ_{cm} and the deformation modulus *E* of the rock mass can be estimated by means of the spreadsheet given in Table 5 by entering any depth greater than 30 m.

Shallow tunnels and slopes

For shallow tunnel and slopes in which the degree of confinement is reduced, a minor principal stress range of $0 < \sigma_3 < \sigma_v$ is used, where σ_v = depth x unit weight of the rock mass. In this case, depth is defined as the depth below surface of the tunnel crown or the average depth of a failure surface in a slope in which a circular type can be assumed, i.e. where the failure is not structurally controlled.

In the case of shallow tunnels or slopes, the spreadsheet presented in Table 5 allows the user to enter the depth below surface and the unit weight of the rock mass. The vertical stress σ_v calculated from the product of these two quantities is then used to calculate the rock mass properties.

Table 5: Spreadsheet for the calculation of rock mass properties

Input:

sigci =	10	MPa	mi =	10		GSI =	30	
Depth of failure surface or tunnel below slope* =				25	m	Unit wt. =	0.027	MN/n3

Output:

stress =	0.68	MPa	mb =	0.82		s =	0.0004	
a =	0.5		sigtm =	-0.0051	MPa	A =	0.4516	
B =	0.7104		k =	3.95		phi =	36.58	degrees
coh =	0.136	MPa	sigcm =	0.54	MPa	E =	1000.0	MPa

Calculation:

									Sums
sig3	1E-10	0.10	0.19	0.29	0.39	0.48	0.58	0.68	2.70
sig1	0.20	1.01	1.47	1.84	2.18	2.48	2.77	3.04	14.99
ds1ds3	21.05	5.50	4.22	3.64	3.29	3.05	2.88	2.74	46.36
sign	0.01	0.24	0.44	0.62	0.80	0.98	1.14	1.31	5.54
tau	0.04	0.33	0.50	0.64	0.76	0.86	0.96	1.05	5.14
x	-2.84	-1.62	-1.35	-1.20	-1.09	-1.01	-0.94	-0.88	-10.94
y	-2.37	-1.48	-1.30	-1.19	-1.12	-1.06	-1.02	-0.98	-10.53
xy	6.74	2.40	1.76	1.43	1.22	1.07	0.96	0.86	16.45
xsq	8.08	2.61	1.83	1.44	1.19	1.02	0.88	0.78	17.84
sig3sig1	0.00	0.10	0.28	0.53	0.84	1.20	1.60	2.05	7
sig3sq	0.00	0.01	0.04	0.08	0.15	0.23	0.33	0.46	1
taucalc	0.04	0.32	0.49	0.63	0.76	0.87	0.97	1.07	
sig1sig3fit	0.54	0.92	1.30	1.68	2.06	2.45	2.83	3.21	
signtaufit	0.14	0.31	0.46	0.60	0.73	0.86	0.98	1.11	

Cell formulae:

σ_n	stress =	if(depth>30, sigci*0.25,depth*unitwt*0.25)
m_b	mb =	mi*EXP((GSI-100)/28)
s	s =	IF(GSI>25,EXP((GSI-100)/9),0)
a	a =	IF(GSI>25,0.5,0.65-GSI/200)
σ_{tm}	sigtm =	0.5*sigci*(mb-SQRT(mb^2+4*s))
σ_3	sig3 =	Start at 1E-10 (to avoid zero errors) and increment in 7 steps of stress/28 to stress/4
σ_1	sig1 =	sig3+sigci*(((mb*sig3)/sigci)+s)^a
$\delta\sigma_1/\delta\sigma_3$	ds1ds3 =	IF(GSI>25,(1+(mb*sigci)/(2*(sig1-sig3))),1+(a*mb^a)*(sig3/sigci)^(a-1))
σ_n	sign =	sig3+(sig1-sig3)/(1+ds1ds3)
τ	tau =	(sign-sig3)*SQRT(ds1ds3)
x	x =	LOG((sign-sigtm)/sigci)
y	y =	LOG(tau/sigci)
	xy =	x*y x sq = x^2
A	A =	acalc = 10^(sumy/8 - bcalc*sumx/8)
B	B =	bcalc = (sumxy - (sumx*sumy)/8)/(sumxsq - (sumx^2)/8)
k	k =	(sumsig3sig1 - (sumsig3*sumsig1)/8)/(sumsig3sq-(sumsig3^2)/8)
ϕ	phi =	ASIN((k-1)/(k+1))*180/PI()
c	coh =	sigcm/(2*SQRT(k))
σ_{cm}	sigcm =	sumsig1/8 - k*sumsig3/8
E	E =	IF(sigci>100,1000*10^((GSI-10)/40),SQRT(sigci/100)*1000*10^((GSI-10)/40))
	phit =	(ATAN(acalc*bcalc*((signt-sigtm)/sigci)^(bcalc-1)))*180/PI()
	coht =	acalc*sigci*((signt-sigtm)/sigci)^bcalc-signt*TAN(phit*PI()/180)
	sig3sig1=	sig3*sig1 sig3sq = sig3^2
	taucalc =	acalc*sigci*((sign-sigtm)/sigci)^bcalc
	s3sifit =	sigcm+k*sig3
	sntaufit =	coh+sign*TAN(phi*PI()/180)

* For depths below surface of less than 30 m, the average stress on the failure surface is calculated by the spreadsheet. For depths greater than 30 m the average stress level is kept constant at the value for 30 m depth.

The example included in Table 5 is for a rock mass with an intact rock strength σ_{ci} = 10 MPa, a constant m_i = 10 and a Geological Strength value of GSI = 30. The depth below surface is 25 m. The estimated properties for this rock mass are a cohesive strength c = 0.136 MPa, a friction angle ϕ = 36.6°, a rock mass compressive strength σ_{cm} = 0.54 MPa and a deformation modulus E = 1000 MPa.

Acknowledgements

The development of the methodology presented in this paper was carried out by the authors as part of their consulting services to Egnatia Odos S.A., an organisation responsible for the design and construction of a 680 km highway across northern Greece. Particular acknowledgements are due to Mr Nikos Kazilis, head of the tunnelling department of Egnatia Odos S.A, Mr George Agistalis, Mr Nikos Syrtariotis and Miss Maria Benissi for their assistance of in the preparation of this paper.

References

Brown E.T. (Ed). 1981. Rock characterization, testing and monitoring - ISRM suggested methods, 171-183. Oxford, Pergamon.

Hoek E., Kaiser P.K. and Bawden W.F. 1995. *Support of underground excavations in hard rock*. Rotterdam, Balkema.

Hoek, E. and Brown, E.T. 1997. Practical estimates or rock mass strength. *Int. J. Rock Mech. & Mining Sci. & Geomechanics Abstracts.* **34**(8), 1165-1186.

Hoek, E., Marinos, P. and Benissi, M. (1998) Applicability of the Geological Strength Index (GSI) classification for very weak and sheared rock masses. The case of the Athens Schist Formation. *Bull. Engg. Geol. Env.* 57(2), 151-160.

Jaeger, J.C. 1971. Friction of rocks and stability of rock slopes. The 11th Rankine Lecture. *Géotechnique* **21**(2), 97-134.

Rock mass properties for underground mines

Evert Hoek

Published in *Underground Mining Methods: Engineering Fundamentals and International Case Studies.* (Edited by W. A. Hustrulid and R. L. Bullock), Litleton, Colorado: Society for Mining, Metallurgy, and Exploration (SME) 2001

Rock mass properties for underground mines

Evert Hoek*

1.1 INTRODUCTION

Reliable estimates of the strength and deformation characteristics of rock masses are required for almost any form of analysis used for the design of underground excavations. Hoek and Brown (1980a, 1980b) proposed a method for obtaining estimates of the strength of jointed rock masses, based upon an assessment of the interlocking of rock blocks and the condition of the surfaces between these blocks. This method was modified over the years in order to meet the needs of users who applied it to problems that were not considered when the original criterion was developed (Hoek 1983, Hoek and Brown 1988). The application of the method to very poor quality rock masses required further changes (Hoek, Wood and Shah 1992) and, eventually, the development of a new classification called the Geological Strength Index (Hoek 1994, Hoek, Kaiser and Bawden 1995, Hoek and Brown 1997, Hoek, Marinos and Benissi (1998)). A review of the development of the criterion and of the equations proposed at various stages in this development is given in Hoek and Brown (1997).

This chapter presents the Hoek-Brown criterion in a form that has been found practical in the field and that appears to provide the most reliable set of results for use as input for methods of analysis currently used in rock engineering.

1.2 GENERALISED HOEK-BROWN CRITERION

The Generalised Hoek-Brown failure criterion for jointed rock masses is defined by:

$$\sigma_1' = \sigma_3' + \sigma_{ci}\left(m_b \frac{\sigma_3'}{\sigma_{ci}} + s\right)^a \tag{1.1}$$

where σ_1' and σ_3' are the maximum and minimum effective stresses at failure,

m_b is the value of the Hoek-Brown constant m for the rock mass,

s and a are constants which depend upon the rock mass characteristics, and

σ_{ci} is the uniaxial compressive strength of the intact rock pieces.

The Mohr envelope, relating normal and shear stresses, can be determined by the method proposed by Hoek and Brown (1980a). In this approach, equation 1.1 is used

* Consulting engineer, Vancouver, Canada.

to generate a series of triaxial test values, simulating full scale field tests, and a statistical curve fitting process is used to derive an equivalent Mohr envelope defined by the equation:

$$\tau = A\sigma_{ci}\left(\frac{\sigma_n' - \sigma_{tm}}{\sigma_{ci}}\right)^B \tag{1.2}$$

where A and B are material constants

σ_n' is the normal effective stress, and

σ_{tm} is the 'tensile' strength of the rock mass.

In order to use the Hoek-Brown criterion for estimating the strength and deformability of jointed rock masses, three 'properties' of the rock mass have to be estimated. These are

1. the uniaxial compressive strength σ_{ci} of the intact rock elements,
2. the value of the Hoek-Brown constant m_i for these intact rock elements, and
3. the value of the Geological Strength Index *GSI* for the rock mass.

1.3 INTACT ROCK PROPERTIES

For the intact rock pieces that make up the rock mass equation 1.1 simplifies to:

$$\sigma_1' = \sigma_3' + \sigma_{ci}\left(m_i \frac{\sigma_3'}{\sigma_{ci}} + 1\right)^{0.5} \tag{1.3}$$

The relationship between the principal stresses at failure for a given rock is defined by two constants, the uniaxial compressive strength σ_{ci} and a constant m_i. Wherever possible the values of these constants should be determined by statistical analysis of the results of a set of triaxial tests on carefully prepared core samples. When laboratory tests are not possible, Table 1.1 and Table 1.2 can be used to obtain estimates of σ_{ci} and m_i.

In the case of mineralised rocks, the effects of alteration can have a significant impact on the properties of the intact rock components and this should be taken into account in estimating the values of σ_{ci} and m_i. For example, the influence of quartz-seritic alteration of andesite and porphyry is illustrated in the Figure 1.1, based upon data provided by Karzulovic (2000). Similar trends have been observed for other forms of alteration and, where this type of effect is considered likely, the geotechnical engineer would be well advised to invest in a program of laboratory testing to establish the appropriate properties for the intact rock.

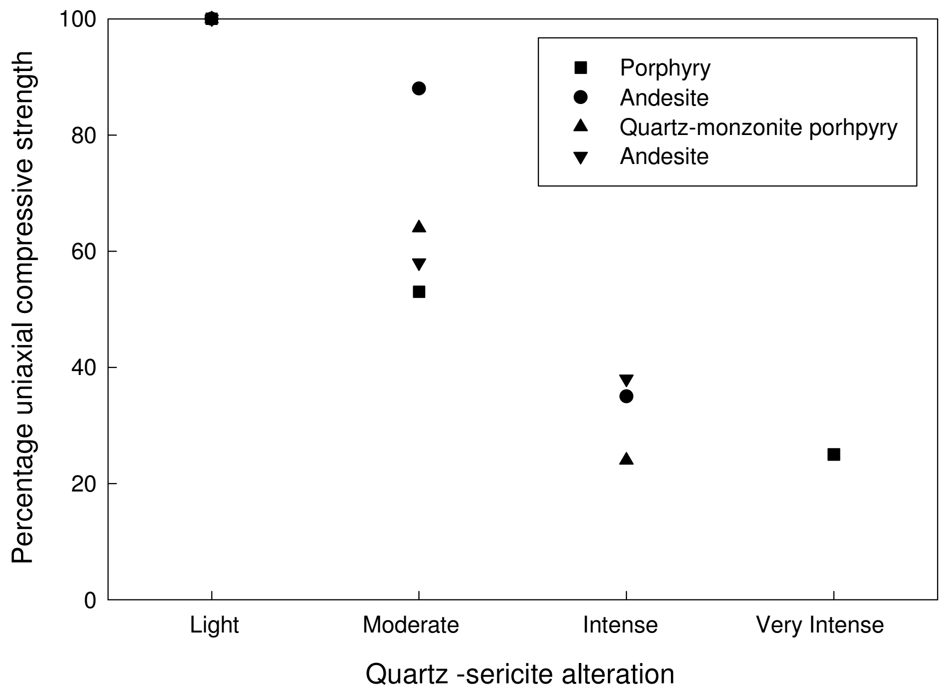

Figure 1.1: Influence of quartz-seritic alteration on the uniaxial compressive strength of "intact" specimens of andesite and porphyry. (After Karzulovic, 2000)

The Hoek-Brown failure criterion, which assumes isotropic rock and rock mass behaviour, should only be applied to those rock masses in which there are a sufficient number of closely spaced discontinuities, with similar surface characteristics, that isotropic behaviour involving failure on multiple discontinuities can be assumed. When the structure being analysed is large and the block size small in comparison, the rock mass can be treated as a Hoek-Brown material.

Where the block size is of the same order as that of the structure being analysed or when one of the discontinuity sets is significantly weaker than the others, the Hoek-Brown criterion should not be used. In these cases, the stability of the structure should be analysed by considering failure mechanisms involving the sliding or rotation of blocks and wedges defined by intersecting structural features. Figure 1.2 summarises these statements in a graphical form.

1.4 GEOLOGICAL STRENGTH INDEX

The strength of a jointed rock mass depends on the properties of the intact rock pieces and also upon the freedom of these pieces to slide and rotate under different stress conditions. This freedom is controlled by the geometrical shape of the intact rock pieces as well as the condition of the surfaces separating the pieces. Angular rock pieces with clean, rough discontinuity surfaces will result in a much stronger rock mass than one which contains rounded particles surrounded by weathered and altered material.

Table 1.1: Field estimates of uniaxial compressive strength.

Grade*	Term	Uniaxial Comp. Strength (MPa)	Point Load Index (MPa)	Field estimate of strength	Examples
R6	Extremely Strong	> 250	>10	Specimen can only be chipped with a geological hammer	Fresh basalt, chert, diabase, gneiss, granite, quartzite
R5	Very strong	100 - 250	4 - 10	Specimen requires many blows of a geological hammer to fracture it	Amphibolite, sandstone, basalt, gabbro, gneiss, granodiorite, peridotite , rhyolite, tuff
R4	Strong	50 - 100	2 - 4	Specimen requires more than one blow of a geological hammer to fracture it	Limestone, marble, sandstone, schist
R3	Medium strong	25 - 50	1 - 2	Cannot be scraped or peeled with a pocket knife, specimen can be fractured with a single blow from a geological hammer	Concete, phyllite, schist, siltstone
R2	Weak	5 - 25	**	Can be peeled with a pocket knife with difficulty, shallow indentation made by firm blow with point of a geological hammer	Chalk, claystone, potash, marl, siltstone, shale, rocksalt,
R1	Very weak	1 - 5	**	Crumbles under firm blows with point of a geological hammer, can be peeled by a pocket knife	Highly weathered or altered rock, shale
R0	Extremely weak	0.25 - 1	**	Indented by thumbnail	Stiff fault gouge

* Grade according to Brown (1981).

** Point load tests on rocks with a uniaxial compressive strength below 25 MPa are likely to yield highly ambiguous results.

Table 1.2: Values of the constant m_i for intact rock, by rock group. Note that values in parenthesis are estimates.

Rock type	Class	Group	Texture: Coarse	Texture: Medium	Texture: Fine	Texture: Very fine
SEDIMENTARY	Clastic		Conglomerates (21 ± 3) Breccias (19 ± 5)	Sandstones 17 ± 4	Siltstones 7 ± 2 Greywackes (18 ± 3)	Claystones 4 ± 2 Shales (6 ± 2) Marls (7 ± 2)
SEDIMENTARY	Non-Clastic	Carbonates	Crystalline Limestone (12 ± 3)	Sparitic Limestones (10 ± 2)	Micritic Limestones (9 ± 2)	Dolomites (9 ± 3)
SEDIMENTARY	Non-Clastic	Evaporites		Gypsum 8 ± 2	Anhydrite 12 ± 2	
SEDIMENTARY	Non-Clastic	Organic				Chalk 7 ± 2
METAMORPHIC	Non Foliated		Marble 9 ± 3	Hornfels (19 ± 4) Metasandstone (19 ± 3)	Quartzites 20 ± 3	
METAMORPHIC	Slightly foliated		Migmatite (29 ± 3)	Amphibolites 26 ± 6		
METAMORPHIC	Foliated*		Gneiss 28 ± 5	Schists 12 ± 3	Phyllites (7 ± 3)	Slates 7 ± 4
IGNEOUS	Plutonic	Light	Granite 32 ± 3 Granodiorite (29 ± 3)	Diorite 25 ± 5		
IGNEOUS	Plutonic	Dark	Gabbro 27 ± 3 Norite 20 ± 5	Dolerite (16 ± 5)		
IGNEOUS	Hypabyssal		Porphyries (20 ± 5)		Diabase (15 ± 5)	Peridotite (25 ± 5)
IGNEOUS	Volcanic	Lava		Rhyolite (25 ± 5) Andesite 25 ± 5	Dacite (25 ± 3) Basalt (25 ± 5)	Obsidian (19 ± 3)
IGNEOUS	Volcanic	Pyroclastic	Agglomerate (19 ± 3)	Breccia (19 ± 5)	Tuff (13 ± 5)	

* These values are for intact rock specimens tested normal to bedding or foliation. The value of m_i will be significantly different if failure occurs along a weakness plane.

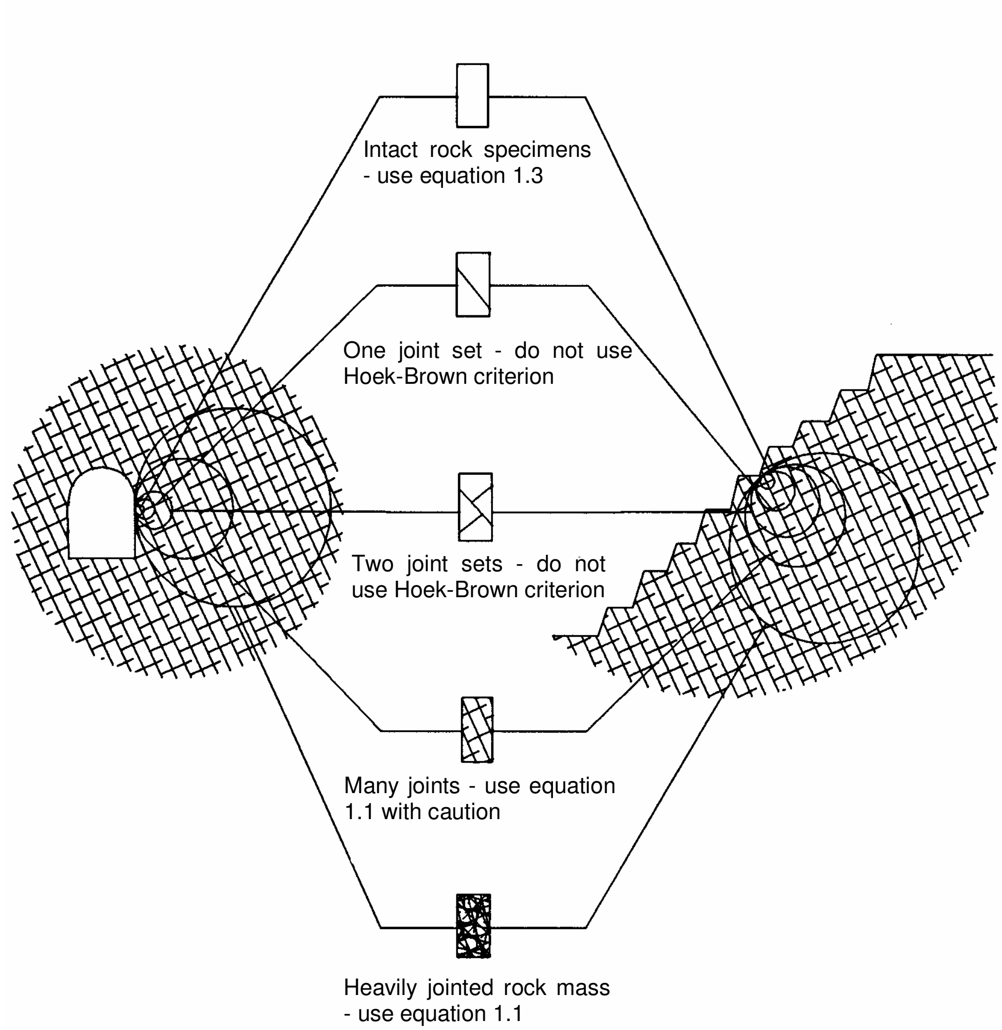

Figure 1.2: Idealised diagram showing the transition from intact to a heavily jointed rock mass with increasing sample size.

The Geological Strength Index (GSI), introduced by Hoek (1994) and Hoek, Kaiser and Bawden (1995) provides a system for estimating the reduction in rock mass strength for different geological conditions. This system is presented in Table 1.3, for blocky rock masses, and Table 1.4 for schistose metamorphic rocks.

Once the Geological Strength Index has been estimated, the parameters that describe the rock mass strength characteristics, are calculated as follows:

$$m_b = m_i \exp\left(\frac{GSI - 100}{28}\right) \tag{1.4}$$

For GSI > 25, i.e. rock masses of good to reasonable quality:

$$s = \exp\left(\frac{GSI - 100}{9}\right) \tag{1.5}$$

and

$$a = 0.5 \tag{1.6}$$

For GSI < 25, i.e. rock masses of very poor quality:

$$s = 0 \tag{1.7}$$

and

$$a = 0.65 - \frac{GSI}{200} \tag{1.8}$$

For better quality rock masses (GSI > 25), the value of GSI can be estimated directly from the 1976 version of Bieniawski's Rock Mass Rating, with the Groundwater rating set to 10 (dry) and the Adjustment for Joint Orientation set to 0 (very favourable) (Bieniawski 1976). For very poor quality rock masses the value of RMR is very difficult to estimate and the balance between the ratings no longer gives a reliable basis for estimating rock mass strength. Consequently, Bieniawski's RMR classification should not be used for estimating the GSI values for poor quality rock masses (RMR < 25) and the GSI charts should be used directly.

If the 1989 version of Bieniawski's RMR classification (Bieniawski 1989) is used, then GSI = RMR_{89}' - 5 where RMR_{89}' has the Groundwater rating set to 15 and the Adjustment for Joint Orientation set to zero.

1.5 MOHR-COULOMB PARAMETERS

Most geotechnical software is written in terms of the Mohr-Coulomb failure criterion in which the rock mass strength is defined by the cohesive strength c' and the angle of friction ϕ'. The linear relationship between the major and minor principal stresses, σ_1' and σ_3', for the Mohr-Coulomb criterion is

$$\sigma_1' = \sigma_{cm} + k\sigma_3' \tag{1.9}$$

where σ_{cm} is the uniaxial compressive strength of the rock mass and k is the slope of the line relating σ_1' and σ_3'. The values of ϕ' and c' can be calculated from

$$\sin\phi' = \frac{k-1}{k+1} \tag{1.10}$$

$$c' = \frac{\sigma_{cm}(1 - \sin\phi')}{2\cos\phi'} \tag{1.11}$$

Table 1.3: Characterisation of a blocky rock masses on the basis of particle interlocking and discontinuity condition. After Hoek, Marinos and Benissi (1998).

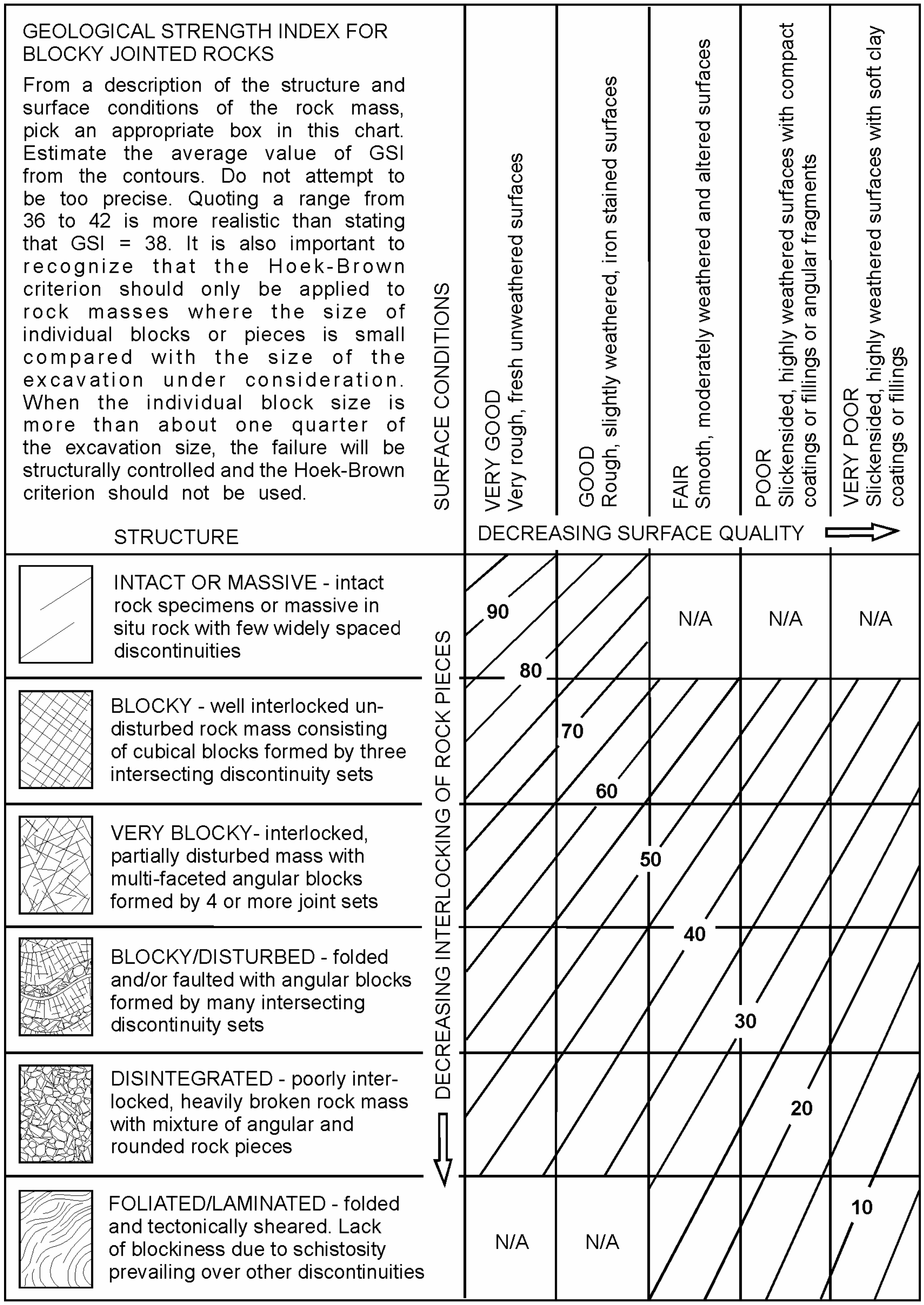

Table 1.4: Characterisation of a schistose metamorphic rock masses on the basis of foliation and discontinuity condition. (After M. Truzman, 1999)

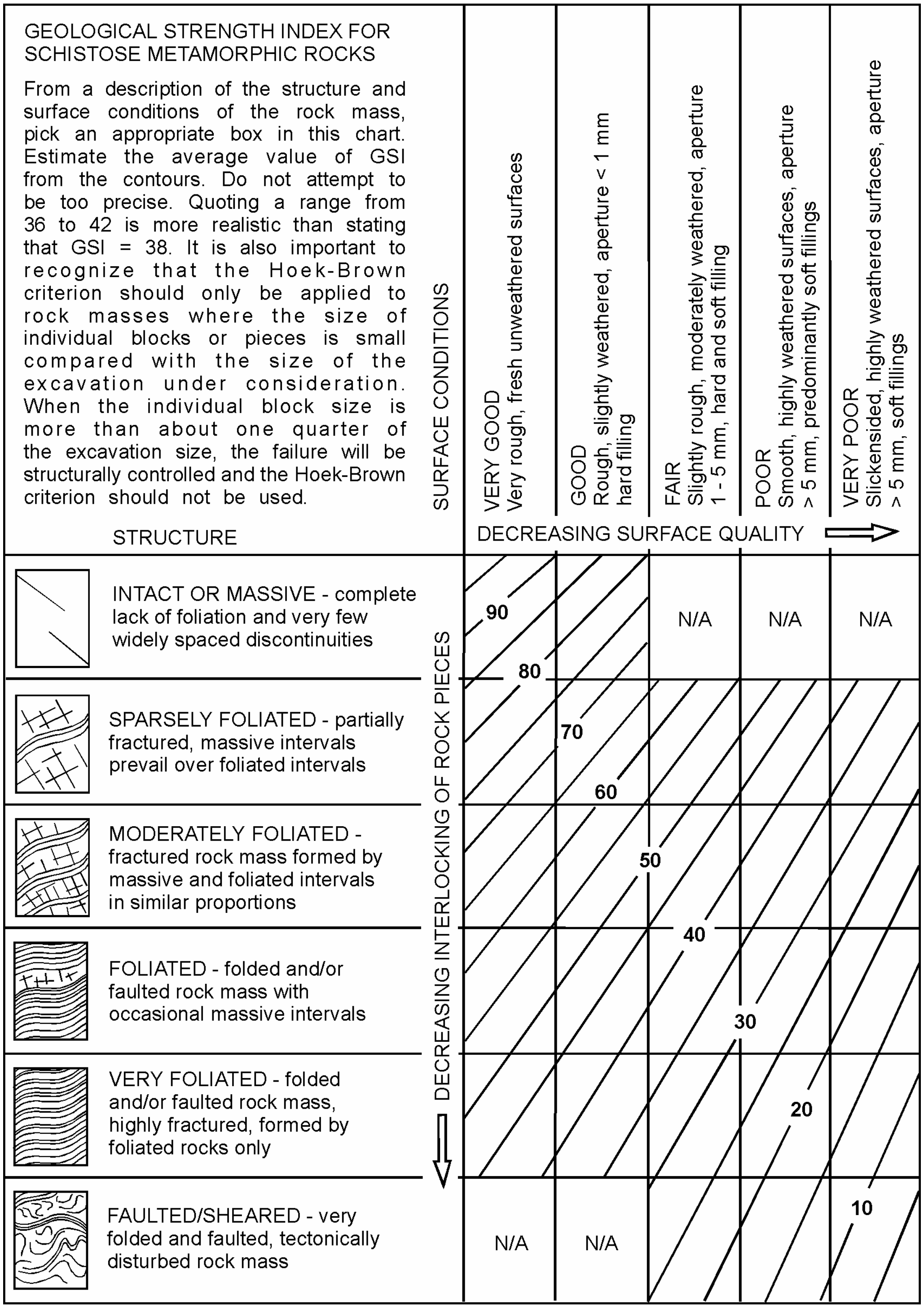

There is no direct correlation between equation 1.9 and the non-linear Hoek-Brown criterion defined by equation 1.1. Consequently, determination of the values of c' and ϕ' for a rock mass that has been evaluated as a Hoek-Brown material is a difficult problem.

Having considered a number of possible approaches, it has been concluded that the most practical solution is to treat the problem as an analysis of a set of full-scale triaxial strength tests. The results of such tests are simulated by using the Hoek-Brown equation 1.1 to generate a series of triaxial test values. Equation 1.9 is then fitted to these test results by linear regression analysis and the values of c' and ϕ' are determined from equations 1.11 and 1.10. A full discussion on the steps required to carry out this analysis is presented in the Appendix, together with a spreadsheet for implementing this analysis.

The range of stresses used in the curve fitting process described above is very important. For the confined conditions surrounding tunnels at depths of more than about 30 m, the most reliable estimates are given by using a confining stress range from zero to $0.25\sigma_{ci}$, where σ_{ci} is the uniaxial compressive strength of the intact rock elements. A series of plots showing the uniaxial compressive strength of the rock mass σ_{cm}, the cohesive strength c and the friction angle ϕ are given in Figures 1.3 and 1.4.

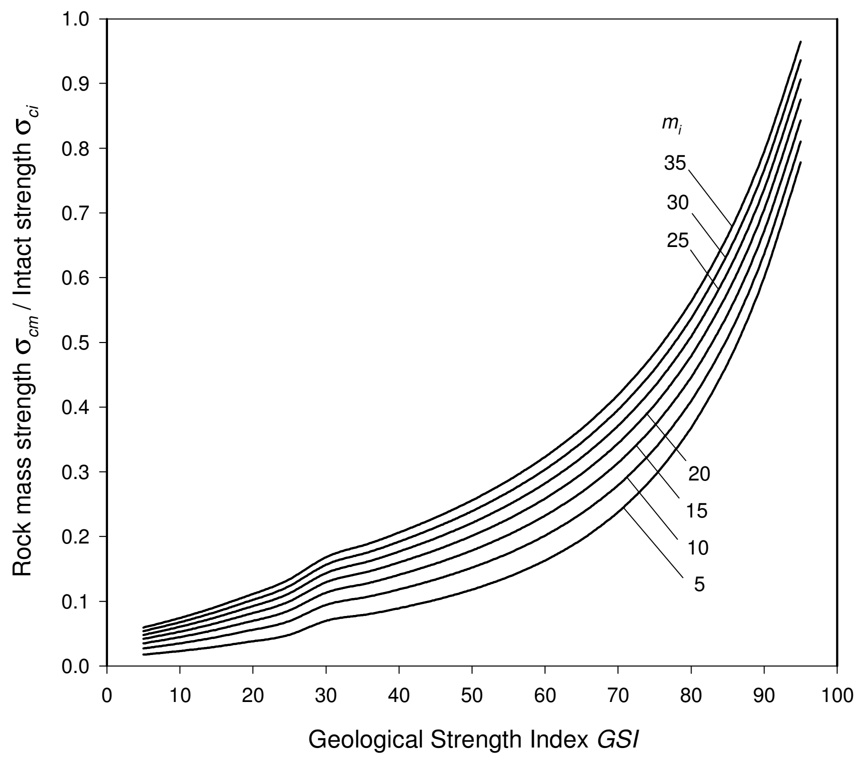

Figure 1.3: Ratio of uniaxial compressive strength of rock mass to intact rock versus Geological Strength Index GSI.

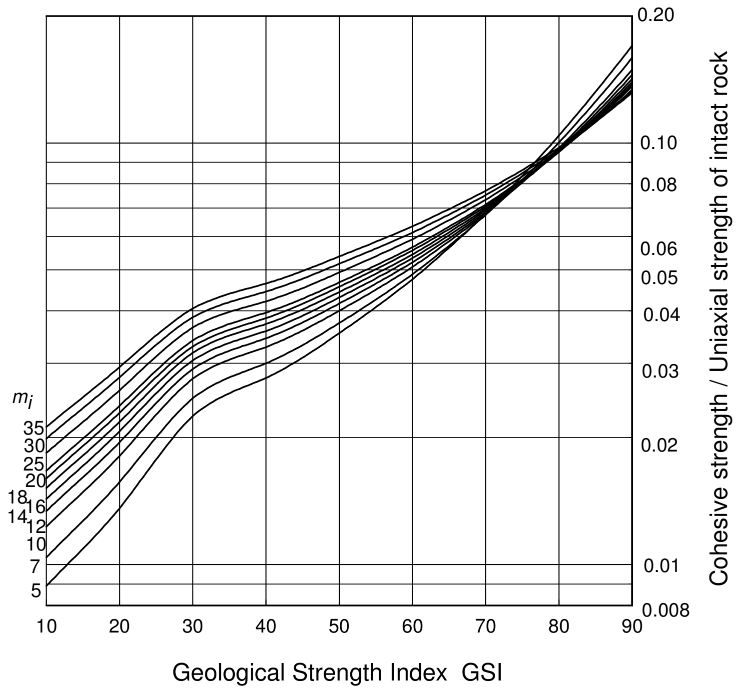

a. Plot of ratio of cohesive strength c' to uniaxial compressive strength σ_{ci} .

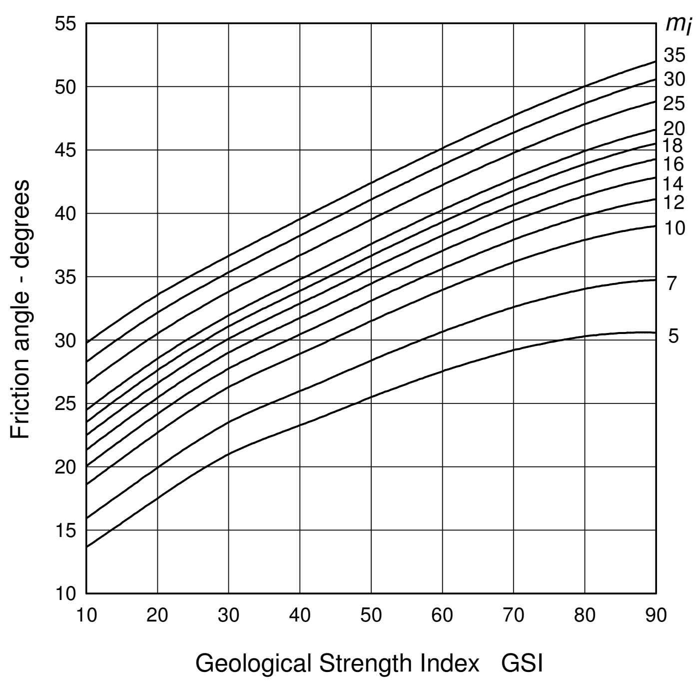

b. Plot of friction angle ϕ'

Figure 1.4: Cohesive strengths and friction angles for different GSI and m_i values.

1.6 DEFORMATION MODULUS

Serafim and Pereira (1983) proposed a relationship between the in situ modulus of deformation and Bieniawski's RMR classification. This relationship is based upon back analysis of dam foundation deformations and it has been found to work well for better quality rocks. However, for many of the poor quality rocks it appears to predict deformation modulus values that are too high. Based upon practical observations and back analysis of excavation behaviour in poor quality rock masses, the following modification to Serafim and Pereira's equation is proposed for $\sigma_{ci} < 100$:

$$E_m = \sqrt{\frac{\sigma_{ci}}{100}}\,10^{\left(\frac{GSI-10}{40}\right)} \tag{1.12}$$

Note that GSI has been substituted for RMR in this equation and that the modulus E_m is reduced progressively as the value of σ_{ci} falls below 100. This reduction is based upon the reasoning that the deformation of better quality rock masses is controlled by the discontinuities while, for poorer quality rock masses, the deformation of the intact rock pieces contributes to the overall deformation process.

Based upon measured deformations, equation 1.12 appears to work reasonably well in those cases where it has been applied. However, as more field evidence is gathered it may be necessary to modify this relationship.

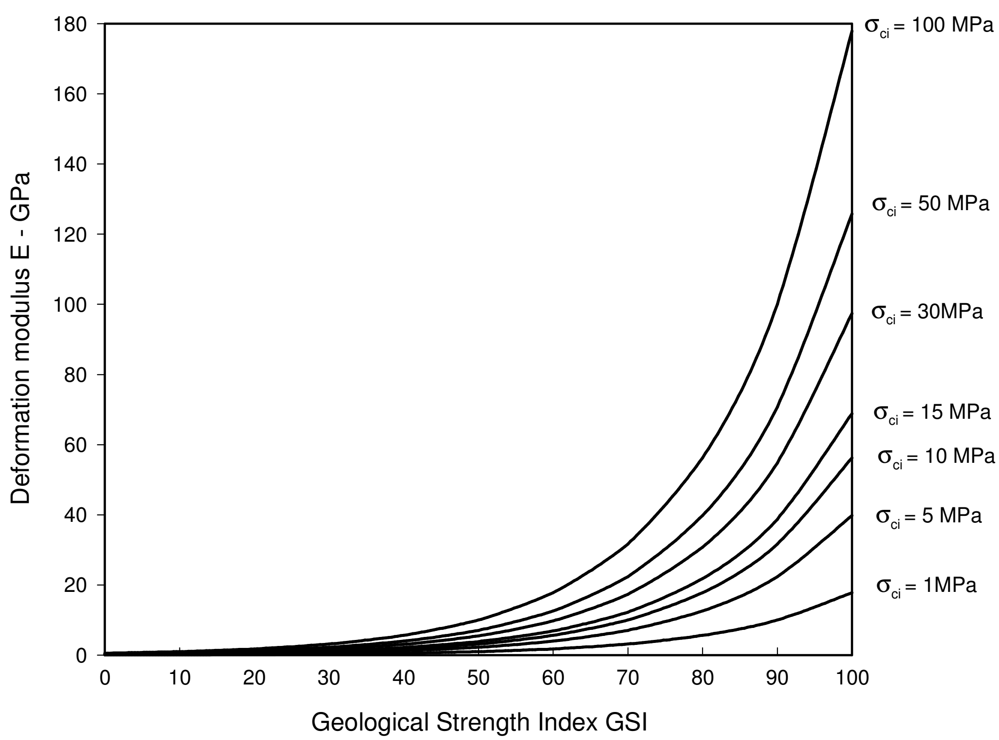

Figure 1.5: Deformation modulus versus Geological Strength Index GSI.

1.7 POST-FAILURE BEHAVIOUR

When using numerical models to study the progressive failure of rock masses, estimates of the post-peak or post-failure characteristics of the rock mass are required. In some of these models, the Hoek-Brown failure criterion is treated as a yield criterion and the analysis is carried out using plasticity theory. No definite rules for dealing with this problem can be given but, based upon experience in numerical analysis of a variety of practical problems, the post-failure characteristics illustrated in Figures 1.6 to 1.8 are suggested as a starting point.

1.7.1 Very good quality hard rock masses

For very good quality hard rock masses, such as massive granites or quartzites, the analysis of spalling around highly stressed openings (Hoek, Kaiser and Bawden 1995) suggests that the rock mass behaves in an elastic brittle manner as shown in Figure 1.6. When the strength of the rock mass is exceeded, a sudden strength drop occurs. This is associated with significant dilation of the broken rock pieces. If this broken rock is confined, for example by rock support, then it can be assumed to behave as a rock fill with a friction angle of approximately $\phi' = 38°$ and zero cohesive strength.

Typical properties for this very good quality hard rock mass may be as shown in Table 1.7. Note that, in some numerical analyses, it may be necessary to assign a very small cohesive strength in order to avoid numerical instability.

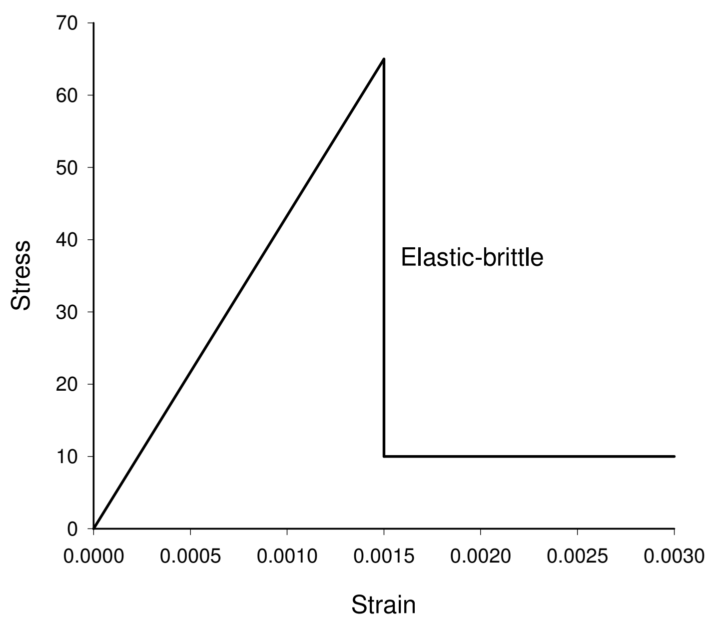

Figure 1.6: Very good quality hard rock mass

Table 1.7: Typical properties for a very good quality hard rock mass

Intact rock strength	σ_{ci}	150 MPa
Hoek-Brown constant	m_i	25
Geological Strength Index	GSI	75
Friction angle	ϕ'	46°
Cohesive strength	c'	13 MPa
Rock mass compressive strength	σ_{cm}	64.8 MPa
Rock mass tensile strength	σ_{tm}	-0.9 MPa
Deformation modulus	E_m	42000 MPa
Poisson's ratio	ν	0.2
Dilation angle	α	$\phi'/4 = 11.5°$
Post-peak characteristics		
Friction angle	ϕ_{f}'	38°
Cohesive strength	c_{f}'	0
Deformation modulus	E_{fm}	10000 MPa

1.7.2 Average quality rock mass

In the case of an average quality rock mass it is reasonable to assume that the post-failure characteristics can be estimated by reducing the GSI value from the in situ value to a lower value which characterises the broken rock mass.

The reduction of the rock mass strength from the in situ to the broken state corresponds to the strain softening behaviour illustrated in Figure 1.7. In this figure it has been assumed that post failure deformation occurs at a constant stress level, defined by the compressive strength of the broken rock mass. The validity of this assumption is uncertain.

Typical properties for this average quality rock mass may be as shown in Table 1.8.

Table 1.8: Typical properties for an average rock mass.

Intact rock strength	σ_{ci}	80 MPa
Hoek-Brown constant	m_i	12
Geological Strength Index	GSI	50
Friction angle	ϕ'	33°
Cohesive strength	c'	3.5 MPa
Rock mass compressive strength	σ_{cm}	13 MPa
Rock mass tensile strength	σ_{tm}	-0.15
Deformation modulus	E_m	9000 MPa
Poisson's ratio	ν	0.25
Dilation angle	α	$\phi'/8 = 4°$
Post-peak characteristics		
Broken rock mass strength	σ_{fcm}	8 MPa
Deformation modulus	E_{fm}	5000 MPa

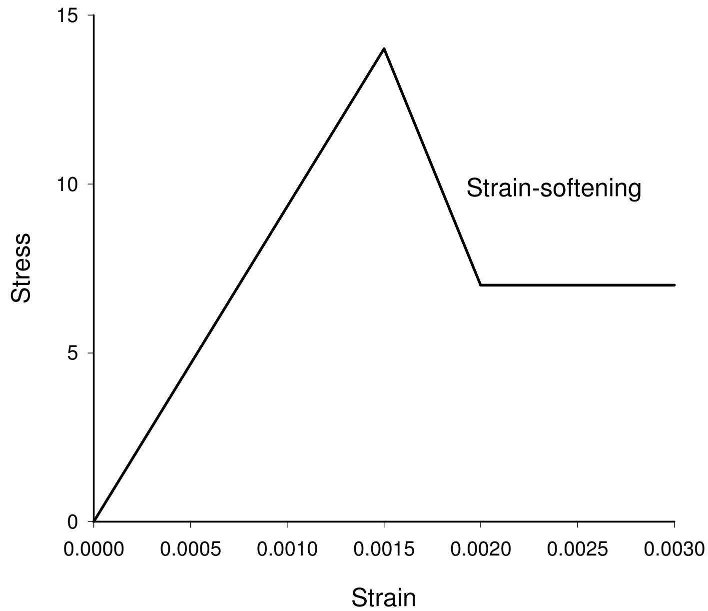

Figure 1.7: Average quality rock mass

1.7.3 Very poor quality rock mass

Analysis of the progressive failure of very poor quality rock masses surrounding tunnels suggests that the post-failure characteristics of the rock are adequately represented by assuming that it behaves perfectly plastically. This means that it continues to deform at a constant stress level and that no volume change is associated with this ongoing failure. This type of behaviour is illustrated in Figure 1.8.

Typical properties for this very poor quality rock mass may be as shown in Table 1.9:

Table 1.9: Typical properties for a very poor quality rock mass

Intact rock strength	σ_{ci}	20 MPa
Hoek-Brown constant	m_i	8
Geological Strength Index	GSI	30
Friction angle	ϕ'	24°
Cohesive strength	c'	0.55 MPa
Rock mass compressive strength	σ_{cm}	1.7 MPa
Rock mass tensile strength	σ_{tm}	-0.01 MPa
Deformation modulus	E_m	1400 MPa
Poisson's ratio	ν	0.3
Dilation angle	α	zero
Post-peak characteristics		
Broken rock mass strength	σ_{fcm}	1.7 MPa
Deformation modulus	E_{fm}	1400 MPa

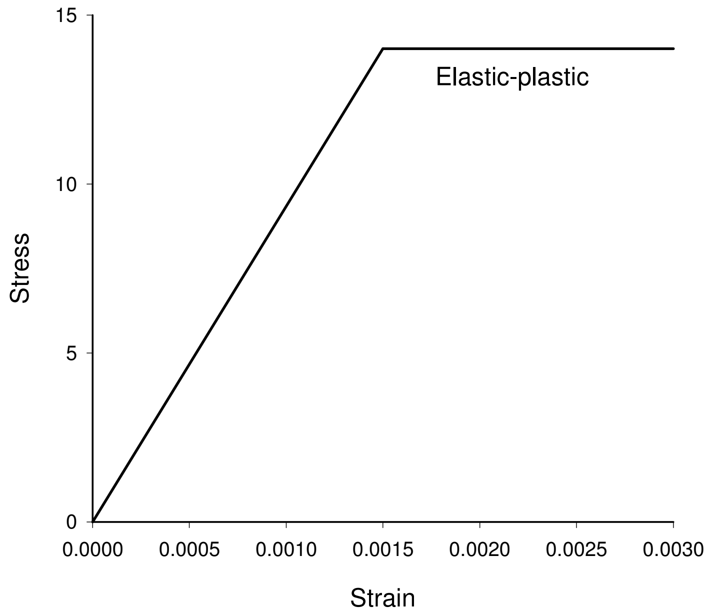

Figure 1.8: Very poor quality soft rock mass

1.8 REFERENCES

Balmer G. 1952. A general analytical solution for Mohr's envelope. Am. Soc. Test. Mat. 52, 1260-1271.

Bieniawski Z.T. 1989. Engineering Rock Mass Classifications. p. 251. New York, Wiley.

Bieniawski Z.T. 1976. Rock mass classification in rock engineering. In Exploration for Rock Engineering, Proc. of the Symp., (Edited by Bieniawski Z.T.) 1, 97-106. Cape Town, Balkema.

Brown E.T. (Ed). 1981. Rock characterization, testing and monitoring - ISRM suggested methods, 171-183. Oxford, Pergamon.

Hoek E. and Brown E.T. 1980. *Underground excavations in rock*, p. 527. London, Instn Min. Metall.

Hoek E. and Brown E.T. 1988 The Hoek-Brown failure criterion - a 1988 update. In Rock Engineering for Underground Excavations, Proc. 15th Canadian Rock Mech. Symp. (Edited by Curran J.C.), 31-38. Toronto, Dept. Civil Engineering, University of Toronto.

Hoek E. Strength of jointed rock masses, 1983. 23rd Rankine Lecture. Géotechnique 33(3), 187-223.

Hoek E. 1994. Strength of rock and rock masses, ISRM News Journal, 2(2), 4-16.

Hoek E., Kaiser P.K. and Bawden W.F. 1995. *Support of underground excavations in hard rock*. p. 215. Rotterdam, Balkema.

Hoek E., Wood D. and Shah S. 1992. A modified Hoek-Brown criterion for jointed rock masses. *Proc. Rock Characterization, Symp. Int. Soc. Rock Mech.: Eurock '92*, (Edited by Hudson J.A.), 209-214. London, Brit. Geotech. Soc.

Hoek, E. and Brown, E.T. 1980. Empirical strength criterion for rock masses. *J. Geotech. Engng. Div., ASCE,* **106** (GT 9), 1013-1035.

Hoek, E. and Brown, E.T. 1997. Practical estimates or rock mass strength. *Int. J. Rock Mech. & Mining Sci. & Geomechanics Abstracts.* **34**(8), 1165-1186.

Hoek, E., Marinos, P. and Benissi, M. 1998. Applicability of the Geological Strength Index (GSI) classification for very weak and sheared rock masses. The case of the Athens Schist Formation. *Bull. Engg. Geol. Env.* 57(2), 151-160.

Karzulovic, A. 2000, personal communication.

Serafim, J.L. and Pereira, J.P. 1983. Consideration of the Geomechanics Classification of Bieniawski. *Proc. Intnl. Symp. Engng. Geol. And Underground Construction.* Lisbon, Portugal, Vol. 1, Part 11, 33-44.

Truzman, M, 1999, personal communication.

1.9 APPENDIX – DETERMINATION OF MOHR COULOMB CONSTANTS

The steps required to determine the parameters A, B, c' and ϕ' are given below. A spreadsheet for carrying out this analysis, with a listing of all the cell formulae, is given in Figure 1.9.

The relationship between the normal and shear stresses can be expressed in terms of the corresponding principal effective stresses as suggested by Balmer (1952):

$$\sigma_n' = \sigma_3' + \frac{\sigma_1' - \sigma_3'}{\partial\sigma_1'/\partial\sigma_3' + 1} \tag{1.13}$$

$$\tau = (\sigma_1' - \sigma_3')\sqrt{\partial\sigma_1'/\partial\sigma_3'} \tag{1.14}$$

For the $GSI > 25$, when $a = 0.5$:

$$\frac{\partial\sigma_1'}{\partial\sigma_3'} = 1 + \frac{m_b\sigma_{ci}}{2(\sigma_1' - \sigma_3')} \tag{1.15}$$

For $GSI < 25$, when $s = 0$:

$$\frac{\partial\sigma_1'}{\partial\sigma_3'} = 1 + am_b^a\left(\frac{\sigma_3'}{\sigma_{ci}}\right)^{a-1} \tag{1.16}$$

The tensile strength of the rock mass is calculated from:

$$\sigma_{tm} = \frac{\sigma_{ci}}{2}\left(m_b - \sqrt{m_b^2 + 4s}\right) \tag{1.17}$$

The equivalent Mohr envelope, defined by equation 1.2, may be written in the form

$$Y = \log A + BX \tag{1.18}$$

where

$$Y = \log\left(\frac{\tau}{\sigma_{ci}}\right),\ X = \log\left(\frac{\sigma_n' - \sigma_{tm}}{\sigma_{ci}}\right) \tag{1.19}$$

Using the value of σ_{tm} calculated from equation 1.17 and a range of values of τ and σ_n' calculated from equations 1.13 and 1.14 the values of A and B are determined by linear regression where :

$$B = \frac{\sum XY - (\sum X \sum Y)/T}{\sum X^2 - (\sum X)^2/T} \tag{1.20}$$

$$A = 10\hat{}\left(\sum Y/T - B(\sum X/T)\right) \tag{1.21}$$

and T is the total number of data pairs included in the regression analysis.

The most critical step in this process is the selection of the range of σ_3' values. As far as the author is aware, there are no theoretically correct methods for choosing this range and a trial and error method, based upon practical compromise, has been used for selecting the range included in the spreadsheet presented in Figure 1.9.

For a Mohr envelope defined by equation 1.2, the friction angle ϕ_i' for a specified normal stress σ_{ni}' is given by:

$$\phi_i' = \arctan\left(AB\left(\frac{\sigma_{ni}' - \sigma_{tm}}{\sigma_{ci}}\right)^{B-1}\right) \tag{1.22}$$

The corresponding cohesive strength c_i' is given by:

$$c_i' = \tau - \sigma_{ni}' \tan \phi_i' \tag{1.23}$$

and the corresponding uniaxial compressive strength of the rock mass is :

$$\sigma_{cmi} = \frac{2c_i' \cos\phi_i'}{1 - \sin\phi_i'} \tag{1.24}$$

The values of c' and ϕ' obtained from this analysis are very sensitive to the range of values of the minor principal stress σ_3' used to generate the simulated full-scale triaxial test results. On the basis of trial and error, it has been found that the most consistent results for deep excavations (depth > 30 m below surface) are obtained when 8 equally spaced values of σ_3' are used in the range $0 < \sigma_3' < 0.25\sigma_{ci}$.

Figure 1.9 Spreadsheet for calculation of Hoek-Brown and equivalent Mohr-Coulomb parameters for excavations deeper than 30 m.

Hoek-Brown and equivalent Mohr-Coulomb failure criteria

Input:	sigci = 60 MPa	mi = 19	GSI = 50
Output:	mb = 3.19	s = 0.0039	a = 0.5
	sigtm = -0.0728 MPa	A = 0.6731	B = 0.7140
	k = 4.06	phi = 37.20 degrees	coh = 2.930 MPa
	sigcm = 11.80 MPa	E = 7746.0 MPa	

Calculation:

									Sums
sig3	1E-10	2.14	4.29	6.4	8.57	10.71	12.86	15.00	60.00
sig1	3.73	22.72	33.15	41.68	49.22	56.12	62.57	68.68	337.88
ds1ds3	26.62	5.64	4.31	3.71	3.35	3.10	2.92	2.78	52.45
sign	0.14	5.24	9.72	13.91	17.91	21.78	25.53	29.20	123.43
tau	0.70	7.36	11.28	14.42	17.10	19.49	21.67	23.68	115.69
x	-2.46	-1.05	-0.79	-0.63	-0.52	-0.44	-0.37	-0.31	-6.58
y	-1.93	-0.91	-0.73	-0.62	-0.55	-0.49	-0.44	-0.40	-6.07
xy	4.76	0.96	0.57	0.39	0.29	0.21	0.16	0.13	7.47
xsq	6.05	1.11	0.62	0.40	0.27	0.19	0.14	0.10	8.88
sig3sig1	0.00	48.69	142.07	267.95	421.89	601.32	804.50	1030.15	3317
sig3sq	0.00	4.59	18.37	41.33	73.47	114.80	165.31	225.00	643
taucalc	0.71	7.15	11.07	14.28	17.09	19.63	21.99	24.19	
sig1sig3fit	11.80	20.50	29.19	37.89	46.58	55.28	63.97	72.67	
signtaufit	3.03	6.91	10.31	13.49	16.53	19.46	22.31	25.09	

Cell formulae:

```
      mb = mi*EXP((GSI-100)/28)
       s = IF(GSI>25,EXP((GSI-100)/9),0)
       a = IF(GSI>25,0.5,0.65-GSI/200)
   sigtm = 0.5*sigci*(mb-SQRT(mb^2+4*s))
    sig3 = Start at 1E-10 (to avoid zero errors) and increment in 7 steps of  sigci/28 to 0.25*sigci
    sig1 = sig3+sigci*(((mb*sig3)/sigci)+s)^a
  ds1ds3 = IF(GSI>25,(1+(mb*sigci)/(2*(sig1-sig3))),1+(a*mb^a)*(sig3/sigci)^(a-1))
    sign = sig3+(sig1-sig3)/(1+ds1ds3)
     tau = (sign-sig3)*SQRT(ds1ds3)
       x = LOG((sign-sigtm)/sigci)
       y = LOG(tau/sigci)
      xy = x*y                x sq = x^2
       A =    acalc =    10^(sumy/8 - bcalc*sumx/8)
       B =    bcalc =    (sumxy - (sumx*sumy)/8)/(sumxsq - (sumx^2)/8)
       k = (sumsig3sig1 - (sumsig3*sumsig1)/8)/(sumsig3sq-(sumsig3^2)/8)
     phi = ASIN((k-1)/(k+1))*180/PI()
     coh = sigcm/(2*SQRT(k))
   sigcm = sumsig1/8 - k*sumsig3/8
       E = IF(sigci>100,1000*10^((GSI-10)/40),SQRT(sigci/100)*1000*10^((GSI-10)/40))
    phit = (ATAN(acalc*bcalc*((signt-sigtm)/sigci)^(bcalc-1)))*180/PI()
    coht = acalc*sigci*((signt-sigtm)/sigci)^bcalc-signt*TAN(phit*PI()/180)
sig3sig1= sig3*sig1        sig3sq = sig3^2
 taucalc = acalc*sigci*((sign-sigtm)/sigci)^bcalc
  s3sifit = sigcm+k*sig3
sntaufit =  coh+sign*TAN(phi*PI()/180)
```

Rock mass properties for underground mines

Evert Hoek

Published in *Underground Mining Methods: Engineering Fundamentals and International Case Studies.* (Edited by W. A. Hustrulid and R. L. Bullock), Litleton, Colorado: Society for Mining, Metallurgy, and Exploration (SME) 2001

Rock mass properties for underground mines

Evert Hoek[*]

1.1 INTRODUCTION

Reliable estimates of the strength and deformation characteristics of rock masses are required for almost any form of analysis used for the design of underground excavations. Hoek and Brown (1980a, 1980b) proposed a method for obtaining estimates of the strength of jointed rock masses, based upon an assessment of the interlocking of rock blocks and the condition of the surfaces between these blocks. This method was modified over the years in order to meet the needs of users who applied it to problems that were not considered when the original criterion was developed (Hoek 1983, Hoek and Brown 1988). The application of the method to very poor quality rock masses required further changes (Hoek, Wood and Shah 1992) and, eventually, the development of a new classification called the Geological Strength Index (Hoek 1994, Hoek, Kaiser and Bawden 1995, Hoek and Brown 1997, Hoek, Marinos and Benissi (1998)). A review of the development of the criterion and of the equations proposed at various stages in this development is given in Hoek and Brown (1997).

This chapter presents the Hoek-Brown criterion in a form that has been found practical in the field and that appears to provide the most reliable set of results for use as input for methods of analysis currently used in rock engineering.

1.2 GENERALISED HOEK-BROWN CRITERION

The Generalised Hoek-Brown failure criterion for jointed rock masses is defined by:

$$\sigma_1^{'} = \sigma_3^{'} + \sigma_{ci}\left(m_b \frac{\sigma_3^{'}}{\sigma_{ci}} + s \right)^a \qquad (1.1)$$

where $\sigma_1^{'}$ and $\sigma_3^{'}$ are the maximum and minimum effective stresses at failure,

m_b is the value of the Hoek-Brown constant m for the rock mass,

s and a are constants which depend upon the rock mass characteristics, and

σ_{ci} is the uniaxial compressive strength of the intact rock pieces.

The Mohr envelope, relating normal and shear stresses, can be determined by the method proposed by Hoek and Brown (1980a). In this approach, equation 1.1 is used

---

[*] Consulting engineer, Vancouver, Canada.

to generate a series of triaxial test values, simulating full scale field tests, and a statistical curve fitting process is used to derive an equivalent Mohr envelope defined by the equation:

$$\tau = A\sigma_{ci}\left(\frac{\sigma_n^{'} - \sigma_{tm}}{\sigma_{ci}}\right)^B \tag{1.2}$$

where A and B are material constants

$\sigma_n^{'}$ is the normal effective stress, and

σ_{tm} is the 'tensile' strength of the rock mass.

In order to use the Hoek-Brown criterion for estimating the strength and deformability of jointed rock masses, three 'properties' of the rock mass have to be estimated. These are

1. the uniaxial compressive strength σ_{ci} of the intact rock elements,
2. the value of the Hoek-Brown constant m_i for these intact rock elements, and
3. the value of the Geological Strength Index *GSI* for the rock mass.

1.3 INTACT ROCK PROPERTIES

For the intact rock pieces that make up the rock mass equation 1.1 simplifies to:

$$\sigma_1^{'} = \sigma_3^{'} + \sigma_{ci}\left(m_i \frac{\sigma_3^{'}}{\sigma_{ci}} + 1\right)^{0.5} \tag{1.3}$$

The relationship between the principal stresses at failure for a given rock is defined by two constants, the uniaxial compressive strength σ_{ci} and a constant m_i. Wherever possible the values of these constants should be determined by statistical analysis of the results of a set of triaxial tests on carefully prepared core samples. When laboratory tests are not possible, Table 1.1 and Table 1.2 can be used to obtain estimates of σ_{ci} and m_i.

In the case of mineralised rocks, the effects of alteration can have a significant impact on the properties of the intact rock components and this should be taken into account in estimating the values of σ_{ci} and m_i. For example, the influence of quartz-seritic alteration of andesite and porphyry is illustrated in the Figure 1.1, based upon data provided by Karzulovic (2000). Similar trends have been observed for other forms of alteration and, where this type of effect is considered likely, the geotechnical engineer would be well advised to invest in a program of laboratory testing to establish the appropriate properties for the intact rock.

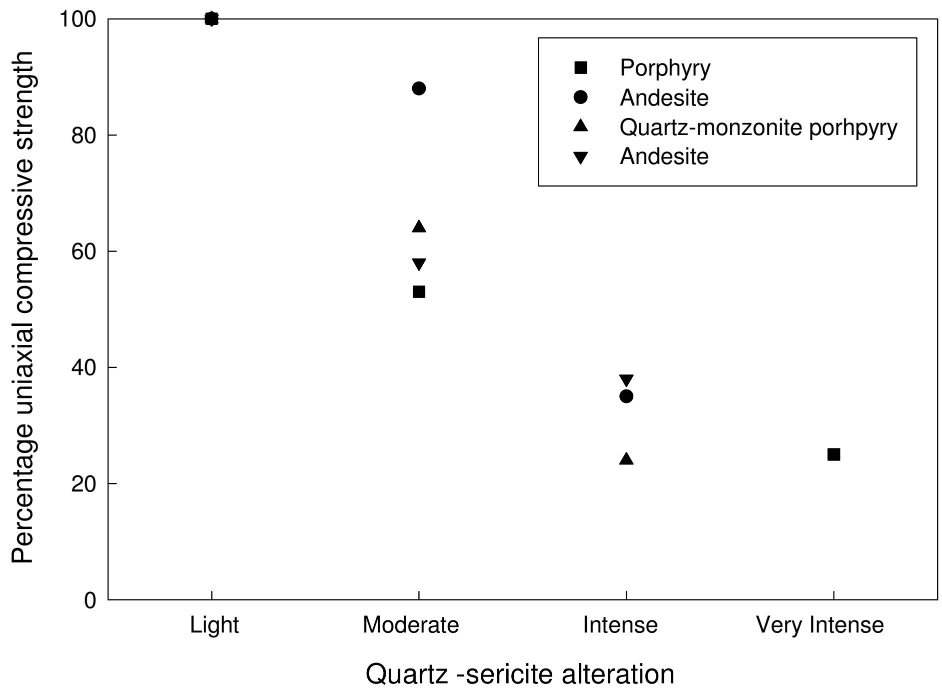

Figure 1.1: Influence of quartz-seritic alteration on the uniaxial compressive strength of "intact" specimens of andesite and porphyry. (After Karzulovic, 2000)

The Hoek-Brown failure criterion, which assumes isotropic rock and rock mass behaviour, should only be applied to those rock masses in which there are a sufficient number of closely spaced discontinuities, with similar surface characteristics, that isotropic behaviour involving failure on multiple discontinuities can be assumed. When the structure being analysed is large and the block size small in comparison, the rock mass can be treated as a Hoek-Brown material.

Where the block size is of the same order as that of the structure being analysed or when one of the discontinuity sets is significantly weaker than the others, the Hoek-Brown criterion should not be used. In these cases, the stability of the structure should be analysed by considering failure mechanisms involving the sliding or rotation of blocks and wedges defined by intersecting structural features. Figure 1.2 summarises these statements in a graphical form.

1.4 GEOLOGICAL STRENGTH INDEX

The strength of a jointed rock mass depends on the properties of the intact rock pieces and also upon the freedom of these pieces to slide and rotate under different stress conditions. This freedom is controlled by the geometrical shape of the intact rock pieces as well as the condition of the surfaces separating the pieces. Angular rock pieces with clean, rough discontinuity surfaces will result in a much stronger rock mass than one which contains rounded particles surrounded by weathered and altered material.

Table 1.1: Field estimates of uniaxial compressive strength.

Grade*	Term	Uniaxial Comp. Strength (MPa)	Point Load Index (MPa)	Field estimate of strength	Examples
R6	Extremely Strong	> 250	>10	Specimen can only be chipped with a geological hammer	Fresh basalt, chert, diabase, gneiss, granite, quartzite
R5	Very strong	100 - 250	4 - 10	Specimen requires many blows of a geological hammer to fracture it	Amphibolite, sandstone, basalt, gabbro, gneiss, granodiorite, peridotite , rhyolite, tuff
R4	Strong	50 - 100	2 - 4	Specimen requires more than one blow of a geological hammer to fracture it	Limestone, marble, sandstone, schist
R3	Medium strong	25 - 50	1 - 2	Cannot be scraped or peeled with a pocket knife, specimen can be fractured with a single blow from a geological hammer	Concete, phyllite, schist, siltstone
R2	Weak	5 - 25	**	Can be peeled with a pocket knife with difficulty, shallow indentation made by firm blow with point of a geological hammer	Chalk, claystone, potash, marl, siltstone, shale, rocksalt,
R1	Very weak	1 - 5	**	Crumbles under firm blows with point of a geological hammer, can be peeled by a pocket knife	Highly weathered or altered rock, shale
R0	Extremely weak	0.25 - 1	**	Indented by thumbnail	Stiff fault gouge

* Grade according to Brown (1981).
** Point load tests on rocks with a uniaxial compressive strength below 25 MPa are likely to yield highly ambiguous results.

Table 1.2: Values of the constant m_i for intact rock, by rock group. Note that values in parenthesis are estimates.

Rock type	Class	Group	Texture			
			Coarse	Medium	Fine	Very fine
SEDIMENTARY	Clastic		Conglomerates (21 ± 3) Breccias (19 ± 5)	Sandstones 17 ± 4	Siltstones 7 ± 2 Greywackes (18 ± 3)	Claystones 4 ± 2 Shales (6 ± 2) Marls (7 ± 2)
	Non-Clastic	Carbonates	Crystalline Limestone (12 ± 3)	Sparitic Limestones (10 ± 2)	Micritic Limestones (9 ± 2)	Dolomites (9 ± 3)
		Evaporites		Gypsum 8 ± 2	Anhydrite 12 ± 2	
		Organic				Chalk 7 ± 2
METAMORPHIC	Non Foliated		Marble 9 ± 3	Hornfels (19 ± 4) Metasandstone (19 ± 3)	Quartzites 20 ± 3	
	Slightly foliated		Migmatite (29 ± 3)	Amphibolites 26 ± 6		
	Foliated*		Gneiss 28 ± 5	Schists 12 ± 3	Phyllites (7 ± 3)	Slates 7 ± 4
IGNEOUS	Plutonic	Light	Granite 32 ± 3 Granodiorite (29 ± 3)	Diorite 25 ± 5		
		Dark	Gabbro 27 ± 3 Norite 20 ± 5	Dolerite (16 ± 5)		
	Hypabyssal		Porphyries (20 ± 5)		Diabase (15 ± 5)	Peridotite (25 ± 5)
	Volcanic	Lava		Rhyolite (25 ± 5) Andesite 25 ± 5	Dacite (25 ± 3) Basalt (25 ± 5)	Obsidian (19 ± 3)
		Pyroclastic	Agglomerate (19 ± 3)	Breccia (19 ± 5)	Tuff (13 ± 5)	

* These values are for intact rock specimens tested normal to bedding or foliation. The value of m_i will be significantly different if failure occurs along a weakness plane.

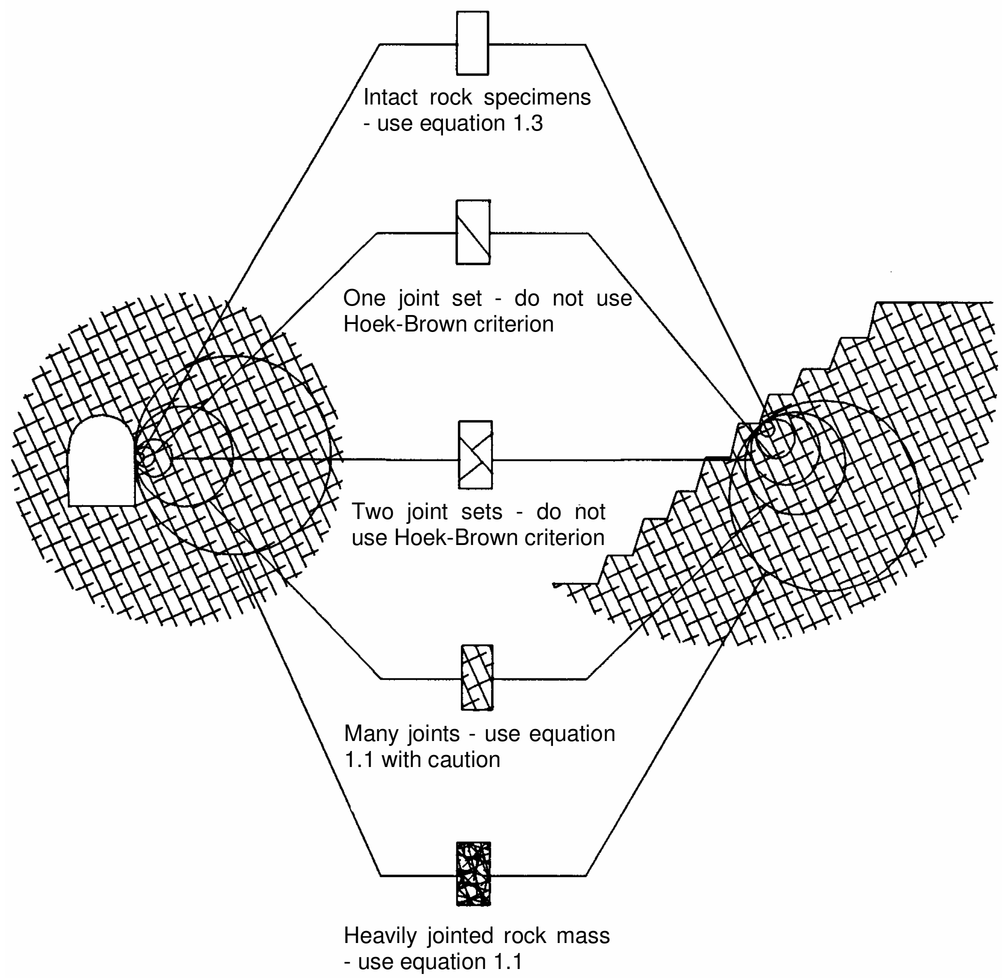

Figure 1.2: Idealised diagram showing the transition from intact to a heavily jointed rock mass with increasing sample size.

The Geological Strength Index (GSI), introduced by Hoek (1994) and Hoek, Kaiser and Bawden (1995) provides a system for estimating the reduction in rock mass strength for different geological conditions. This system is presented in Table 1.3, for blocky rock masses, and Table 1.4 for schistose metamorphic rocks.

Once the Geological Strength Index has been estimated, the parameters that describe the rock mass strength characteristics, are calculated as follows:

$$m_b = m_i \exp\left(\frac{GSI - 100}{28}\right) \tag{1.4}$$

For GSI > 25, i.e. rock masses of good to reasonable quality:

$$s = \exp\left(\frac{GSI - 100}{9}\right) \tag{1.5}$$

and

$$a = 0.5 \tag{1.6}$$

For GSI < 25, i.e. rock masses of very poor quality:

$$s = 0 \tag{1.7}$$

and

$$a = 0.65 - \frac{GSI}{200} \tag{1.8}$$

For better quality rock masses (GSI > 25), the value of GSI can be estimated directly from the 1976 version of Bieniawski's Rock Mass Rating, with the Groundwater rating set to 10 (dry) and the Adjustment for Joint Orientation set to 0 (very favourable) (Bieniawski 1976). For very poor quality rock masses the value of RMR is very difficult to estimate and the balance between the ratings no longer gives a reliable basis for estimating rock mass strength. Consequently, Bieniawski's RMR classification should not be used for estimating the GSI values for poor quality rock masses (RMR < 25) and the GSI charts should be used directly.

If the 1989 version of Bieniawski's RMR classification (Bieniawski 1989) is used, then GSI = RMR_{89}' - 5 where RMR_{89}' has the Groundwater rating set to 15 and the Adjustment for Joint Orientation set to zero.

1.5 MOHR-COULOMB PARAMETERS

Most geotechnical software is written in terms of the Mohr-Coulomb failure criterion in which the rock mass strength is defined by the cohesive strength c' and the angle of friction ϕ'. The linear relationship between the major and minor principal stresses, σ_1' and σ_3', for the Mohr-Coulomb criterion is

$$\sigma_1' = \sigma_{cm} + k\sigma_3' \tag{1.9}$$

where σ_{cm} is the uniaxial compressive strength of the rock mass and k is the slope of the line relating σ_1' and σ_3'. The values of ϕ' and c' can be calculated from

$$\sin\phi' = \frac{k-1}{k+1} \tag{1.10}$$

$$c' = \frac{\sigma_{cm}(1 - \sin\phi')}{2\cos\phi'} \tag{1.11}$$

Table 1.3: Characterisation of a blocky rock masses on the basis of particle interlocking and discontinuity condition. After Hoek, Marinos and Benissi (1998).

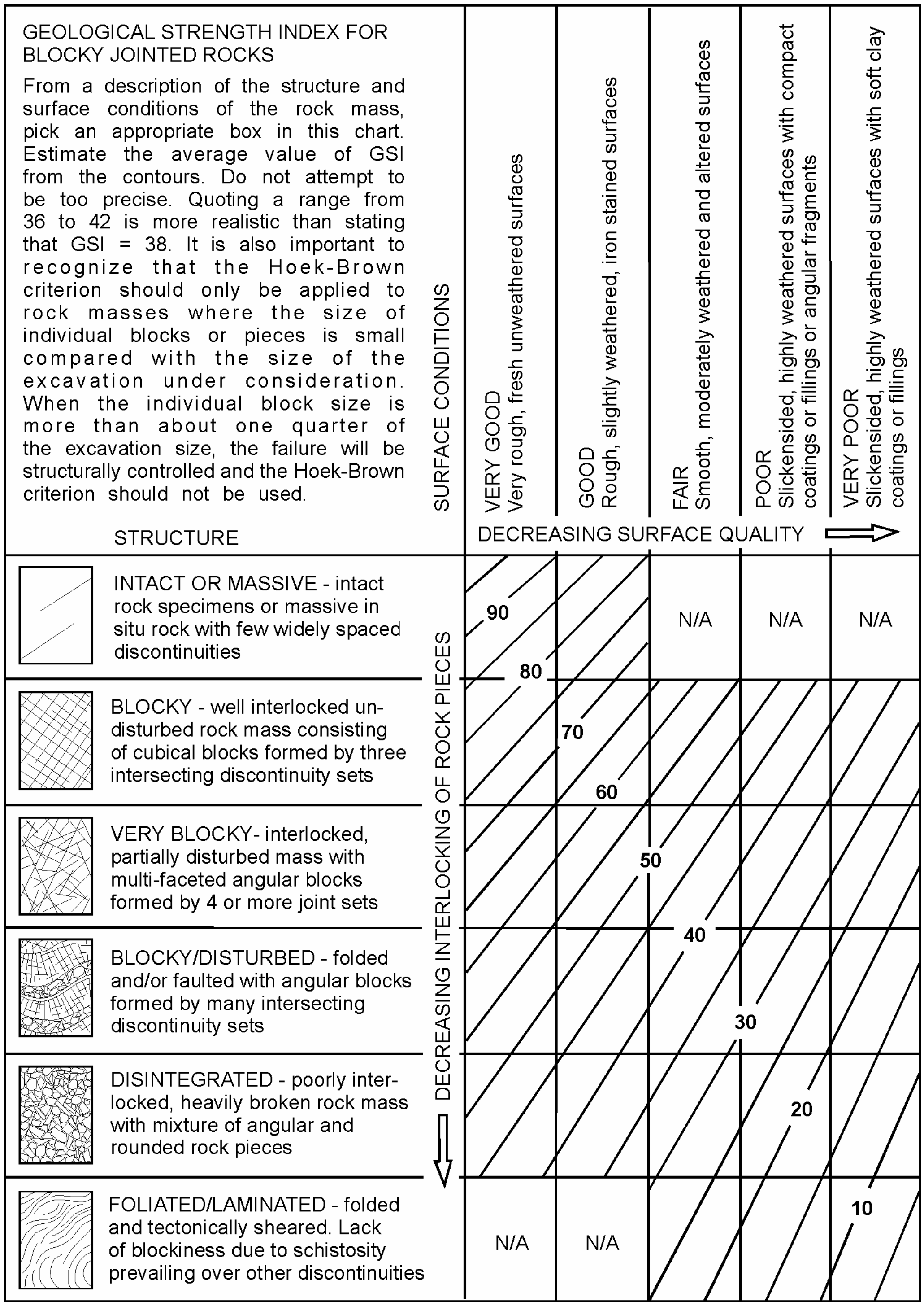

Table 1.4: Characterisation of a schistose metamorphic rock masses on the basis of foliation and discontinuity condition. (After M. Truzman, 1999)

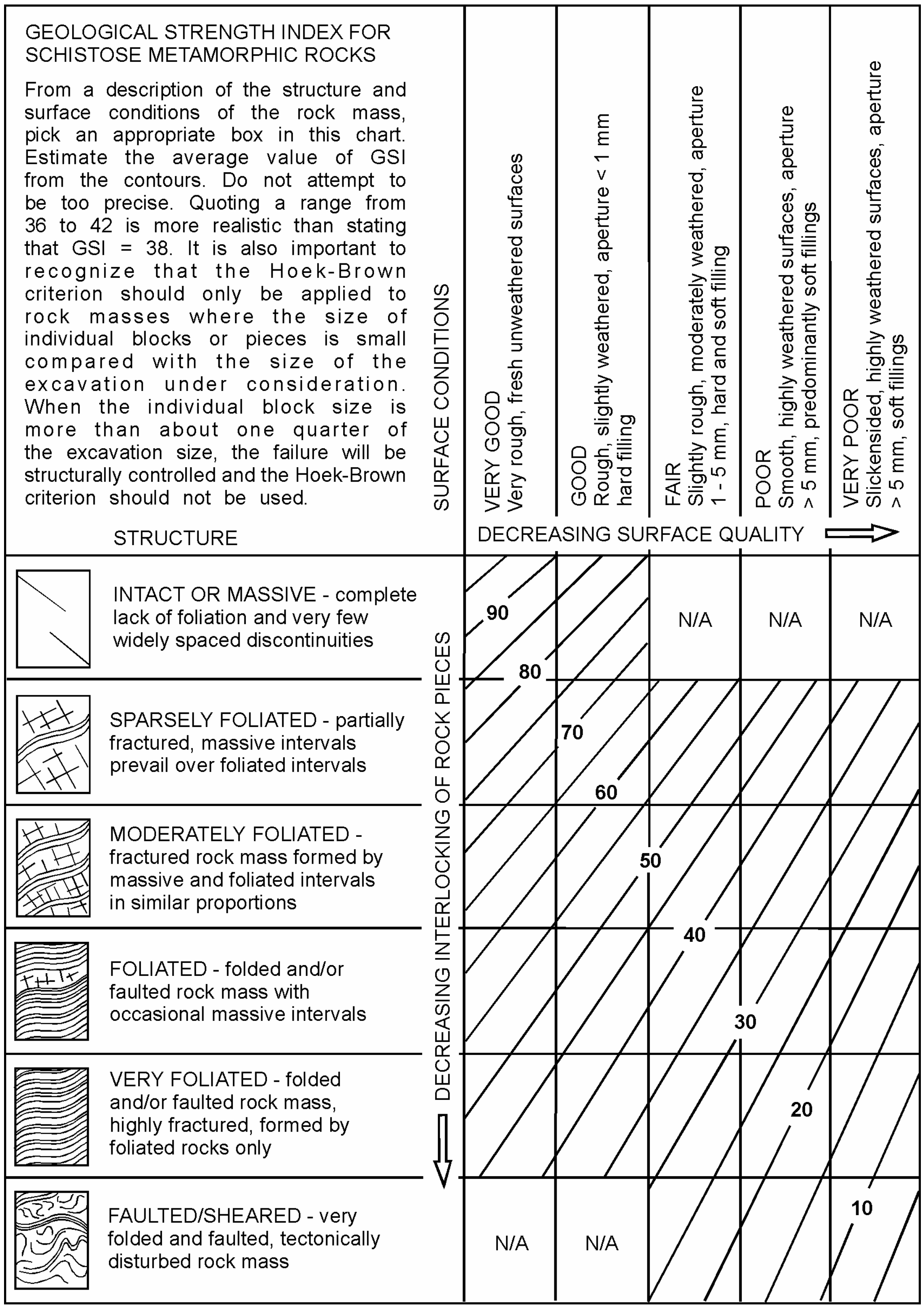

There is no direct correlation between equation 1.9 and the non-linear Hoek-Brown criterion defined by equation 1.1. Consequently, determination of the values of c' and ϕ' for a rock mass that has been evaluated as a Hoek-Brown material is a difficult problem.

Having considered a number of possible approaches, it has been concluded that the most practical solution is to treat the problem as an analysis of a set of full-scale triaxial strength tests. The results of such tests are simulated by using the Hoek-Brown equation 1.1 to generate a series of triaxial test values. Equation 1.9 is then fitted to these test results by linear regression analysis and the values of c' and ϕ' are determined from equations 1.11 and 1.10. A full discussion on the steps required to carry out this analysis is presented in the Appendix, together with a spreadsheet for implementing this analysis.

The range of stresses used in the curve fitting process described above is very important. For the confined conditions surrounding tunnels at depths of more than about 30 m, the most reliable estimates are given by using a confining stress range from zero to $0.25\sigma_{ci}$, where σ_{ci} is the uniaxial compressive strength of the intact rock elements. A series of plots showing the uniaxial compressive strength of the rock mass σ_{cm}, the cohesive strength c and the friction angle ϕ are given in Figures 1.3 and 1.4.

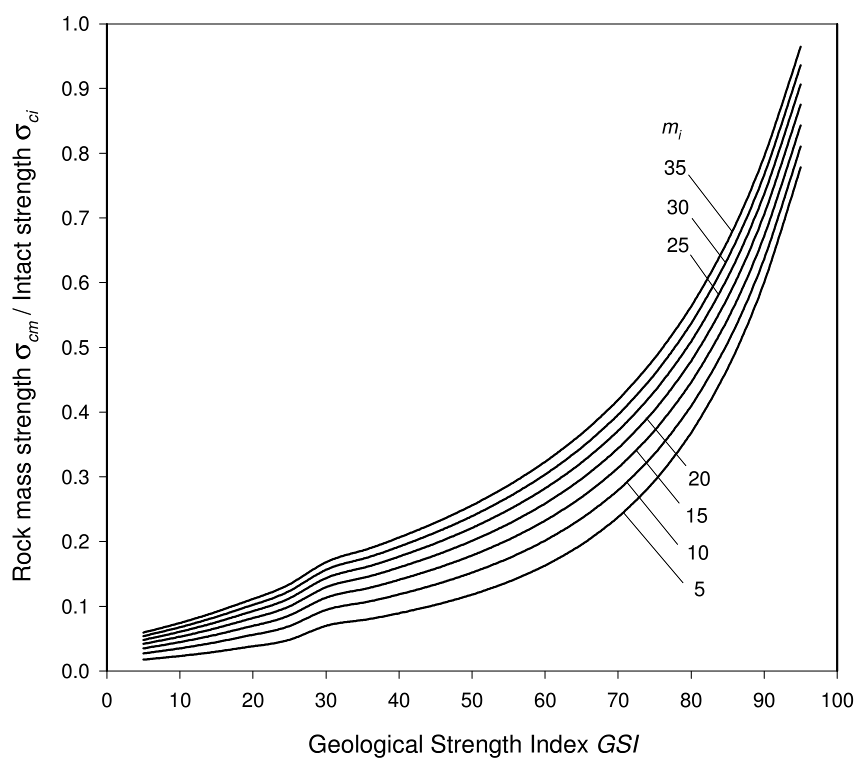

Figure 1.3: Ratio of uniaxial compressive strength of rock mass to intact rock versus Geological Strength Index GSI.

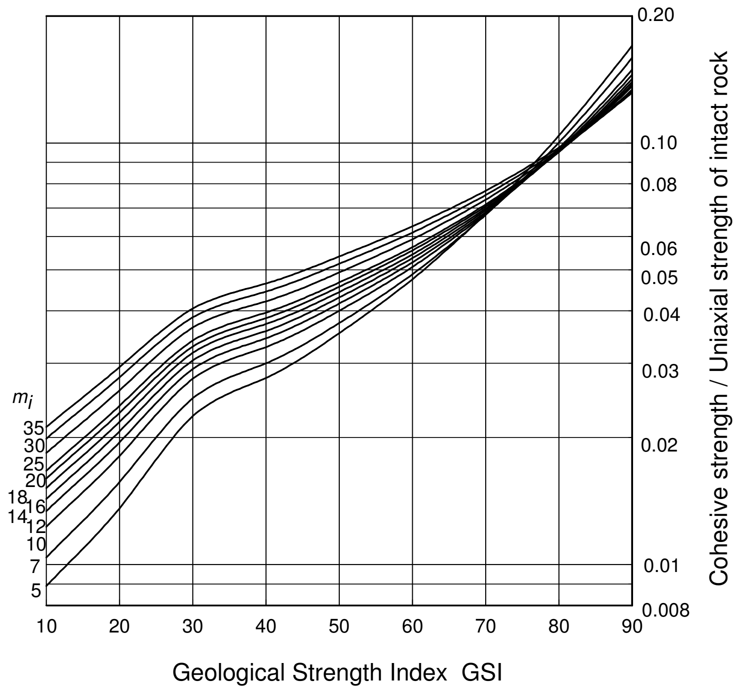

a. Plot of ratio of cohesive strength c' to uniaxial compressive strength σ_{ci} .

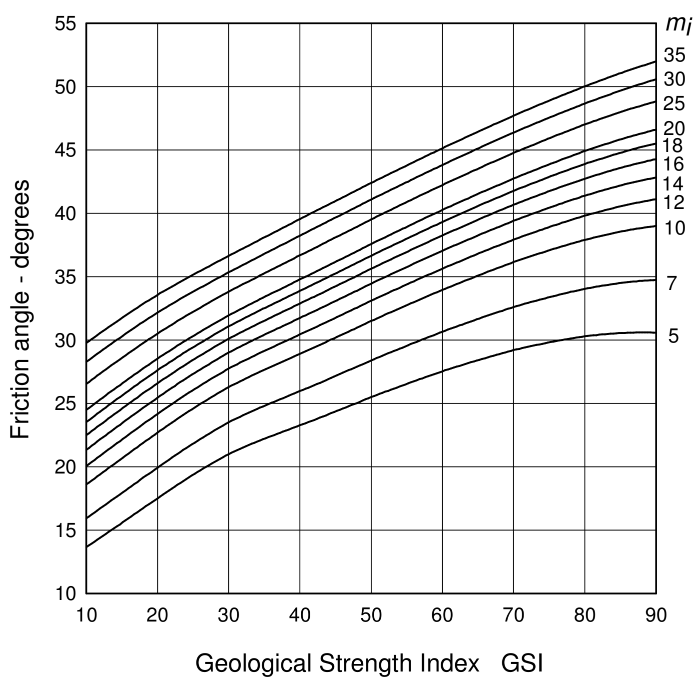

b. Plot of friction angle ϕ'

Figure 1.4: Cohesive strengths and friction angles for different GSI and m_i values.

1.6 DEFORMATION MODULUS

Serafim and Pereira (1983) proposed a relationship between the in situ modulus of deformation and Bieniawski's RMR classification. This relationship is based upon back analysis of dam foundation deformations and it has been found to work well for better quality rocks. However, for many of the poor quality rocks it appears to predict deformation modulus values that are too high. Based upon practical observations and back analysis of excavation behaviour in poor quality rock masses, the following modification to Serafim and Pereira's equation is proposed for $\sigma_{ci} < 100$:

$$E_m = \sqrt{\frac{\sigma_{ci}}{100}}\,10^{\left(\frac{GSI-10}{40}\right)} \tag{1.12}$$

Note that GSI has been substituted for RMR in this equation and that the modulus E_m is reduced progressively as the value of σ_{ci} falls below 100. This reduction is based upon the reasoning that the deformation of better quality rock masses is controlled by the discontinuities while, for poorer quality rock masses, the deformation of the intact rock pieces contributes to the overall deformation process.

Based upon measured deformations, equation 1.12 appears to work reasonably well in those cases where it has been applied. However, as more field evidence is gathered it may be necessary to modify this relationship.

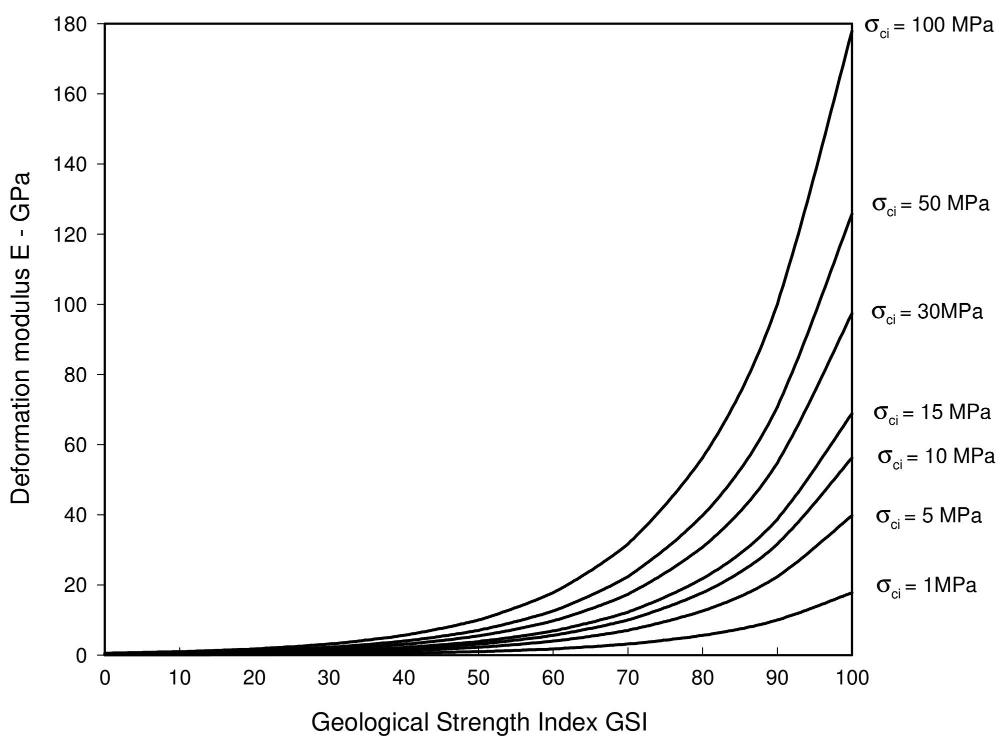

Figure 1.5: Deformation modulus versus Geological Strength Index GSI.

1.7 POST-FAILURE BEHAVIOUR

When using numerical models to study the progressive failure of rock masses, estimates of the post-peak or post-failure characteristics of the rock mass are required. In some of these models, the Hoek-Brown failure criterion is treated as a yield criterion and the analysis is carried out using plasticity theory. No definite rules for dealing with this problem can be given but, based upon experience in numerical analysis of a variety of practical problems, the post-failure characteristics illustrated in Figures 1.6 to 1.8 are suggested as a starting point.

1.7.1 Very good quality hard rock masses

For very good quality hard rock masses, such as massive granites or quartzites, the analysis of spalling around highly stressed openings (Hoek, Kaiser and Bawden 1995) suggests that the rock mass behaves in an elastic brittle manner as shown in Figure 1.6. When the strength of the rock mass is exceeded, a sudden strength drop occurs. This is associated with significant dilation of the broken rock pieces. If this broken rock is confined, for example by rock support, then it can be assumed to behave as a rock fill with a friction angle of approximately $\phi' = 38°$ and zero cohesive strength.

Typical properties for this very good quality hard rock mass may be as shown in Table 1.7. Note that, in some numerical analyses, it may be necessary to assign a very small cohesive strength in order to avoid numerical instability.

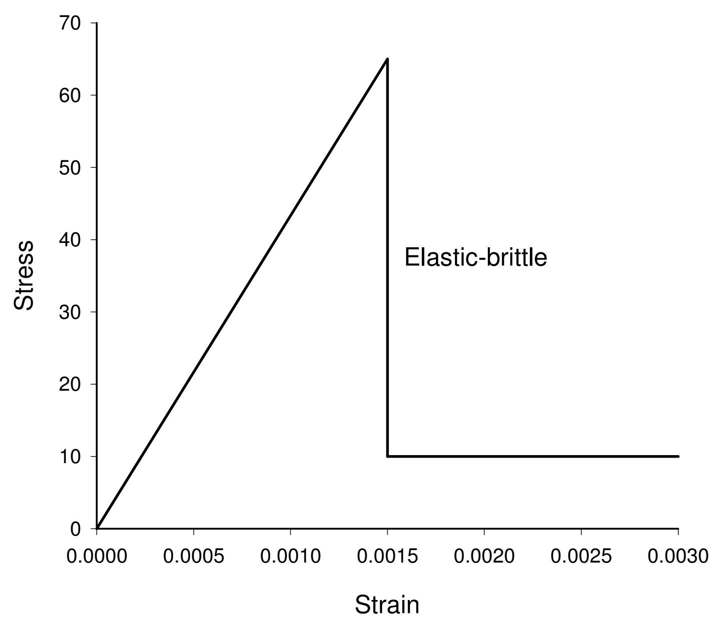

Figure 1.6: Very good quality hard rock mass

Table 1.7: Typical properties for a very good quality hard rock mass

Intact rock strength	σ_{ci}	150 MPa
Hoek-Brown constant	m_i	25
Geological Strength Index	GSI	75
Friction angle	ϕ'	46°
Cohesive strength	c'	13 MPa
Rock mass compressive strength	σ_{cm}	64.8 MPa
Rock mass tensile strength	σ_{tm}	-0.9 MPa
Deformation modulus	E_m	42000 MPa
Poisson's ratio	ν	0.2
Dilation angle	α	$\phi'/4 = 11.5°$
Post-peak characteristics		
Friction angle	ϕ_{f}'	38°
Cohesive strength	c_{f}'	0
Deformation modulus	E_{fm}	10000 MPa

1.7.2 Average quality rock mass

In the case of an average quality rock mass it is reasonable to assume that the post-failure characteristics can be estimated by reducing the GSI value from the in situ value to a lower value which characterises the broken rock mass.

The reduction of the rock mass strength from the in situ to the broken state corresponds to the strain softening behaviour illustrated in Figure 1.7. In this figure it has been assumed that post failure deformation occurs at a constant stress level, defined by the compressive strength of the broken rock mass. The validity of this assumption is uncertain.

Typical properties for this average quality rock mass may be as shown in Table 1.8.

Table 1.8: Typical properties for an average rock mass.

Intact rock strength	σ_{ci}	80 MPa
Hoek-Brown constant	m_i	12
Geological Strength Index	GSI	50
Friction angle	ϕ'	33°
Cohesive strength	c'	3.5 MPa
Rock mass compressive strength	σ_{cm}	13 MPa
Rock mass tensile strength	σ_{tm}	-0.15
Deformation modulus	E_m	9000 MPa
Poisson's ratio	ν	0.25
Dilation angle	α	$\phi'/8 = 4°$
Post-peak characteristics		
Broken rock mass strength	σ_{fcm}	8 MPa
Deformation modulus	E_{fm}	5000 MPa

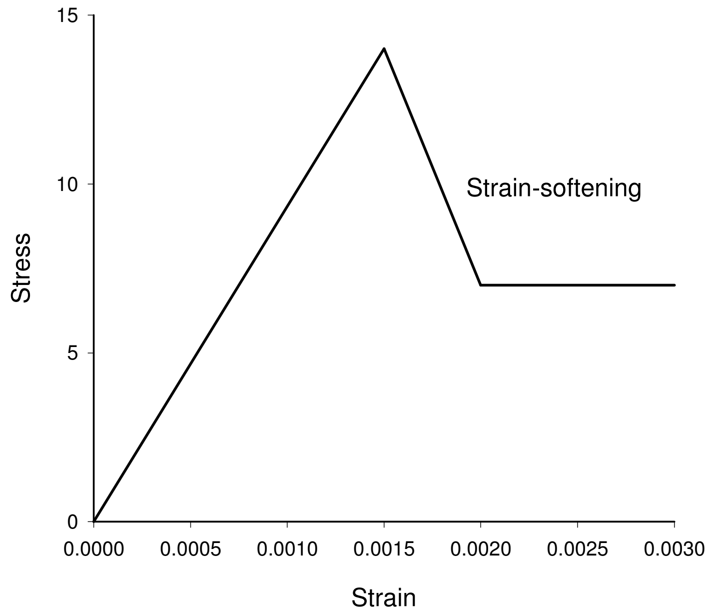

Figure 1.7: Average quality rock mass

1.7.3 Very poor quality rock mass

Analysis of the progressive failure of very poor quality rock masses surrounding tunnels suggests that the post-failure characteristics of the rock are adequately represented by assuming that it behaves perfectly plastically. This means that it continues to deform at a constant stress level and that no volume change is associated with this ongoing failure. This type of behaviour is illustrated in Figure 1.8.

Typical properties for this very poor quality rock mass may be as shown in Table 1.9:

Table 1.9: Typical properties for a very poor quality rock mass

Intact rock strength	σ_{ci}	20 MPa
Hoek-Brown constant	m_i	8
Geological Strength Index	GSI	30
Friction angle	ϕ'	24°
Cohesive strength	c'	0.55 MPa
Rock mass compressive strength	σ_{cm}	1.7 MPa
Rock mass tensile strength	σ_{tm}	-0.01 MPa
Deformation modulus	E_m	1400 MPa
Poisson's ratio	ν	0.3
Dilation angle	α	zero
Post-peak characteristics		
Broken rock mass strength	σ_{fcm}	1.7 MPa
Deformation modulus	E_{fm}	1400 MPa

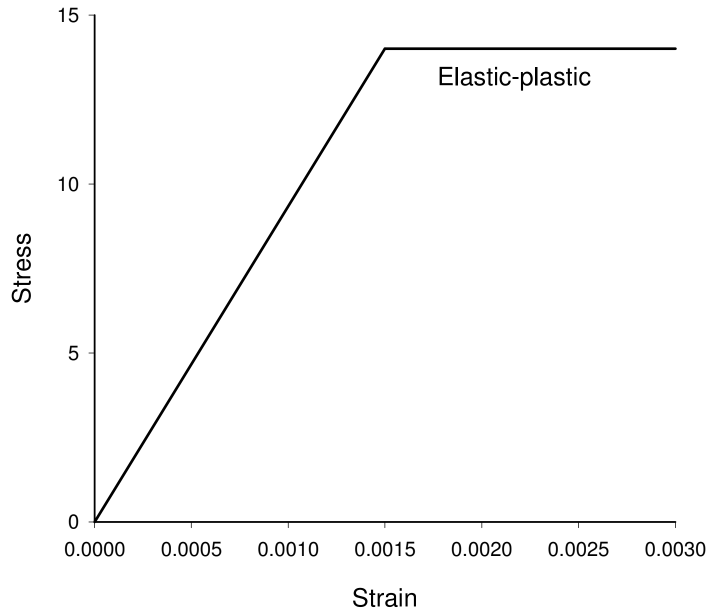

Figure 1.8: Very poor quality soft rock mass

1.8 REFERENCES

Balmer G. 1952. A general analytical solution for Mohr's envelope. Am. Soc. Test. Mat. 52, 1260-1271.

Bieniawski Z.T. 1989. Engineering Rock Mass Classifications. p. 251. New York, Wiley.

Bieniawski Z.T. 1976. Rock mass classification in rock engineering. In Exploration for Rock Engineering, Proc. of the Symp., (Edited by Bieniawski Z.T.) 1, 97-106. Cape Town, Balkema.

Brown E.T. (Ed). 1981. Rock characterization, testing and monitoring - ISRM suggested methods, 171-183. Oxford, Pergamon.

Hoek E. and Brown E.T. 1980. *Underground excavations in rock*, p. 527. London, Instn Min. Metall.

Hoek E. and Brown E.T. 1988 The Hoek-Brown failure criterion - a 1988 update. In Rock Engineering for Underground Excavations, Proc. 15th Canadian Rock Mech. Symp. (Edited by Curran J.C.), 31-38. Toronto, Dept. Civil Engineering, University of Toronto.

Hoek E. Strength of jointed rock masses, 1983. 23rd Rankine Lecture. Géotechnique 33(3), 187-223.

Hoek E. 1994. Strength of rock and rock masses, ISRM News Journal, 2(2), 4-16.

Hoek E., Kaiser P.K. and Bawden W.F. 1995. *Support of underground excavations in hard rock*. p. 215. Rotterdam, Balkema.

Hoek E., Wood D. and Shah S. 1992. A modified Hoek-Brown criterion for jointed rock masses. *Proc. Rock Characterization, Symp. Int. Soc. Rock Mech.: Eurock '92*, (Edited by Hudson J.A.), 209-214. London, Brit. Geotech. Soc.

Hoek, E. and Brown, E.T. 1980. Empirical strength criterion for rock masses. *J. Geotech. Engng. Div., ASCE,* **106** (GT 9), 1013-1035.

Hoek, E. and Brown, E.T. 1997. Practical estimates or rock mass strength. *Int. J. Rock Mech. & Mining Sci. & Geomechanics Abstracts.* **34**(8), 1165-1186.

Hoek, E., Marinos, P. and Benissi, M. 1998. Applicability of the Geological Strength Index (GSI) classification for very weak and sheared rock masses. The case of the Athens Schist Formation. *Bull. Engg. Geol. Env.* 57(2), 151-160.

Karzulovic, A. 2000, personal communication.

Serafim, J.L. and Pereira, J.P. 1983. Consideration of the Geomechanics Classification of Bieniawski. *Proc. Intnl. Symp. Engng. Geol. And Underground Construction.* Lisbon, Portugal, Vol. 1, Part 11, 33-44.

Truzman, M, 1999, personal communication.

1.9 APPENDIX – DETERMINATION OF MOHR COULOMB CONSTANTS

The steps required to determine the parameters A, B, c' and ϕ' are given below. A spreadsheet for carrying out this analysis, with a listing of all the cell formulae, is given in Figure 1.9.

The relationship between the normal and shear stresses can be expressed in terms of the corresponding principal effective stresses as suggested by Balmer (1952):

$$\sigma_n^{'} = \sigma_3^{'} + \frac{\sigma_1^{'} - \sigma_3^{'}}{\partial\sigma_1^{'} / \partial\sigma_3^{'} + 1} \tag{1.13}$$

$$\tau = (\sigma_1^{'} - \sigma_3^{'})\sqrt{\partial\sigma_1^{'} / \partial\sigma_3^{'}} \tag{1.14}$$

For the $GSI > 25$, when $a = 0.5$:

$$\frac{\partial\sigma_1^{'}}{\partial\sigma_3^{'}} = 1 + \frac{m_b \sigma_{ci}}{2(\sigma_1^{'} - \sigma_3^{'})} \tag{1.15}$$

For $GSI < 25$, when $s = 0$:

$$\frac{\partial\sigma_1^{'}}{\partial\sigma_3^{'}} = 1 + a m_b^a \left(\frac{\sigma_3^{'}}{\sigma_{ci}}\right)^{a-1} \tag{1.16}$$

The tensile strength of the rock mass is calculated from:

$$\sigma_{tm} = \frac{\sigma_{ci}}{2}\left(m_b - \sqrt{m_b^2 + 4s}\right) \tag{1.17}$$

The equivalent Mohr envelope, defined by equation 1.2, may be written in the form

$$Y = \log A + BX \tag{1.18}$$

where

$$Y = \log\left(\frac{\tau}{\sigma_{ci}}\right), \; X = \log\left(\frac{\sigma_n^{'} - \sigma_{tm}}{\sigma_{ci}}\right) \tag{1.19}$$

Using the value of σ_{tm} calculated from equation 1.17 and a range of values of τ and $\sigma_n^{'}$ calculated from equations 1.13 and 1.14 the values of A and B are determined by linear regression where :

$$B = \frac{\sum XY - (\sum X \sum Y)/T}{\sum X^2 - (\sum X)^2 / T} \tag{1.20}$$

$$A = 10\wedge\left(\sum Y/T - B(\sum X/T)\right) \tag{1.21}$$

and T is the total number of data pairs included in the regression analysis.

The most critical step in this process is the selection of the range of σ_3' values. As far as the author is aware, there are no theoretically correct methods for choosing this range and a trial and error method, based upon practical compromise, has been used for selecting the range included in the spreadsheet presented in Figure 1.9.

For a Mohr envelope defined by equation 1.2, the friction angle ϕ_i' for a specified normal stress σ_{ni}' is given by:

$$\phi_i' = \arctan\left(AB\left(\frac{\sigma_{ni}' - \sigma_{tm}}{\sigma_{ci}}\right)^{B-1}\right) \tag{1.22}$$

The corresponding cohesive strength c_i' is given by:

$$c_i' = \tau - \sigma_{ni}' \tan \phi_i' \tag{1.23}$$

and the corresponding uniaxial compressive strength of the rock mass is :

$$\sigma_{cmi} = \frac{2c_i' \cos\phi_i'}{1 - \sin\phi_i'} \tag{1.24}$$

The values of c' and ϕ' obtained from this analysis are very sensitive to the range of values of the minor principal stress σ_3' used to generate the simulated full-scale triaxial test results. On the basis of trial and error, it has been found that the most consistent results for deep excavations (depth > 30 m below surface) are obtained when 8 equally spaced values of σ_3' are used in the range $0 < \sigma_3' < 0.25\sigma_{ci}$.

Figure 1.9 Spreadsheet for calculation of Hoek-Brown and equivalent Mohr-Coulomb parameters for excavations deeper than 30 m.

Hoek-Brown and equivalent Mohr-Coulomb failure criteria

Input:	sigci = 60 MPa	mi = 19	GSI = 50

Output:	mb = 3.19	s = 0.0039	a = 0.5
	sigtm = -0.0728 MPa	A = 0.6731	B = 0.7140
	k = 4.06	phi = 37.20 degrees	coh = 2.930 MPa
	sigcm = 11.80 MPa	E = 7746.0 MPa	

Calculation:

									Sums
sig3	1E-10	2.14	4.29	6.4	8.57	10.71	12.86	15.00	60.00
sig1	3.73	22.72	33.15	41.68	49.22	56.12	62.57	68.68	337.88
ds1ds3	26.62	5.64	4.31	3.71	3.35	3.10	2.92	2.78	52.45
sign	0.14	5.24	9.72	13.91	17.91	21.78	25.53	29.20	123.43
tau	0.70	7.36	11.28	14.42	17.10	19.49	21.67	23.68	115.69
x	-2.46	-1.05	-0.79	-0.63	-0.52	-0.44	-0.37	-0.31	-6.58
y	-1.93	-0.91	-0.73	-0.62	-0.55	-0.49	-0.44	-0.40	-6.07
xy	4.76	0.96	0.57	0.39	0.29	0.21	0.16	0.13	7.47
xsq	6.05	1.11	0.62	0.40	0.27	0.19	0.14	0.10	8.88
sig3sig1	0.00	48.69	142.07	267.95	421.89	601.32	804.50	1030.15	3317
sig3sq	0.00	4.59	18.37	41.33	73.47	114.80	165.31	225.00	643
taucalc	0.71	7.15	11.07	14.28	17.09	19.63	21.99	24.19	
sig1sig3fit	11.80	20.50	29.19	37.89	46.58	55.28	63.97	72.67	
signtaufit	3.03	6.91	10.31	13.49	16.53	19.46	22.31	25.09	

Cell formulae:

```
      mb = mi*EXP((GSI-100)/28)
       s = IF(GSI>25,EXP((GSI-100)/9),0)
       a = IF(GSI>25,0.5,0.65-GSI/200)
   sigtm = 0.5*sigci*(mb-SQRT(mb^2+4*s))
    sig3 = Start at 1E-10 (to avoid zero errors) and increment in 7 steps of  sigci/28 to 0.25*sigci
    sig1 = sig3+sigci*(((mb*sig3)/sigci)+s)^a
  ds1ds3 = IF(GSI>25,(1+(mb*sigci)/(2*(sig1-sig3))),1+(a*mb^a)*(sig3/sigci)^(a-1))
    sign = sig3+(sig1-sig3)/(1+ds1ds3)
     tau = (sign-sig3)*SQRT(ds1ds3)
       x = LOG((sign-sigtm)/sigci)
       y = LOG(tau/sigci)
      xy = x*y                x sq = x^2
       A =    acalc =     10^(sumy/8 - bcalc*sumx/8)
       B =    bcalc =     (sumxy - (sumx*sumy)/8)/(sumxsq - (sumx^2)/8)
       k = (sumsig3sig1 - (sumsig3*sumsig1)/8)/(sumsig3sq-(sumsig3^2)/8)
     phi = ASIN((k-1)/(k+1))*180/PI()
     coh = sigcm/(2*SQRT(k))
   sigcm = sumsig1/8 - k*sumsig3/8
       E = IF(sigci>100,1000*10^((GSI-10)/40),SQRT(sigci/100)*1000*10^((GSI-10)/40))
    phit = (ATAN(acalc*bcalc*((signt-sigtm)/sigci)^(bcalc-1)))*180/PI()
    coht = acalc*sigci*((signt-sigtm)/sigci)^bcalc-signt*TAN(phit*PI()/180)
sig3sig1= sig3*sig1         sig3sq = sig3^2
 taucalc = acalc*sigci*((sign-sigtm)/sigci)^bcalc
  s3sifit = sigcm+k*sig3
sntaufit =   coh+sign*TAN(phi*PI()/180)
```

Characterization and engineering properties of tectonically undisturbed but lithologically varied sedimentary rock masses

Evert Hoek, Paul G. Marinos and Vassillis P. Marinos

Paper submitted for publication in the *International Journal of Rock Mechanics and Mining Sciences*

CHARACTERIZATION AND ENGINEERING PROPERTIES OF TECTONICALLY UNDISTURBED BUT LITHOLOGICALLY VARIED SEDIMENTARY ROCK MASSES

Evert Hoek[1], Paul G. Marinos[2] and Vassilis P. Marinos[2]

Abstract

Tectonically undisturbed sedimentary rocks deposited in a quiescent shallow marine environment often include a sequence of strata that may present significant lithological variety at the scale of an engineering structure. Such rock masses exhibit engineering properties that are significantly different from tectonically disturbed rock masses of similar composition. For example, molasse consists of a series of tectonically undisturbed sediments of sandstones, conglomerates, siltstones and marls, produced by the erosion of mountain ranges after the final phase of an orogeny. They behave quite differently from flysch which has the same composition but which was tectonically disturbed during the orogeny. The molasses behave as continuous rock masses when they are confined at depth and the bedding planes do not appear as clearly defined discontinuity surfaces. Close to the surface the layering of the formations is discernible and only then similarities may exist with the structure of some types of flysch. Therefore extreme care is necessary in the use of geotechnical classification systems for the selection of design parameters, in order to avoid penalizing the rock mass unnecessarily. A discussion on the use Geological Strength Index, GSI, for the characterization of such rock masses is presented. Two GSI charts are proposed for estimating the mechanical properties of these masses, one mainly for tunnels and the second for surface excavations. An example is given to illustrate the process of tunnel design in molassic rocks.

1. Introduction

In many mountainous regions a sequence of alternations of clastic and pelitic sediments were deposited during a quiescent period after the main orogenesis. The behaviour of these deposits, known as molasses in Europe, is quite different from that of flysch, a sequence of strata of similar composition associated with the same orogenesis. Although the cases on which this discussion is based come from the molassic formation of Northern Greece, we believe that the proposed characterisation can be of general application to sedimentary rocks deposited in a quiescent shallow marine environment and not associated with significant tectonic disturbance.

2. General geological setting.

Molasse comes from a provincial Swiss name originally given to soft sandstone associated with marl and conglomerates belonging to the Miocene Tertiary period, extensively developed in the low country of Switzerland and composed of Alpine detritus. The term is now applied to all orogenic deposits of similar genesis e.g. to describe sediments produced by the erosion of mountain ranges after the final phase of an orogeny.

The molasse consist of an almost undisturbed sequence of great overall thickness of sandstones and siltstones, mudstones or marls. These rocks can alternate in layers of tens of centimetres or they can be present as massive strata (mainly the sandstones with occasional siltstone intercalations). Conglomerates occur rather commonly, forming thick bands in some cases. Rather restricted limestone horizons may also be present. Due to the facts that the sedimentation of the detritus material took place close to the sea shore line and the ongoing subsidence of the newly formed basin, an alternation of sea, lacustrine and terrestrial deposits, may characterise the molasses together with lateral transitions from one lithological type of layer to the other. A Stratigraphic column and a geologic profile of molassic formations from Greece are presented in Figures 1 and 2.

[1] Consulting Engineer, Vancouver, Canada, e-mail: ehoek@attglobal.net
[2] National Technical University of Athens, School of Civil Engineering, 9, Iroon Politechniou str., 157 80 Zografou, Greece, e-mail: marinos@central.ntua.gr

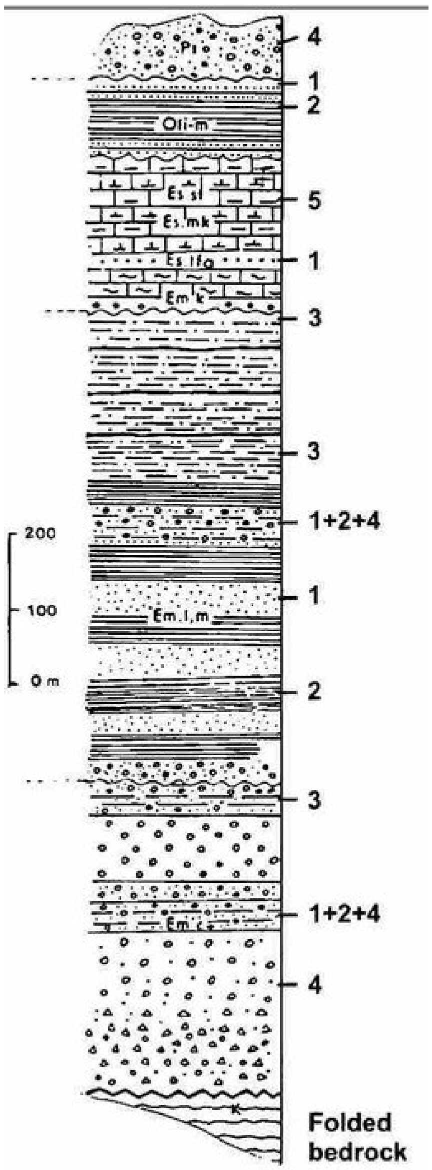

Figure 1: Schematic column of the mollassic formations in the Rhodope basin, NE Greece.

1. sandstones,
2. clay shales or siltstones,
3. sandstones with siltstones or clayey sandstones,
4. conglomerates,
5. limestones, marly limestones or marles.

(from the Geolgical map of Greece, 1:50000, IGME, 1980)

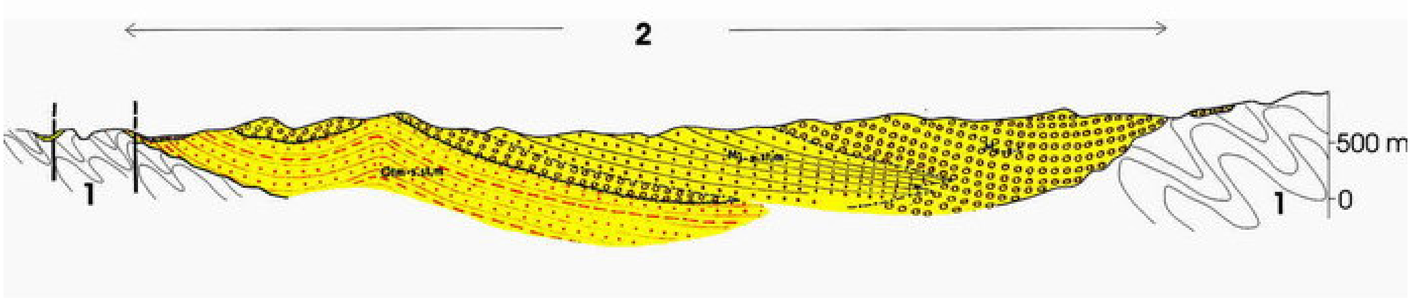

Figure 2: Geologic section in a molassic country, NW Greece (from the Geological map of Greece, sheet Ayiofillo, 1:50.000, IGME, 1979, slightly modified)

1: Bed rock of the already formed mountain belt.
2: Molassic country: alternation of sandstones, conglomerates, siltstones and marls.

In some cases sandstones are very weak and can be assimilated with sands; in such weak molasses, clays and silts are also present and the material can be treated as soil. These types of molasses are not considered in this paper.

As the molasse characterise a series of sediments that were formed and developed after the main orogenesis, they have not suffered from compression or shear. They are thus unfolded or contain mild gravity folds or flexures. Inclination of strata is generally low and cases with dips of more than 30° are infrequent or local. Gravity faults are present, as in all post-tectonic basins but their impact on the deterioration of the quality of the rock is limited. In certain ranges molassic formations may be deformed and overthrust by the final advance of tectonic nappes. Again the decrease of their quality is localised.

3. Molasse vs Flysch

In contrast to molasses, the term flysch is used to describe sediments produced early in the mountain building process by the erosion of uprising and developing fold structures. These are subsequently deformed by later stages in the development of the same fold structures. Flysch is thus produced in front of the advancing orogenesis, folded with the other strata or even overthrust by the advancing mountain belt. On the other hand, molasses in the basins behind the already formed mountain belt remain over the folded belt and are undisturbed by the mountain building process.

Flysch, in contrast to molasses, has more rhythmic and thinner alternations of sandstone and pelitic layers. These suffered strong compressional deformations which produced folds of many scales, sizeable sheared zones and weaker surfaces, primarily in the form of well developed bedding planes.

4. Lithology

The sandstones members of the molasse are often silty or marly and these exhibit low strength values. Their unconfined compression strength may be about 10 MPa if they are marly or silty and more than 50 MPa in their typical granular form. A value of 20 MPa may reasonably describe the typical unconfined compression strength of the sandstone component of the molasses in NW Greece.

The unconfined compressive strength of a typical siltstone can be about 15 MPa. However, siltstones may have a significant presence of clayey materials (mudstones) and in the case of a clayey-siltstone, mudstone or marl, the unconfined compressive strength may be in the range of 5 to 10 MPa.

All of these siltstones are very vulnerable to weathering and development of fissility parallel to the bedding when these rocks are exposed or are close to the surface. In outcrops they appear thinly layered like siltstone shales and when they alternate with sandstones, their appearance resemblances similar alternation in flysch. The weathering of outcrops shown in Figure 3 can be misleading when considering the behaviour of these molassic rocks in a confined underground environment in which the process of air slaking is restricted. This can be seen by comparing the appearance of freshly drilled core in Figure 4 with that of the same core after storage in a core shed for approximately 6 months, shown in Figure 5.

Figure 3: Surface exposure showing alternating sandstone and siltstone layers in a molassic rock mass in NW Greece.

In the freshly drilled core it is sometimes difficult to distinguish between the sandstone and siltstone components of the molasse since the core may be continuous over significant lengths. It is only after exposure that the siltstone cores start to develop a fissile appearance and, after a few months they collapse to a silty-muddy loose mass. This process, which also affects the silty-sandstones, can result in a dramatic misinterpretation of the engineering characteristics of molasses if inspection of the core is not done immediately. Similarly, testing for the unconfined compressive strength must be performed as soon as possible after drilling and, in some extreme cases, it has been found that this testing will only produce reliable results if it is done on site immediately after drilling.

Figure 4: Appearance of molassic rock core immediately after drilling. Sandstones and siltstones are present but the bedding planes (mainly of the siltstone) do not appear as defined discontinuity surfaces.

Figure 5: Appearance of the same core as shown in Figure 4 but after storage in a core shed for six months. The sandstone remains intact but the siltstones exhibit fissility followed by collapse.

Figures 6 and 7 show very similar behaviour to that described above in cores from rock from the site of the Drakensberg Pumped Storage Project in South Africa where site investigations were carried out in the early 1970s. The appearance of surface outcrops resulted in an extremely conservative assessment of the rock mass behaviour. It was only after an exploratory adit was mined and freshly drilled core was inspected and tested and that realistic excavation designs were developed.

Figure 8 shows the main powerhouse cavern of the Drakensberg Pumped Storage Scheme during construction in about 1975. Based on tests carried out on site and on the behaviour of exploration adits on the project [1], a final design was developed using tensioned and grouted rockbolts (6 m long and 25 mm diameter) and a 15 cm thick shotcrete lining. A 5 cm thick protective coating of shotcrete was applied as soon as possible to all exposed rock surfaces in order to prevent air slaking. A further 10 cm of wire-reinforced shotcrete was applied later to complete the lining. No additional lining or reinforcement was used and a suspended steel ceiling was used to catch water drips and to improve the appearance of the interior of the cavern. The system has performed without any problems for more than 25 years.

5. The application of GSI to molassic rock masses

The molasses form rock masses with dramatically different structure when they outcrop or are close to the surface as compared to those confined in depth. This means that care has to be exercised in the use of the Geological Strength Index (GSI) charts for assessment of rock mass properties.

In the undisturbed in situ rock mass encountered in tunnelling, the rock mass is generally continuous as illustrated in the freshly drilled core photographs described above. Even when lithological variation is present the bedding planes do not appear as clearly defined discontinuity surfaces. They are taken into account by the intact strength σ_{ci} of the mass. In such cases the use of the GSI chart for blocky rock [2, 3] reproduced in Figure 9, is recommended and the zone designated M1 is applicable. The fractures and other joints that are present, given the history of the formation, are generally not numerous and the rock mass should be assigned a GSI value of 50 to 60 or more. Due to the benign geological history it is even expected that the molasses will exhibit very few or no discontinuities in several stretches of the tunnels. In these cases GSI values are very high and indeed the rock mass can be treated as intact with engineering parameters given by direct laboratory testing.

Figure 6: Freshly drilled sandstones and siltstones from the Drakensberg Pumped Storage Project in South Africa (1972).

Figure 7: Similar core to that shown in Figure 6 but after storage for 6 months.

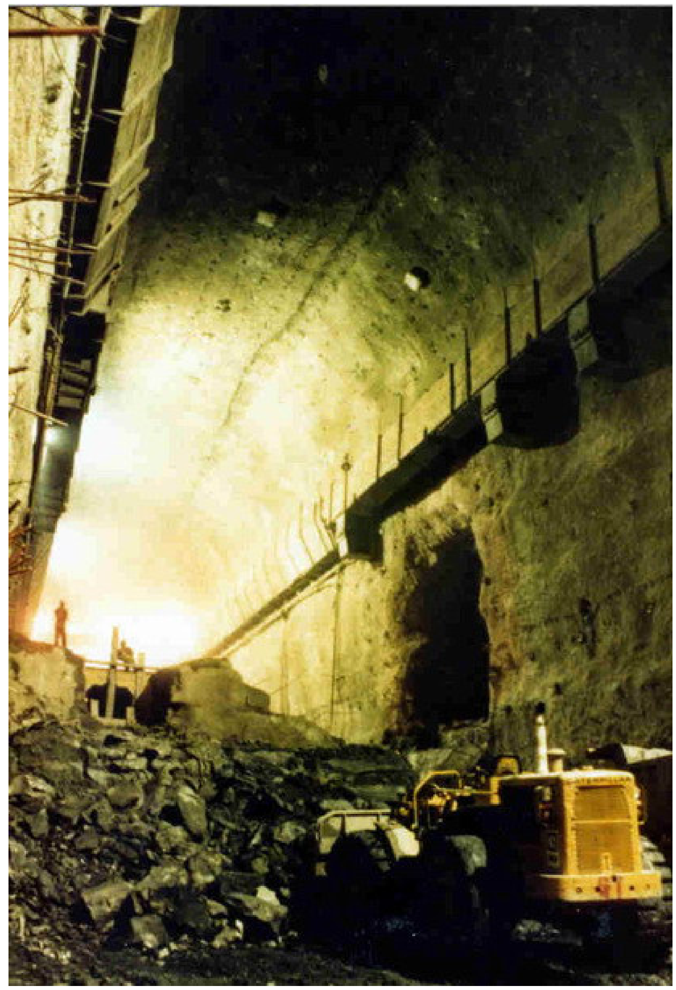

Figure 8: The 17 m span, 32 m high underground powerhouse of the Drakensberg Pumped Storage in South Africa. This cavern was excavated in the undisturbed sedimentary rock mass illustrated in Figure 6 and it was supported using rockbolts and shotcrete only. A 5 cm thick layer was applied immediately to all exposed rock surfaces and this was followed later by a layer of wire mesh and an additional 10 cm of shotcrete. The project has recently completed 25 years of trouble-free operation. Note: The extreme degradation of the Drakensberg rocks was partly because some of the units were tuffaceous

When fault zones are encountered in tunnelling through these molassic rocks, the rock mass may be heavily broken and brecciated but it will not have been subjected to air slaking. Hence the blocky rock GSI chart given in Figure 9 can be used but the GSI value will lie in the range of 25 to 40 as shown by the area designated M2.

In outcrops the heterogeneity of the formation is discernible and similarities exist with the structure of some types of flysch. Hence the GSI chart for heterogeneous rock masses such as flysch [4, 5] can be used with the exclusion of sheared and deformed types and with a slight shifting to the left of the flysch chart categories. This version of the chart, for use with fissile molassic rocks, is presented in Figure 10. The M3 to M7 designations in Figure 10 are largely self-explanatory. However, the user should read the descriptions in both rows and columns carefully and should not rely only on the pictures in choosing GSI values.

6. Estimates of the mechanical properties of molassic rock masses

For massive units of sandstone or siltstone, where no significant bedding planes or discontinuities are present, the rock mass should be treated as intact and the design values for strength and deformation modulus should be taken directly from laboratory tests. Note that these tests have to be performed very carefully in order to obtain reliable results. As mentioned earlier, some of the siltstone units can break down very quickly on exposure and it is essential to test than as soon after recovery of the core as possible. In some cases, testing in the field using portable equipment has been necessary in order to obtain reliable results.

The use of point load tests is not recommended for these low strength materials since the penetration of the loading points can invalidate the results. Compression testing should always be carried out normal to the bedding direction and the results from specimens in which the failure is controlled by structural features should be rejected. A first estimate of the deformation modulus for these massive rock units can be obtained from $E \approx 200\sigma_{ci}$ (all units in MPa).

For molassic rock masses in which significant bedding planes or discontinuities are present the charts presented in Figures 9 and 10 can be used to estimate the GSI values which can then be used to downgrade the strength of the intact rock in accordance with the Hoek-Brown criterion.

7. Brittle failure in massive molassic units

Research over many years, dating back to the pioneering work on the fracture of glass aircraft windshields by Griffith [6, 7], has established that brittle fracture in massive rocks is associated with propagation of tensile cracks which originate at defects such as grain boundaries in the material. These cracks propagate parallel to the major principal stress direction and their length is controlled by the ratio of minor to major principal stresses at the point under consideration. At the excavated boundary of an underground excavation the minor principal stress is zero and hence these tensile cracks propagate parallel to the boundary forming the slabs and spalls. Recent thinking on brittle fracture in hard massive rocks has been summarized by Kaiser et al [8] and by Diederichs [9].

Since the tensile crack propagation described above does not mobilize any frictional forces within the rock mass, the Mohr Coulomb criterion for the initiation of these cracks can be expressed in terms of cohesive strength only, with the friction angle set to zero. Laboratory tests and back analyses of the extent brittle failure in underground excavations show that the appropriate cohesive strength is approximately equal to one third of the uniaxial compressive strength of the intact rock, i.e. $c \approx 0.33\sigma_{ci}$, $\phi = 0$. The broken material that remains within the failure zone surrounding an underground excavation can be characterized as a highly frictional, cohesionless rock mass, i.e. $c = 0$, $\phi \approx 33°$.

This failure process has been used in modelling an unsupported tunnel in molasse and the results are shown in Figure 11. The properties of the sandstone and siltstone layers in this model are as follows:

Sandstone: Intact rock: $c = 7$ MPa, $\phi = 0$,
$E = 4000$ MPa ($\sigma_{ci} = 20$ MPa)
Residual strength: $c = 0$, $\phi = 35°$, dilation angle 5°.
Siltstone: Intact rock: $c = 3$ MPa, $\phi = 0$,
$E = 1800$ MPa ($\sigma_{ci} = 9$ MPa)
Residual strength: $c = 0$, $\phi = 25°$, dilation angle 5°.

Figure 9: GSI chart for confined molasse (mainly applicable for tunnels).

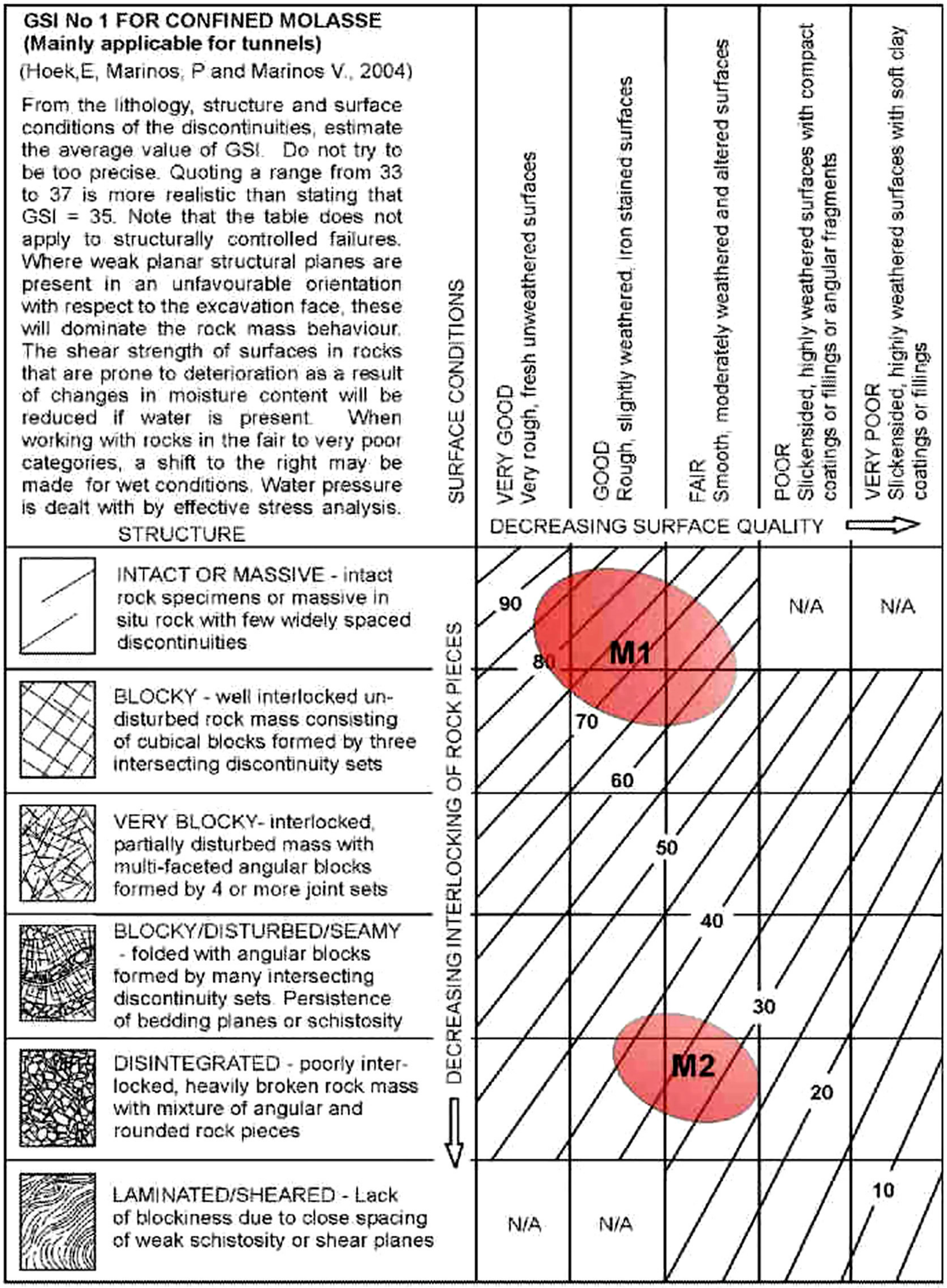

Notes: When there are no discontinuities, use laboratory test results directly
M1 - Confined molasse, either homogeneous or with sandstone and siltstone alterations
M2 - Heavily broken or brecciated molasse in fault zones
The GSI chart should not be used for loose conglomerates - treat as weakly cemented river gravel

Figure 10: GSI chart for fissile Molasse where bedding planes of siltstones-mudstones are frequent and well defined. (Surface excavations and slopes)

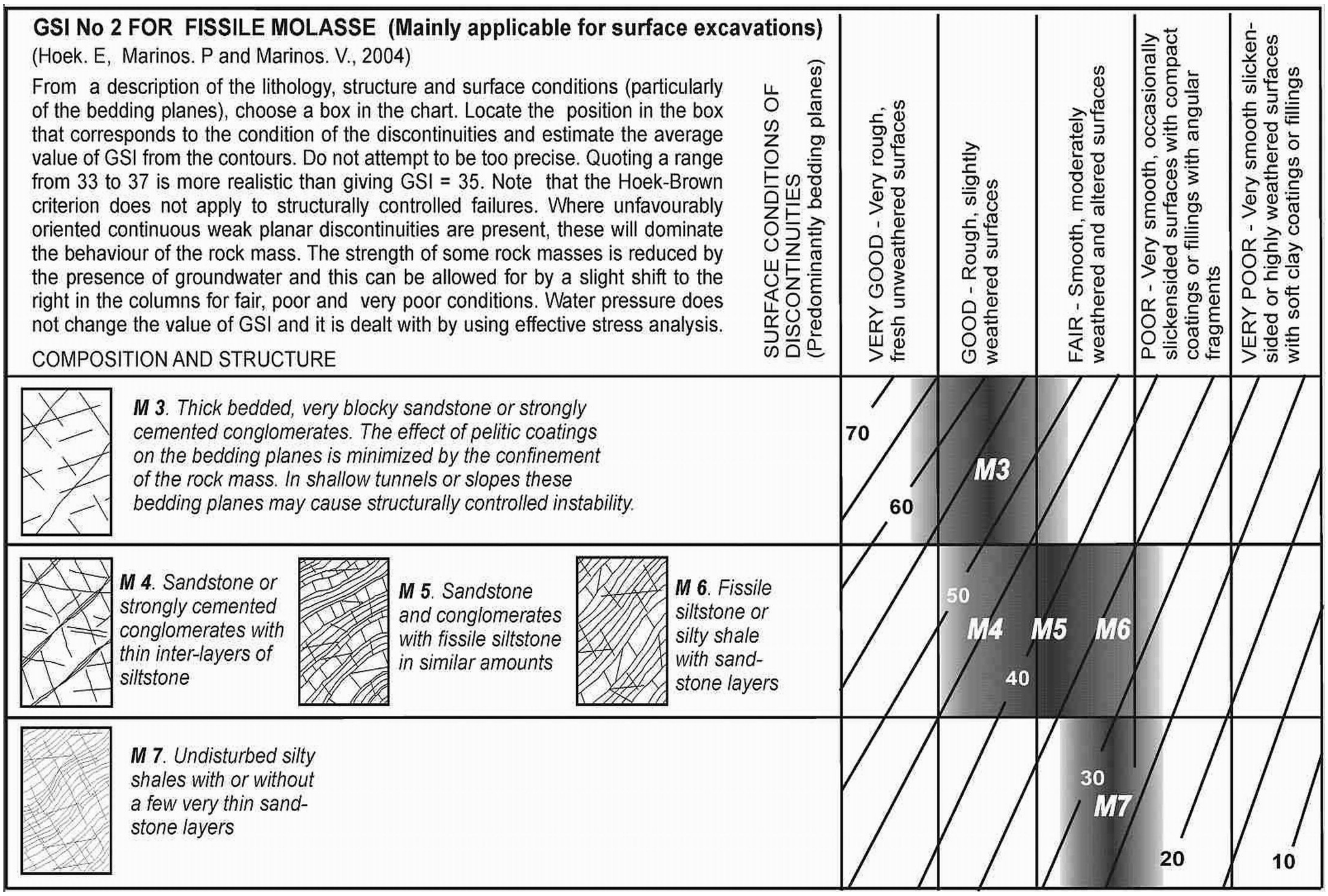

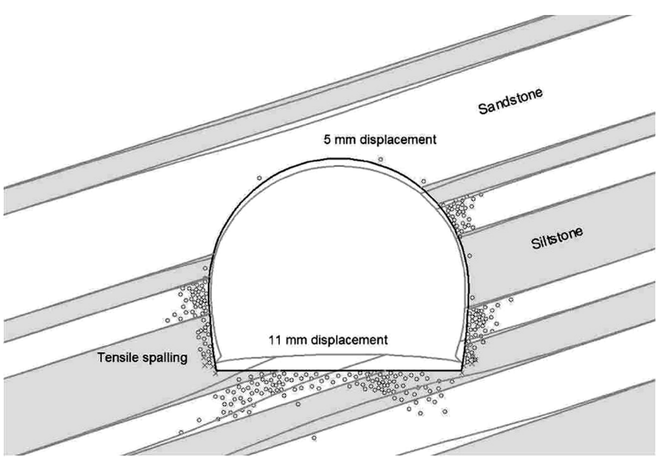

Figure 11: Tensile failure in sandstone and siltstone molasse surrounding an unsupported tunnel.

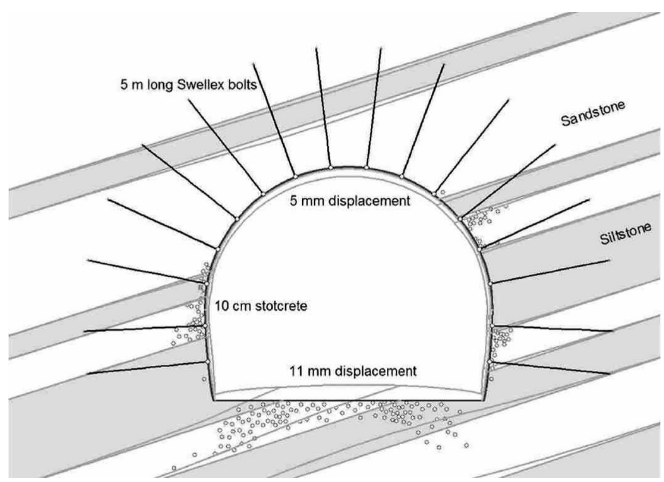

Figure 12: Typical support in molassic rock masses under moderate stress levels.

Zero tensile strength was assumed for all cases. The depth of cover over the tunnel is assumed to be 100 m and the ratio of horizontal to vertical stress $k = 0.5$.

Note that the failure process is almost entirely tensile (denoted by the **o** symbol in Figures 11 and 12) and the propagation of the failure is quite limited and concentrated largely in the sandstone layers which are "dragged" by the softer siltstones. The deformations are also small as would be expected for the relatively high deformation modulus and the modest in situ stress level.

Sensitivity studies showed that the distribution and extent of failure is quite sensitive to the ratio of horizontal to vertical stress. This suggests that, where no in situ stress measurements are available, the designer should check the design for both $k = 0.5$ and $k = 2$ which can be considered reasonable lower and upper bounds for the molassic rock masses under consideration.

The influence of jointing was also checked and found to be not very significant on the results shown in Figure 11. This is because the joints are tensile failures created by differential strains in the sandstone and siltstone layers. Consequently, their surfaces are rough and they exhibit high frictional strength. Obviously there are situations in which the creation of a free surface by the excavation of the tunnel can combine with joints and bedding planes to release blocks and wedges that will fall under gravity. Predicting the location and size of these failures is difficult and, where they are or concern, it is prudent to use pattern rockbolting to stabilize the tunnel roof and walls.

Figure 12 shows the results of an analysis of the same tunnel shown in Figure 11 except that a pattern of 5 m long Swellex rockbolts and a 10 cm layer of shotcrete have been added. It can be seen that, apart from a reduction of spalling and deformation in the lower sidewalls of the tunnel, the support system does not have a dramatic impact upon the behaviour of the tunnel. However, this support plays the following critical roles:

1. The application of a 3 to 5 cm thick layer of shotcrete to exposed rock faces as soon as possible (typically at the and of each excavation round) provides sealing and protection of the siltstone layers against air slaking.
2. The pattern of rockbolts reinforces the rock mass by maintaining the confinement and preventing gravity falls of loose structurally defined blocks or wedges or falls due to decompression of the sealing of bedding planes.
3. The addition of a second layer of shotcrete, with either wire mesh or fibre reinforcement, forms a bridging shell between rockbolts and prevents progressive ravelling from falling of small "key blocks" from the surface of the excavation.

4. Support design for discontinuous, broken and weak molassic rocks

For broken and weak molassic rocks in the vicinity of faults (M2 in Figure 9) or in the cases where discontinuous weak masses occur (M3 to M7 in Figure 10), there is clearly a need to provide heavier support than that shown in Figure 12. In addition, stabilization of the face may be required in order to prevent progressive ravelling and chimney formation. A typical primary support design is illustrated in Figure 13 and this closely resembles the design used in tunnels in flysch in many Alpine highway projects. An important difference is the application of a protective layer of shotcrete to exposed molassic rock surfaces to prevent air slacking and the resultant deterioration of the rock mass.

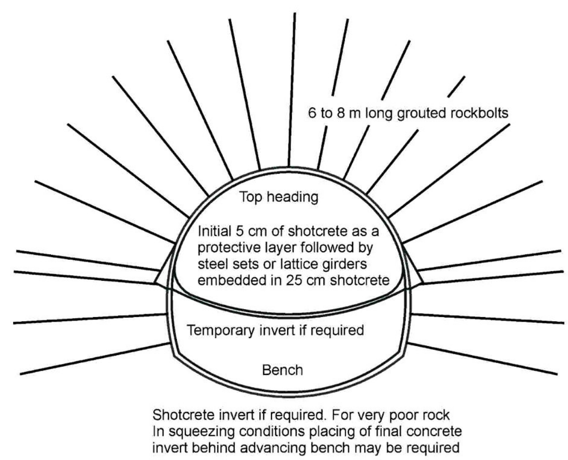

Figure 13: Typical primary support design for broken molassic rocks with frequent and well defined discontinuities, mainly bedding planes. A final concrete lining (not shown) is placed later.

The treatment of the invert depends upon the rock mass characteristics and in situ stress levels. If heavy squeezing conditions are anticipated [4, 10] consideration can be given to the installation of the final concrete invert as close as practicable to the bench face. Where the cover is relatively modest it may be possible to proceed without an invert in the top heading and a relative light final invert (mainly for trafficability).

8. Conclusions

Extreme care has to be taken when classifying tectonically undisturbed sedimentary rock masses with lithological variation formed in a quiescent depositional environment. Although the cases on which this paper are based come from molassic formations, we believe that the proposed characterization can be of general application for this type of undisturbed geologic formation.

For massive units of sandstone or siltstone, where no significant bedding planes or discontinuities are present, the rock mass should be treated as intact and the design values for strength and deformation modulus should be taken directly from laboratory tests.

For rock masses in which bedding planes or discontinuities are present the GSI charts can be used to estimate the values to be used to downgrade the strength of the intact rock in accordance with the Hoek-Brown criterion. The use of the program RocLab[1] is recommended for the estimation of rock mass properties. For the confined conditions encountered in tunnels, these rock masses are generally continuous with few discontinuities and zone M1 in the the basic GSI chart for blocky rock given in Figure 9. Zone M2 in this chart corresponds to broken and brecciated masses as a result of faulting. Typical GSI values of 60 to 70 can be anticipated in the first case and values of 30 to 40 in the second.

In such massive rocks under confined conditions, brittle failure is considered to be the most likely failure mode and this results in spalling and slabbing of tunnel boundaries. Laboratory tests and back analyses of the extent brittle failure in underground excavations show that the appropriate cohesive strength is approximately equal to one third of the uniaxial compressive strength of the intact rock ($c \approx 0.33\sigma_{ci}$) and the friction angle is zero ($\phi = 0$) since the failure process is predominantly tensile and no shear is mobilized. Simple tunnelling conditions and good advance rates can be anticipated for confined masses which can be treated as intact rock or classified as M1 in Figure 9.

An example of the analysis of tunnel behaviour in these rocks is presented in Figures 11 and 12 and a typical primary support design for a 12 m span tunnel excavated by top heading and benching is given in Figure 13.

For surface excavations such as portals and cuts, where air slaking occurs as a result of the exposure of the rock mass, the use of a new GSI chart is recommended. This chart, presented in Figure 10, is derived from a GSI chart for heterogeneous rocks such as flysch with the elimination of the deformation and sheared features that govern the behaviour of flysch.

In surface excavations or where faulting and brecciation have disrupted the rock mass, more conventional rock mass failure characteristics, defined by the Hoek-Brown failure criterion are appropriate.

9. Acknowledgement:

The constructive comments provided by Dr Trevor Carter or Golder Associates of Toronto, Canada, Mr Nikos Kazilis of Engatia Odos S.A, Greece and Mr Kostas Anastasopoulos or the Public Power Corporation of Greece are gratefully acknowledged.

10. References

1. Bowcock, J.B., Boyd, J.M., Hoek, E. and Sharp, J.C. 1976. Drakensberg pumped storage scheme, rock engineering aspects. In *Exploration for Rock Engineering* (ed. Z.T. Bieniawski) **2** , 121-139. Rotterdam: Balkema.
2. Hoek, E. and Brown, E.T. 1997. Practical estimates or rock mass strength. *Intnl. J. Rock Mech. & Mining Sci. & Geomechanics Abstracts.* **34**(8), 1165-1186.
3. Marinos, P and Hoek, E. 2000. GSI – A geologically friendly tool for rock mass strength estimation. *Proc. GeoEng2000 Conference, Melbourne.*

[1] This program can be downloaded free from www.rocscience.com.

4. Hoek, E. and Marinos, P. (2000) Predicting Tunnel Squeezing. *Tunnels and Tunnelling International*. Part 1 - November Issue 2000,. 45-51, Part 2 - December, 2000, 34-36.

5. Marinos. P, and Hoek, E. (2001) – Estimating the geotechnical properties of heterogeneous rock masses such as flysch. *Bulletin of the Engineering Geology & the Environment (IAEG)*, 60, 85-92.

6. Griffith, A.A. 1921. The phenomenon of rupture and flow in solids. *Phil. Trans. Roy. Soc., London* Vol. A221 , 163-198.

7. Griffith, A.A. 1924. Theory of rupture. *Proc. 1st congr. applied mechanics*, Delft, 55-63. Delft: Technische Bockhandel en Drukkerij.

8. Kaiser, P.K., Diederichs, M.S., Martin, D., Sharp, J. and Steiner, W. 2000, Underground works in hard rock tunnelling and mining. *Proc. GeoEng2000*, Melbourne.

9. Diederichs, M.S. 2002, Stress induced damage accumulation and implications for hard rock engineering. *Proc. NARMS-TAC Conference*, Toronto, 2002, **1**, 3-12.

10. Hoek, E. 2000. Big tunnels in bad rock, 2000 Terzaghi lecture. *ASCE Journal of Gotechnical and Geoenvironmental Engineering*, Vol. 127, No. 9, Sept 2001, pages 726-740.

Characterization of Granite and the Underground Construction in Metro do Porto, Portugal.

Babendererde, S, Hoek, E., Marinos, P. and Cardoso, A.S.

Proc. International Conference on Site Characterization, Porto, Portugal, 19-22 September, 2004

Characterization of Granite and the Underground Construction in Metro do Porto, Portugal.

S. Babendererde

Am Lotsenberg 8, D-23570 Lubeck-Travemunde, Germany, Email: contact@bab-ing.com

E. Hoek

3034 Edgemont Boulevard, P.O. Box 75516, North Vancouver, B.C, Canada, V7R 4X1, Email: ehoek@attglobal.ne

P. Marinos

National Technical University of Athens, 9 Iroon Polytechniou str. 15780, Greece, Email:marinos@central.ntua.gr

A. S. Cardoso

Faculdade de Engenharia, Rua Roberto Frias, 4200-465 Porto, Portugal, Email: scardoso@pe.up.pt

Keywords: Rockmass classification, granite, tunnelling

ABSTRACT: The characterization of the granitic mass of Porto for the design and construction of the Metro works of the city was based on weathering grades and structural features which were used for the derivation of the design parameters. The highly variable nature of the deeply weathered Oporto granite posed significant challenges in the driving of the 2.3 km long C line and the 4 km long S line of the project. Two 8.7 m diameter Herrenknecht EPB TBMs were used to excavate these tunnels but the nature of the rock mass made it extremely difficult to differentiate between the qualities of the mass and apply an open or a closed mode operation of the TBM accordingly. Thus early problems were encountered due to over excavation and face collapse. The matter was finally resolved by the introduction of an Active Support System, which involves the injection of pressurized bentonite slurry to compensate for deficiencies in the face support pressure when driving in mixed face conditions. Both the C and S lines have now been completed with minimal surface subsidence and no face instability.

1. INTRODUCTION

In late 1998 the Municipality of Porto took a decision to upgrade its existing railway network to an integrated metropolitan transport system with 70 km of track and 66 stations. Seven kilometres of this track and 10 stations are located under the picturesque and densely populated city of Porto, an UNESCO world heritage site. A map of the surface and underground routes is presented in Figure 1. Metro do Porto SA, a public company, is implementing the project. The design, construction and operation of this concession were awarded to Normetro, a joint venture. The civil works design and construction was awarded to Transmetro, a joint venture of Soares da Costa, Somague and Impregilio.

The underground tunnel, driven by two Earth Pressure Balance (EPB) TBMs, has an internal diameter of 7.8 m and accommodates two tracks with trains. Line C stretches 2,350 m from Campanhã to Trindade and has five underground stations, a maximum cover of 32 m and a minimum of 3m before reaching Trinidad station. Line S is 3,950m long and runs from Salgueiros to São Bento with 7 stations and a maximum overburden of 21 m.

Figure 1: Map of Metro do Porto routes. Underground tunnels are Line C from Campanhã to Trindande and Line S from Salgeuiros to São Bento.

Tunnel driving was started in August 2000 with the drive from Campanhã to Trindade. It was originally planned that the EPB TBM would be run with a partially full, unpressurized working chamber in the better quality granite in order to take advantage of the higher rates of advance in this mode as compared with operating with a fully pressurized working chamber. It was soon found that the highly variable nature of the rock mass made it extremely difficult to differentiate between the better quality rock masses in which the working chamber could be operated safely with no pressure and the weathered material in which a positive support pressure was required on the face. There were indications of over-excavation and two collapses reached the surface. The second occurred on 12 January 2001, almost a month after the passage of the TBM on 16 to 18 December 2000. This collapse resulted in the death of a citizen in a house overlying the tunnel.

At the invitation of Professor Manuel de Oliveira Marques, Chief Executive Officer of Metro do Porto S.A., one of the authors (E.H) visited Porto from in early February 2001 to review the geotechnical and tunnelling issues of the C Line tunnel. As a result of this visit a Panel of Experts, consisting of the authors of this paper, was established in order to provide advice to Metro do Porto.

2. GEOLOGICAL CONDITIONS

The underground portion of the line passes through the granite batholith which was intruded into the Porto-Tomar regional fault in the late Hercinian period (Figure 2). The Porto Granite, a medium grained two mica granite, is characterized by deep weathering and the tunnel passes unevenly through six grades of weathering and alteration ranging from fresh granite to residual soil. The granite is crossed randomly by aplitic/pegmatitic dykes which display much less weathering, following tectonically determined tension joints.

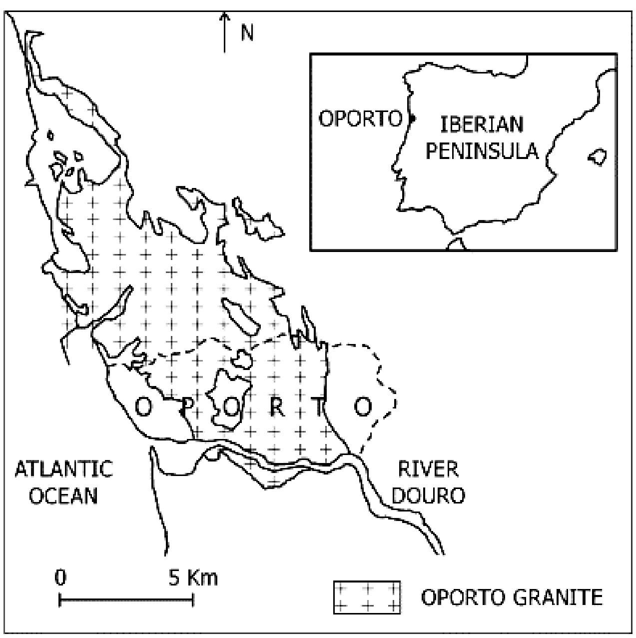

Figure 2: Distribution of granite in the City of Oporto (from A. Begonha and M. A. Sequeira Braga, 2002)

3. CHARACTERISATION OF WEATHERING

The particular feature of most engineering significance of the rock mass is its weathering. All weathering grades (W1 to W6, as established in the engineering geological classification according to the scheme proposed by the Geological Society of London, 1995, and the recommendations of ISRM) can be encountered. Through analyzing the associated geomechanical properties from laboratory tests, the designers developed a re-classification of the degree of weathering aiming to better define the characteristic values of each class and to reduce the overlap between classes (Table 1, Russo et al., 2001).

Table 1: Weathering classes over the uniaxial compressive strength range (clear bars indicate classification based only on qualitative evaluation, shaded bars indicate re-classification after statistical analysis, from Russo et al., 2001)

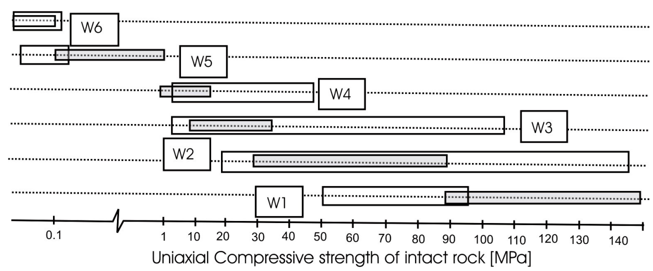

The depth of weathering is of the order of few tens of meters as weathering was assisted by the stress relief regime due to the deepening of Duro valley. Depths of weathering of 30m are reported by Begonha and Sequeira Braga, 2002. Hence, the ground behaviour varies from a strong rock mass to a low cohesion or even cohesionless granular soil. The granularity and frictional behaviour is retained, as the kaolinitisation of feldspaths is not complete and the clay part not important. Furthermore, the spatial development of the weathered rock is completely irregular and erratic. The change from one weathered zone to another is neither progressive nor transitional. It is thus possible to move abruptly from a good granitic mass to a very weathered soil like mass. The thickness of the weathered parts varies very quickly from several meters to zero. Blocks of sound rock, “bolas”, of various dimensions can “float” inside a completely decomposed granite. Weathered material, either transported or in situ, also occurs in discontinuities.

A particularly striking feature is that, due to the erratic weathering of the granite, weathered zones of considerable size well beyond the size of typical “bolas” can be found under zones of sound granite (see Figure 3). While this phenomenon is an exception rather than the rule and it was expected to disappear with depth, it could not be ignored in the zone intersected by the construction of the metro works. A typical case of such setting is in Heroismo station where weathered granite with floating cores of granite occurs under a surficial part of a sound granitic rock mass (Figure 5).

Figure 3: Appearance of different degrees of weathering in granite in a core recovered from a site investigation borehole on the tunnel alignment. Note that the weathered granite in the left box is at a depth of about 24m under the sound granite of the right box. This must therefore correspond to a huge boulder (core).

Figure 4: Appearance of Oporto granite in the face of an excavation for the new (2002) football stadium. Fracturing of the rock mass and heterogeneity in weathering is obvious

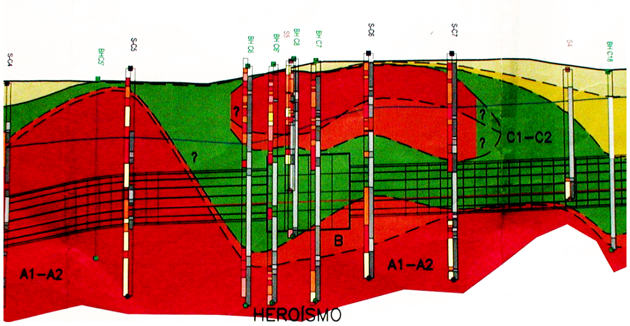

Figure 5: Predicted geology for the Heroismo mined station (Assessment by Transmetro, documents of Metro do Porto). Heterogeneity in weathering and its erratic geometry is evident.

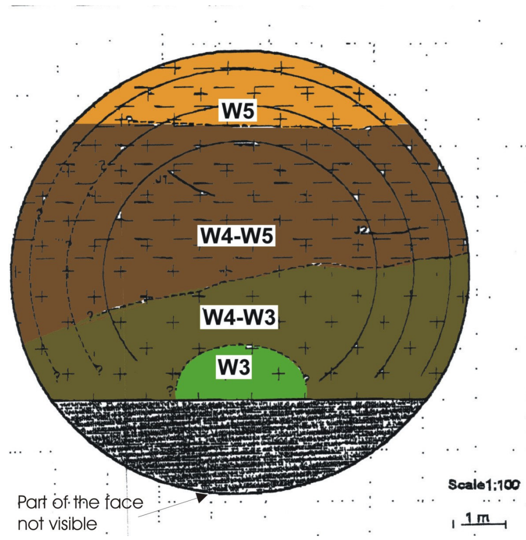

Figure 6: As typical distribution of weathered granite in the face of the EPB driven Tunnel.

4. CHARACTERIZATION OF GRANITIC ROCK MASSES

The definition of rock mass properties for use in the face stability analyses and the machine selection, in the design of stations and the settlement- risk analysis, was based on a geotechnical characterization of the granitic mass in various groups. The approach applied in the design is illustrated in Table 2 and the values of the geotechnical parameters selected after statistical analysis are shown in Table 3 (Russo et al., 2001, Quelhas et al., 2004). Groups g5, g6 and g7 refer to material with soil-like behaviour. Thus it was generally possible to apply principles of soil mechanics to define the geotechnical parameters and the design values of the soil mass were based on sample properties, taking into account the results of the available in situ tests (SPT, etc).

Deformations modulus for groups g2 and g3 was derived from empirical correlations and the results of the 136 Menard tests conducted in the boreholes. It is worth noting that the values of the pressiometric modulus showed significant variability when only associated with the weathering class. On the other hand, when the structure of the mass was considered, variability and discrepancies were significantly reduced (Russo et al., 2001).

It is clear that this characterization cannot be integrated in the design for the selection of parameters, without taking into account the spatial development and variation of geotechnical groups along the alignment or in the area around the stations.

The significance of this comment was shown dramatically soon after boring with the EPB TBM has started. Thus, for the needs of this specific mechanized excavation such a characterization was meaningless and the mode of operation of the TBM had to be selected in such a way that the worst anticipated conditions could be dealt with at any time.

Table 2. Conceptual procedure for the geotechnical characterization of the granitic rock mass and for design (from Russo et al., 2001)

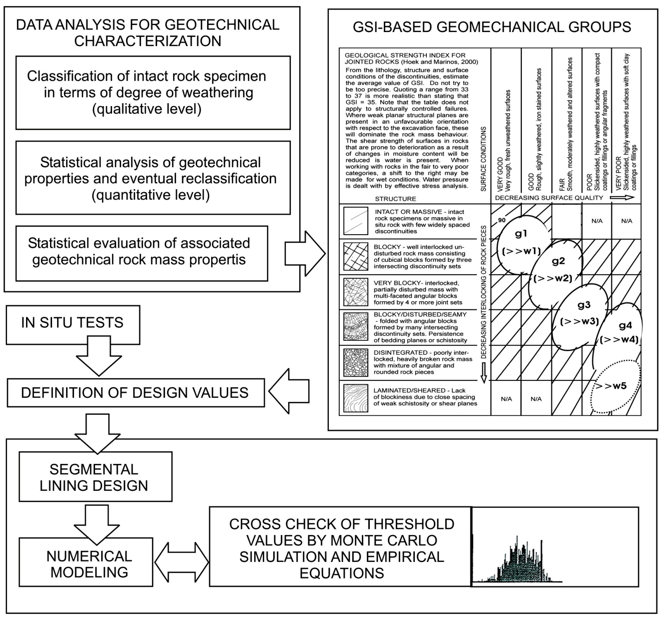

Table 3 Geotechnical parameters (average values, with brackets are given the standard deviations, from Russo et al., 2001 and from Quelhas et al., 2004)

Geotech-nical groups	σ_{ci}	γ (KN/m^3)	Hoek-Brown criterion parameters		Ed (GPa)
			mb	s	
g1	90-150	25-27	7.45 (1.15)	6.9E-2 (3.2E-2)	35 (10)
g2	30-90	25-27	3.2 (0.5)	7.5E-3 (3.4E-3)	10.7 (3.0)
g3	10-35	23-25	0.98 (0.07)	7.5E-4 (1.7E-4)	1.0 (0.5)
g4	1-15	22-24	0.67 (0.12)	0	0.4 (0.2)

Geotechnical groups	N_{SPT}	γ (KN/m^3)	c´ (MPa)	φ´ (°)	Ed (GPa)
g5	>50	19-21	0.01-0.05	32-36	0.05-0.20
g6	<50	18-20	0-0.02	30-34	0.02-0.07
g7	Var.	18-20	0	27-29	<0.05

5. PERMEABILITY

The permeability of the rock mass is dependent upon the weathering grade and the associated fractures. In the less weathered rock the flow is related primarily to the fracture system while, in the more heavily weathered material, the ground behaves more like a porous medium. Porosity in the latter case may have been increased from leaching and this together with the highly variable permeability of the rock mass, has resulted in a very complex groundwater regime. The overall permeability is rather low; of the order of 10^{-6}m/s or lower. However higher permeabilities were measured in pumping tests. We consider that preferential drainage paths exist within the granite mass. The very weathered material, having little or no cohesion, may be erodible under high hydraulic gradients.

The frequent occurrence of old wells connected by drainage galleries was a hazard for tunnelling. Opinion was expressed that long term exploitation of these wells had led to the washing out of fines increasing permeability and formation of an unstable soil structure (Grasso et al., 2003)

6. EPB TBM CHARACTERISTICS

The complex geological and hydrogeological conditions described above resulted in a decision by Transmetro to utilize an 8.7 m diameter Herrenknecht EPB TBM (see Fruguglietti et al. 1999, and 2001). Initially, only one machine was to be used to drive both lines but following start-up problems, a second machine was added in order to make it possible to complete the tunnel drives on schedule.

The TBMs are equipped with a soil conditioning system capable of injecting foam, polymer or bentonite slurry into the working chamber. Muck removal is by continuous belt conveyor from the TBM back-up to the portal and then by truck to the muck disposal areas. Tunnel lining is formed from 30 cm thick, 1.4 m wide pre-cast concrete segments. The lining comprises six segments and a key and dowel connectors are used in the radial joints while guidance rods are used in the longitudinal joints. The features of the EPB TBM are illustrated in Figure 7. In a review paper by N. Della Valle (Tunnels and Tunnelling, 2002) details are presented. Gugliementi et al. (2004), in a recent paper, offer a full presentation of the control of ground response and face stability during excavation. In those papers issues proposed by the authors of the present paper and discussed here are described.

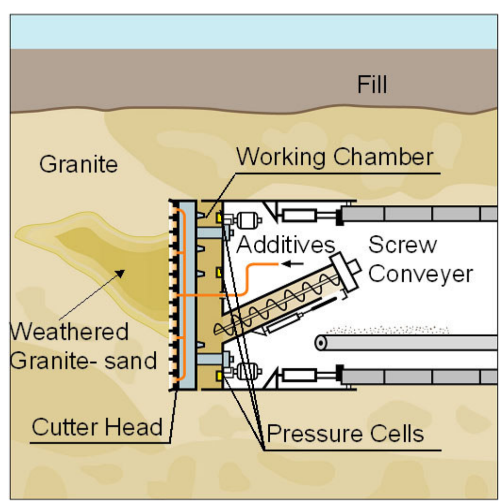

Figure 7: Characteristics of the Herrenknecht EPB TBM used in Oporto.

7. CHARACTERIZATION OF GEOLOGICAL CONDITIONS IN TERMS OF THE TBM OPERATION

The geological conditions discussed above can be translated to the following geological models in front, at the face and immediately above the TBM:

1. Granitic mass of sound or slightly weathered rock, no weathered material in the discontinuities;
2. Granitic mass of sound or slightly weathered rock but with very weathered material (filled or in situ) in substantial fractures; these fractures may communicate with overlaying parts of completely weathered granite;
3. Very weathered or completely weathered granite, W5 (almost granular soil with little or no cohesion);
4. Very weathered or completely weathered granite with blocks of the rock core;
5. Mixed conditions with both sound mass and completely weathered granite appearing in the face.

In all cases the water table is above the tunnel crown

Only the first of these geological models can be excavated using an EPB TBM operating in an open mode. However, because of the unpredictable changes in the geological conditions described above, we considered that the risk of operating in an open mode was unacceptable unless there was unambiguous evidence that this condition persisted for a considerable length of tunnel drive. This was not the case in this tunnel and we recommended that the entire drive should be carried out with the TBM operating in a closed mode.

Indeed in all other models, uncontrolled over-excavation could occur unless the chamber of the machine was full of appropriately conditioned excavated material with the necessary support pressure and control of the evacuation of the muck through the screw conveyor. Lack of adequate face support could result in piping of the weathered material in the fractures that could, in turn, induce collapse of the overlying weathered granite. The mixed face conditions described in item 5 above were considered to be particularly difficult because of the uneven pressure distribution on the face induced by the different stiffness of the rock and soil masses. The successfully handling of this problem is discussed in a following section.

A significant number of wells and old galleries exist in the area and, while most were located on old city maps and by inspection of existing properties, there remained the possibility that some unpredicted wells and galleries could be encountered. The wells usually end above the tunnel but some were deep enough to interfere with the construction. The crossing of such features clearly involved some risk but this was substantially lower when operating the TBM in a fully closed and pressurised mode than in an open or partially open mode.

6. FACE SUPPORT PRESSURE

The face support pressure of EPB - TBMs was controlled by measuring the pressure at the bulkhead with pressure cells, approximately 1.5 m from the face, as shown in Figure 8. In closed mode operation, the working chamber is completely filled with conditioned excavated material, the earth paste. The earth paste is pressurized by the advancing forces induced by the advance jacks via the bulkhead. The pressure level is controlled by the effectiveness of the excavating cutter head in relation to the discharging screw conveyor.

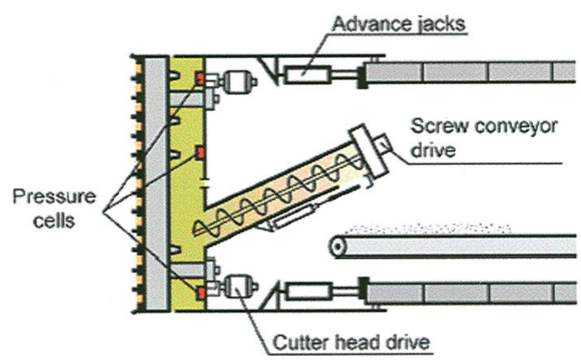

Figure 8: Measurement devices for face support pressure

To verify complete filling of the working chamber, the density of the earth paste in the working chamber was controlled by pressure cells on the bulkhead at different levels. This method satisfies the demand of preventing a sudden instability of the face caused by a partially empty working chamber but it does not guarantee a reliable face support pressure.

Pressure measurement at the bulkhead, 1.5 m behind the face, provides only partial information about the support pressure at the face. The support medium, the earth paste created from excavated ground, conditioned by a suspension with different additives, must have the physical properties of a viscous liquid. However, the shear resistance in that viscous liquid reduces the support forces which can be transferred onto the face. The shear resistance of the earth paste depends on the excavated ground and the conditioning, which is a complex and sensitive procedure. Consequently, the shear resistance of the support medium often varied considerably.

Therefore, the fluctuation of the face support pressure could exceed 0.5 bars. This fluctuation may be acceptable in homogeneous geology but in mixed ground, as found in the Oporto granite, the variable support pressure entailed the danger of significant over excavation.

One of the processes which can cause a drop in the face support pressure is illustrated in Figure 9 which shows a situation in which the lower part of the face is in unweathered granite while the upper part of the face is in residual soil. A major part of the thrust of the machine is consumed by the cutter forces required to excavate the unweathered granite and there is a deficiency in the forces available to generate the pressure in the earth paste in the upper part of the working chamber. This results is an imbalance between the soil and water pressure in the unweathered granite and the support pressure in the upper part of the working chamber. If this deficiency is too large, the face will collapse inwards into the working chamber and this will result in progressive over excavation ahead and above the face.

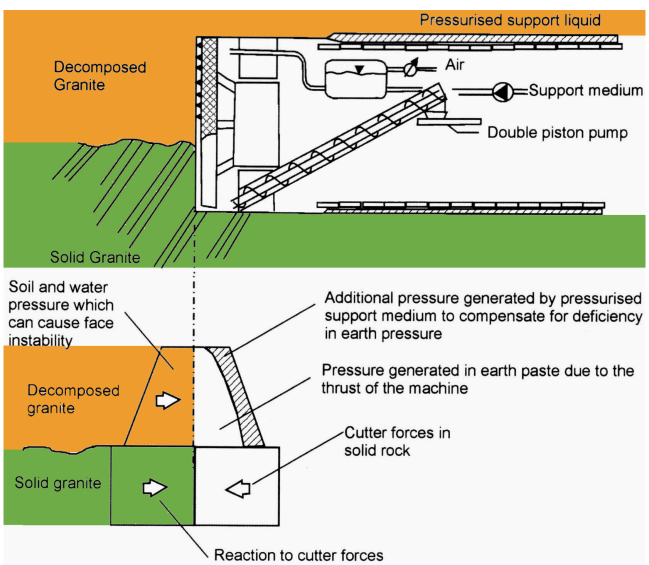

Figure 9: Face support pressures in mixed face conditions in Oporto granite. An Active Support System for overcoming the support pressure deficiency is also illustrated.

The deficiency of face support pressure can be compensated for by the addition of an Active Support System, proposed by Dr Siegmund Babendererde (one of the authors of this paper) and shown in Figure 9. This system is positioned on the back-up train and consists of a container filled with pressurized bentonite slurry linked to a regulated compressed air reservoir. The Bentonite slurry container is connected with the crown area of the working chamber of the EPB TBM. If the support pressure in the working chamber drops below a predetermined level, the Active Support System automatically injects pressurized slurry until the pressure level loss in the working chamber is compensated. The addition of this Active Support System to the EPB TMB results in an operation similar to that of a Slurry TBM. This automatic pressure control system reduces the range of fluctuations of the face support pressure to about 0.2 bar.

In the case of an open and potentially collapsible structure in the weathered granite surrounding the wells, resulting from leaching of the fines, we considered that stable face conditions can be maintained by the correct operation of the TBM in fully closed EPB mode with supplementary fluid pressure application. However, care was required in the formulation and preparation of the pressurizing fluid in order to ensure that an impermeable filter cake was formed at the face. This was necessary in order to prevent fluid loss into the open structure of the leached granite mass.

The application of the Active Support System in the Metro do Porto project was the first time that this system had been used. There was initial concern that the addition of the bentonite slurry would alter the characteristics of the muck to the point where it could no longer be contained on the conveyor system and that an additional slurry muck handling facility may be required. This concern proved to be unfounded since the volume of bentonite slurry injected proved to be very small and there was no discernable change on the characteristics of the muck.

The predetermined support pressure was determined from calculations using the method published by Anagnostou and Kovari (1996) which proved to be reliable for these conditions. The Active Support System was extremely effective in maintaining the predetermined support pressure and no serious face instability or over excavation problems were encountered after it was introduced. In fact, the system permitted the 8.7 m diameter tunnel to pass under old houses with a cover of 3 m to the foundations, without any pre-treatment of the ground. Surface settlements of less than 5 mm were measured in this case. The boring of the section under this shallow cover is described in a paper of Diez and Williams, 2003.

The Active Support System was also connected to the steering gap abound the shield and the filling of this gap with bentonite slurry provided a reliable means of maintaining a predetermined pressure in this gap.

CONCLUSIONS

The highly variable characteristics of the weathered granite in Oporto and their sudden changes imposed substantial risks on the driving of the C and S lines by means of EPB TBMs. The impossibility of accurately predicting and maintaining the correct face support pressure resulted in significant over excavation and two collapses to surface during the first 400 m of the C line drive. Characterization in different geotechnical groups for the selection of the mode of operation of the EPB was almost meaningless and the mode of operation of the TBM had to be selected in such a way that the worst anticipated conditions could be dealt with at any time.

The introduction of the Active Support System, which involves the injection of pressurized bentonite slurry to compensate for deficiencies in the face support pressure when driving in mixed face conditions, proved to be a very effective solution. The remaining C and S line drives have now been completed without further difficulty although the rate of progress was less than that originally projected when the project was planned.

The final breakthrough of the C line drive is illustrated in Figure 13.

Figure 13: Final breakthrough of the TBM S-203 on the completion of the drive from Salgueiros to Trindade on Thursday 16 October 2003.

ACKNOWLEDGEMENTS

The authors wish to acknowledge the permission of Metro do Porto to publish the details contained in this paper. The cooperation of Transmetro and particularly of Ing. Giovanni Giacomin in working with the Panel of Experts is also acknowledged. Part of this paper was presented in a workshop in Aveiro, Portugal, April 2004.

REFERENCES

Anagnostou, G and Kovari, K. 1996. "Face stability conditions with earth-pressure balanced shields". *Tunnelling and Underground Space Technolog*y. Vol 11, No 2, pp 163-173.

Begonha, A. and Sequeira Braga, M. A. 2002. "Weathering of the Oporto granite: geotechnical and physical properties". *Caten*a. Vol. 49, pp. 57-76

Della Valle, N. 2002. "Challenging soil conditions at Oporto". *Tunnels and Tunnelling Internationa*l. December 2002, pp. 16-19.

Diez R. nad Williams R. "TBM tunneling under very low cover- Approach to Trindade station, Porto Metro (Portugal)"

Fruguglietti, A., Ferrara, G, Gasparini, M and Centis, S. 2001 "Influence of geotechnical conditions on the excavation methods of Metro do Porto project".*Proceedings, Congress ITA*. Milan, pp. 135-141

Fruguglietti, A., Guglielmetti, V., Grasso, P., Carrieri, G and Xu, S. 1999. "Selection of the right TBM to excavate weathered rocks and soils". *Proceedings Conference: Challenges for the 21 st Centur*y, Allen et al (eds), Balkema Publ.. pp. 839-947.

Geological Society of London 1995. "The description and classification of weathered rocks for engineering purposes". *QJE*G, pp 28

Grasso P., Xu Sh., Fedele M., Russo G. and Ch. E. 2003. "Particular failure mechanisms of weathered granite observed during construction of metro tunnels by TBM". *Proc. ITA World Tunnelling Congress,* 2, Amsterdam

Guglielmetti V., Grasso P., Gaj F. and Giacomin G. 2003. "Mechanized tunneling in urban environment: control of ground response and face stability, when excavating with an EPB Machine". *Proc. ITA World Tunnelling Congress,* 2, Amsterdam

Quelhas, J., Gomez, J., Ferreira, P., Pires, A., Andrade, c., Baiao, C., Maia, C., Pistone, R. 2004. "Estacoes mineiras do metro do Porto – Metodos construtivos". *9th Portugeuse Congress of Geotechnics (9th CNG),* Aveiro.

Russo, G., Kalamaras, G.S., Origlia, P and Grasso, P. 2001. "A probabilistic approach for characterizing the complex geological environment for the design of the new Metro do Porto". *Proceedings, Congress IT*A. Milan, pp 463-470.

Rock mass properties for surface mines

Evert Hoek and Antonio Karzulovic

Published in *Slope Stability in Surface Mining,* (Edited by W.A. Hustralid, M.K. McCarter and D.J.A. van Zyl), Littleton, Colorado: Society for Mining, Metallurgical and Exploration (SME), 2000, pages 59-70.

Rock mass properties for surface mines

Evert Hoek[*] and Antonio Karzulovic**

1.1 INTRODUCTION

Reliable estimates of the strength and deformation characteristics of rock masses are required for almost any form of analysis used for the design of surface excavations. Hoek and Brown (1980a, 1980b) proposed a method for obtaining estimates of the strength of jointed rock masses, based upon an assessment of the interlocking of rock blocks and the condition of the surfaces between these blocks. This method was modified over the years in order to meet the needs of users who applied it to problems that were not considered when the original criterion was developed (Hoek 1983, Hoek and Brown 1988). The application of the method to very poor quality rock masses required further changes (Hoek, Wood and Shah 1992) and, eventually, the development of a new classification called the Geological Strength Index (Hoek 1994, Hoek, Kaiser and Bawden 1995, Hoek and Brown 1997, Hoek, Marinos and Benissi (1998)). A review of the development of the criterion and of the equations proposed at various stages in this development is given in Hoek and Brown (1997).

This chapter presents the Hoek-Brown criterion in a form that has been found practical in the field and that appears to provide the most reliable set of results for use as input for methods of analysis currently used in rock engineering.

For surface excavations, the rock mass properties are particularly sensitive to stress relief and blast damage and these two factors are discussed in his chapter.

1.2 GENERALISED HOEK-BROWN CRITERION

The Generalised Hoek-Brown failure criterion for jointed rock masses is defined by:

$$\sigma_1' = \sigma_3' + \sigma_{ci}\left(m_b \frac{\sigma_3'}{\sigma_{ci}} + s\right)^a \qquad (1.1)$$

where σ_1' and σ_3' are the maximum and minimum effective stresses at failure,

m_b is the value of the Hoek-Brown constant m for the rock mass,

s and a are constants which depend upon the rock mass characteristics, and

σ_{ci} is the uniaxial compressive strength of the intact rock pieces.

* Consulting engineer, Vancouver, Canada.
** Professor, Department of Mining Engineering, University of Chile, Santiago, Chile

The Mohr envelope, relating normal and shear stresses, can be determined by the method proposed by Hoek and Brown (1980a). In this approach, equation 1.1 is used to generate a series of triaxial test values, simulating full scale field tests, and a statistical curve fitting process is used to derive an equivalent Mohr envelope defined by the equation:

$$\tau = A\sigma_{ci}\left(\frac{\sigma_n' - \sigma_{tm}}{\sigma_{ci}}\right)^B \tag{1.2}$$

where A and B are material constants

σ_n' is the normal effective stress, and

σ_{tm} is the 'tensile' strength of the rock mass.

In order to use the Hoek-Brown criterion for estimating the strength and deformability of jointed rock masses, three 'properties' of the rock mass have to be estimated. These are

1. the uniaxial compressive strength σ_{ci} of the intact rock elements,
2. the value of the Hoek-Brown constant m_i for these intact rock elements, and
3. the value of the Geological Strength Index *GSI* for the rock mass.

1.3 INTACT ROCK PROPERTIES

For the intact rock pieces that make up the rock mass equation 1.1 simplifies to:

$$\sigma_1' = \sigma_3' + \sigma_{ci}\left(m_i \frac{\sigma_3'}{\sigma_{ci}} + 1\right)^{0.5} \tag{1.3}$$

The relationship between the principal stresses at failure for a given rock is defined by two constants, the uniaxial compressive strength σ_{ci} and a constant m_i. Wherever possible the values of these constants should be determined by statistical analysis of the results of a set of triaxial tests on carefully prepared core samples. When laboratory tests are not possible, Table 1.1 and Table 1.2 can be used to obtain estimates of σ_{ci} and m_i.

In the case of mineralised rocks, the effects of alteration can have a significant impact on the properties of the intact rock components and this should be taken into account in estimating the values of σ_{ci} and m_i. For example, the influence of quartz-seritic alteration of andesite and porphyry is illustrated in the Figure 1.1. Similar trends have been observed for other forms of alteration and, where this type of effect is considered likely, the geotechnical engineer would be well advised to invest in a program of laboratory testing to establish the appropriate properties for the intact rock.

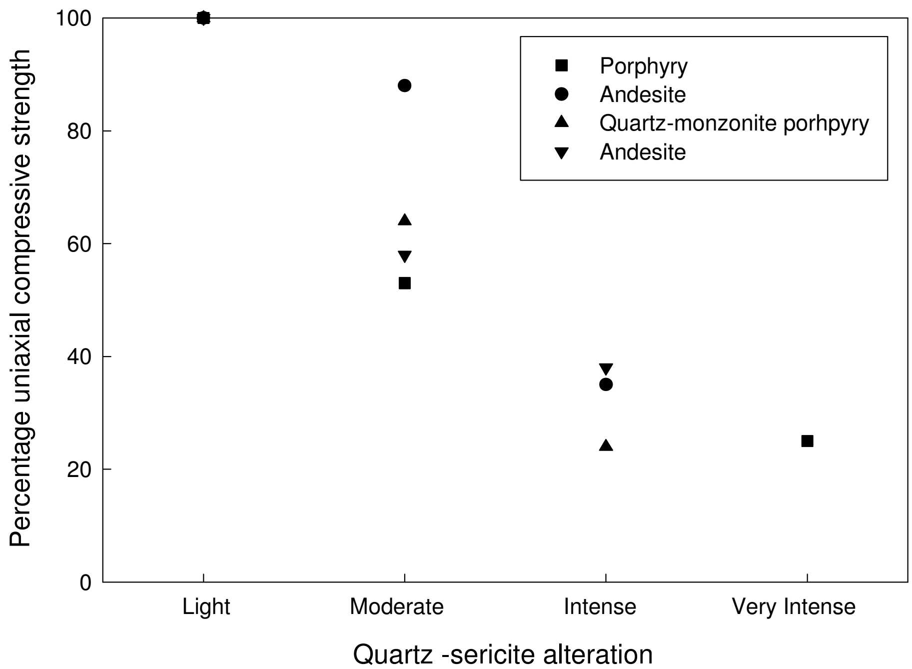

Figure 1.1: Influence of quartz-seritic alteration on the uniaxial compressive strength of “intact” specimens of andesite and porphyry.

The Hoek-Brown failure criterion, which assumes isotropic rock and rock mass behaviour, should only be applied to those rock masses in which there are a sufficient number of closely spaced discontinuities, with similar surface characteristics, that isotropic behaviour involving failure on multiple discontinuities can be assumed. When the structure being analysed is large and the block size small in comparison, the rock mass can be treated as a Hoek-Brown material.

Where the block size is of the same order as that of the structure being analysed or when one of the discontinuity sets is significantly weaker than the others, the Hoek-Brown criterion should not be used. In these cases, the stability of the structure should be analysed by considering failure mechanisms involving the sliding or rotation of blocks and wedges defined by intersecting structural features. Figure 1.2 summarises these statements in a graphical form.

1.4 GEOLOGICAL STRENGTH INDEX

The strength of a jointed rock mass depends on the properties of the intact rock pieces and also upon the freedom of these pieces to slide and rotate under different stress conditions. This freedom is controlled by the geometrical shape of the intact rock pieces as well as the condition of the surfaces separating the pieces. Angular rock pieces with clean, rough discontinuity surfaces will result in a much stronger rock mass than one which contains rounded particles surrounded by weathered and altered material.

Table 1.1: Field estimates of uniaxial compressive strength.

Grade*	Term	Uniaxial Comp. Strength (MPa)	Point Load Index (MPa)	Field estimate of strength	Examples
R6	Extremely Strong	> 250	>10	Specimen can only be chipped with a geological hammer	Fresh basalt, chert, diabase, gneiss, granite, quartzite
R5	Very strong	100 - 250	4 - 10	Specimen requires many blows of a geological hammer to fracture it	Amphibolite, sandstone, basalt, gabbro, gneiss, granodiorite, peridotite , rhyolite, tuff
R4	Strong	50 - 100	2 - 4	Specimen requires more than one blow of a geological hammer to fracture it	Limestone, marble, sandstone, schist
R3	Medium strong	25 - 50	1 - 2	Cannot be scraped or peeled with a pocket knife, specimen can be fractured with a single blow from a geological hammer	Concete, phyllite, schist, siltstone
R2	Weak	5 - 25	**	Can be peeled with a pocket knife with difficulty, shallow indentation made by firm blow with point of a geological hammer	Chalk, claystone, potash, marl, siltstone, shale, rocksalt,
R1	Very weak	1 - 5	**	Crumbles under firm blows with point of a geological hammer, can be peeled by a pocket knife	Highly weathered or altered rock, shale
R0	Extremely weak	0.25 - 1	**	Indented by thumbnail	Stiff fault gouge

* Grade according to Brown (1981).
** Point load tests on rocks with a uniaxial compressive strength below 25 MPa are likely to yield highly ambiguous results.

Table 1.2: Values of the constant m_i for intact rock, by rock group. Note that values in parenthesis are estimates.

Rock type	Class	Group	Texture: Coarse	Medium	Fine	Very fine
SEDIMENTARY	Clastic		Conglomerates (21 ± 3) Breccias (19 ± 5)	Sandstones 17 ± 4	Siltstones 7 ± 2 Greywackes (18 ± 3)	Claystones 4 ± 2 Shales (6 ± 2) Marls (7 ± 2)
	Non-Clastic	Carbonates	Crystalline Limestone (12 ± 3)	Sparitic Limestones (10 ± 2)	Micritic Limestones (9 ± 2)	Dolomites (9 ± 3)
		Evaporites		Gypsum 8 ± 2	Anhydrite 12 ± 2	
		Organic				Chalk 7 ± 2
METAMORPHIC	Non Foliated		Marble 9 ± 3	Hornfels (19 ± 4) Metasandstone (19 ± 3)	Quartzites 20 ± 3	
	Slightly foliated		Migmatite (29 ± 3)	Amphibolites 26 ± 6		
	Foliated*		Gneiss 28 ± 5	Schists 12 ± 3	Phyllites (7 ± 3)	Slates 7 ± 4
IGNEOUS	Plutonic	Light	Granite 32 ± 3 Granodiorite (29 ± 3)	Diorite 25 ± 5		
		Dark	Gabbro 27 ± 3 Norite 20 ± 5	Dolerite (16 ± 5)		
	Hypabyssal		Porphyries (20 ± 5)		Diabase (15 ± 5)	Peridotite (25 ± 5)
	Volcanic	Lava		Rhyolite (25 ± 5) Andesite 25 ± 5	Dacite (25 ± 3) Basalt (25 ± 5)	Obsidian (19 ± 3)
		Pyroclastic	Agglomerate (19 ± 3)	Breccia (19 ± 5)	Tuff (13 ± 5)	

* These values are for intact rock specimens tested normal to bedding or foliation. The value of m_i will be significantly different if failure occurs along a weakness plane.

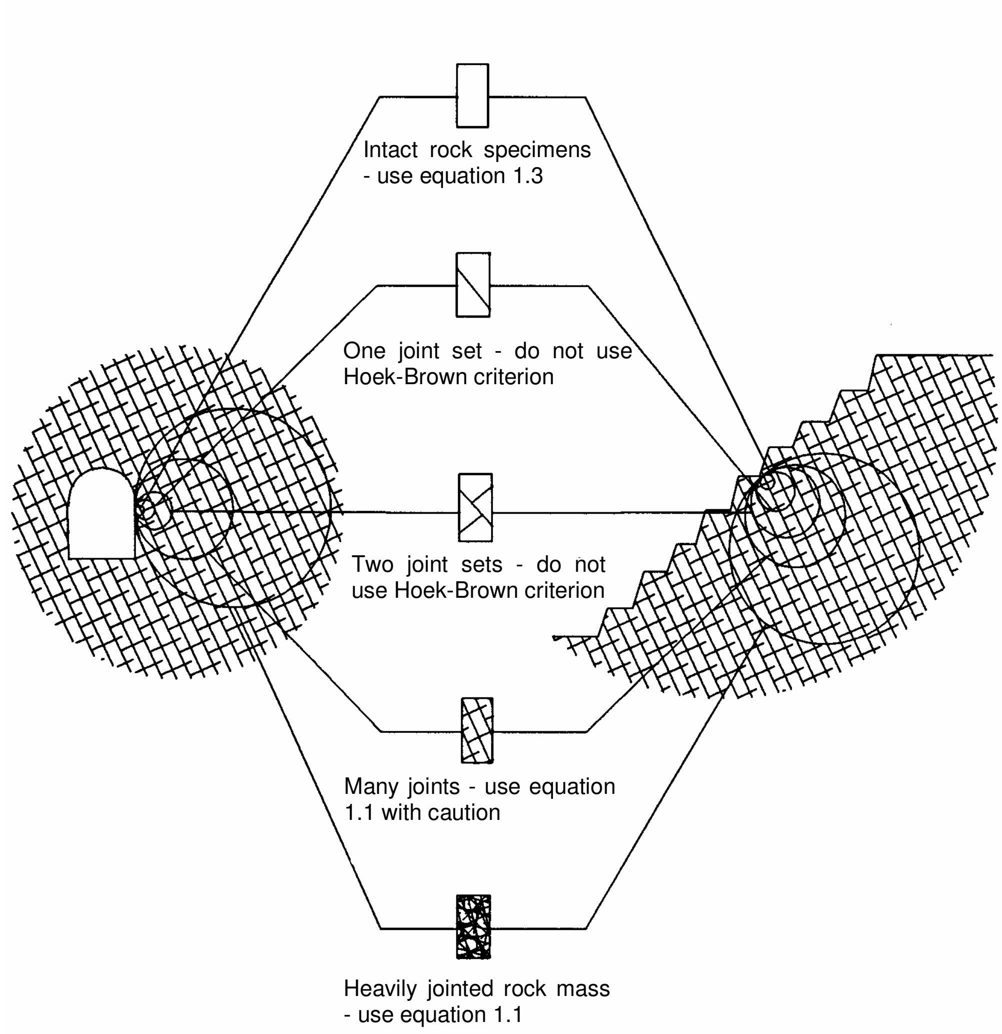

Figure 1.2: Idealised diagram showing the transition from intact to a heavily jointed rock mass with increasing sample size.

The Geological Strength Index (GSI), introduced by Hoek (1994) and Hoek, Kaiser and Bawden (1995) provides a system for estimating the reduction in rock mass strength for different geological conditions. This system is presented in Table 1.3, for blocky rock masses, and Table 1.4 for schistose metamorphic rocks.

Once the Geological Strength Index has been estimated, the parameters that describe the rock mass strength characteristics, are calculated as follows:

$$m_b = m_i \exp\left(\frac{GSI - 100}{28}\right) \tag{1.4}$$

For GSI > 25, i.e. rock masses of good to reasonable quality:

$$s = \exp\left(\frac{GSI - 100}{9}\right) \tag{1.5}$$

and

$$a = 0.5 \tag{1.6}$$

For GSI < 25, i.e. rock masses of very poor quality:

$$s = 0 \tag{1.7}$$

and

$$a = 0.65 - \frac{GSI}{200} \tag{1.8}$$

For better quality rock masses (GSI > 25), the value of GSI can be estimated directly from the 1976 version of Bieniawski's Rock Mass Rating, with the Groundwater rating set to 10 (dry) and the Adjustment for Joint Orientation set to 0 (very favourable) (Bieniawski 1976). For very poor quality rock masses the value of RMR is very difficult to estimate and the balance between the ratings no longer gives a reliable basis for estimating rock mass strength. Consequently, Bieniawski's RMR classification should not be used for estimating the GSI values for poor quality rock masses (RMR < 25) and the GSI charts should be used directly.

If the 1989 version of Bieniawski's RMR classification (Bieniawski 1989) is used, then GSI = RMR_{89}' - 5 where RMR_{89}' has the Groundwater rating set to 15 and the Adjustment for Joint Orientation set to zero.

1.5 MOHR-COULOMB PARAMETERS

Most geotechnical software is written in terms of the Mohr-Coulomb failure criterion in which the rock mass strength is defined by the cohesive strength c' and the angle of friction ϕ'. The linear relationship between the major and minor principal stresses, σ_1' and σ_3', for the Mohr-Coulomb criterion is

$$\sigma_1' = \sigma_{cm} + k\sigma_3' \tag{1.9}$$

where σ_{cm} is the uniaxial compressive strength of the rock mass and k is the slope of the line relating σ_1' and σ_3'. The values of ϕ' and c' can be calculated from

$$\sin\phi' = \frac{k-1}{k+1} \tag{1.10}$$

$$c' = \frac{\sigma_{cm}(1 - \sin\phi')}{2\cos\phi'} \tag{1.11}$$

Table 1.3: Characterisation of a blocky rock masses on the basis of particle interlocking and discontinuity condition. After Hoek, Marinos and Benissi (1998).

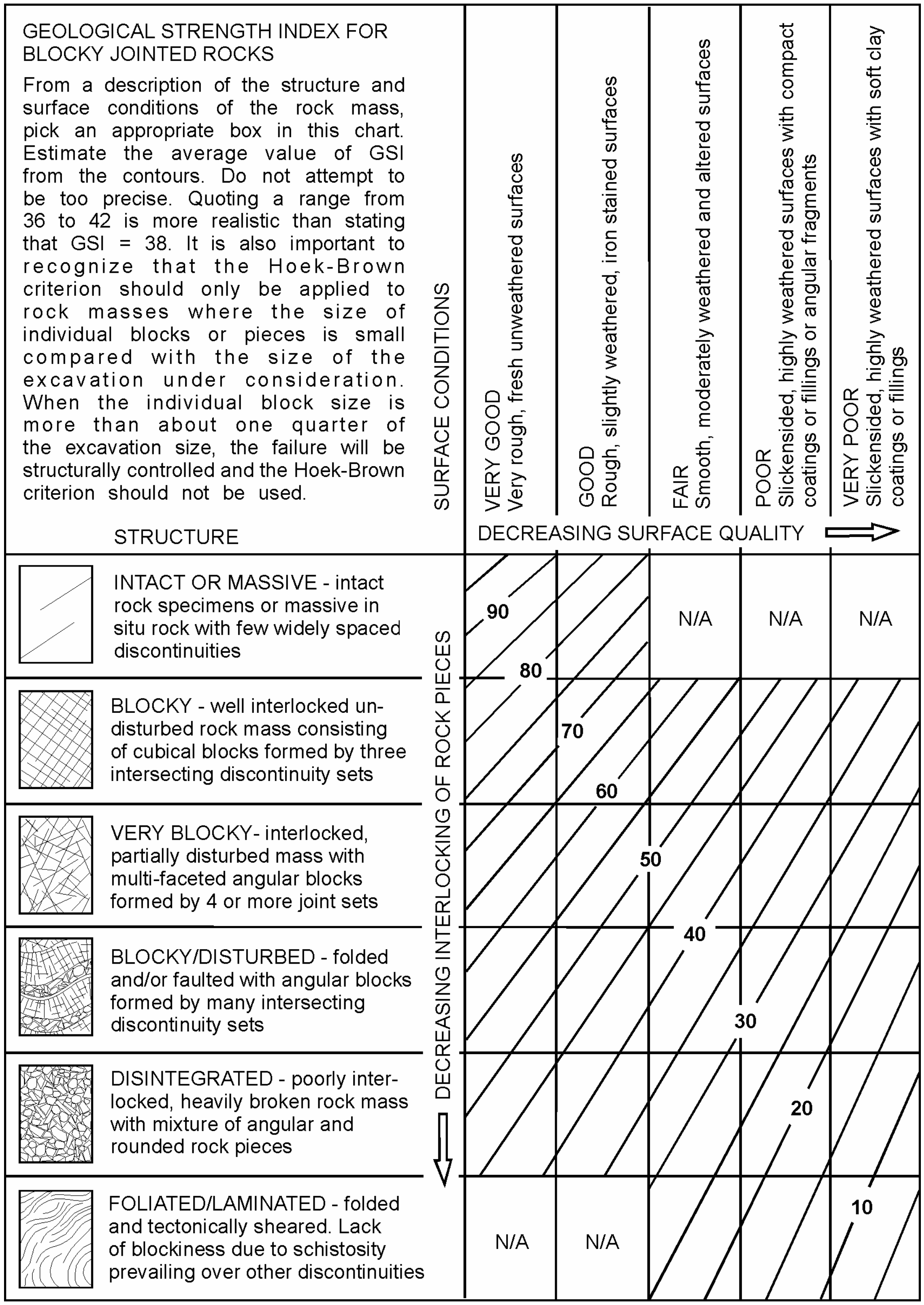

Table 1.4: Characterisation of a schistose metamorphic rock masses on the basis of foliation and discontinuity condition. (After M. Truzman, 1999)

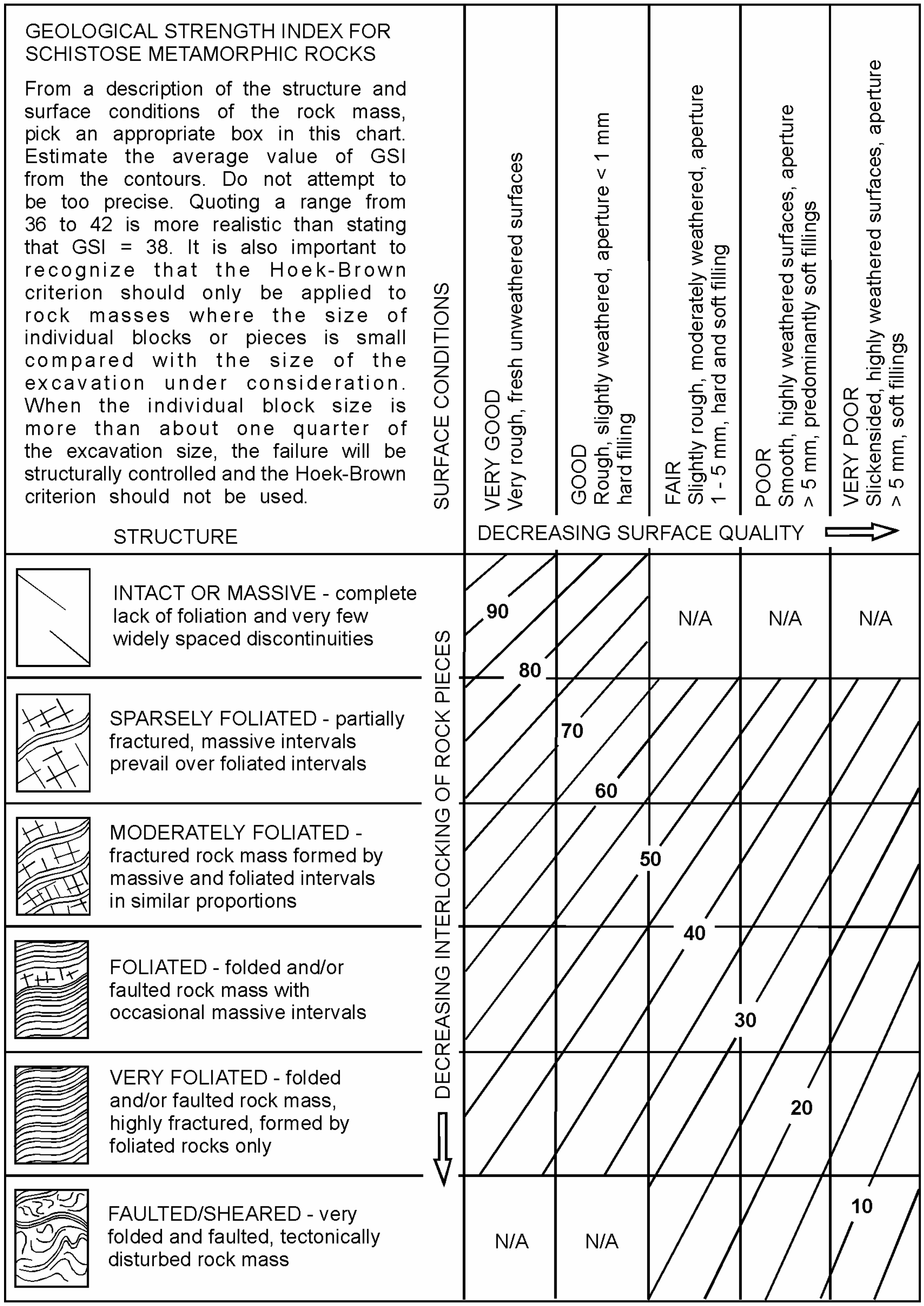

There is no direct correlation between equation 1.9 and the non-linear Hoek-Brown criterion defined by equation 1.1. Consequently, determination of the values of c' and ϕ' for a rock mass that has been evaluated as a Hoek-Brown material is a difficult problem.

Having considered a number of possible approaches, it has been concluded that the most practical solution is to treat the problem as an analysis of a set of full-scale triaxial strength tests. The results of such tests are simulated by using the Hoek-Brown equation 1.1 to generate a series of triaxial test values. Equation 1.9 is then fitted to these test results by linear regression analysis and the values of c' and ϕ' are determined from equations 1.11 and 1.10. A full discussion on the steps required to carry out this analysis is presented in the Appendix, together with a spreadsheet for implementing this analysis.

The range of stresses used in the curve fitting process described above is very important. For the confined conditions surrounding tunnels at depths of more than about 30 m, the most reliable estimates are given by using a confining stress range from zero to $0.25\sigma_{ci}$, where σ_{ci} is the uniaxial compressive strength of the intact rock elements. For this stress range, the uniaxial compressive strength of the rock mass σ_{cm}, the cohesive strength c and the friction angle ϕ are given in Figures 1.3 and 1.4.

For slopes and shallow excavations the user is given the choice of the stress range for this curve fitting process. This is discussed in full in the Appendix.

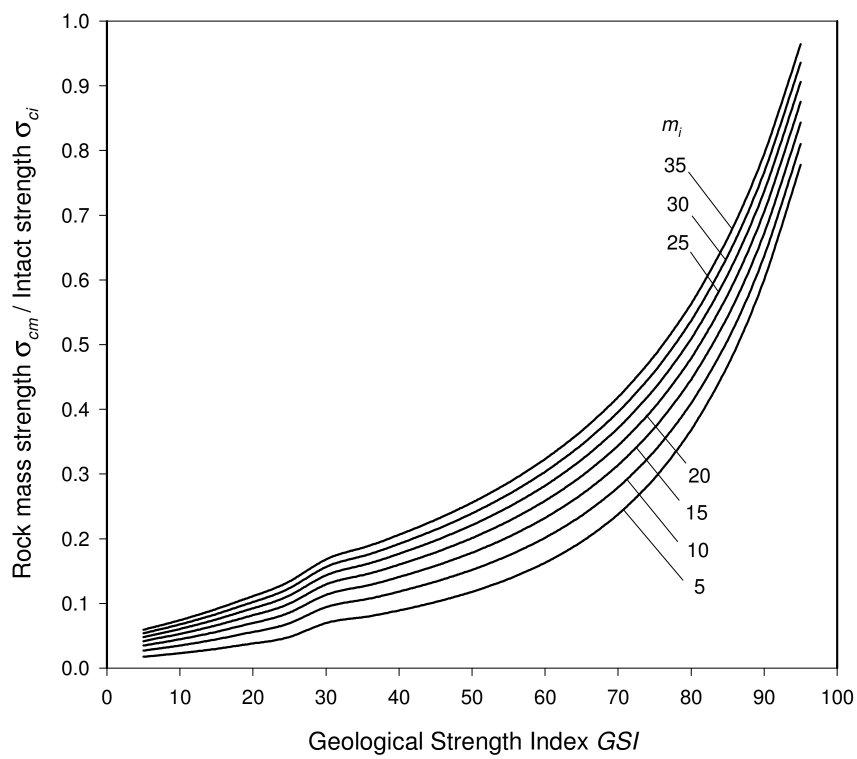

Figure 1.3: Ratio of uniaxial compressive strength of rock mass to intact rock versus Geological Strength Index GSI for depths of more than 30 m.

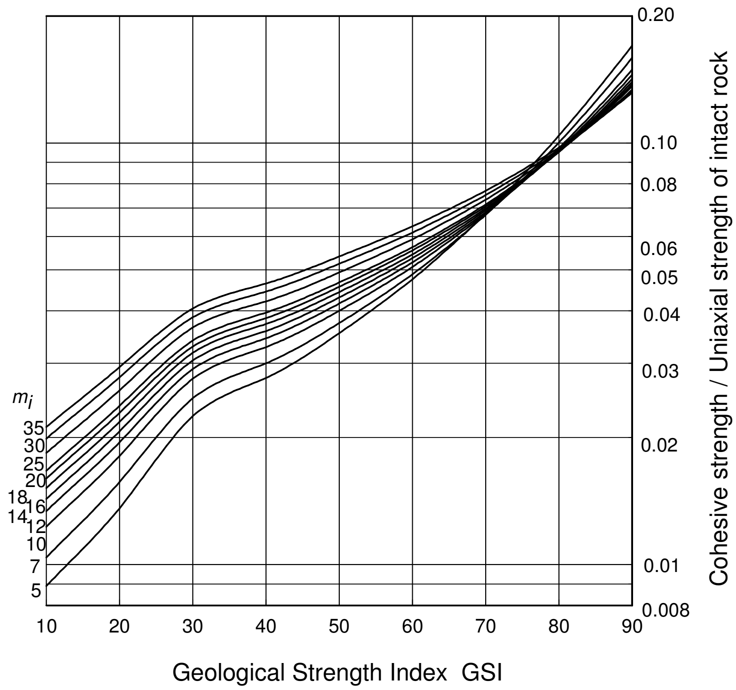

a. Plot of ratio of cohesive strength c' to uniaxial compressive strength σ_{ci} for depths of more than 30 m.

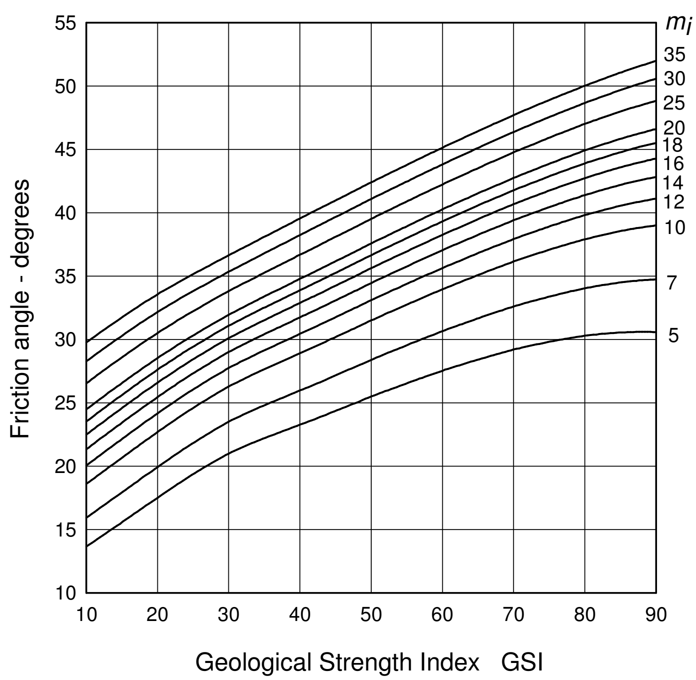

b. Plot of friction angle ϕ'

Figure 1.4: Cohesive strengths and friction angles for different GSI and m_i values for depths of more than 30 m.

1.6 DEFORMATION MODULUS

Serafim and Pereira (1983) proposed a relationship between the in situ modulus of deformation and Bieniawski's RMR classification. This relationship is based upon back analysis of dam foundation deformations and it has been found to work well for better quality rocks. However, for many of the poor quality rocks it appears to predict deformation modulus values that are too high. Based upon practical observations and back analysis of excavation behaviour in poor quality rock masses, the following modification to Serafim and Pereira's equation is proposed for $\sigma_{ci} < 100$:

$$E_m = \sqrt{\frac{\sigma_{ci}}{100}} 10^{\left(\frac{GSI-10}{40}\right)} \tag{1.12}$$

Note that GSI has been substituted for RMR in this equation and that the modulus E_m is reduced progressively as the value of σ_{ci} falls below 100. This reduction is based upon the reasoning that the deformation of better quality rock masses is controlled by the discontinuities while, for poorer quality rock masses, the deformation of the intact rock pieces contributes to the overall deformation process.

Based upon measured deformations, equation 1.12 appears to work reasonably well in those cases where it has been applied. However, as more field evidence is gathered it may be necessary to modify this relationship.

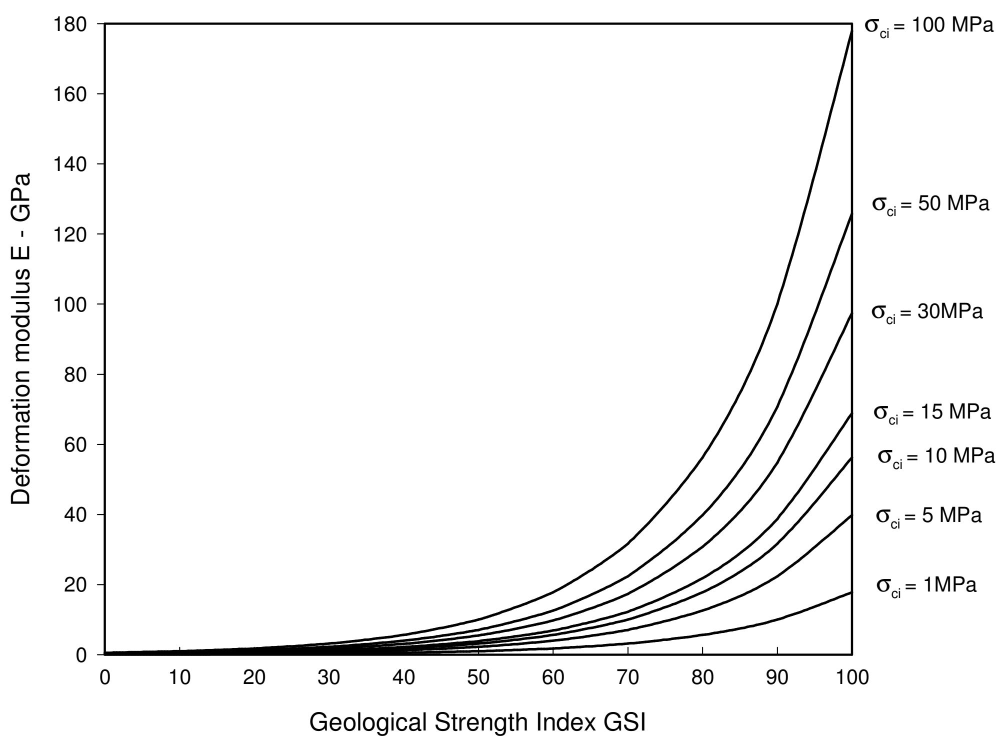

Figure 1.5: Deformation modulus versus Geological Strength Index GSI.

1.7 STRESS RELAXATION

When the rock mass adjacent to a tunnel wall or a slope is excavated, a relaxation of the confining stresses occurs and the remaining material is allowed to expand in volume or to dilate. This has a profound influence on the strength of the rock mass since, in jointed rocks, this strength is strongly dependent upon the interlocking between the intact rock particles that make up the rock mass.

As far as the authors are aware, there is very little research evidence relating the amount of dilation to the strength of a rock mass. One set of observations that gives an indication of the loss of strength associated with dilation is derived from the support required to stabilise tunnels. Sakurai (1983) suggested that tunnels in which the 'strain', defined as the ratio of tunnel closure to tunnel diameter, exceeds 1% are likely to suffer significant instability unless adequately supported. This suggestion was confirmed in observations by Chern et al (1998) who recorded the behaviour of a number of tunnels excavated in Taiwan. They found that all of those tunnels that exhibited strains of greater than 1 to 2% required significant support. Tunnels exhibiting strains as high as 10% were successfully stabilised but the amount of effort required to achieve this stability increased in proportion to the amount of strain.

While it is not possible to derive a direct relationship between rock mass strength and dilation from these observations, it is possible to conclude that the strength loss is significant. An unconfined surface that has deformed more than 1 or 2% (based upon Sakurai's definition of strain) has probably reached residual strength in which all of the effective 'cohesive' strength of the rock mass has been lost. While there are no similar observations for rock slopes, it is reasonable to assume that a similar loss of strength occurs as a result of dilation. Hence, a 100 m high slope which has suffered a total crest displacement of more than 1 m (i.e. more than 1% strain) may start to exhibit significant signs of instability as a result of loss of strength of the rock mass.

1.8 BLAST DAMAGE

Blast damage results in a loss of rock mass strength due to the creation of new fractures and the wedging open of existing fractures by the penetration of explosive gasses. In the case of very large open pit mine blasts, this damage can extend as much as 100 m behind the final row of blast holes.

In contrast to the strength loss due to stress relaxation or dilation, discussed in the previous section, it is possible to arrive at an approximate quantification of the strength loss due to blast damage. This is because the blast is designed to achieve a specific purpose which is generally to produce a fractured rock mass that can be excavated by means of a given piece of equipment.

Figure 1.6 presents a plot of 23 case histories of excavation by digging, ripping and blasting published by Abdullatif and Cruden (1983). These case histories are summarised in Table 1.5. The values of GSI are estimated from the data contained in the paper by Abdullatif and Cruden while the rock mass strength values were calculated by means of the spreadsheet given in the appendix, assuming an average slope height of 15 m.

These examples shows that rock masses can be dug, obviously with increasing difficulty, up to GSI values of about 40 and rock mass strength values of about 1 MPa. Ripping can be used up to GSI values of about 60 and rock mass strength values of about 10 MPa, with two exceptions where heavy equipment was used to rip strong rock masses. Blasting was used for GSI values of more than 60 and rock mass strengths of more than about 15 MPa.

Consider the case of an open pit slope excavated in granodiorite. The uniaxial compressive strength of the intact rock is σ_{ci} = 60 MPa and the Geological Strength Index is GSI = 55. For granodiorite, Table 2 gives the value of m_i = 30. Substitution of these values into the spreadsheet given in the appendix, for a single 18 m high bench, gives a rock mass strength σ_{cm}= 5.7 MPa. In order to create conditions for easy digging, the blast is designed to reduce the GSI value to below 40 and/or the rock mass strength to less than 1 MPa. In this case the controlling parameter is the rock mass strength and the spreadsheet given in the appendix shows that the GSI value has to be reduced to about 22 on order to achieve this rock mass strength.

In another example of a 15 m high slope in weak sandstone, the compressive strength of the intact rock is σ_{ci} = 10 MPa, m_i = 17 and GSI = 60. These values give a rock mass strength σ_{cm}= 1.4 MPa and this is reduced to 0.7 by reducing the GSI to 40. Hence, in this case, both the conditions for efficient digging in this soft rock are satisfied by designing the blast to give a GSI value of 40.

.

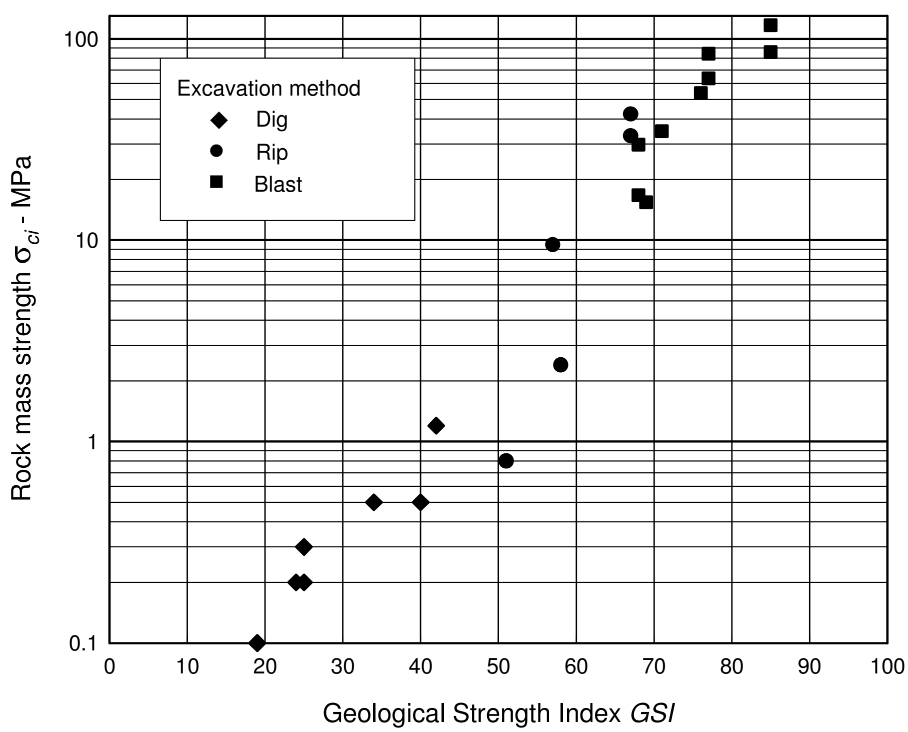

Figure 1.6: Plot of rock mass strength versus GSI for different excavation methods, after Abdullatif and Cruden (1983).

Table 1.5: Summary of methods used to excavate rock masses with a range of uniaxial compressive strength values, based on data published by Abdullatif and Cruden (1983).

GSI	Rock mass strength σ_{cm} - MPa	Excavation method
85	86	Blasting
85	117	Blasting
77	64	Blasting
77	135	Blasting
77	84	Blasting
76	54	Blasting
71	35	Blasting
69	15	Blasting
68	17	Blasting
68	30	Blasting
67	42	Ripping by D9L bulldozer
67	33	Ripping by D9L bulldozer
58	2.4	Ripping by track loader
57	9.5	Ripping by 977L track loader
51	0.8	Ripping by track loader
42	1.2	Digging by 977L track loader
40	0.5	Digging by wheel loader
34	0.5	Digging by hydraulic face shovel
25	0.3	Digging by 977L track loader
24	0.2	Digging by wheel loader
25	0.2	Digging by hydraulic backhoe
19	0.1	Digging by D9 bulldozer
19	0.1	Digging by 977L track loader

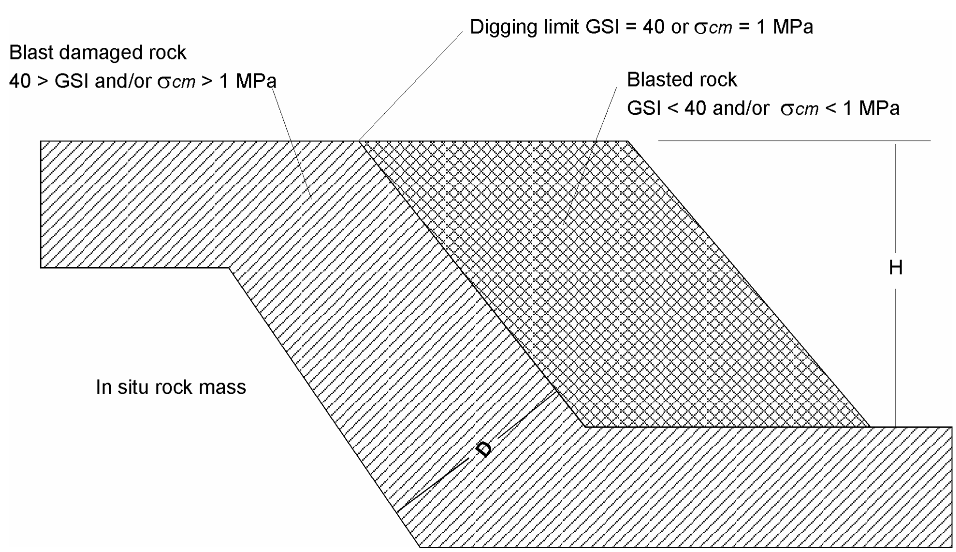

Figure 1.7: Diagrammatic representation of the transition between the in situ rock mass and blasted rock that is suitable for digging.

Figure 1.7 summarises the conditions for a muckpile that can be dug efficiently and the blast damaged rock mass that lies between the digging limit and the in situ rock mass. The properties of this blast damaged rock mass will control the stability of the slope that remains after digging of the muckpile has been completed.

The thickness D of the blast damaged zone will depend upon the design of the blast. Based upon experience, the authors suggest that the following approximate relationships can be used as a starting point in judging the extent of the blast damaged zone resulting from open pit mine production blasting:

- Large production blast, confined and with little or no control — D = 2 to 2.5 H
- Production blast with no control but blasting to a free face — D = 1 to 1.5 H
- Production blast, confined but with some control, e.g. one or more buffer rows — D = 1 to 1.2 H
- Production blast with some control, e.g. one or more buffer rows, and blasting to a free face — D = 0.5 to 1 H
- Carefully controlled production blast with a free face — D = 0.3 to 0.5 H

1.9 REFERENCES

Abdullatif, O.M. and Cruden, D.M. 1983. The relationship between rock mass quality and ease of excavation. *Bull. Intnl. Assoc. Eng. Geol.* No. 28. 183-187.

Balmer G. 1952. A general analytical solution for Mohr's envelope. Am. Soc. Test. Mat. 52, 1260-1271.

Bieniawski Z.T. 1976. Rock mass classification in rock engineering. In Exploration for Rock Engineering, Proc. of the Symp., (Edited by Bieniawski Z.T.) 1, 97-106. Cape Town, Balkema.

Bieniawski Z.T. 1989. Engineering Rock Mass Classifications. p. 251. New York, Wiley.

Brown E.T. (Ed). 1981. Rock characterization, testing and monitoring - ISRM suggested methods, 171-183. Oxford, Pergamon.

Chern, J.C., Yu, C.W. and Shiao, F.Y. 1998. Tunnelling in squeezing ground and support estimation. *Proc. Regional Symposium on Sedimentary Rock Engineering, Taipei.* 192-202.

Hoek E. 1994. Strength of rock and rock masses, ISRM News Journal, 2(2), 4-16.

Hoek E. and Brown E.T. 1980. *Underground excavations in rock*, p. 527. London, Instn Min. Metall.

Hoek E. and Brown E.T. 1988 The Hoek-Brown failure criterion - a 1988 update. In Rock Engineering for Underground Excavations, Proc. 15th Canadian Rock Mech. Symp. (Edited by Curran J.C.), 31-38. Toronto, Dept. Civil Engineering, University of Toronto.

Hoek E. Strength of jointed rock masses, 1983. 23rd Rankine Lecture. Géotechnique 33(3), 187-223.

Hoek E., Kaiser P.K. and Bawden W.F. 1995. *Support of underground excavations in hard rock*. p. 215. Rotterdam, Balkema.

Hoek E., Wood D. and Shah S. 1992. A modified Hoek-Brown criterion for jointed rock masses. *Proc. Rock Characterization, Symp. Int. Soc. Rock Mech.: Eurock '92*, (Edited by Hudson J.A.), 209-214. London, Brit. Geotech. Soc.

Hoek, E. and Brown, E.T. 1980. Empirical strength criterion for rock masses. *J. Geotech. Engng. Div., ASCE,* **106** (GT 9), 1013-1035.

Hoek, E. and Brown, E.T. 1997. Practical estimates or rock mass strength. *Int. J. Rock Mech. & Mining Sci. & Geomechanics Abstracts.* **34**(8), 1165-1186.

Hoek, E., Marinos, P. and Benissi, M. 1998. Applicability of the Geological Strength Index (GSI) classification for very weak and sheared rock masses. The case of the Athens Schist Formation. *Bull. Engg. Geol. Env.* 57(2), 151-160.

Sakurai, S. 1983. Displacement measurements associated with the design of underground openings. *Proc. Intnl. Symp. Field Measurements in Geomechanics, Zurich.* Vol. 2, 1163-1178.

Serafim, J.L. and Pereira, J.P. 1983. Consideration of the Geomechanics Classification of Bieniawski. *Proc. Intnl. Symp. Engng. Geol. And Underground Construction.* Lisbon, Portugal, Vol. 1, Part 11, 33-44.

Truzman, M, 1999, personal communication.

1.10 APPENDIX – DETERMINATION OF MOHR COULOMB CONSTANTS

The steps required to determine the parameters A, B, c' and ϕ' are given below. A spreadsheet for carrying out this analysis, with a listing of all the cell formulae, is given in Figure 1.8.

The relationship between the normal and shear stresses can be expressed in terms of the corresponding principal effective stresses as suggested by Balmer (1952):

$$\sigma_n' = \sigma_3' + \frac{\sigma_1' - \sigma_3'}{\partial\sigma_1' / \partial\sigma_3' + 1} \tag{1.13}$$

$$\tau = (\sigma_1' - \sigma_3')\sqrt{\partial\sigma_1' / \partial\sigma_3'} \tag{1.14}$$

For the $GSI > 25$, when $a = 0.5$:

$$\frac{\partial\sigma_1'}{\partial\sigma_3'} = 1 + \frac{m_b \sigma_{ci}}{2(\sigma_1' - \sigma_3')} \tag{1.15}$$

For $GSI < 25$, when $s = 0$:

$$\frac{\partial\sigma_1'}{\partial\sigma_3'} = 1 + a m_b^a \left(\frac{\sigma_3'}{\sigma_{ci}}\right)^{a-1} \tag{1.16}$$

The tensile strength of the rock mass is calculated from:

$$\sigma_{tm} = \frac{\sigma_{ci}}{2}\left(m_b - \sqrt{m_b^2 + 4s}\right) \tag{1.17}$$

The equivalent Mohr envelope, defined by equation 1.2, may be written in the form

$$Y = \log A + BX \tag{1.18}$$

where

$$Y = \log\left(\frac{\tau}{\sigma_{ci}}\right), \; X = \log\left(\frac{\sigma_n' - \sigma_{tm}}{\sigma_{ci}}\right) \tag{1.19}$$

Using the value of σ_{tm} calculated from equation 1.17 and a range of values of τ and σ_n' calculated from equations 1.13 and 1.14 the values of A and B are determined by linear regression where :

$$B = \frac{\sum XY - (\sum X \sum Y)/T}{\sum X^2 - (\sum X)^2 / T} \tag{1.20}$$

$$A = 10\hat{}\left(\sum Y/T - B(\sum X/T)\right) \quad (1.21)$$

and T is the total number of data pairs included in the regression analysis.

The most critical step in this process is the selection of the range of σ_3' values. As far as the authors are aware, there are no theoretically correct methods for choosing this range and a trial and error method, based upon practical compromise, has been used for selecting the range included in the spreadsheet presented in Figure 1.9.

For a Mohr envelope defined by equation 1.2, the friction angle ϕ_i' for a specified normal stress σ_{ni}' is given by:

$$\phi_i' = \arctan\left(AB\left(\frac{\sigma_{ni}' - \sigma_{tm}}{\sigma_{ci}} \right)^{B-1} \right) \quad (1.22)$$

The corresponding cohesive strength c_i' is given by:

$$c_i' = \tau - \sigma_{ni}' \tan \phi_i' \quad (1.23)$$

and the corresponding uniaxial compressive strength of the rock mass is :

$$\sigma_{cmi} = \frac{2c_i' \cos\phi_i'}{1 - \sin\phi_i'} \quad (1.24)$$

The values of c' and ϕ' obtained from this analysis are very sensitive to the range of values of the minor principal stress σ_3' used to generate the simulated full-scale triaxial test results. On the basis of trial and error, it has been found that the most consistent results for deep excavations (depth > 30 m below surface) are obtained when 8 equally spaced values of σ_3' are used in the range $0 < \sigma_3' < 0.25\sigma_{ci}$. For shallow excavations and slopes, the user should input the depth below surface of the anticipated failure surface and the unit weight of the rock mass. For typical slopes, the depth of the failure surface can be assumed to be equal to the slope height.

Figure 1.8: Spreadsheet for calculation of Hoek-Brown and equivalent Mohr-Coulomb parameters for shallow excavations and slopes.

Input:

sigci =	30	MPa	mi =	15		GSI =	55	
Depth of failure surface or tunnel below slope =				25	m	Unit wt. =	0.027	MN/n3

Output:

stress =	0.68	MPa	mb =	3.01		s =	0.0067	
a =	0.5		sigtm =	-0.0672	MPa	A =	0.7086	
B =	0.7263		k =	9.19		phi =	53.48	degrees
coh =	0.494	MPa	sigcm =	3.00	MPa	E =	7304.0	MPa

Calculation:

									Sums
sig3	1E-10	0.10	0.19	0.29	0.39	0.48	0.58	0.68	2.70
sig1	2.46	3.94	5.04	5.96	6.78	7.52	8.21	8.86	48.77
ds1ds3	19.32	12.74	10.31	8.95	8.06	7.41	6.91	6.51	80.20
sign	0.12	0.38	0.62	0.86	1.09	1.32	1.54	1.76	7.70
tau	0.53	1.00	1.38	1.70	2.00	2.28	2.54	2.78	14.21
x	-2.20	-1.83	-1.64	-1.51	-1.41	-1.34	-1.27	-1.21	-12.42
y	-1.75	-1.48	-1.34	-1.25	-1.18	-1.12	-1.07	-1.03	-10.21
xy	3.85	2.71	2.19	1.88	1.66	1.49	1.36	1.25	16.41
xsq	4.85	3.35	2.69	2.28	2.00	1.78	1.61	1.47	20.04
sig3sig1	0.00	0.38	0.97	1.72	2.61	3.63	4.75	5.98	20
sig3sq	0.00	0.01	0.04	0.08	0.15	0.23	0.33	0.46	1
taucalc	0.53	1.00	1.37	1.70	2.00	2.28	2.54	2.79	
sig1sig3fit	3.00	3.88	4.77	5.65	6.54	7.42	8.31	9.20	
signtaufit	0.66	1.00	1.33	1.65	1.97	2.28	2.58	2.88	

Cell formulae:

```
   stress = if(depth>30, sigci*0.25,depth*unitwt*0.25)
       mb = mi*EXP((GSI-100)/28)
        s = IF(GSI>25,EXP((GSI-100)/9),0)
        a = IF(GSI>25,0.5,0.65-GSI/200)
    sigtm = 0.5*sigci*(mb-SQRT(mb^2+4*s))
     sig3 = Start at 1E-10 (to avoid zero errors) and increment in 7 steps of  stress/28 to stress/4
     sig1 = sig3+sigci*(((mb*sig3)/sigci)+s)^a
   ds1ds3 = IF(GSI>25,(1+(mb*sigci)/(2*(sig1-sig3))),1+(a*mb^a)*(sig3/sigci)^(a-1))
     sign = sig3+(sig1-sig3)/(1+ds1ds3)
      tau = (sign-sig3)*SQRT(ds1ds3)
        x = LOG((sign-sigtm)/sigci)
        y = LOG(tau/sigci)
       xy = x*y                  x sq = x^2
        A =    acalc =     10^(sumy/8 - bcalc*sumx/8)
        B =    bcalc =     (sumxy - (sumx*sumy)/8)/(sumxsq - (sumx^2)/8)
        k = (sumsig3sig1 - (sumsig3*sumsig1)/8)/(sumsig3sq-(sumsig3^2)/8)
      phi = ASIN((k-1)/(k+1))*180/PI()
      coh = sigcm/(2*SQRT(k))
    sigcm = sumsig1/8 - k*sumsig3/8
        E = IF(sigci>100,1000*10^((GSI-10)/40),SQRT(sigci/100)*1000*10^((GSI-10)/40))
     phit = (ATAN(acalc*bcalc*((signt-sigtm)/sigci)^(bcalc-1)))*180/PI()
     coht = acalc*sigci*((signt-sigtm)/sigci)^bcalc-signt*TAN(phit*PI()/180)
 sig3sig1= sig3*sig1         sig3sq = sig3^2
  taucalc = acalc*sigci*((sign-sigtm)/sigci)^bcalc
   s3sifit = sigcm+k*sig3
 sntaufit =   coh+sign*TAN(phi*PI()/180)
```

Strength of jointed rock masses

Evert Hoek, Golder Associates, Vancouver, Canada

Twenty-third Rankine Lecture
presented to the British Geological Society in London on February 23, 1983
and published in *Géotechnique*, Vol. 23, No. 3, 1983, pp. 187-223.

Strength of jointed rock masses

Evert Hoek, Golder Associates, Vancouver, Canada

Synopsis

Jointed rock masses comprise interlocking angular particles or blocks of hard brittle material separated by discontinuity surfaces which may or may not be coated with weaker materials. The strength of such rock masses depends on the strength of the intact pieces and on their freedom of movement which, in turn, depends on the number, orientation, spacing and shear strength of the discontinuities. A complete understanding of this problem presents formidable theoretical and experimental problems and, hence, simplifying assumptions are required in order to provide a reasonable basis for estimating the strength of jointed rock masses for engineering design purposes. This paper summarizes some of the basic information upon which such simplifying assumptions can be made. A simple empirical failure criterion is presented and its application in engineering design is illustrated by means of a number of practical examples.

Introduction

The past twenty years have seen remarkable developments in the field of geotechnical engineering, particularly in the application of computers to the analysis of complex stress distribution and stability problems. There have also been advances in the field of geotechnical equipment and instrumentation and in the understanding of concepts such as the interaction between a concrete or steel structure and the soil foundation upon which it is built or, in the case of a tunnel, the interaction between the rock mass surrounding the tunnel and the support system installed in the tunnel. Similarly, there have been significant advances in our ability to understand and to analyze the role of structural features such as joints, bedding planes and faults in controlling the stability of both surface and underground excavations.

In spite of these impressive advances, the geotechnical engineer is still faced with some areas of major uncertainty and one of these relates to the strength of jointed rock masses. This problem is summed up very well in a paper on rockfill materials by Marachi, Chan and Seed (1972) when they say 'No stability analysis, regardless of how intricate and theoretically exact it may be, can be useful for design if an incorrect estimation of the shearing strength of the construction material has been made'. These authors go on to show that, although laboratory tests on rockfill are difficult and expensive because of the size of the equipment involved, there are techniques available to permit realistic and reliable evaluation of the shear strength of typical rockfill used for dam construction.

Unfortunately, this is not true for jointed rock masses where a realistic evaluation of shear strength presents formidable theoretical and experimental problems. However, since this question is of fundamental importance in almost all major designs involving foundations, slopes or underground excavations in rock, it is essential that such strength estimates be made and that these estimates should be as reliable as possible.

In this paper the author has attempted to summarize what is known about the strength of jointed rock masses, to deal with some of the theoretical concepts involved and to explore their limitations and to propose some simple empirical approaches which have been found useful in solving real engineering problems. Examples of such engineering problems are given.

Definition of the problem

Figure 1 summarises the range of problems to be considered. In order to understand the behaviour of jointed rock masses, it is necessary to start with the components which go together to make up the system - the intact rock material and individual discontinuity surfaces. Depending upon the number, orientation and nature of the discontinuities, the intact rock pieces will translate, rotate or crush in response to stresses imposed upon the rock mass. Since there are a large number of possible combinations of block shapes and sizes, it is obviously necessary to find any behavioural trends which are common to all of these combinations. The establishment of such common trends is the most important objective of this paper.

Before embarking upon a study of the individual components and of the system as a whole, it is necessary to set down some basic definitions.

Intact rock refers to the unfractured blocks which occur between structural discontinuities in a typical rock mass. These pieces may range from a few millimetres to several metres in size and their behaviour is generally elastic and isotropic. Their failure can be classified as brittle which implies a sudden reduction in strength when a limiting stress level is exceeded. In general, viscoelastic or time-dependent behaviour such as creep is not considered to be significant unless one is dealing with evaporites such as salt or potash.

Joints are a particular type of geological discontinuity but the term tends to be used generically in rock mechanics and it usually covers all types of structural weakness.
Strength, in the context of these notes, refers to the maximum stress level which can be carried by a specimen. No attempt is made to relate this strength to the amount of strain which the specimen undergoes before failure nor is consideration given to the post-peak behaviour or the relationship between peak and residual strength. It is recognised that these factors are important in certain engineering applications but such problems are beyond the scope of this paper.

The presentation of rock strength data and its incorporation into a failure criterion depends upon the preference of the individual and upon the end use for which the criterion is intended. In dealing with slope stability problems where limit equilibrium methods of analyses are used, the most useful failure criterion is one which expresses the shear strength in terms of the effective normal stress acting across a particular weakness plane or shear zone. The presentation which is most familiar to soil mechanics engineers is the Mohr failure envelope. On the other hand, when analysing the stability of underground excavations, the response of the rock to the principal stresses acting upon each element is of paramount interest. Consequently, a plot of triaxial test data in terms of the major principal stress at failure versus minimum principal stress or confining pressure is the most useful form of failure criterion for the underground excavation engineer. Other forms of failure criterion involving induced tensile strain, octahedral shear stress or energy considerations will not be dealt with.

In recognition of the soil mechanics background of many of the readers, most of the discussion on failure criteria will be presented in terms of Mohr failure envelopes. It is, however, necessary to point out that the author's background in underground excavation engineering means that the starting point for most of his studies is the triaxial test and the presentation of failure criteria in terms of principal stresses rather than shear and normal stresses. As will become obvious later, this starting point has an important bearing upon the form of the empirical failure criterion presented here.

Strength of intact rock

A vast amount of information on the strength of intact rock has been published during the past fifty years and it would be inappropriate to attempt to review all this information here. Interested readers are referred to the excellent review presented by Professor J.C. Jaeger in the eleventh Rankine lecture (1971).

In the context of this discussion, one of the most significant steps was a suggestion by Murrell (1958) that the brittle fracture criterion proposed by Griffith (1921,1924) could be applied to rock. Griffith postulated that, in brittle materials such as glass, fracture initiated when the tensile strength of the material is exceeded by stresses generated at the ends of microscopic flaws in the material. In rock, such flaws could be pre-existing cracks, grain boundaries or other discontinuities. Griffith's theory, summarized for rock mechanics application by Hoek (1968), predicts a parabolic Mohr failure envelope defined by the equation:

$$\tau = 2(|\sigma_t|(|\sigma_t| + \sigma'))^{1/2} \tag{1}$$

Where τ is the shear stress

σ' is the effective normal stress and

σ_t is the tensile strength of the material (note that tensile stresses are considered negative throughout this paper).

Griffith's theory was originally derived for predominantly tensile stress fields. In applying this criterion to rock subjected to compressive stress conditions, it soon became obvious that the frictional strength of closed crack has to be allowed for, and McClintock and Walsh (1962) proposed a modification to Griffith's theory to account for these frictional forces. The Mohr failure envelope for the modified Griffith theory is defined by the equation:

$$\tau = 2|\sigma_t| + \sigma' Tan\,\phi' \tag{2}$$

Where ϕ' is the angle of friction on the crack surfaces. (Note, this equation is only valid for $\sigma > 0$.

	Description	Strength characteristics	Strength testing	Theoretical considerations
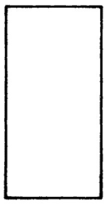	Hard intact rock	Brittle, elastic and generally isotropic	Triaxial testing of core specimens in laboratory relatively simple and inexpensive and results usually reliable	Theoretical behaviour of isotropic elastic brittle rock adequately understood for most practical applications
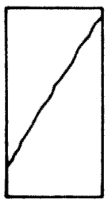	Intact rock with single inclined discontinuity	Highly anisotropic, depending on shear strength and inclination of discontinuity	Triaxial testing of core with inclined joints difficult and expensive but results reliable. Direct shear testing of joints simple and inexpensive but results require careful interpretation	Theoretical behaviour of individual joints and of schistose rock adequately understood for most practical applications
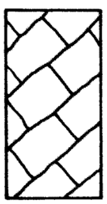	Massive rock with a few sets of discontinuities	Anisotropic, depending on number, shear strength and continuity of discontinuities	Laboratory testing very difficult because of sample disturbance and equipment size limitations	Behaviour of jointed rock poorly understood because of complex interaction of interlocking blocks
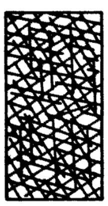	Heavily jointed rock	Reasonably isotropic. Highly dilatant at low normal stress levels with particle breakage at high normal stress	Triaxial testing of undisturbed core samples extremely difficult due to sample disturbance and preparation problems	Behaviour of heavily jointed rock very poorly understood because of interaction of interlocking angular pieces
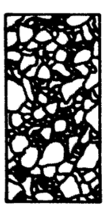	Compacted rockfill	Reasonably isotropic. Less dilatant and lower shear strength than in situ jointed rock but overall behaviour generally similar	Triaxial testing simple but expensive because of large equipment size required to accommodate representative samples	Behaviour of compacted rockfill reasonably well understood from soil mechanics studies on granular materials
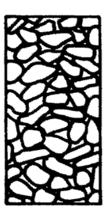	Loose waste rock	Poor compaction and grading allow particle rotation and movement resulting in mobility of waste rock dumps	Triaxial or direct shear testing relatively simple but expensive because of large equipment size required	Behaviour of waste rock adequately understood for most applications

Figure 1 : Summary of range of rock mass characteristics

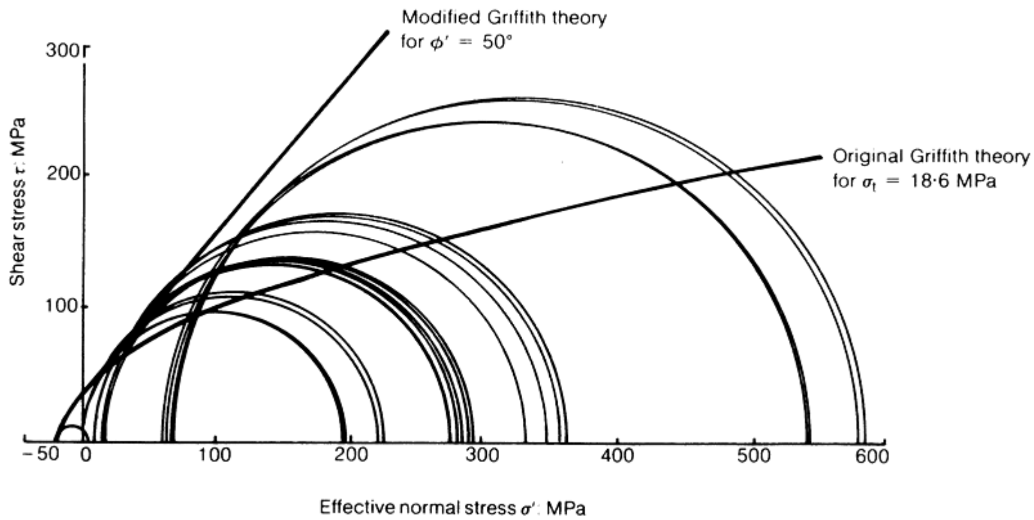

Figure 2 : Mohr circles for failure of specimens of quartzite tested by Hoek (1965). Envelopes included in the figure are calculated by means of the original and modified Griffith theories of brittle fracture initiation.

Detailed studies of crack initiation and propagation by Hoek and Bieniawski (1965) and Hoek (1968) showed that the original and modified Griffith theories are adequate for the prediction of fracture initiation in rocks but that they fail to describe fracture propagation and failure of a sample. Figure 2 gives a set of Mohr circles representing failure of the quartzite tested triaxially (Hoek, 1965). Included in this figure are Mohr envelopes calculated by means of equations 1 and 2 (for $\sigma_t = 18.6$ MPa and $\phi = 50°$). It will be noted that neither of these curves can be considered acceptable envelopes to the Mohr circles representing failure of the quartzite under compressive stress conditions. In spite of the inadequacy of the specimens, a study of the mechanics of fracture initiation and of the shape of the Mohr envelopes predicted by these theories was a useful starting point in deriving the empirical failure criterion discussed in this chapter.

Jaeger (1971), in discussing failure criteria for rock, comments that 'Griffith theory has proved extraordinarily useful as a mathematical model for studying the effect of cracks on rock, but it is essentially only a mathematical model; on the microscopic scale rocks consist of an aggregate of anisotropic crystals of different mechanical properties and it is these and their grain boundaries which determine the microscopic behaviour'

Recognition of the difficulty involved in developing a mathematical model which adequately predicts fracture propagation and failure in rock led a number of authors to propose empirical relationships between principal stresses or between shear and normal stresses at failure. Murrell (1965), Hoek (1968), Hobbs (1970) and Bieniawski (1974) all proposed different forms of empirical criteria. The failure criterion put forward here is based on that presented by Hoek and Brown (1980a, 1980b) and resulted from their efforts to produce an acceptable failure criterion for the design of underground excavations in rock.

An empirical failure criterion for rock

In developing their empirical failure criterion, Hoek and Brown (1980a) attempted to satisfy the following conditions:

(a) The failure criterion should give good agreement with experimentally determined rock strength values.
(b) The failure criterion should be expressed by mathematically simple equations based, to the maximum extent possible, upon dimensionless parameters.
(c) The failure criterion should offer the possibility of extension to deal with anisotropic failure and the failure of jointed rock masses.

The studies on fracture initiation and propagation, discussed earlier, suggested that the parabolic Mohr envelope predicted by the original Griffith theory adequately describes both fracture initiation and failure of brittle materials under conditions where the effective normal stress acting across a pre-existing crack is tensile (negative). This is because fracture propagation follows very quickly upon fracture initiation under tensile stress conditions, and hence fracture initiation and failure of the specimen are practically indistinguishable.

Figure 2 shows that, when the effective normal stress is compressive (positive), the envelope to the Mohr circles tends to be curvilinear, but not to the extent predicted by the original Griffith theory.

Based on these observations, Hoek and Brown (1980a) experimented with a number of distorted parabolic curves to find one which gave good coincidence with the original Griffith theory for tensile effective normal stresses, and which fitted the observed failure conditions for brittle rocks subjected to compressive stress conditions.

Note that the process used by Hoek and Brown in deriving their empirical failure criterion was one of pure trial and error. Apart from the conceptual starting point provided by Griffith theory, there is no fundamental relationship between the empirical constants included in the criterion and any physical characteristics of the rock. The justification for choosing this particular criterion over the numerous alternatives lies in the adequacy of its predictions of observed rock fracture behaviour, and the convenience of its application to a range of typical engineering problems.

As stated earlier, the author's background in designing underground excavations in rock resulted in the decision to present the failure criterion in terms of the major and minor principal stresses at failure. The empirical equation defining the relationship between these stresses is

$$\sigma_1' = \sigma_3' + (m\sigma_c\sigma_3' + s\sigma_c^2)^{1/2} \qquad (3)$$

where σ_1' is the major principal effective stress at failure

σ_3' is the minor principal effective stress or, in the case of a triaxial test, the confining pressure

σ_c is the uniaxial compressive strength of the intact rock material from which the rock mass is made up *m* and *s* are empirical constants

The constant *m* always has a finite positive value which ranges from about 0.001 for highly disturbed rock masses, to about 25 for hard intact rock. The value of the constant *s* ranges from 0 for jointed masses, to 1 for intact rock material.

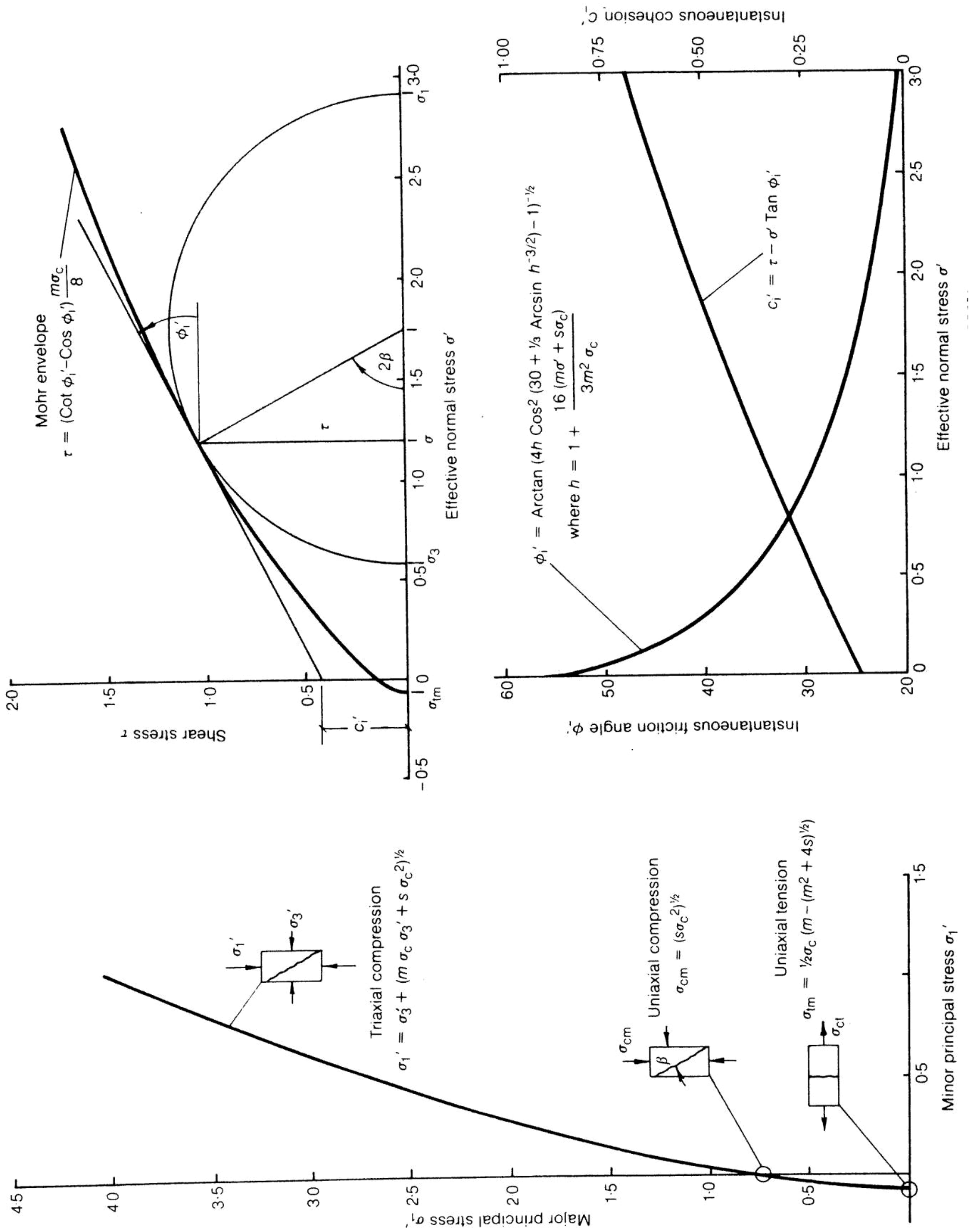

Figure 3. Summary of equations with the non-linear failure criterion proposed by Hoek & Brown (1980b)

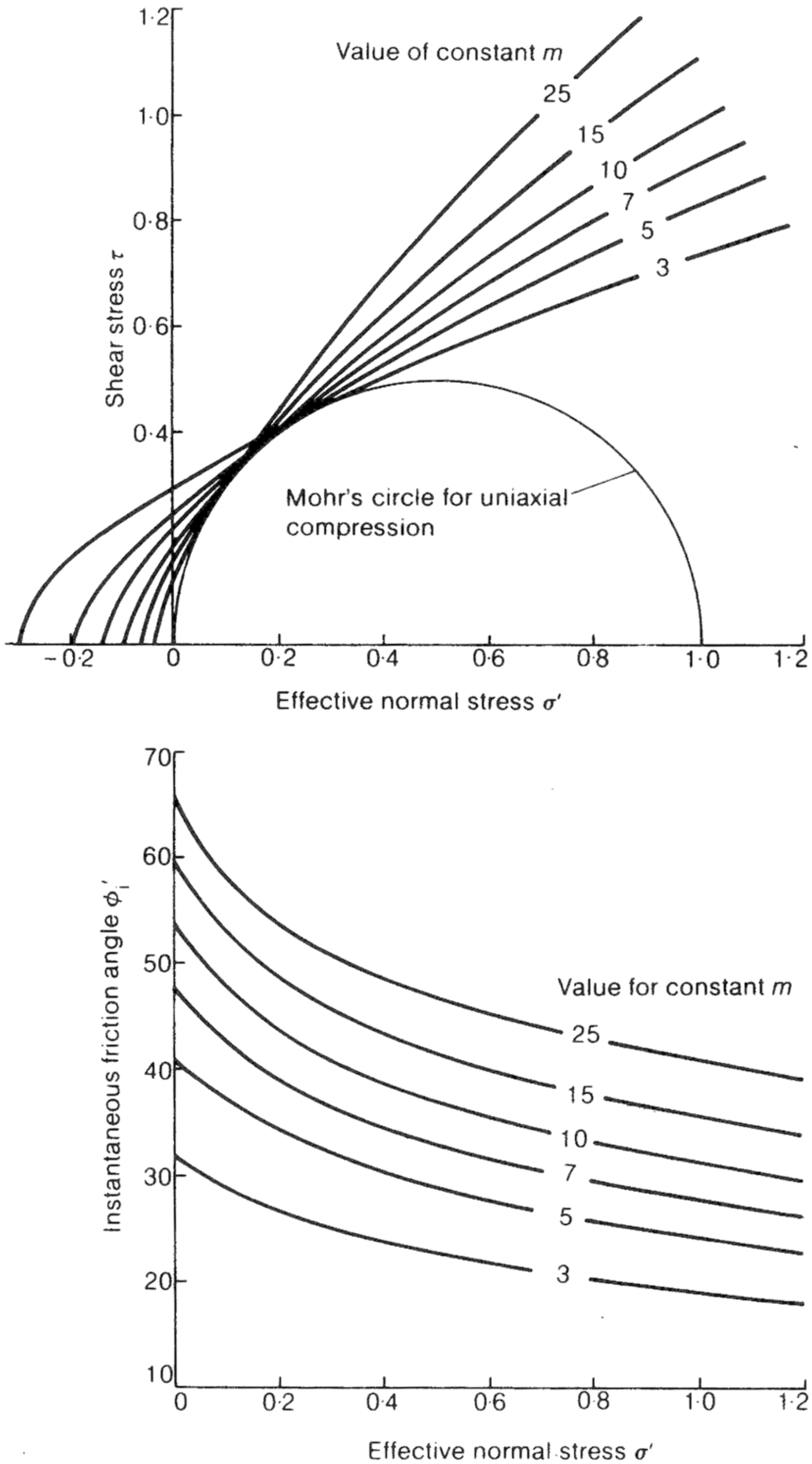

Figure 4. Influence of the value of the constant *m* on the shape of the Mohr failure envelope and on the instantaneous friction angle at different effective normal stress levels.

Substitution of $\sigma_3^{'}$ = 0 into equation 3 gives the unconfined compressive strength of a rock mass as

$$\sigma_1^{'} = \sigma_c = (s\sigma_c^2)^{1/2} \tag{4}$$

Similarly, substitution $\sigma_1^{'}$ of = 0 in equation 3, and solution of the resulting quadratic equation for $\sigma_3^{'}$, gives the uniaxial tensile strength of a rock mass as

$$\sigma_3^1 = \sigma_t = \frac{1}{2}\sigma_c\left(m - (m^2 + 4s)^{1/2}\right) \tag{5}$$

The physical significance of equations 3, 4 and 5 is illustrated in the plot of $\sigma_1^{'}$ versus $\sigma_3^{'}$ given in figure 3.

While equation 3 is very useful in designing underground excavations, where the response of individual rock elements to in situ and induced stresses is important, it is of limited value in designing rock slopes where the shear strength of a failure surface under specified effective normal stress conditions is required.

The Mohr failure envelope corresponding to the empirical failure criterion defined by equation 3 was derived by Dr. John Bray of Imperial College and is given by:

$$\tau = (Cot\,\phi_i^{'} - Cos\,\phi_i^{'})\frac{m\sigma_c}{8} \tag{6}$$

where τ is the shear stress at failure

$\phi_i^{'}$ is the instantaneous friction angle at the given values of τ and σ' i.e. the inclination of the tangent to the Mohr failure envelope at the point (σ', τ) as shown in figure 3.

The value of the instantaneous friction angle $\phi_i^{'}$ is given by:

$$\phi_i^{'} = Arc\tan\left(4h\,Cos^2(30 + \frac{1}{3}Arc\sin h^{-3/2}) - 1\right)^{-1/2} \tag{7}$$

where

$$h = 1 + \frac{16(m\sigma^{'} + s\sigma_c)}{3m^2\sigma_c}$$

and σ' is the effective normal stress.

The instantaneous cohesive strength $c_i^{'}$, shown in figure 3, is given by:

$$c_i^{'} = \tau - \sigma^{'}\,Tan\,\phi_i^{'} \tag{8}$$

From the Mohr circle construction given in figure 3, the failure plane inclination β is given by

$$\beta = 45 - \frac{1}{2}\phi_i^{'} \tag{9}$$

An alternative expression for the failure plane inclination, in terms of the principal stresses $\sigma_1^{'}$ and $\sigma_3^{'}$, was derived by Hoek and Brown (1980a):

$$\beta = \frac{1}{2} Arc \sin \frac{\tau_m}{\tau_m + m\sigma_c/8} \left(1 + m\sigma_c/4\tau_m\right)^{1/2} \tag{10}$$

where $\tau = 1/2(\sigma_1^{'} - \sigma_3^{'})$.

Characteristics of empirical criterion

The empirical failure criterion presented in the preceding section contains three constants *m*, *s* and σ_c. The significance of each of these will be discussed in turn later.

Constants *m* and *s* are both dimensionless and are very approximately analogous to the angle of friction, ϕ, and the cohesive strength, c', of the conventional Mohr-Coulomb failure criterion.

Figure 4 illustrates the influence of different values of the constant *m* upon the Mohr failure envelope for intact rock. Note that in plotting these curves, the values of both *s* and σ_c are assumed equal to unity.

Large values of *m*, in the order of 15 to 25, give steeply inclined Mohr envelopes and high instantaneous friction angles at low effective normal stress levels. These large *m* values tend to be associated with brittle igneous and metamorphic rocks such as andesites, gneisses and granites. Lower *m* values, in the order of 3 to 7, give lower instantaneous friction angles and tend to be associated with more ductile carbonate rocks such as limestone and dolomite.

The influence of the value of the constant *s* upon the shape of the Mohr failure envelope and upon the instantaneous friction angle at different effective normal stress levels is illustrated in figure 5. The maximum value of *s* is 1.00, and this applies to intact rock specimens which have a finite tensile strength (defined by equation 5). The minimum value of *s* is zero, and this applies to heavily jointed or broken rock in which the tensile strength has been reduced to zero and where the rock mass has zero cohesive strength when the effective normal stress is zero.

The third constant, σ_c, the uniaxial compressive strength of the intact rock material, has the dimensions of stress. This constant was chosen after very careful consideration of available rock strength data. The unconfined compressive strength is probably the most widely quoted constant in rock mechanics, and it is likely that an estimate of this strength will be available in cases where no other rock strength data are available.

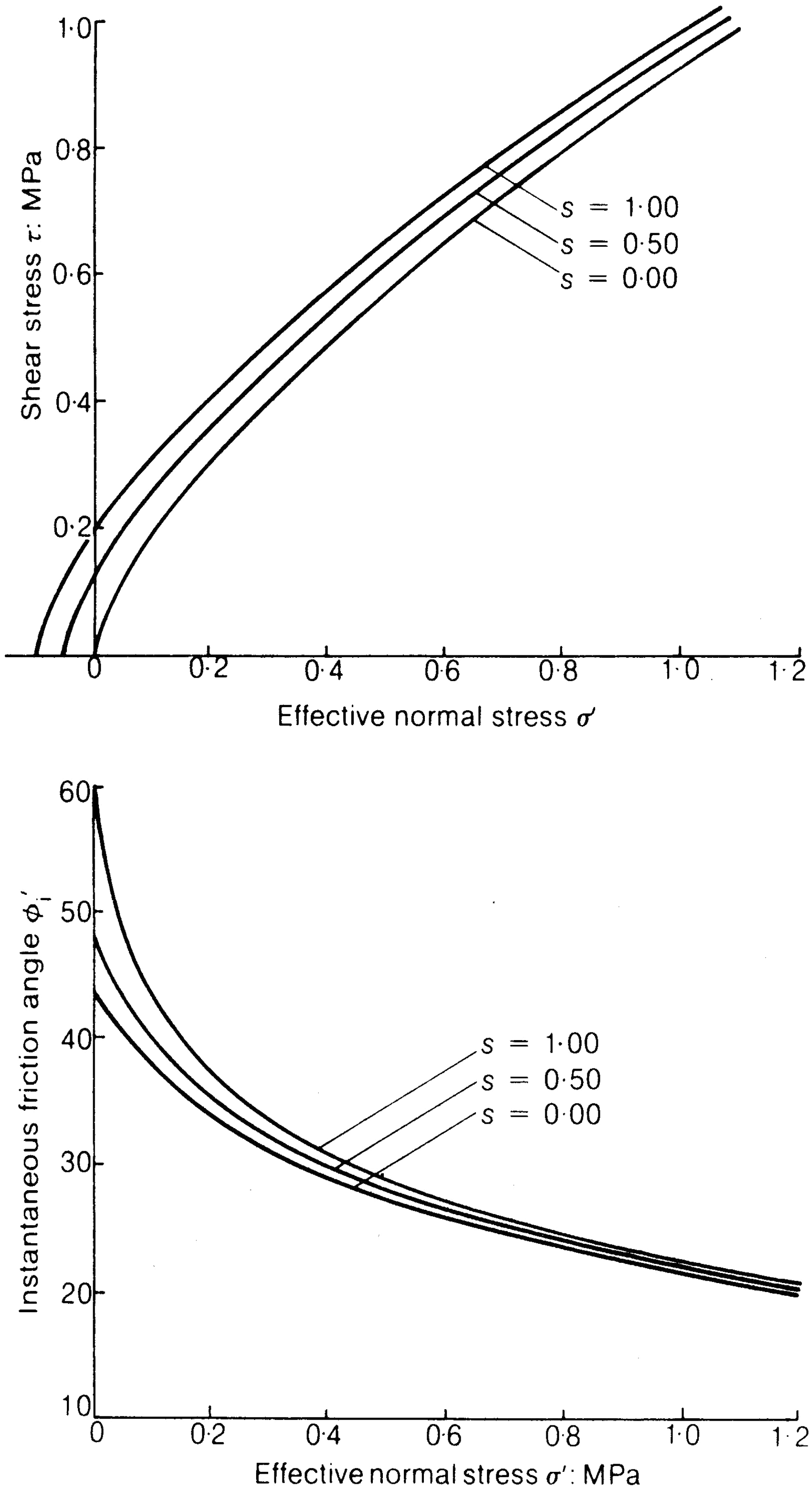

Figure 5. Influence of the value of the constant *s* on the shape of the Mohr failure envelope and on the instantaneous friction angle at different effective stress levels

Consequently, it was decided that the uniaxial compressive strength σ_c would be adopted as the basic unit of measurement in the empirical failure criterion.

Note that the failure criterion defined by equation 3 can be made entirely dimensionless by dividing both sides by the uniaxial compressive strength:

$$\sigma_1^{'} / \sigma_c = \sigma_3^{'} / \sigma_c + (m\sigma_3^{'} / \sigma_c + s)^{1/2} \qquad (11)$$

This formulation, which can also be achieved by simply putting $\sigma_c = 1$ in equation 3, is very useful when comparing the shape of Mohr failure envelopes for different rock materials.

A procedure for the statistical determination of the values of the constants *m, s* and σ_c from experimental data is given in appendix 1.

Triaxial data for intact rock

Hoek and Brown (1980a) analyzed published data from several hundred triaxial tests on intact rock specimens and found some useful trends. These trends will be discussed in relationship to two sets of data plotted as Mohr failure circles in figure 6. The sources of the triaxial data plotted in figure 6 are given in table 1.

Figure 6a gives Mohr failure envelopes for five different granites from the USA and UK. Tests on these granites were carried out in five different laboratories using entirely different triaxial equipment. In spite of these differences, the failure characteristics of these granites follow a remarkably consistent pattern, and the Mohr failure envelope predicted by equations 6 and 7 (for $\sigma_c = 1$, $m = 29.2$, and $s = 1$) fits all of these Mohr circles very well. Table 1 shows that a correlation coefficient of 0.99 was obtained by statistically fitting the empirical failure criterion defined by equation 3 to all of the granite strength data. The term granite defines a group of igneous rocks having very similar mineral composition, grain size and angularity, hence it is not too surprising that the failure characteristics exhibited by these rocks should be very similar, irrespective of the source of the granite. The trend illustrated in figure 6a has very important practical implications, since it suggests that it should be possible, given a description of the rock and an estimate of its uniaxial compressive strength, to predict its Mohr failure envelope with a relatively high degree of confidence. This is particularly important in early conceptual or feasibility studies where the amount of reliable laboratory data is very limited.

In contrast to the trends illustrated in figure 6a for granite, the plot given in figure 6b for limestone is less convincing. In this case, eleven different limestones, tested in three different laboratories, have been included in the plot. Table 1 shows that the values of the constant *m*, derived from statistical analyses of the test data, vary from 3.2 to 14.1, and that the correlation coefficient for the complete data set is only 0.68.

The scatter of the data included in figure 6b is attributed to the fact that the generic term limestone applies to a range of carbonate rocks formed by deposition of a variety of organic and inorganic materials. Consequently, mineral composition, grain size and shape, and the nature of cementing materials between the grains will vary from one limestone to another.

Comparison of the two plots given in figure 6 suggests that the empirical failure criterion presented in this paper gives a very useful indication of the general trend of the Mohr failure envelope for different rock types. The accuracy of each prediction will depend upon the adequacy of the description of the particular rock under consideration. In comparing the granites and limestones included in figure 6, there would obviously be a higher priority in carrying out confirmatory laboratory tests on the limestone than on the granite.

Hoek and Brown (1980) found that there were definite trends which emerged from the statistical fitting of their empirical failure criterion (equation 3) to published triaxial data. For intact rock (for which $s = 1$), these trends are characterized by the value of the constant s which, as illustrated in figure 4, defines the shape of the Mohr failure envelope. The trends suggested by Hoek and Brown (1980) are as follows:

a) Carbonate rocks with well-developed crystal cleavage (dolomite, limestone and marble): $m = 7$
b) Lithified argillaceous rocks (mudstone, shale and slate (normal to cleavage)): $m = 10$
c) Arenaceous rocks with strong crystals and poorly developed crystal cleavage (sandstone and quartzite): $m = 15$
d) Fine grained polymineralic igneous crystalline rocks (andesite, dolerite, diabase and rhyotite): $m = 17$
e) Coarse grained polymineralic igneous and metamorphic rocks (amphibolite, gabbro, gneiss, granite, norite and granodiorite): $m = 25$

Before leaving the topic of intact rock strength, the fitting of the empirical failure criterion defined by equation 3 to a particular set of triaxial data is illustrated in figure 7. The Mohr circles plotted in this figure were obtained by Bishop and Garga (1969) from a series of carefully performed triaxial tests on undisturbed samples of London clay (Bishop et al, 1965). The Mohr envelope plotted in figure 7 was determined from a statistical analysis of Bishop and Garga's data (using the technique described in appendix 1), and the values of the constants are $\sigma_c = 211.8$ kPa, $m = 6.475$ and σ_c = 1. The correlation coefficient for the fit of the empirical criterion to the experimental data is 0.98.

This example was chosen for its curiosity value rather than its practical significance, and because of the strong association between the British Geotechnical Society and previous Rankine lecturers and London clay. The example does serve to illustrate the importance of limiting the use of the empirical failure criterion to a low effective normal stress range. Tests on London clay at higher effective normal stress levels by Bishop et al (1965) gave approximately linear Mohr failure envelopes with friction angles of about 11°.

As a rough rule-of-thumb, when analyzing intact rock behaviour, the author limits the use of the empirical failure criterion to a maximum effective normal stress level equal to the unconfined compressive strength of the material. This question is examined later in a discussion on brittle-ductile transition in intact rock.

Table 1. Sources of data included in Figure 6*

Rock type	Location	Reference	Number tested	Uniaxial compressive strength		Each sample		Rock type	
				lb/in²	MPa	*m*	r^2†	*m*	r^2†
Granite	Westerley, USA	Heard *et al.* (1974)	17	31 040	214·0	26·7	1·00		
	Westerley, USA	Wawersik & Brace (1971)	7	43 310	298·6	27·0	1·00		
	Westerley, USA	Brace (1964)	7	49 820	343·5	28·3	0·98		
	Westerley, USA	Mogi (1967)	6	32 440	223·7	32·8	0·99		
	Stone Mountain, USA	Schwartz (1964)	14	16 850	116·2	28·9	0·93	29·2	0·99
	Blackingstone, UK	Franklin & Hoek (1970)	48	30 410	209·7	20·8	0·91		
	Mount Sorrel, UK	Misra (1972)	5	39 910	275·2	26·5	0·99		
	Carnmarth, Redruth, UK	Misra (1972)	5	23 540	162·3	27·7	0·99		
Limestone	Portland, UK	Franklin & Hoek (1970)	30	13 300	91·7	7·5	0·72		
	Indiana, USA	Schwartz (1964)	6	7090	48·9	3·2	0·95		
	Bath, UK	Misra (1972)	7	6830	47·1	5·5	0·97		
	Grindling Stubbs, UK	Misra (1972)	6	19 450	134·1	8·8	0·97		
	Kirbymoorside, UK	Misra (1972)	5	23 830	164·3	12·3	0·98		
	Blackwell, UK	Misra (1972)	5	29 211	201·4	10·0	0·92	5·4	0·68
	Foster Yeoman, UK	Misra (1972)	5	24 265	167·3	14·1	0·95		
	Gigglewick, UK	Misra (1972)	5	22 423	154·6	8·8	0·97		
	Kelmac, UK	Misra (1972)	5	16 897	116·5	7·3	1·00		
	Threshfield, UK	Misra (1972)	5	21 423	147·7	6·9	0·98		
	Swinden Cracoe, UK	Misra (1972)	5	16 027	110·5	8·4	0·96		

* Material constant $s = 1$ for intact rock.

† r^2. is coefficient of deremination or correlation coefficient.

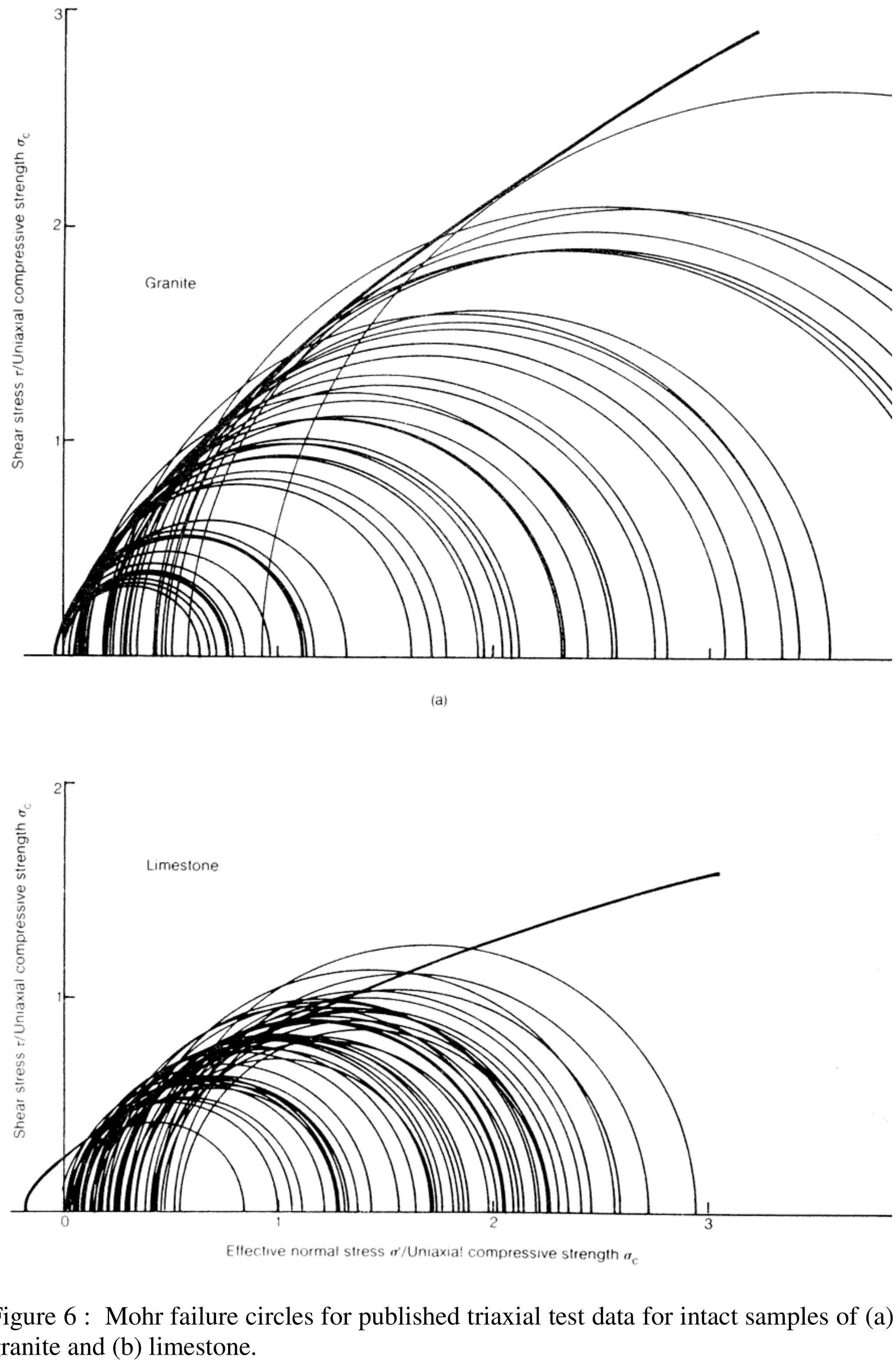

Figure 6 : Mohr failure circles for published triaxial test data for intact samples of (a) granite and (b) limestone.

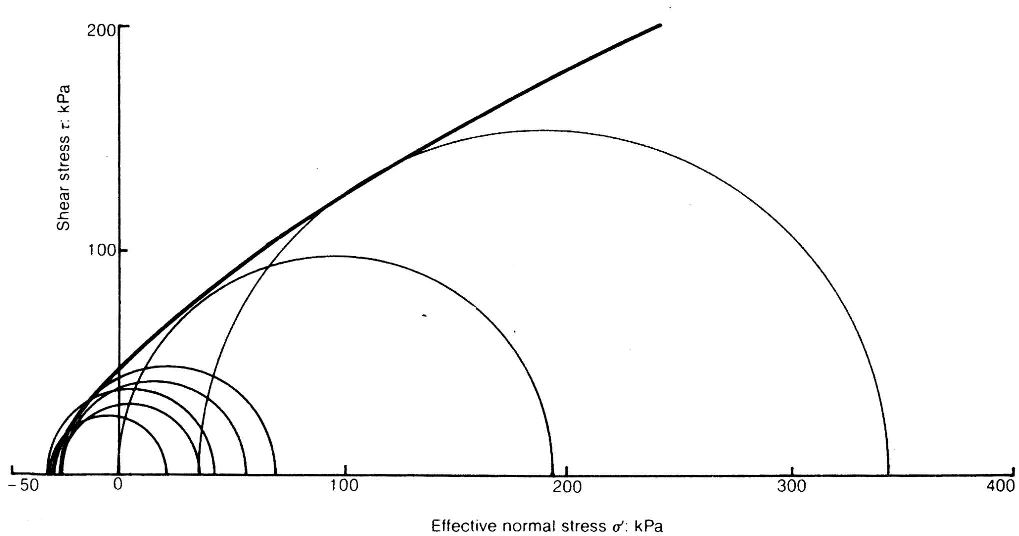

Figure 7 : Mohr failure envelope for drained triaxial tests at very low normal stress levels carried out bu Bishop and Garga (1969) on undisturbed samples of London clay.

Assumptions included in empirical failure criterion

A number of simplifying assumptions have been made in deriving the empirical failure criterion, and it is necessary briefly to discuss these assumptions before extending the criterion to deal with jointed rock masses.

Effective stress

Throughout this discussion, it is assumed that the empirical failure criterion is valid for effective stress conditions. In other words, the effective stress σ' used in equations 7 and 8 is obtained from $\sigma' = \sigma - u$, where σ is the applied normal stress and *u* is the pore or joint water pressure in the rock. In spite of some controversy on this subject, discussed by Jaeger and Cook (1969), Brace and Martin (1969) demonstrate that the effective stress concept appears to be valid in intact rocks of extremely low permeability, provided that loading rates are sufficiently low to permit pore pressures to equalize. For porous rocks such as sandstone, normal laboratory loading rates will generally satisfy effective stress conditions (Handin et al, (1963)) and there is no reason to suppose that they will not apply in the case of jointed rocks.

Influence of pore fluid on strength

In addition to the influence of pore pressure on strength, it is generally accepted that the pore fluid itself can have a significant influence on rock strength. For example, Colback and Wiid (1965) and Broch (1974) showed that the unconfined compressive strength of quartzitic shale, quartzdiorite, gabbro and gneiss can be reduced by as much as 2 by saturation in water as compared with oven dried specimens. Analyses of their results suggest that this reduction takes place in the unconfined compressive strength σ_c and not in the constant *m* of the empirical failure criterion.

It is important, in testing rock materials or in comparing data from rock strength tests, that the moisture content of all specimens be kept within a narrow range. In the author's own experience in testing samples of shale which had been left standing on the laboratory shelf for varying periods of time, the very large amount of scatter in strength data was almost eliminated by storing the specimens in a concrete curing room to bring them close to saturation before testing. Obviously, in testing rocks for a particular practical application, the specimens should be tested as close to in situ moisture content as possible.

Influence of loading rate

With the exception of effective stress tests on very low porosity materials (e.g. Brace and Martin (1968)), or tests on viscoelastic materials such as salt or potash, it is generally assumed that the influence of loading rate is insignificant when dealing with rock. While this may be an oversimplification, the author believes that it is sufficiently accurate for most practical applications.

Influence of specimen size

Hoek and Brown (1980a) have analyzed the influence of specimen size on the results of strength tests on the intact rock samples. They found that the influence of specimen size can be approximated by the relationship

$$\sigma_c = \sigma_{c50}(50/d)^{0.18} \tag{12}$$

where σ_c is the unconfined compressive strength,
d is the diameter of the specimen in millimeters, and
σ_{c50} is the unconfined compressive strength of a 50 mm diameter specimen of the same material.

In the case of jointed rocks, the influence of size is controlled by the relationship between the spacing of joints and the size of the sample. This problem is dealt with in the discussion on jointed rock masses given later in this paper.

Influence of intermediate principal stress

In deriving the empirical failure criterion presented in this paper, Hoek and Brown (1980) assumed that the failure process is controlled by the major and minor principal stresses σ_1' and σ_3', and that the intermediate principal stress σ_2' has no significant influence upon this process. This is almost certainly an over-simplification, but there appears to be sufficient evidence (reviewed by Jaeger and Cook (1967)) to suggest that the influence of the intermediate principle stress can be ignored without introducing unacceptably large errors.

Failure surface inclination

The inclination of an induced failure plane in an intact rock specimen is given by equation 9 or equation 10. Note that this inclination is measured from the direction of the maximum principal stress σ_1', as illustrated in figure 3.

The results of a series of triaxial tests by Wawersik (1968) on Tennessee marble are listed in table 2, and plotted as Mohr circles in figure 8. Also listed in table 2 and plotted in figure 8, are observed failure plane inclinations.

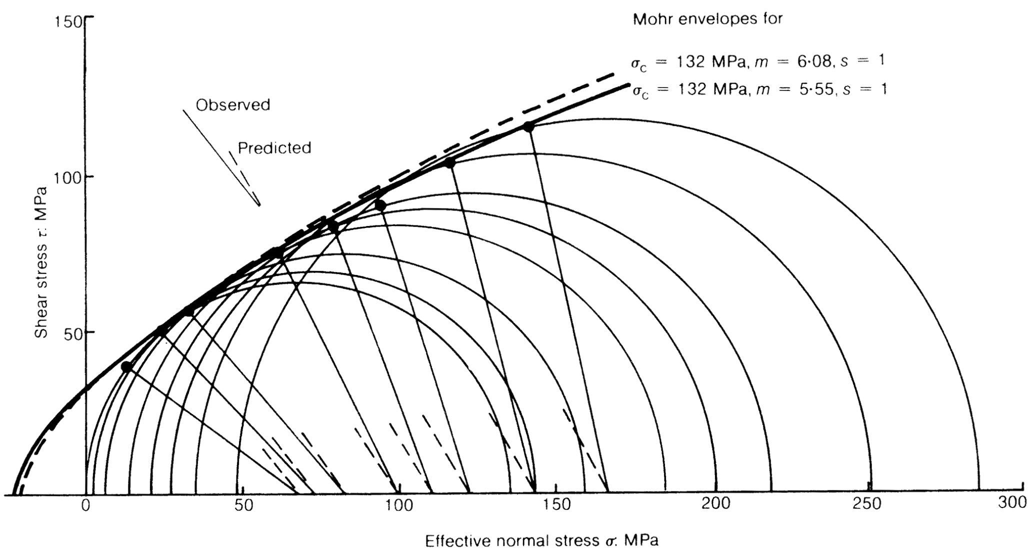

Figure 8 : Plot of Mohr failure circles for Tennessee marble tested by Wawersik (1968) giving comparison between predicted and observed failure plane inclination.

Table 2. Observed and predicted failure plane inclination for Tennesee marble (Wawersik, 1968).

Confining pressure: MPa	Axial strength: MPa	Observed fracture angle	Predicted fracture angle
0	134·48	18·0	26·61
3·45	143·45	23·4	27·0
6·90	160·00	24·8	27·7
13·79	186·21	31·7	28·7
20·69	201·38	35·1	29·1
27·59	220·00	36·3	29·7
34·48	251·03	37·8	30·6
48·28	286·21	38·8	31·4

A statistical analysis of the triaxial test data gives the following constants: σ_c = 132.0 MPa, m = 6.08, s = 1, with a correlation coefficient of 0.99. The Mohr envelope defined by these constants is plotted as a dashed curve in figure 8.

The predicted fracture angles listed in Table 2 have been calculated for σ_c = 132.0 MPa and m = 6.08 by means of equation 10, and it will be noted that there are significant differences between observed and predicted fracture angles.

On the other hand, a Mohr envelope fitted through the shear stress (τ) and effective normal stress (σ') points defined by construction (using the Mohr circles), gives a value of m = 5.55 for σ_c = 132 MPa and s = 1.00. The resulting Mohr envelope, plotted as a full line in figure 8, is not significantly different from the Mohr envelope determined by analysis of the principal stresses.

These findings are consistent with the author's own experience in rock testing. The fracture angle is usually very difficult to define, and is sometimes obscured altogether. This is because, as discussed earlier in this paper, the fracture process is complicated and does not always follow a clearly defined path. When the failure plane is visible, the inclination of this plane cannot be determined to better than plus or minus 5°. In contrast, the failure stresses determined from a carefully conducted set of triaxial tests are usually very clearly grouped, and the pattern of Mohr circles plotted in figure 8 is not unusual in intact rock testing.

The conclusion to be drawn from this discussion is that the failure plane inclinations predicted by equations 9 or 10 should be regarded as approximate only, and that, in many rocks, no clearly defined failure surfaces will be visible.

Brittle-ductile transition

The results of a series of triaxial tests carried out by Schwartz (1964) on intact specimens of Indiana limestone are plotted in figure 9. A transition from brittle to ductile behaviour appears to occur at a principal stress ratio of approximately $\sigma_1^{'} / \sigma_3^{'} = 4.3$.

A study of the failure characteristics of a number of rocks by Mogi (1966) led him to conclude that the brittle-ductile transition for most rocks occurs at an average principal stress ratio $\sigma_1^{'} / \sigma_3^{'} = 3.4$.

Examination of the results plotted in figure 9, and of similar results plotted by Mogi, shows that there is room for a wide variety of interpretations of the critical principal stress ratio, depending upon the curve fitting procedure employed and the choice of the actual brittle-ductile transition point. The range of possible values of $\sigma_1^{'} / \sigma_3^{'}$ appears to lie between 3 and 5.

A rough rule-of-thumb used by this author is that the confining pressure σ_1' must always be less than the unconfined compressive strength σ_c of the material for the behaviour to be considered brittle. In the case of materials characterized by very low values of the constant *m,* such as the Indiana limestone considered in figure 9 (m = 3.2), the value of $\sigma_1' = \sigma_c$ may fall beyond the brittle-ductile transition. However, for most rocks encountered in practical engineering applications, this rule-of-thumb appears to be adequate.

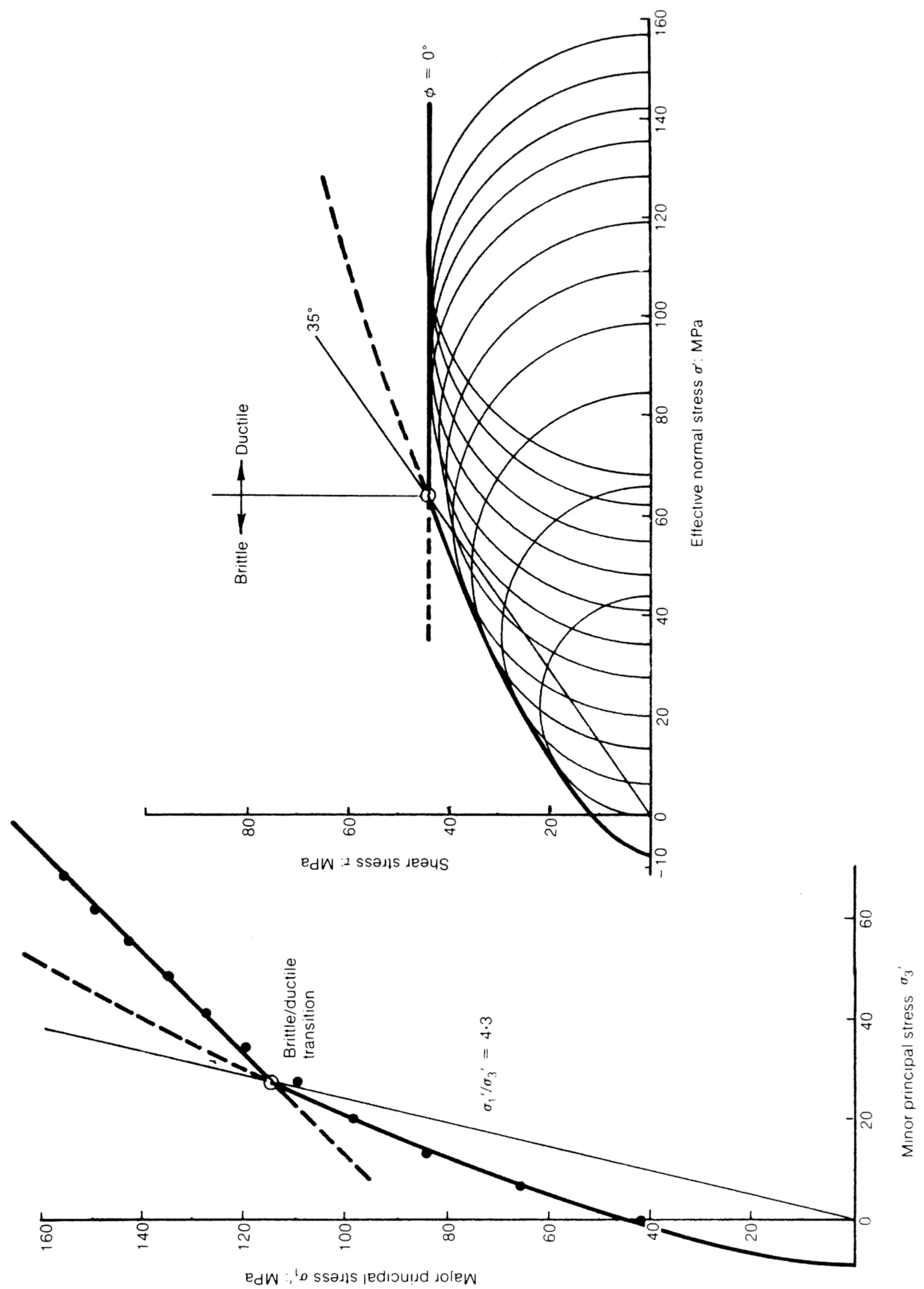

Figure 9. Results of triaxial tests on Indiana limestone carried out by Schwartz (1964) illustrating the brittle-ductile transition.

Shear strength of discontinuities

The shear strength of discontinuities in rock has been extensively discussed by a number of authors such as Patton (1966), Goodman (1970), Ladanyi and Archambault (1970), Barton (1971, 1973, 1974), Barton and Choubey (1977), and Richards and Cowland (1982). These discussions have been summarized by Hoek and Bray (1981).

For practical field applications involving the estimation of the shear strength of rough discontinuity surfaces in rock, the author has no hesitation in recommending the following empirical relationship between shear strength (τ) and effective normal stress (σ') proposed by Barton (1971, 1973).

$$\tau = \sigma' Tan\left(\phi_b' + JRC\, Log_{10}\,(JCS/\sigma')\right) \tag{13}$$

where ϕ_b' is the 'basic' friction angle of smooth planar discontinuities in the rock under consideration, *JRC* is a joint roughness coefficient which ranges from 5 for smooth surfaces, to 20 for rough undulating surfaces, and *JCS* is joint wall compressive strength which, for clean unweathered discontinuities, equals the uniaxial compressive strength of the intact rock material.
While Barton's equation is very useful for field applications, it is by no means the only one which can be used for fitting to laboratory shear test data such as that published by Krsmanovic (1967), Martin and Miller (1974), and Hencher and Richards (1982).

Figure 10 gives a plot of direct shear strength data obtained by Martin and Miller (1974) from tests on 150 mm by 150 mm joint surfaces in moderately weathered greywacke (grade 3, test sample number 7). Barton's empirical criterion (equation 13) was fitted by trial and error, and the dashed curve plotted in figure 10 is defined by ϕ_b' = 20°, JRC = 17, and JCS = 20 MPa.

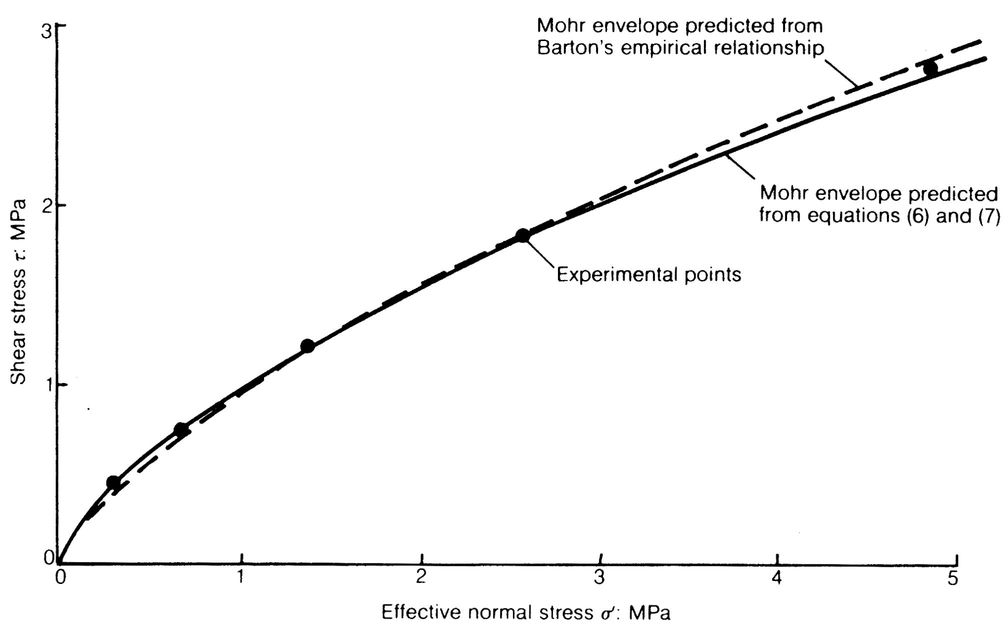

Figure 10 : Results of direct shear tests on moderately weathered greywacke, tested by Martin and Miller (1974), compared with empirical failure envelopes

Also included in figure 10 is a Mohr envelope defined by equations 6 and 7 in this paper for σ_c = 20 MPa, *m* = 0.58 and *s* = 0 (determined by the method described in appendix 1). It will be seen that this curve is just as good a fit to the experimental data as Barton's curve.

A number of analyses, such as that presented in Figure 10, have convinced the author that equations 6 and 7 provide a reasonably accurate prediction of the shear strength of rough discontinuities in rock under a wide range of effective normal stress conditions. This fact is useful in the study of schistose and jointed rock mass strength which follows.

Strength of schistose rock

In the earlier part of these notes, the discussion on the strength of intact rock was based upon the assumption that the rock was isotropic, i.e. its strength was the same in all directions. A common problem encountered in rock mechanics involves the determination of the strength of schistose or layered rocks such as slates or shales.

If it is assumed that the shear strength of the discontinuity surfaces in such rocks is defined by an instantaneous friction angle ϕ_i' and an instantaneous cohesion c_i' (see figure 3), then the axial strength σ_1' of a triaxial specimen containing inclined discontinuities is given by the following equation (see Jaeger and Cook (1969), pages 65 to 68):

$$\sigma_1' = \sigma_3' + \frac{2(c_i' + \sigma_3' \, Tan\,\phi_i')}{(1 - Tan\,\phi_i' Tan\,\beta)\, Sin\, 2\beta} \tag{14}$$

where σ_3' is the minimum principal stress or confining pressure,

and β is the inclination of the discontinuity surfaces to the direction of the major principal stress σ_1 as shown in figure 11a.

Equation 14 can only be solved for values of β within about 25º of the friction angle ϕ'. Very small values of β will give very high values for σ_1', while values of β close to 90º will give negative (and hence meaningless) values for σ_1'. The physical significance of these results is that slip on the discontinuity surfaces is not possible, and failure will occur through the intact material as predicted by equation 3. A typical plot of the axial strength σ_1' versus the angle β is given in figure 11b.

If it is to be assumed that the shear strength of the discontinuity surfaces can be defined by equations 6 and 7, as discussed in the previous section, then in order to determine the values of ϕ_i' and c_1' for substitution into equation 14, the effective normal stress σ' acting across the discontinuity must be known. This is found from:

$$\sigma' = \frac{1}{2}(\sigma_1' + \sigma_3') - \frac{1}{2}(\sigma_1' - \sigma_3')\, Cos\, 2\beta \tag{15}$$

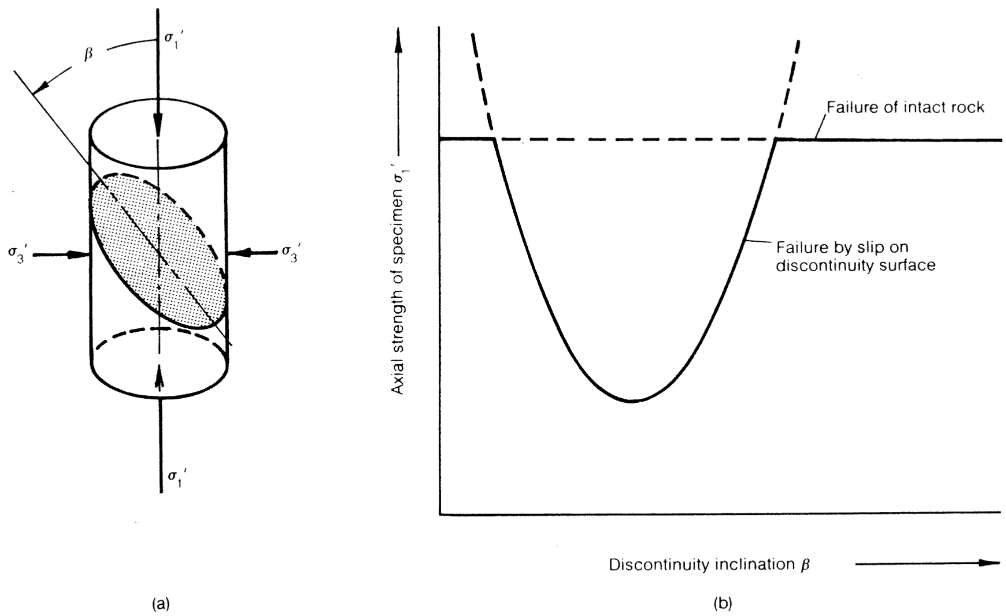

Figure 11 : (a) Configuration of triaxial test specimens containing a pre-existing discontinuity;(b) strength of specimen predicted by means of equations 14 and15.

However, since σ_1' is the strength to be determined, the following iterative process can be used:

a) Calculate the strength σ_{1i}' of the intact material by means of equation 3, using the appropriate values of σ_c, *m* and *s*.
b) Determine values of m_j and s_j for the joint (discontinuity) surfaces from direct shear or triaxial test data. Note that the value of σ_c, the unconfined compressive strength, is the same for the intact material and the discontinuity surfaces in this analysis.
c) Use the value σ_{1i}', calculated in step 1, to obtain the first estimate of the effective normal stress σ' from equation 15.
d) Calculate τ, ϕ_i' and c_i' from equations 7, 6 and 8, using the value of m_j and s_j from step *b*, and the value of σ' from step *c*.
e) Calculate the axial strength σ_{1j}' from equation 14.
f) If σ_{1j}' is negative or greater than σ_{1i}', the failure of the intact material occurs in preference to slip on the discontinuity, and the strength of the specimen is defined by equation 3.
g) If σ_{1j}' is less than σ_{1i}' then failure occurs as a result of slip on the discontinuity. In this case, return to step *c* and use the axial strength calculated in step 5 to calculate a new value for the effective normal stress σ'.
h) Continue this iteration until the difference between successive values of σ_{1j}' in step *e* is less than 1%. It will be found that only three or four iterations are required to achieve this level of accuracy.

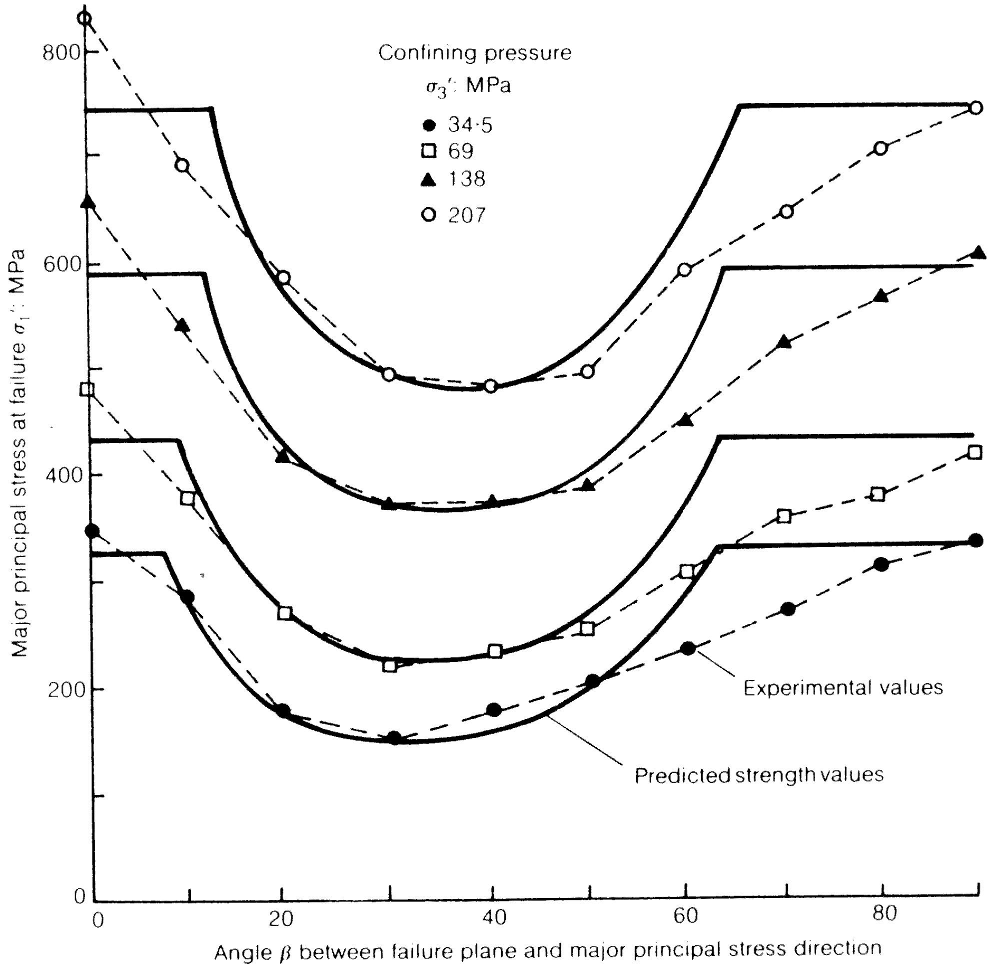

Figure 12 : Triaxial test results for slate with different failure plane inclinations, obtained by McLamore and Gray (1967), compared with strength predictions from equations 3 and 14.

Examples of the analysis described above are given in figures 12 and 13.

The results of triaxial tests on slate tested by McLamore and Gray (1967) for a range of confining pressures and cleavage orientations are plotted in figure 12. The solid curves have been calculated, using the method outlined above, for $\sigma_c = 217$ MPa (unconfined strength of intact rock), $m = 5.25$ and $s = 1.00$ (constants for intact rock), and $m_j = 1.66$ and $s_j = 0.006$ (constants for discontinuity surfaces).

The values of the constants m_j and s_j for the discontinuity surfaces were determined by statistical analysis of the minimum axial strength values, using the procedure for broken rock, described in Appendix 1.

A similar analysis is presented in figure 13, which gives results from triaxial tests on sandstone by Horino and Ellikson (1970). In this case the discontinuity surfaces were created by intentionally fracturing intact sandstone in order to obtain very rough fresh surfaces. The constants used in plotting the solid curves in figure 13 were σ_c = 177.7 MPa (intact rock strength), m = 22.87 and s = 1.00 (constants for intact rock), m_j = 4.07 and s_j = 0 (constants for induced fracture planes).

The rougher failure surfaces in the sandstone, as compared with the slate (compare values of m_j), give more sudden changes in axial strength with discontinuity inclination. In both of these cases, and in a number of other examples analyzed, the agreement between measured and predicted strengths is adequate for most practical design purposes.

An example of the application of the analysis of anisotropic failure, presented on the preceding pages, is given later. This example involves the determination of the stress distribution and potential failure zones in highly stressed schistose rock surrounding a tunnel.

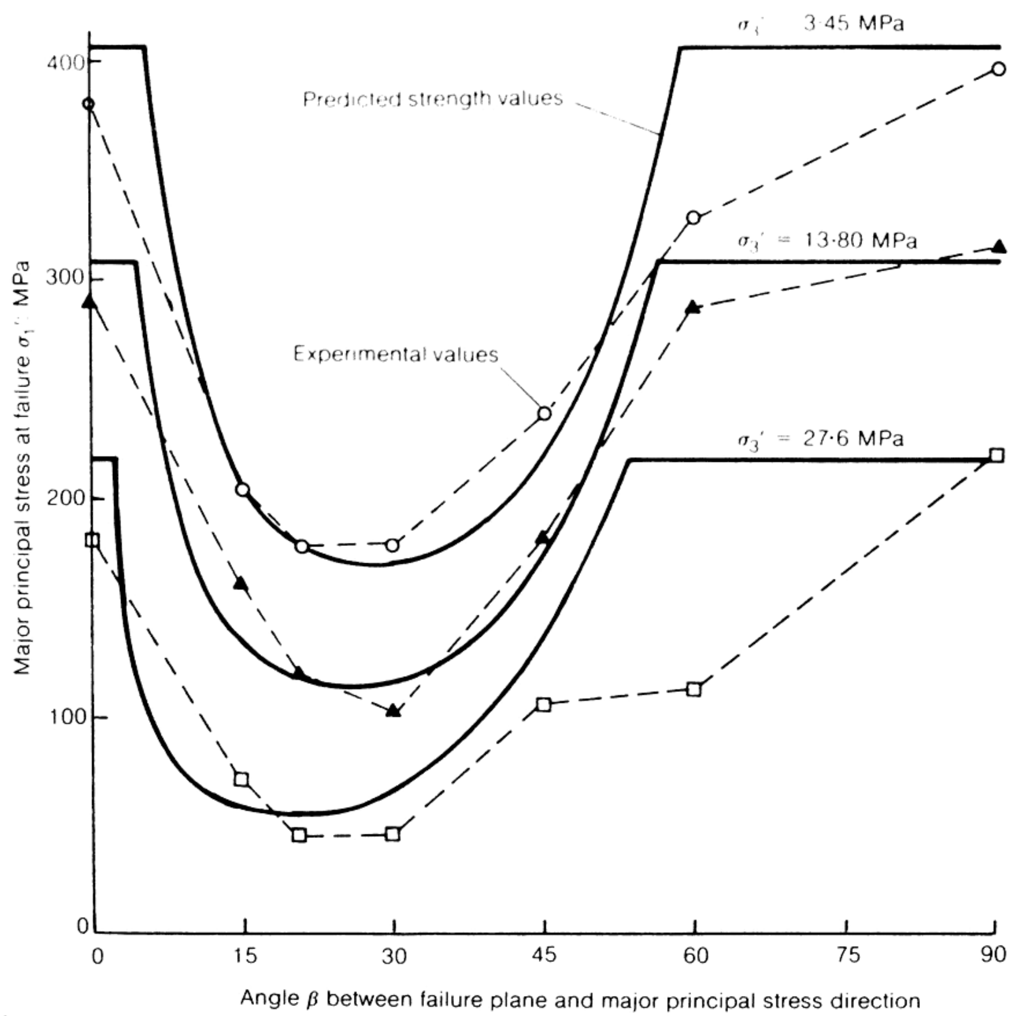

Figure 13 : Triaxial test results for fractured sandstone, tested by Horino and Ellikson (1970), compared with predicted anisotropic strength

Failure of jointed rock masses

Having studied the strength of intact rock and of discontinuities in rock, the next logical step is to attempt to predict the behaviour of a jointed rock mass containing several sets of discontinuities. The simplest approach to this problem is to superimpose a number of analyses for individual discontinuity sets, such as those presented in figures 12 and 13, in the hope that the overall behaviour pattern obtained would be representative of the behaviour of an actual jointed rock mass.

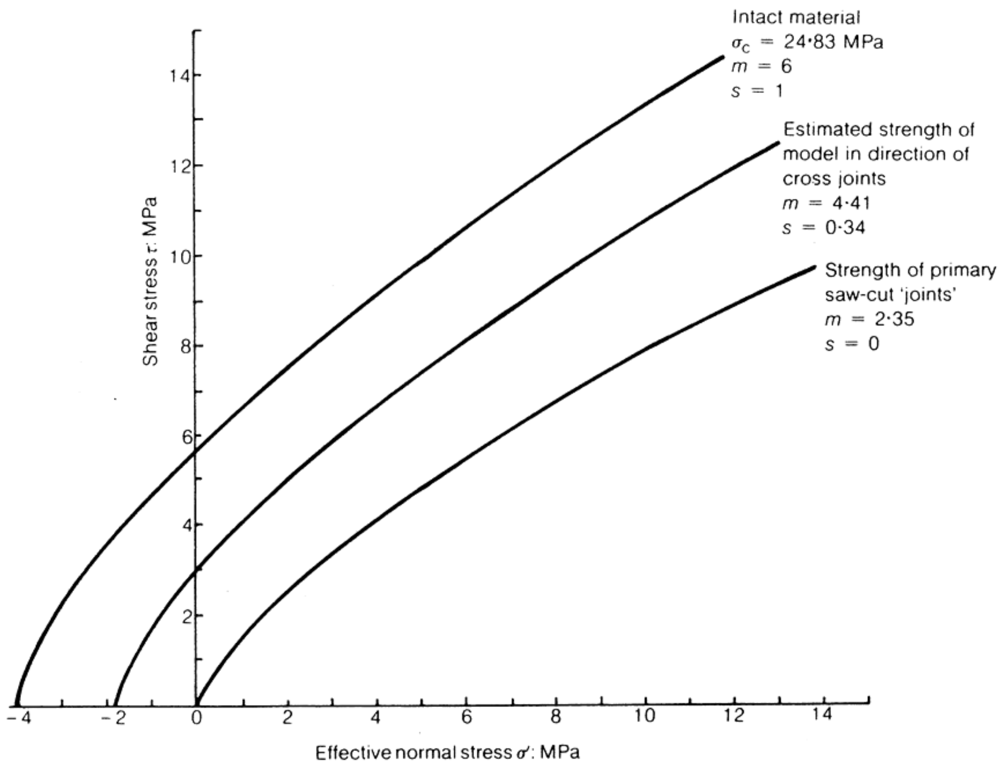

Figure 14 : Mohr failure envelopes for brickwall model tested by Ladanyi and Archambault (1972)

Verification of the results of such predictions presents very complex experimental problems, and many research workers have resorted to the use of physical models in an attempt to minimize these experimental difficulties. Lama and Vutukuri (1978) have presented a useful summary of the results of model studies carried out by John (1962), Muller and Packer (1965), Lajtai (1967), Einstein et al (1969), Ladanyi and Archambault (1970, 1972), Brown (1970), Brown and Trollope (1970), Walker (1971) and others. One of these studies, published by Ladanyi and Archambault (1972), will be considered here.

Ladanyi and Archambault constructed models from rods, with a square cross-section of 12.7 mm and a length of 63.5 mm, which had been sawn from commercial compressed concrete bricks. The Mohr failure envelopes for the intact concrete material and for the sawn 'joints' in the model are given in figure 14. These curves were derived by statistical analysis of raw test data supplied to the author by Professor B. Ladanyi.

One of the model configurations used by Ladanyi and Archambault (1972) is illustrated in figure 15. As will be seen from this drawing, failure of the model in the direction of the 'cross joints' (inclined at an angle α to the major principal stress direction) would involve fracture of intact material as well as sliding on the joints. A crude first approximation of the model strength in the α direction is obtained by simple averaging of the Mohr failure envelopes for the intact material and the through-going joints. The resulting strength estimate is plotted as a Mohr envelope in figure 14.

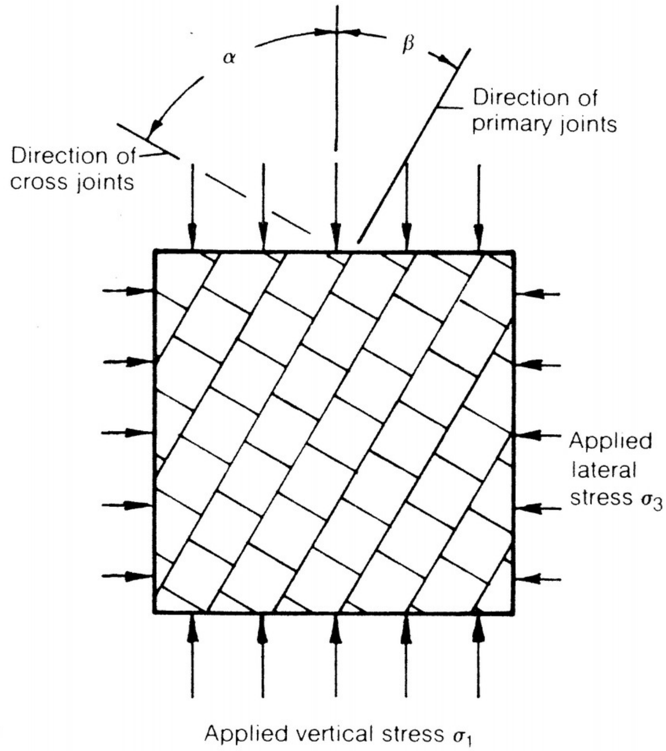

Figure 15 : Configuration of brickwall model tested by Ladanyi and Archambault (1972)

The predicted strength behaviour of Ladanyi and Archambault's 'brickwall' model, for different joint orientations and lateral stress levels, is given in figure 16a. These curves have been calculated, from the strength values given in figure 14, by means of equations 14, 15 and 3, as discussed in the previous section. The actual strength values measured by Ladanyi and Archambault are plotted in figure 16b. Comparison between these two figures leads to the following conclusions:

1. There is an overall similarity between predicted and observed strength behaviour which suggests that the approach adopted in deriving the curves plotted in figure 16a is not entirely inappropriate.

2. The observed strengths are generally lower than the predicted strengths. The intact material strength is not achieved, even at the most favourable joint

orientations. The sharply defined transitions between different failure modes, predicted in figure 16a, are smoothed out by rotation and crushing of individual blocks. This behaviour is illustrated in the series of photographs reproduced in figure 17. In particular, the formation of 'kink bands', as illustrated in figure 17c, imparts a great deal of mobility to the model and results in a significant strength reduction in the zone defined by15° > α > 45°, as shown in figure 16b.

3. Intuitive reasoning suggests that the degree of interlocking of the model blocks is of major significance in the behaviour of the model since this will control the freedom of the blocks to rotate. In other words, the freedom of a rock mass to dilate will depend upon the interlocking of individual pieces of rock which, in turn, will depend upon the particle shape and degree of disturbance to which the mass has been subjected. This reasoning is supported by experience in strength determination of rock fill where particle strength and shape, particle size distribution and degree of compaction are all important factors in the overall strength behaviour.

4. Extension of the principle of strength prediction used in deriving the curves presented in figure 16a to rock masses containing thee, four or five sets of discontinuities, suggests that the behaviour of such rock masses would approximate to that of a homogeneous isotropic system. In practical terms, this means that, for most rock masses containing a number of joint sets with similar strength characteristics, the overall strength behaviour will be similar to that of a very tightly interlocking rock fill.

The importance of the degree of interlocking between particles in a homogeneous rock mass can be illustrated by considering the results of an ingenious experiment carried out by Rosengren and Jaeger (1968), and repeated by Gerogiannopoulis (1979). By heating specimens of coarse grained marble to about 600ºC, the cementing material between grains is fractured by different thermal expansion of the grains themselves. The material produced by this process is a very low porosity assemblage of extremely tightly interlocking but independent grains. This 'granulated' marble was tested by Rosengren and Jaeger (1969) and Gerogiannopoulis (1979) in an attempt to simulate the behaviour of an undisturbed jointed rock mass.

The results obtained by Gerogiannopoulis from triaxial tests on both intact and granulated Carrara marble are plotted in figure 18. In order to avoid confusion, Mohr failure circles for the granulated material only are included in this figure. However, statistical analyses of the data sets for both intact and granulated material to obtain σ_c, m and s values gave correlation coefficients in excess of 90%.

Figure 18 shows that the strength difference between intact material and a very tightly interlocking assemblage of particles of the same material is relatively small. It is unlikely that this degree of interlocking would exist in an in situ rock mass, except in very massive rock at considerable depth below surface. Consequently, the Mohr failure envelope for granulated marble, presented in figure 18, represents the absolute upper bound for jointed rock mass strength.

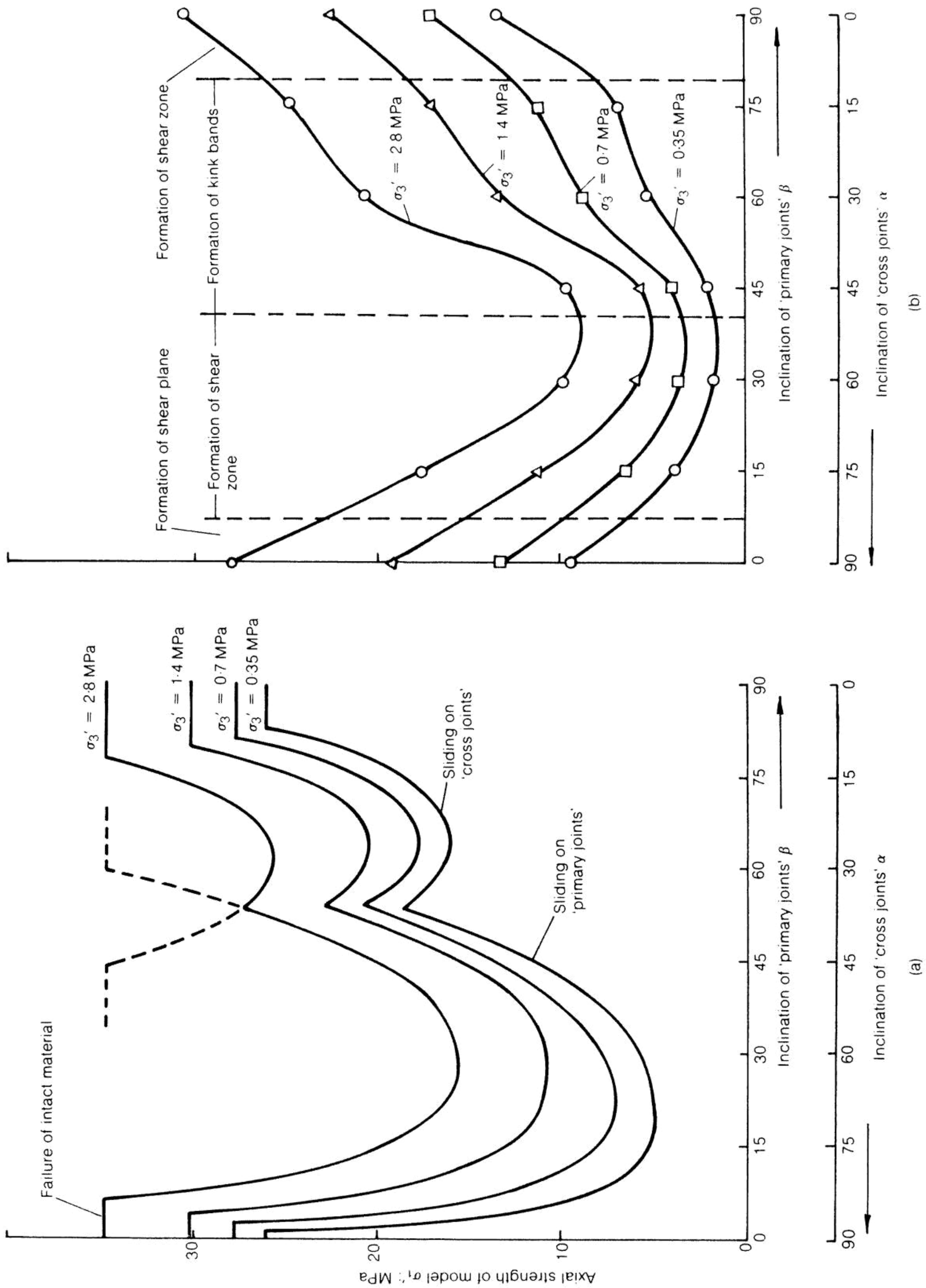

Figure 16. Comparison between a) predicted and b) observed strength of brickwall model tested by Ladanyi & Archambault (1972).

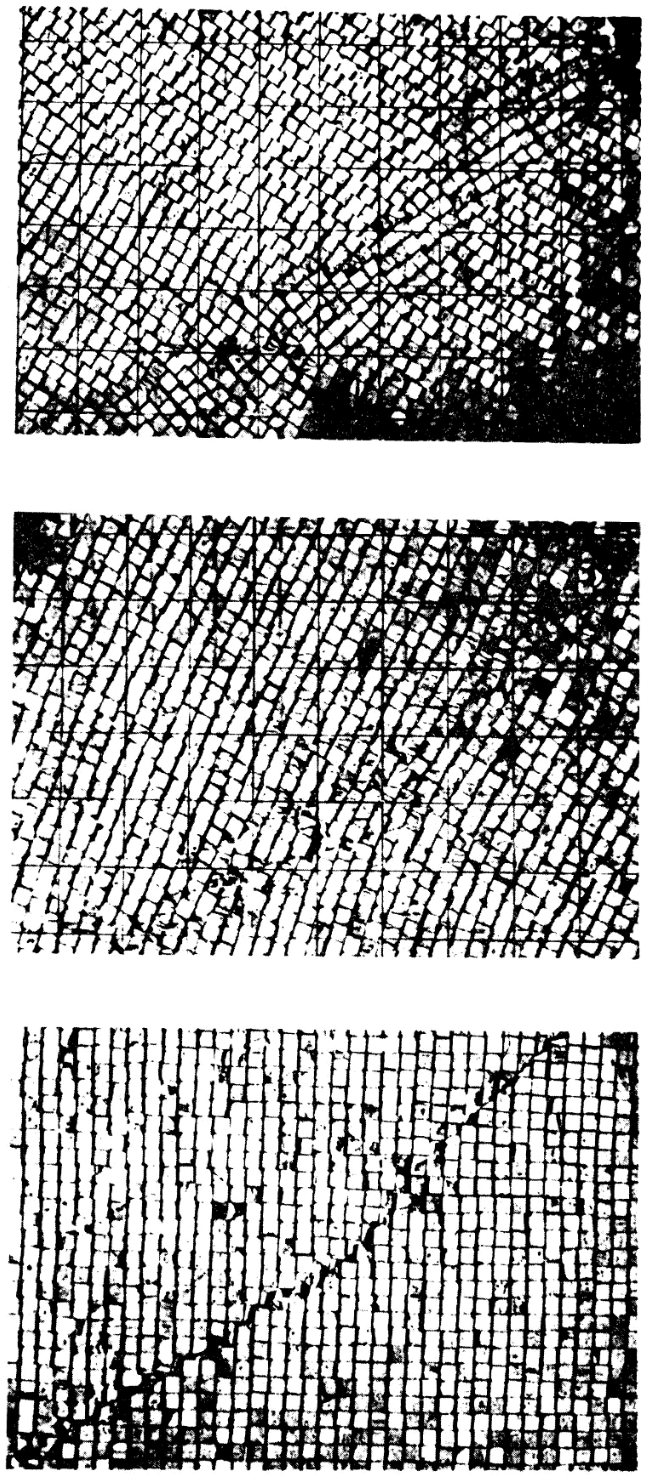

Figure 17. (a) Shear plane failure; (b) shear zone failure; and (c) kink band failure observed in concreate brick models tested by Ladanyi & Archambault (1972). Photograph reproduced with the permission of Professor B. Ladanyi.

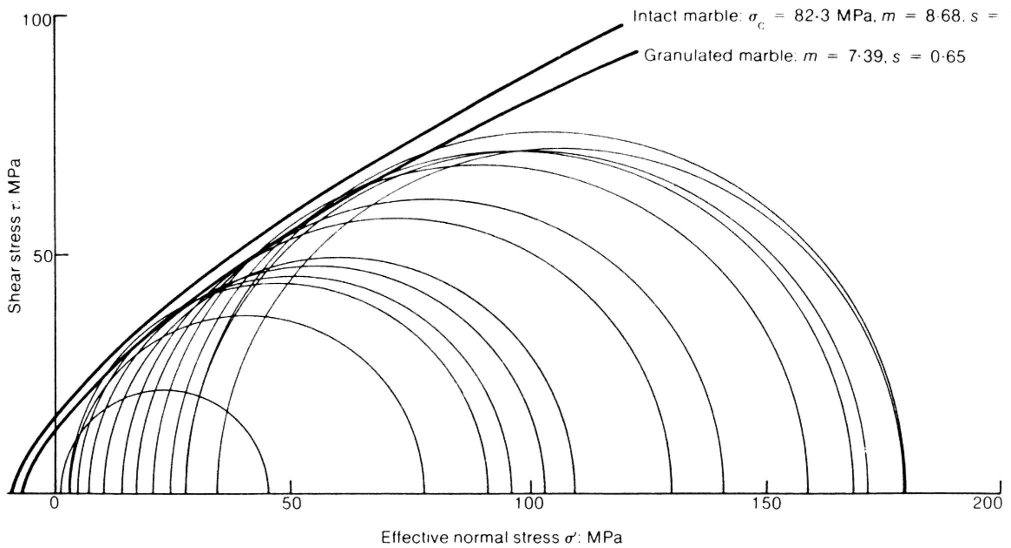

Figure 18 : Comparison between the strength of intact and granulated Carrara marble tested by Gerogiannopoulos (1979).

A more realistic assessment of the strength of heavily jointed rock masses can be made on the basis of triaxial test data obtained in connection with the design of the slopes for the Bougainville open pit copper mine in Papua New Guinea. The results of some of these tests, carried out by Jaeger (1970), the Snowy Mountain Engineering Corporation and in mine laboratories, have been summarized by Hoek and Brown (1980a).

The results of tests on Panguna Andesite are plotted as Mohr envelopes in figure 19. Figure 19a has been included to show the large strength difference between the intact material and the jointed rock mass. Figure 19b is a 100X enlargement of the low stress portion of figure 19a, and gives details of the test results on the jointed material. Details of the materials tested are given in table 3.

Particular mention must be made of the 'undisturbed' 152 mm diameter core samples of jointed Panguna Andesite tested by Jaeger (1970). These samples were obtained by very careful triple-tube diamond core drilling in an exploration adit in the mine. The samples were shipped to Professor Jaeger's laboratory in Canberra, Australia, in the inner tubes of the core barrels, and then carefully transferred onto thin copper sheets which were soldered to form containers for the specimens. These specimens were rubber sheathed and tested triaxially. This series of tests is, as far as the author is aware, the most reliable set of tests ever carried out on 'undisturbed' jointed rock.

The entire Bougainville testing programme, with which the author has been associated as a consultant since its inception, extended over a ten year period and cost several hundred thousand pounds. This level of effort was justified because of the very large economic and safety considerations involved in designing a final slope of almost 1000 m high for one side of the open pit. Unfortunately, it is seldom possible to justify testing programmes of this magnitude in either mining or civil engineering projects, and hence the results summarized in figure 19 represent a very large proportion of the sum total of all published data on this subject.

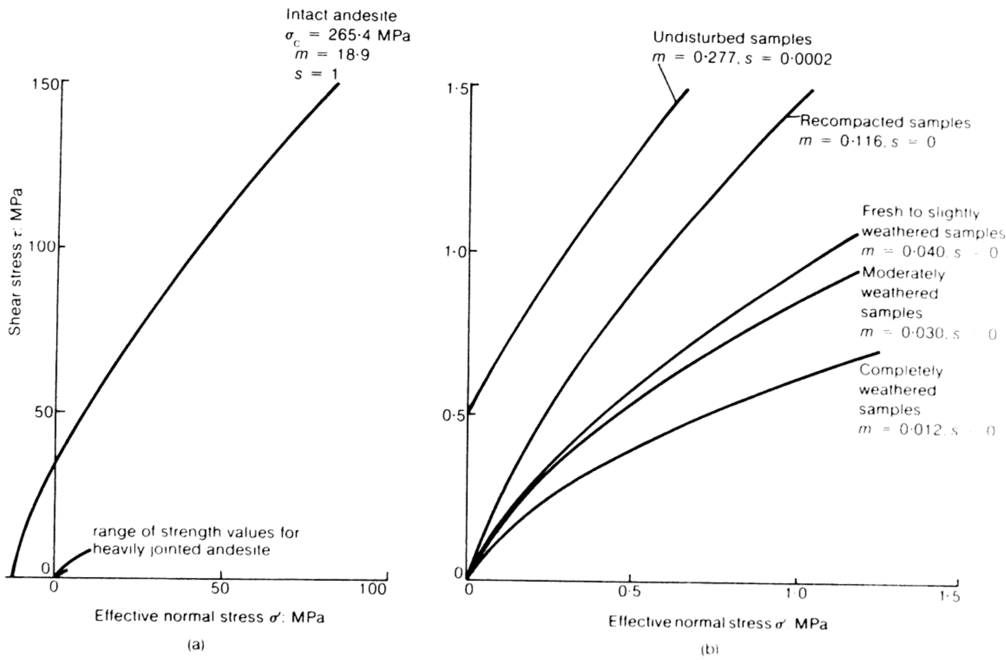

Figure 19 : Mohr failure envelopes for (a) intact and (b) heavily jointed Panguna andesite from Bougainville, Papua New Guinea (see Table 3 for description of materials).

Table 3. Details of matierials and test procedures for Panguna andesite.

Material	Tested by	Sample diameter: mm	Material constants
Intact Panguna andesite	Jaeger (1970) Golder Associates	25 50	$\sigma_c = 265{\cdot}4$ MPa $m = 18{\cdot}9$ $s = 1$ Correlation coefficient 0·85
Undisturbed core samples of heavily jointed andesite obtained by triple-tube diamond core drilling in exploration adit	Jaeger (1970)	152	$m = 0{\cdot}277$ $s = 0{\cdot}0002$ Correlation coefficient 0·99
Recompacted sample of heavily jointed andesite collected from mine benches (equivalent to compacted fresh rock-fill)	Bougainville Copper	152	$m = 0{\cdot}116$ $s = 0$
Fresh to slightly weathered andesite, lightly recompacted	Snowy Mountains Engineering Corporation	570	$m = 0{\cdot}040$ $s = 0$
Moderately weathered andesite, lightly recompacted	Snowy Mountains Engineering Corporation	570	$m = 0{\cdot}030$ $s = 0$
Completely weathered andesite (equivalent to poor quality waste rock)	Snowy Mountains Engineering Corporation	570	$m = 0{\cdot}012$ $s = 0$

A similar, although less ambitious, series of tests was carried out on a highly fractured greywacke sandstone by Raphael and Goodman (1979). The results of these tests, plotted in figure 20, show a much lower reduction from intact to jointed rock mass strength than for the Panguna Andesite (figure 19). This is presumably because the intact sandstone tested by Raphael and Goodman is significantly weaker than the andesite tested by Jaeger, and hence there is less possibility of the block rotation mechanism (see figure 17c) which appears to contribute so much to the weakness of jointed systems in strong materials. The author freely admits that this suggestion is highly speculative, and is based upon intuitive reasoning rather than experimental facts.

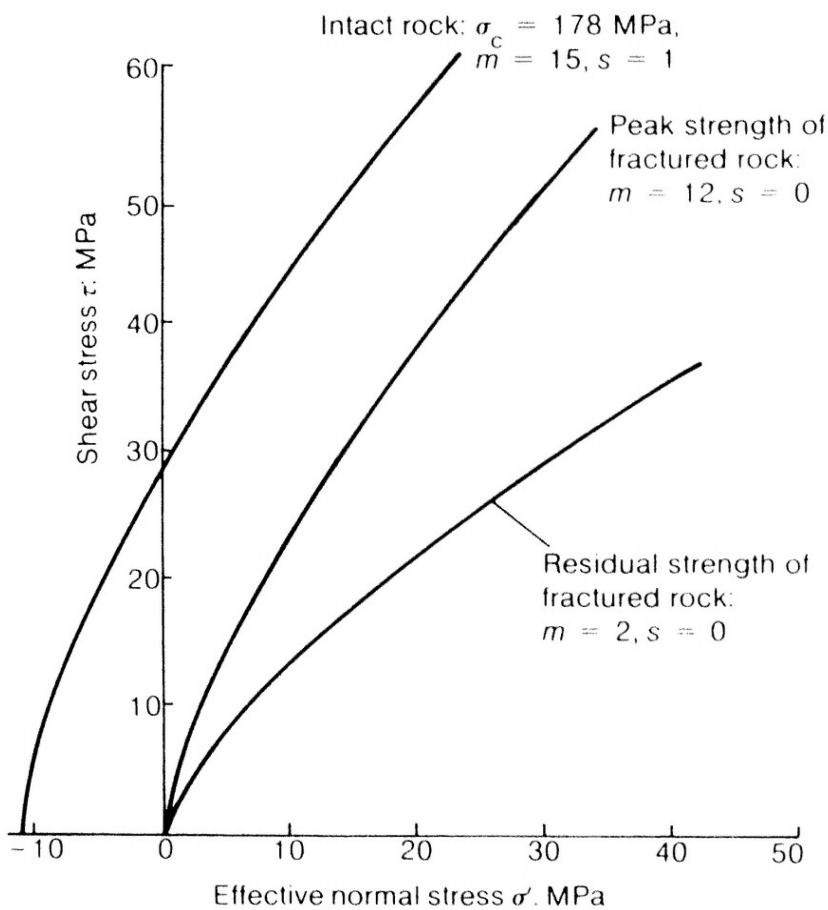

Figure 20 : Mohr failure envelopes estimated from plotted triaxial test data (Raphael and Goodman, 1979) for highly fractured, fresh to slightly altered greywacke sandstone.

Estimating the strength of jointed rock

Based on their analyses of the results from tests on models, jointed rock masses and rock fill, Hoek and Brown (1980b) proposed an approximate method for estimating the strength of jointed rock masses. This method, summarized in Table 4, involves estimating the values of the empirical constants *m* and *s* from a description of the rock mass. These estimates, together with an estimate of the uniaxial compressive strength of the intact pieces of rock, can then be used to construct an approximate Mohr failure envelope for the jointed rock mass.

As a means of assisting the user in describing the rock mass, use is made of the rock mass classification systems proposed by Bieniawski (1974) and Barton et al (1974). Space does not permit a review of these classification systems, and hence the reader is referred to the original papers or to the extensive summary published by Hoek and Brown (1980a).

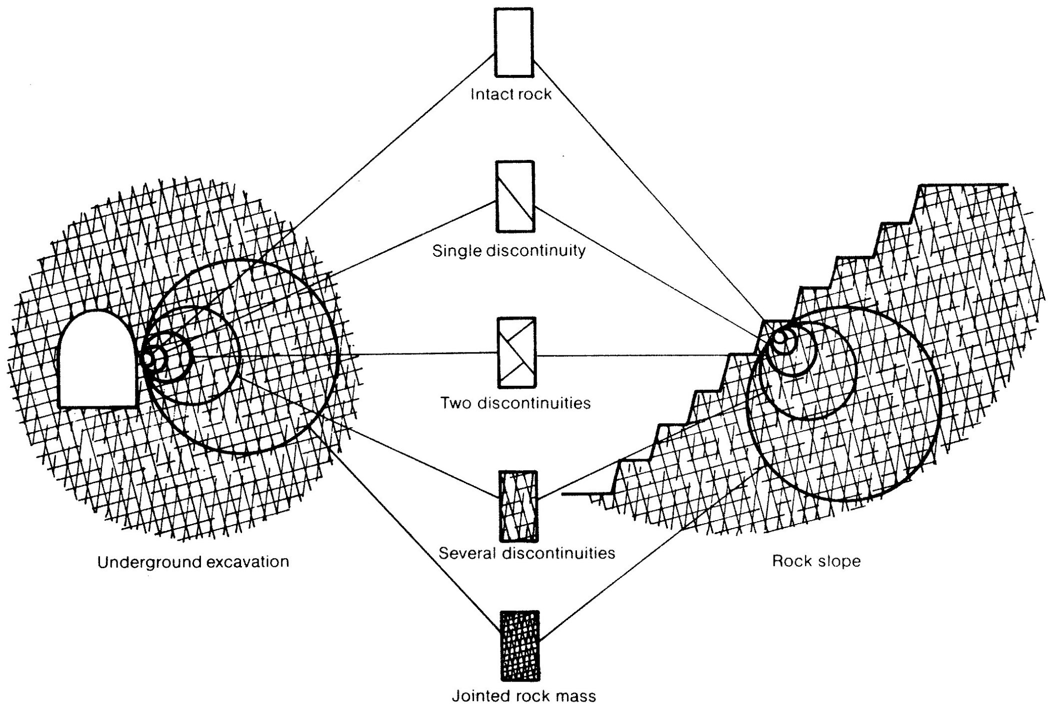

Figure 21 : Simplified representation of the influence of scale on the type of rock mass behaviour model which should be used in designing underground excavations or rock slopes.

The author's experience in using the values listed in Table 4 for practical engineering design suggests that they are somewhat conservative. In other words, the actual rock mass strength is higher than that estimated from the Mohr envelopes plotted from the values listed. It is very difficult to estimate the extent to which the predicted strengths are too low, since reliable field data are almost non-existent. However, based on comparisons between observed and predicted behaviour of rock slopes and underground excavations, the author tends to regard the strength estimates made from Table 4 as lower bound values for design purposes. (For further discussion on this question, see the addendum at the end of this paper). Obviously, in designing an important structure, the user would be well advised to obtain his own test data before deciding to use strength values significantly higher than those given in Table 4.

Table 4. Approximate relationship between rock mass quality and material constants.

Empirical failure criterion $\sigma_1' = \sigma_3' + (m\sigma_c\sigma_3' + s\sigma_c^2)^{1/2}$ σ_1' = major principal stress σ_3' = minor principal stress σ_c = uniaxial compressive strength of intact rock m, s = empirical constants		Carbonate rocks with well developed crystal cleavage, e.g. dolomite, limestone and marble	Lithified argillaceous rocks, e.g. mudstone, siltstone, shale and slate (tested normal to cleavage)	Arenaceous rocks with strong crystals and poorly developed crystal cleavage, e.g. sandstone and quartzite	Fine grained polymineralic igneous crystalline rocks, e.g. andesite, dolerite, diabase and rhyolite	Coarse grained polymineralic igneous and metamorphic crystalline rocks, e.g. amphibolite, gabbro, gneiss, granite, norite and quartzdiorite
Intact rock samples Laboratory size samples free from pre-existing fractures Bieniawski, 1974b (CSIR)* rating Barton *et al.*, 1974 (NGI)† rating	 100 500	$m = 7$ $s = 1$	$m = 10$ $s = 1$	$m = 15$ $s = 1$	$m = 17$ $s = 1$	$m = 25$ $s = 1$
Very good quality rock mass Tightly interlocking undisturbed rock with rough unweathered joints spaced at 1 to 3 m Bieniawski, 1974b (CSIR) rating Barton *et al.*, 1974 (NGI) rating	 85 100	$m = 3{\cdot}5$ $s = 0{\cdot}1$	$m = 5$ $s = 0{\cdot}1$	$m = 7{\cdot}5$ $s = 0{\cdot}1$	$m = 8{\cdot}5$ $s = 0{\cdot}1$	$m = 12{\cdot}5$ $s = 0{\cdot}1$
Good quality rock mass Fresh to slightly weathered rock, slightly disturbed with joints spaced at 1 to 3 m Bieniawski, 1974b (CSIR) rating Barton *et al.*, 1974 (NGI) rating	 65 10	$m = 0{\cdot}7$ $s = 0{\cdot}004$	$m = 1$ $s = 0{\cdot}004$	$m = 1{\cdot}5$ $s = 0{\cdot}004$	$m = 1{\cdot}7$ $s = 0{\cdot}004$	$m = 2{\cdot}5$ $s = 0{\cdot}004$
Fair quality rock mass Several sets of moderately weathered joints spaced at 0·3 to 1 m, disturbed Bieniawski, 1974b (CSIR) rating Barton *et al.*, 1974 (NGI) rating	 44 1	$m = 0{\cdot}14$ $s = 0{\cdot}0001$	$m = 0{\cdot}20$ $s = 0{\cdot}0001$	$m = 0{\cdot}30$ $s = 0{\cdot}0001$	$m = 0{\cdot}34$ $s = 0{\cdot}0001$	$m = 0{\cdot}50$ $s = 0{\cdot}0001$
Poor quality rock mass Numerous weathered joints at 30 to 500 mm with some gouge. Clean, compacted rockfill Bieniawski, 1974b (CSIR) rating Barton *et al.*, 1974 (NGI) rating	 23 0·1	$m = 0{\cdot}04$ $s = 0{\cdot}00001$	$m = 0{\cdot}05$ $s = 0{\cdot}00001$	$m = 0{\cdot}08$ $s = 0{\cdot}00001$	$m = 0{\cdot}09$ $s = 0{\cdot}00001$	$m = 0{\cdot}13$ $s = 0{\cdot}00001$
Very poor quality rock mass Numerous heavily weathered joints spaced at 50 mm with gouge. Waste rock Bieniawski, 1974b (CSIR) rating Barton *et al.*, 1974 (NGI) rating	 3 0·01	$m = 0{\cdot}007$ $s = 0$	$m = 0{\cdot}010$ $s = 0$	$m = 0{\cdot}015$ $s = 0$	$m = 0{\cdot}017$ $s = 0$	$m = 0{\cdot}025$ $s = 0$

* CSIR Commonwealth Scientific and Industrial Research Organization.
† NGI Norway Geotechnical Institute.

In order to use table 4 to make estimates of rock mass strength, the following steps are suggested :

(a) From a geological description of the rock mass, and from a comparison between the size of the structure being designed and the spacing of discontinuities in the rock mass (see figure 21), decide which type of material behaviour model is most appropriate. The values listed in table 4 should only be used for estimating the strength of intact rock or of heavily jointed rock masses containing several sets of discontinuities of similar type. For schistose rock or for jointed rock masses containing dominant discontinuities such as faults, the behaviour will be anisotropic and the strength should be dealt with in the manner described in example 1.

(b) Estimate the unconfined compressive strength σ_c of the intact rock pieces from laboratory test data, index values or descriptions of rock hardness (see Hoek and Bray (1981) or Hoek and Brown (1980a)). This strength estimate is important since it establishes the scale of the Mohr failure envelope.

(c) From a description of the rock mass or, preferably, from a rock mass classification using Barton et al (1974) or Bieniawski's (1974) system, determine the appropriate row and column in table 4, or calculate m and s values from equations 17 to 20.

(d) Using equations 6 and 7, calculate and plot a Mohr failure envelope for the estimated values of σ_c, m and s. Draw an approximate average Mohr Coulomb linear envelope through the plotted points, and estimate the average friction angle and cohesive strength of the rock mass. Compare these values with published data for rock fill (Marachi, Chan and Seed (1972); Marsal (1967, 1973); Charles and Watts (1980)) or with data given in this paper to ensure that the values are reasonable.

(e) Use the estimated strength values for preliminary design purposes and carry out sensitivity studies by varying the values of m and s to determine the importance of rock mass strength in the design.

(f) For critical designs which are found to be very sensitive to variations in rock mass strength, establish a site investigation and laboratory testing programme aimed at refining the strength estimates made on the basis of the procedure outlined in the preceding steps.

Examples of application of rock mass strength estimates in engineering design

In order to illustrate the application of the empirical failure criterion presented to practical engineering design problems, three examples are given. These examples have been carefully chosen to illustrate particular points and, although all of the examples are hypothetical, they are based upon actual engineering problems studied by the author.

Example 1

Figure 22 gives a set of contours of the ratio of available strength to induced stress in a schistose gneiss rock mass surrounding a tunnel. The following assumptions were made in calculating these ratios.

The vertical in situ stress in the rock surrounding the tunnel is 40 MPa, corresponding to a depth below surface of about 1500m. The horizontal in situ stress is 60 MPa or 1.5 times the vertical stress.

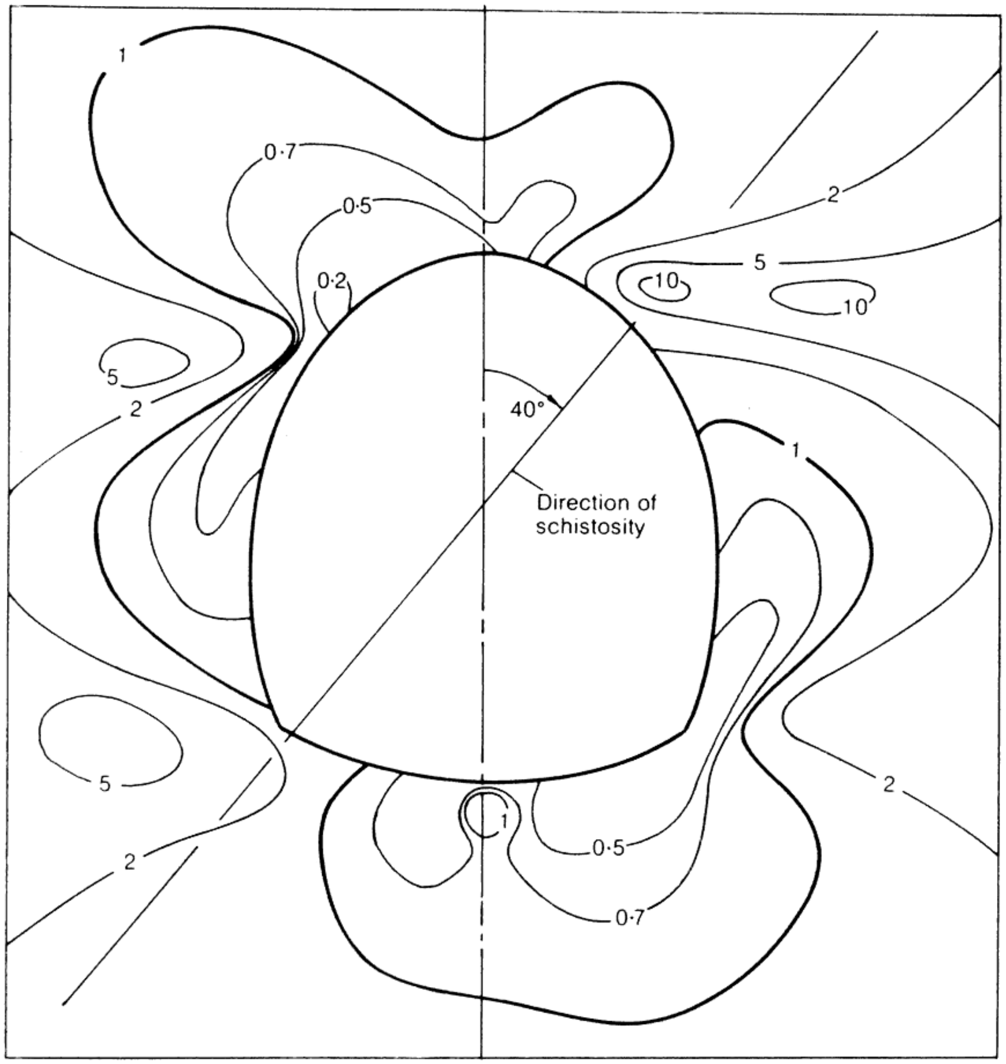

Figure 22 : Contours of ratio of available strength to stress in schistose rock surrounding a highly stressed tunnel.

The rock strength is defined by the following constants: uniaxial compressive strength of intact rock σ_c = 150 MPa, material constants for the isotropic rock mass: m_i = 12.5, s_i = 0.1, material constants for joint strength in the direction of schistosity: m_j = 0.28, s_j = 0.0001.

The direction of schistosity is assumed to be at 40º (measured in a clockwise direction) to the vertical axis of the tunnel.

The rock mass surrounding the tunnel is assumed to be elastic and isotropic. This assumption is generally accurate enough for most practical purposes, provided that the ratio of elastic moduli parallel to and normal to schistosity does not exceed three. In the case of the example illustrated in figure 22, the stress distribution was calculated by means of the two-dimensional boundary element stress analysis technique, using the programming listing published by Hoek and Brown (1980a). A modulus of elasticity of E = 70 GPa and a Poisson's ratio of ν = 0.25 were assumed for this analysis.

The shear and normal stresses τ and σ', acting on a plane inclined at 40º (clockwise) to the vertical axis, were calculated for each point on a grid surrounding the tunnel. The available shear strengths in the direction of this plane, τ_{as} , were calculated by means of equations 7 and 6 for σ_c = 150 MPa, m_j = 0.28 and s_j = 0.0001. Hence, the ratio of available shear strength τ_{as} to the induced shear stress τ was determined for each grid point.

In addition, the available strength σ'_{ai} of the isotropic rock mass was calculated for each grid point by means of equation 3, using the principal stresses σ'_1 and σ'_3 and the isotropic rock mass material properties (σ_c = 150 MPa, m_i = 12.5 and s_i = 0.1). This available strength σ'_{ai} was compared with the induced maximum principal stress σ'_1 to obtain the ratio σ'_{ai} / σ'_1 at each grid point.

In plotting the contours illustrated in figure 22, the lower of the two ratios τ_{as} / τ and σ'_{ai} / σ'_1 was used to define the strength to stress ratio value.

The zones surrounded by the contours defined by a strength to stress ratio of one contain overstressed rock. The general method used in designing tunnels and caverns in highly stressed rock is to attempt to minimize the extent of such overstressed zones by choice of the excavation shape and orientation in relation to the in situ stress direction.

When zones of overstressed rock, such as those illustrated in figure 22, are unavoidable, appropriate support systems have to be designed in order to restrict the propagation of fracture of rock contained in these zones. Unfortunately, the analysis presented in this example cannot be used to predict the extent and direction of fracture propagation from the zones of overstressed rock and the choice of support systems tends to be based upon very crude approximations.

Such approximations involve designing a system of rockbolts with sufficient capacity to support the weight of the rock contained in the overhead overstressed zones and of sufficient length to permit anchoring in the rock outside these zones.

Improved techniques for support design are being developed, but are not yet generally available for complex failure patterns such as that illustrated in figure 22. These techniques, discussed by Hoek and Brown (1980a), involve an analysis of the interaction between displacements, induced by fracturing in the rock surrounding the tunnel, and the response of the support system installed to control these displacements. It is hoped that these support-interaction analyses will eventually be developed to the point where they can be used to evaluate the support requirements for tunnels such as that considered in this example.

Example 2

This example involves a study of the stability of a very large rock slope such as that which would be excavated in a open pit mine. The benched profile of such a slope, having an overall angle of about 30º and a vertical height of 400m, is shown in figure 23.

The upper portion of the slope is in overburden material comprising mixed sands, gravels and clays. Back-analysis of previous failures in this overburden material, assuming a linear Mohr failure envelope, gives a friction angle of $\phi' = 18°$ and a cohesive strength $c' = 0$. The unit weight of this material averages 0.019 MN/m^3.

The overburden is separated from the shale forming the lower part of the slope by a fault which is assumed to have a shear strength defined by $\phi' = 15°$ and $c' = 0$.

No strength data are available for the shale, but examination of the rock exposed in tunnels in this material suggests that the rock mass can be rated as 'good quality'. From Table 4, the material constants $m = 1$ and $s = 0.004$ are chosen as representative of this rock. In order to provide a measure of conservatism in the design, the value of s is downgraded to zero to allow for the influence of stress relaxation which may occur as the slope is excavated. The strength of the intact material is estimated from point load tests (see Hoek and Brown, 1980a) as 30 MPa. The unit weight of the shale is 0.023 MN/m^3.

The phreatic surface in the rock mass forming the slope, shown in figure 23, is estimated from a general knowledge of the hydrogeology of the site and from observations of seepage in tunnels in the slope.

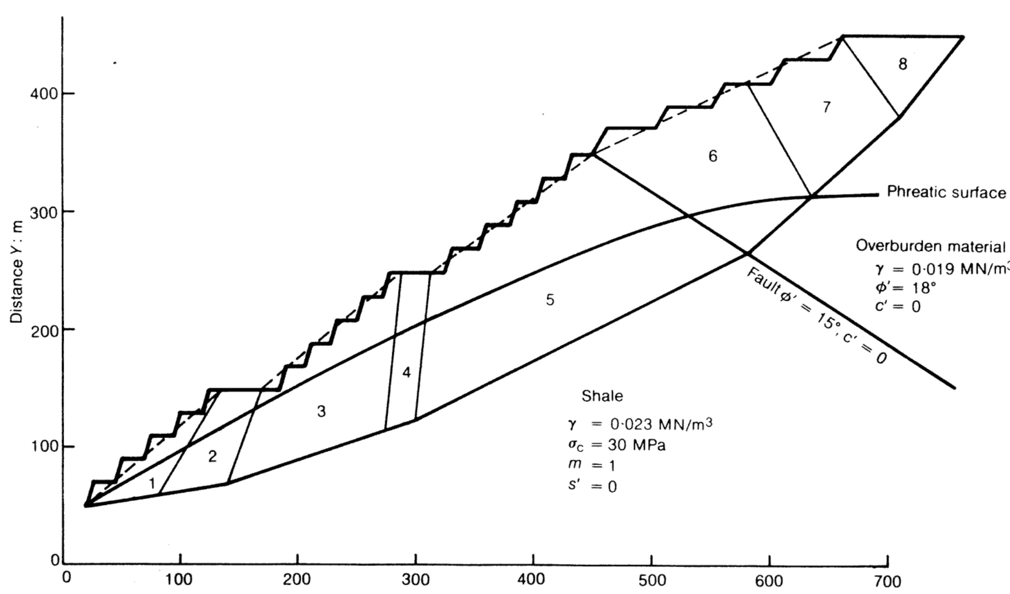

Figure 23 : Rock slope analysed in example 2 (see Table 5 for coordinates of slope profile, phreatic surface and failure surface).

Analysis of the stability of this slope is carried out by means of the non-vertical slice method (Sarma, 1979). This method is ideally suited to many rock slope problems because it permits the incorporation of specific structural features such as the fault illustrated in figure 23.

Sarma's analysis has been slightly modified by this author and programmed for use on a micro-computer (Hoek, 1986).

Table 5: Stability analysis of slope shown in Fig. 23.

Slice	1	2	3	4	5	6	7	8	9
XT	20	135	170	288	312	450	580	660	765
YT	50	150	150	250	250	350	410	450	450
XW	20	106	162	284	308	530	635	710	765
YW	50	100	132	196	210	300	311	380	450
XB	20	82	140	274	300	580	635	710	765
YB	50	60	68	115	123	265	311	380	450
Unit weight γ: MN/m^3	0·023	0·023	0·023	0·023	0·023	0·019	0·019	0·019	Factor of safety
First iteration									
ϕ_B'	30	30	30	30	30	18	18	18	
c_B'	1·0	1·0	1·0	1·0	1·0	0	0	0	
ϕ_S'	0	30	30	30	30	15	18	18	1·69
c_S'	0	1·0	1·0	1·0	1·0	0	0	0	
σ_B'	1·32	0·77	1·40	1·57	1·89	0·58	1·38	0·54	
σ_S'	0	0·09	0·55	0·66	0·75	2·01	1·21	0·52	
Second iteration									
ϕ_B'	40·03	45·08	39·46	38·36	36·58	18	18	18	
c_B'	0·48	0·32	0·51	0·55	0·64	0	0	0	
ϕ_S'	0	62·08	48·11	46·48	45·32	15	18	18	1·57
c_S'	0	0·06	0·25	0·28	0·31	0	0	0	
σ_B'	0·74	1·07	1·31	1·76	1·96	0·57	1·37	0·53	
σ_S'	0	0·16	0·46	0·53	0·62	2·00	1·19	0·51	
Third iteration									
ϕ_B'	45·44	42·02	40·10	37·26	36·23	18	18	18	
c_B'	0·31	0·41	0·48	0·61	0·66	0	0	0	
ϕ_S'	0	58·10	49·67	48·44	47·04	15	18	18	1·57
c_S'	0	0·10	0·21	0·24	0·27	0	0	0	
σ_B'	0·74	1·07	1·31	1·76	1·96	0·57	1·37	0·53	
σ_S'	0	0·15	0·44	0·52	0·61	2·00	1·19	0·51	

Table 5 lists the coordinates of the slope profile (XT, YT), the phreatic surface (XW, YW), and the base or failure surface (YB, YB) which was found, from a number of analyses, to give the lowest factor of safety. As a first approximation, the strength of the shale is assumed to be defined by $\phi' = 30°$ and $c' = 1$ MPa. Analysis of the slope, using these values, gives a factor of safety of 1.69.

The effective normal stresses σ_B' and σ_S' on the slice bases and sides, respectively, are calculated during the course of this analysis and these values are listed, for each slice, in Table 5. These values are used to determine the appropriate values for the instantaneous friction angle ϕ_i' and the instantaneous cohesive strength c_i' for the shale by means of equations 6 and 7 (for σ_c = 30 MPa, m = 1 and s = 0). These values of ϕ_i' and c_i' are used in the second iteration of a stability analysis and, as shown in Table 5, the resulting factor of safety is 1.57.

This process is repeated a third time, using the values of $\phi_i^{'}$ and $c_i^{'}$ calculated from the effective normal stresses given by the second iteration. The factor of safety given by the third iteration is 1.57. An additional iteration, not included in Table 5, gave the same factor of safety and no further iterations were necessary.

This example is typical of the type of analysis which would be carried out during the feasibility or the basic design phase of a large open pit mine or excavation for a dam foundation or spillway. Further analyses of this type would normally be carried out at various stages during excavation of the slope as the rock mass is exposed and more reliable information becomes available. In some cases, a testing programme may be set up to attempt to investigate the properties of materials such as the shale forming the base of the slope shown in figure 23.

Example 3

A problem which frequently arises in both mining and civil engineering projects is that of the stability of waste dumps on sloping foundations. This problem has been studied extensively by the Commonwealth Scientific and Industrial Research Organization in Australia in relation to spoil pile failures in open cast coal mines (see, for example, Coulthard, 1979). These studies have shown that many of these failures involve the same active-passive wedge failure process analysed by Seed and Sultan (1967, 1969) and Horn and Hendron (1968) for the evaluation of dams with sloping clay cores.

In considering similar problems, the author has found that the non-vertical slice method published by Sarma (1979) and Hoek (1986) is well suited to an analysis of this active-passive wedge failure. Identical results to those obtained by Coulthard (1979) are given by assuming a drained spoil pile with a purely frictional shear strength on the interface between the active and passive wedges. However, Sarma's method allows the analysis of a material with non-linear failure characteristics and, if necessary, with ground water pressures in the pile.

The example considered here involves a 75m high spoil pile with a horizontal upper surface and a face angle of 35º. The unit weight of the spoil material is 0.015 MN/m^3. This pile rests on a weak foundation inclined at 12º to the horizontal. The shear strength of the foundation surface is defined by a friction angle of $\phi^{'}$ = 15º and zero cohesion. The pile is assumed to be fully drained.

Triaxial tests on retorted oil shale material forming the spoil pile give the Mohr circles plotted in figure 24. Regression analysis of the triaxial test data, assuming a linear Mohr failure envelope, give $\phi^{'}$ = 29.5º and c' = 0.205 MPa with a correlation coefficient to 1.00. Analysis of the same data, using the 'broken rock' analysis given in appendix 1, for σ_c = 25 MPa (determined by point load testing) gave m = 0.243 and s = 0. Both linear and non-linear Mohr failure envelopes are plotted in figure 24, and both of these envelopes will be used for the analysis of spoil pile stability.

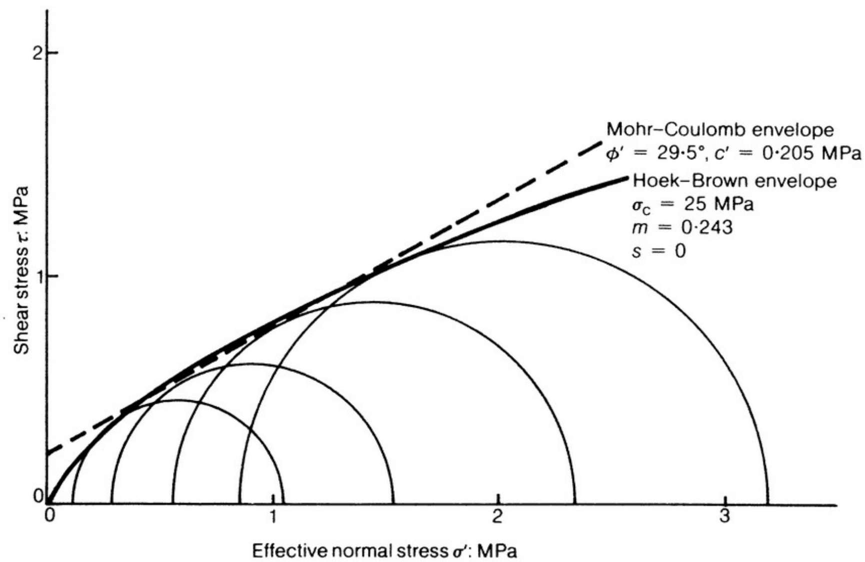

Figure 24 : Mohr circles derived from drained triaxial tests on retorted oil shale waste.

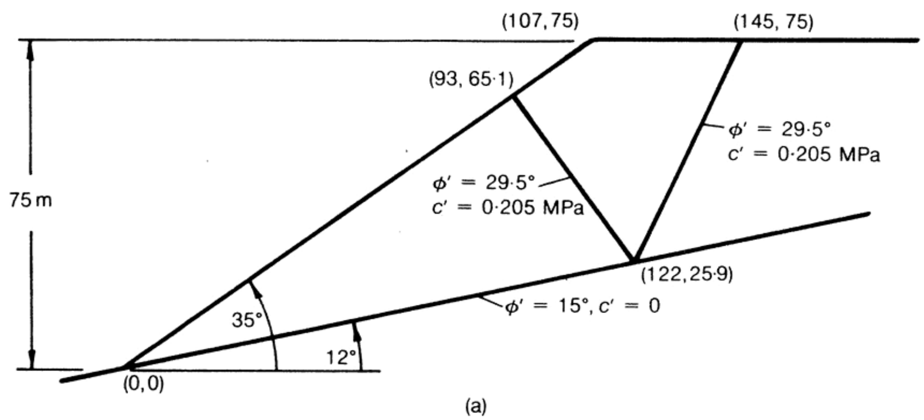

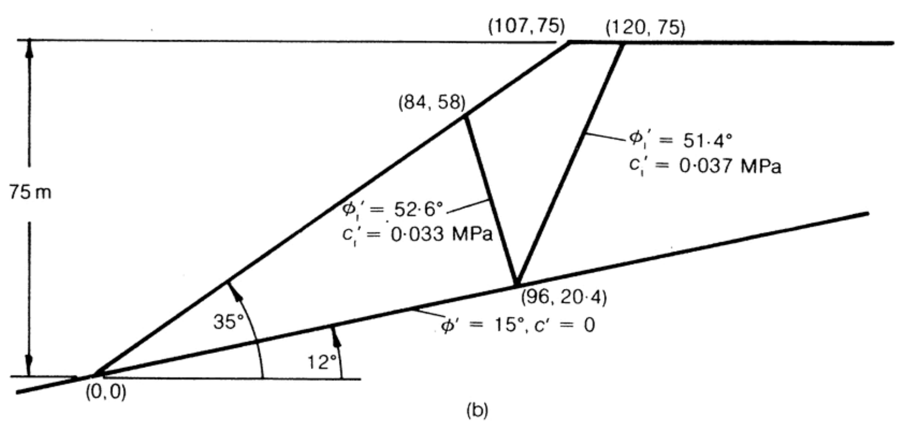

Figure 25 : Analyses of active-passive wedge failure in waste dumps of retorted oil shale resting on weak foundations. (a) Mohr-Coulomb failure criterion, factor of safety = 1.41; (b) Hoek-Brown failure criterion, factor of safety = 1.08

Figure 25 gives the results of stability analyses for the Mohr-Coulomb and Hoek-Brown failure criteria. These analyses were carried out by optimizing the angle of the interface between the active and passive wedge, followed by the angle of the back scarp followed by the distance of the back scarp behind the crest of the spoil pile. In each case, the angles and distances were varied to find the minimum factor of safety in accordance with the procedure suggested by Sarma (1979).

The factor of safety obtained for the Mohr-Coulomb failure criterion ($\phi' = 29.5°$ and $c' = 0.205$) was 1.41, while that obtained for the Hoek-Brown criterion ($\sigma_c = 25$ MPa, $m = 0.243$ and $s = 0$) was 1.08. In studies on the reason for the difference between these two factors of safety, it was found that the normal stresses acting across the interface between the active and passive wedges and on the surface forming the back scarp range from 0.06 to 0.11 MPa. As can be seen from figure 24, this is the normal stress range in which no test data exists and where the linear Mohr-Coulomb failure envelope, fitted to test data at higher normal stress levels, tends to over-estimate the available shear strength.

This example illustrates the importance of carrying out triaxial or direct shear tests at the effective normal stress levels which occur in the actual problem being studied. In the example considered here, it would have been more appropriate to carry out a preliminary stability analysis, based upon assumed parameters, before the testing programme was initiated. In this way, the correct range of normal stresses could have been used in the test. Unfortunately, as frequently happens in the real engineering world, limits of time, budget and available equipment means that it is not always possible to achieve the ideal testing and design sequence.

Conclusion

An empirical failure criterion for estimating the strength of jointed rock masses has been presented. The basis for its derivation, the assumptions made in its development, and its advantages and limitations have all been discussed. Three examples have been given to illustrate the application of this failure criterion in practical geotechnical engineering design.

From this discussion and from some of the questions left unanswered in the examples, it will be evident that a great deal more work remains to be done in this field. A better understanding of the mechanics of jointed rock mass behaviour is a problem of major significance in geotechnical engineering, and it is an understanding to which both the traditional disciplines of soil mechanics and rock mechanics can and must contribute. The author hopes that the ideas presented will contribute towards this understanding and development.

Acknowledgements

The author wishes to acknowledge the encouragement, assistance and guidance provided over many years by Professor E.T. Brown and Dr J.W. Bray of Imperial College. Many of the ideas presented originated from discussions with these colleagues and co-authors.

The simulating and challenging technical environment which is unique to the group of people who make up Golder Associates is also warmly acknowledged. This environment has provided the impetus and encouragement required by this author in searching for realistic solutions to practical engineering problems.

Particular thanks are due to Dr R. Hammett, Dr S. Dunbar, Mr M. Adler, Mr B. Stewart, Miss D. Mazurkewich and Miss S. Kerber for their assistance in the preparation of this paper.

Appendix 1 - Determination of material constants for empirical failure criterion.

Failure criterion

The failure criterion defined by equation 3

$$\sigma_1' = \sigma_3' + (m\sigma_c\sigma_3' + s\sigma_c^2)^{1/2} \tag{3}$$

can be rewritten as

$$y = m\sigma_c x + s\sigma_c^2 \tag{16}$$

where $y = (\sigma_1' - \sigma_3')^2$ and $x = \sigma_3'$

Intact rock

For intact rock, s = 1 and the uniaxial compressive strength σ_c and the material constant *m* are given by:

$$\sigma_c^2 = \frac{\sum y}{n} - \left[\frac{\sum xy - \frac{\sum x \sum y}{n}}{\sum x^2 - \frac{(\sum x)^2}{n}} \right] \frac{\sum x}{n} \tag{17}$$

$$m = \frac{1}{\sigma_c} \left[\frac{\sum xy - \frac{\sum x \sum y}{n}}{\sum x^2 - \frac{(\sum x)^2}{n}} \right] \tag{18}$$

where *n* is the number of data pairs.
The coefficient of determination r^2 is given by:

$$r^2 = \frac{\left(\sum xy - \sum x \sum y / n\right)^2}{\left(\sum x^2 - (\sum x)^2 / n\right)\left(\sum y^2 - (\sum y)^2 / n\right)} \tag{19}$$

Broken rock

For broken or heavily jointed rock, the strength of the intact rock pieces is determined by the analysis given above. The value of the constant *m* for broken or heavily jointed rock is found from equation 18. The value of the constant *s* is given by:

$$s = \frac{1}{\sigma_c^2}\left[\frac{\sum y}{n} - m\sigma_c \frac{\sum x}{n}\right] \tag{20}$$

The coefficient of determination is found from equation 19.

When the value of *s* is very close to zero, equation 20 will sometimes give a small negative value. In such cases, put *s* = 0 and calculate the constant *m* as follows:

$$m = \frac{\sum y}{\sigma_c \sum x} \tag{21}$$

Mohr envelope

The Mohr failure envelope is defined by the following equation, derived by Dr J.W. Bray of Imperial College:

$$\tau = (Cot\phi_i^{'} - Cos\phi_i^{'})\frac{m\sigma_c}{8} \tag{22}$$

The value of the instantaneous friction angle $\phi_i^{'}$ is given by:

$$\phi_i^{'} = Arc\tan\left(4h\, Cos^2(30 + 1/3\, Arc\sin\, h^{-3/2}) - 1\right)^{-1/2} \tag{23}$$

where

$$h = 1 + \frac{16\,(m\sigma' + s\sigma_c)}{3m^2\sigma_c}$$

and the instantaneous cohesive strength $c_i^{'}$ is given by:

$$c_i^{'} = \tau - \sigma'\, Tan\phi_i^{'} \tag{24}$$

where σ' is the effective normal stress.

Determination of m and s from direct shear test data

The following method for determination of the material constants *m* and s from direct shear test data was derived by Dr S. Dunbar (unpublished report) of Golder Associates in Vancouver.

The major and minor principal stresses σ_1' and σ_3' corresponding to each τ, σ' pair can be calculated as follows:

$$\sigma_1' = \frac{(\sigma'^2 + (\tau - c')\tau) + \tau(\sigma'^2 + (\tau - c')^2)^{1/2}}{\sigma'} \tag{25}$$

$$\sigma_3' = \frac{(\sigma'^2 + (\tau - c')\tau) - \tau(\sigma'^2 + (\tau - c')^2)^{1/2}}{\sigma'} \tag{26}$$

where c' is an estimate of the cohesion intercept for the entire τ, σ' data set. This value can be an assumed value greater than or equal to zero or it can be determined by linear regression analysis of the shear test results.

After calculation of the values of σ_1' and σ_3' by means of equations 25 and 26, the determination of the material constants *m* and *s* is carried out as for broken rock.

An estimate of the uniaxial compressive strength σ_c is required in order to complete the analysis.

References

Barton, N.R. (1971). A relationship between joint roughness and joint shear strength. *Proc. Intnl. Symp. Rock Fracture. Nancy, France*, paper No. 1-8.

Barton, N.R. (1973). Review of a new shear strength criterion for rock joints. *Engineering Geol*. Vol. 7, 287-332.

Barton, N.R. (1974). A review of the shear strength of filled discontinuities in rock. *Norwegian Geotech. Inst. Publ*. No. 105. Oslo: Norwegian Geotechnical Institute.

Barton, N.R., Lien, R. and Lunde, J. (1974). Engineering classification of rock masses for the design of tunnel support. *Rock Mechanics*. Vol. 6, No. 4, 189-236.

Barton, N.R. and Choubey, V. (1977). The shear strength of rock joints in theory and practice. *Rock Mechanics*. Vol. 10, No. 1-2, 1-54.

Bieniawski, Z.T. (1974). Estimating the strength of rock materials.*J. South African Inst. Min. Metall*., Vol. 74, No. 8, 312-320.

Bieniawski, Z.T. (1974). Geomechanics classification of rock masses and its application in tunnelling. *Proc. 3rd Intnl. Congr. Soc. Rock Mech*. Denver, 2, Part A, 27-32.

Bieniawski, Z.T. (1976). Rock mass classification in rock engineering. In *Exploration for rock engineering : proceedings of the symposium*, Johannesburg, 1976, A.A. Balkema, Vol. 1, 97-106.

Bishop, A.W., Webb, D.L. and Lewin, P.I. (1965). Undisturbed samples of London clay from the Ashford Common shaft. *Geotechnique*, Vol. 15, No. 1, 1-31.

Bishop, A.W., and Garga, V.K. (1969). Drained tension tests on London clay. *Geotechnique*, Vol. 19, No. 2, 309-313.

Brace, W.F. (1964). Brittle fracture of rocks. In *State of Stress in the Earth's Crust*. (ed. W.R. Judd) 111-174. New York: Elsevier.

Brace, W.F. and Martin, R.J. (1968). A test of the law of effective stress for crystalline rocks of low porosity. *Intnl. J. Rock Mech. Min. Sci.*, Vol. 5, No. 5, 415-426.

Broch, E. (1974). The influence of water on some rock properties. *Proc. 3rd Congr. Intnl. Soc. Rock Mech.* Denver, 2, Part A, 33-38.

Brown, E.T. (1970). Strength of models of rock with intermittent joints. *J. Soil Mech. Found. Div., ASCE,* Vol. 96, SM6, 1935-1949.

Brown, E.T. and Trollope, D.H. (1970). Strength of a model of jointed rock. *J. Soil Mech. Found. Div., ASCE,* Vol. 96, SM2, 685-704.

Charles, J.A. and Watts, K.S. (1980). The influence of confining pressure on the shear strength of compacted rockfill. *Geotechnique*. Vol. 30, No. 4, 353-367.

Colback, P.S.B. and Wiid, B.L. (1965). The influence of moisture con-tent on the compressive strength of rock. *Proc. 3rd Canadian Rock Mechanics Symp*., Toronto, 57-61.

Coulthard, M.A. (1979). Back analysis of observed spoil failures using a two-wedge method. *Australian CSIRO Division of Applied Geomechanics*. Technical report, No. 83, Melbourne: CSIRO.

Einstein, H.H., Nelson, R.A., Bruhn, R.W. and Hirschfeld, R.C. (1969). Model studies of jointed rock behaviour. *Proc. 11th Symp. Rock Mech*., Berkeley, Calif., 83-103.

Franklin, J.A. and Hoek, E. (1970). Developments in triaxial testing equipment. *Rock Mechanics*. Vol. 2, 223-228.

Gerogiannopoulos, N.G.A. (1979). A critical state approach to rock mechanics. *PhD. thesis*. Univ. London (Imperial College).

Goodman, R.E. (1970). The deformability of joints. In *Determination of the in-situ modulus of deformation of rock*. ASTM Special Tech. Publ. No. 477, 174-196. Philadelphia: American Society for Testing and Materials.

Griffith, A.A. (1921). The phenomena of rupture and flow in solids. *Phil. Trans*. Royal Soc. (London) A, Vol. 221, 163-198.

Griffith, A.A. (1925). Theory of rupture. *Proc. 1st Congr. Appl. Mech*., Delft, 1924. Delft: Technische Bockhandel en Drukkerij, 55-63.

Handin, J., Hager, R.V., Friedman, M. and Feather, J.N. (1963). Experimental deformation of sedimentary; rocks under confining pressure; pore pressure tests. *Bull. Amer. Assoc. Petrol. Geol.* Vol. 47, 717-755.

Heard, H.C., Abey, A.E., Bonner, B.P. and Schock, R.N. (1974). Mechanical behaviour of dry Westerly granite at high confining pressure. *UCRL Report*, 51642. California: Lawrence Livermore Laboratory.

Hencher, S.R. and Richards, L.R. (1982). The basic frictional resistance of sheeting joints in Hong Kong granite. *Hong Kong Engineer*. Feb., 21-25.

Hobbs, D.W. (1970). The behaviour of broken rock under triaxial compression. *Intnl. J. Rock Mech. Min. Sci*. Vol. 7, 125-148.

Hoek, E. (1964). Fracture of anisotropic rock. *J. South African Inst. Min. Metall*. Vol. 64, No. 10, 510-518.

Hoek, E. (1965). Rock fracture under static stress conditions. *PhD Thesis*, Univ. Cape Town.

Hoek, E. (1968). Brittle failure of rock. In /it Rock Mechanics in Engineering Practice. (eds K.G. Stagg and O.C. Zienkiewicz) London: Wiley. 99-124.

Hoek, E. and Bieniawski, Z.T. (1965). Brittle fracture propagation in rock under compression. *Intnl. J. Fracture Mechanics*. Vol. 1, No. 3, 137-155.

Hoek, E. and Brown, E.T. (1980a). *Underground Excavations in Rock*. London: Inst. Min. Metall.

Hoek, E. and Brown, E.T. (1980b). Empirical strength criterion for rock masses. *J.*

Geotech. Engin. Div., ASCE, Vol. 106, No. GT9, 1013-1035.

Hoek, E. and Bray, J.W. (1981). *Rock Slope Engineering.* (Third ed.) London: Inst. Min. Metall.

Hoek, E. General two-dimensional slope stability analysis. In *Analytical and Numerical Methods in Rock Engineering* (ed. E.T. Brown). London: Geo. Allen & Unwin. in press.

Horino, F.G. and Ellikson, M.L. (1970). A method of estimating the strength of rock containing planes of weakness. *U.S. Bur. Mines Rept. Invest*. 7449.

Horn, H.M. and Hendron, D.M. (1968). Discussion on 'Stability analysis for a sloping core embankment'. *J. Soil Mech. Found. Div., ASCE*, Vol. 94, SM3, 777-779.

Jaeger, J.C. (1970). The behaviour of closely jointed rock. *Proc. 11th Symp. Rock Mech.*, Berkeley, California, 57-68.

Jaeger, J.C. (1971). Friction of rocks and stability of rock slopes. *Geotechnique*, Vol. 21, No. 2, 97-134.

Jaeger, J.C. and Cook, N.G.W. (1969). *Fundamentals of Rock Mechanics*. London: Chapman and Hall.

John, K.W. (1962). An approach to rock mechanics. *J. Soil Mech. Found. Div., ASCE*, Vol. 88. SM4, 1-30.

Krsmanovic, D. (1967). Initial and residual shear strength of hard rock. *Geotechnique*. Vol. 17, No. 2, 145-160.

Ladanyi, B. and Archambault, G. (1970). Simulation of shear behaviour of a jointed rock mass. *Proc. 11th Symp. Rock. Mech.* , 105-125. New York: American Institute of Mining, Metallurgical and Petroleum Engineers.

Ladanyi, B. and Archambault, G. (1972). Evaluation de la resistance au cisaillement d'un massif rocheux fragmente. *Proc. 24th Intnl. Geol. Cong*., Montreal. Sect. 130, 249-260.

Lajtai, E.Z. (1967). The influence of interlocking rock discontinuities on compressive strength (model experiments). *Rock Mech. Eng. Geol.* Vol. 5, 217-228.

Lama, R.C. and Vutukuri, V.S. (1978). *Handbook on Mechanical Properties of Rocks. Vol.IV - Testing Techniques and Results*. Switzerland: Trans Tech Publications.

Marachi, N.D., Chan, C.K. and Seed, H.B. (1972). Evaluation of properties of rockfill materials. *J. Soil Mechs. Fdns. Div. ASCE*, Vol. 98, SM4, 95-114.

Marsal, R.J. (1967). Large scale testing of rockfill materials. *J. Soil Mech. Fdns. Div. ASCE*, Vol. 93, SM2, 27-44.

Marsal, R.J. (1973). Mechanical properties of rockfill. *Embankment Dam Engineering, Casagrande Vol*., 109-200. New York: Wiley.

Martin, G.R. and Miller, (1974). Joint strength characteristics of a weathered rock. *Proc. 3rd Cong. Intnl. Soc. Rock Mech.*, Denver. Vol. 2, Part A, 263-270.

McClintock, F.A. and Walsh, J.B. (1967). Friction on Griffith cracks under pressure. *Proc. 4th U.S. Congr. Appl. Math.*, Berkeley. 1015-1021.

McLamore, R. and Gray, K.E. (1967). The mechanical behaviour of anisotropic sedimentary rocks. *Trans. Am. Soc. Mech. Engrs*. Series B, 62-76.

Misra, B. (1972). Correlation of rock properties with machine performance. *PhD. Thesis*, Leeds University.

Mogi, K. (1966). Pressure dependence of rock strength and transition from brittle fracture to ductile flow. *Bull. Earthquake Res. Inst. Tokyo University*, Vol. 44, 215-232.

Mogi, K. (1967). Effect of the intermediate principal stress on rock failure. *J. Geophys. Res*., Vol. 72, No. 20, 5117-5131.

Muller, L. and Pacher, F. (1965). Modelevensuch Zur Klarung der Bruchgefahr geklufteter Medien. *Rock Mech. Engng Geol*. Supp. No.2, 7-24.

Murrell, S.A.F. (1958). The strength of coal under triaxial compression. In *Mechanical properties of non-metallic brittle materials*. (ed. W.H. Walton), 123-145. London: Butterworths.

Murrell, S.A.F. (1965). The effect of triaxial stress systems on the strength of rocks at atmospheric temperatures.*Geophysics J*., Vol. 10, 231-281.

Patton, F.D. (1966). Multiple modes of shear failure in rock. *Proc. Inst. Intnl. Cong. Rock Mech*., Lisbon, Vol. 1, 509-513.

Raphael, J.M. and Goodman, R.E. (1979). Strength of deformability of highly fractured rock. *J. Geotech. Eng. Div., ASCE*, Vol. 105, GT11, 1285-1300.

Richards, L.R. and Cowland, J.W. (1982). The effect of surface roughness on field shear strength of sheeting joints in Hong Kong granite. *Hong Kong Engineer*, Oct., 39-43.

Rosengren, K.J. and Jaeger, J.C. (1968). The mechanical properties of a low-porosity interlocked aggregate. *Geotechnique*. Vol. 18, No.3, 317-326.

Sarma, S.K. (1979). Stability analysis of embankments and slopes. *J. Geotech. Eng. Div., ASCE*, Vol. 105, GT12, 1511-1524.

Schwartz, A.E. (1964). Failure of rock in the triaxial shear test. *Proc. 6th Rock Mech. Symp*. Rolla, Missouri, 109-135.

Seed, H.B. and Sultan, H.A. (1967). Stability analysis for sloping core embankment. *J. Geotech. Eng. Div., ASCE*, Vol. 93, SM4, 69 -83.

Walker, P.E. (1971). The shearing behaviour of a block jointed rock model. *PhD Thesis*, Queens Univ. Belfast.

Wawersik, W.R. (1969). Detailed analysis of rock failure in laboratory compression tests. *PhD Thesis*, Univ. of Minnesota.

Wawersik, W.R. and Brace, W.F. (1971). Post failure behaviour of a granite and a diabase. *Rock Mechanics*. Vol. 3, No. 2, 61-85.